Layer-by-Layer Assembled Carbon Nanotube Composites for Neural Interfacing

by

Edward Jan

A dissertation submitted in partial fulfillment
of the requirements for the degree of
Doctor of Philosophy
(Chemical Engineering)
in The University of Michigan
2010

Doctoral Committee:

Professor Nicholas Kotov, Chair
Professor Daryl R. Kipke
Associate Professor Joerg Lahan
Assistant Professor Parag G. Patil

DEDICATION

To my parents, my wife, my family, and my friends.

To Venerable Dharma Master Cheng Yen.

To Buddha, Dharma, Sangha, and all sentient beings.

ACKNOWLEDGMENTS

This dissertation would not have been possible without the guidance, support, friendship, and love from many individuals. I would like to express my sincere gratitude to all of them.

First of all, I am extremely grateful to have Professor Nicholas Kotov as my Ph.D. advisor. I deeply appreciate the support and freedom he gave me during my Ph.D. studies. His encouragements, compliments, and critiques nourished my scientific curiosity and allowed me to discover my potential. Working with him was a valuable and rewarding experience, and I will always be inspired by his diligence, creativity, and kindness as a scientist, a mentor, and a friend.

I would also like to express my gratitude to my committee members, Professor Daryl Kipke, Professor Joerg Lahann, and Professor Parag Patil, for taking time out of their extremely busy schedules to discuss my research, offer me advices, and review my thesis. I also would like to acknowledge the University of Michigan for supporting my research through the Cellular Biotechnology Training Program Fellowship and the Rackham Predoctoral Fellowship.

I would like to thank the current and past members of the Kotov group for their friendship and technical assistances. Dr. Zhiyong Tang, Dr. Paul Podsiadlo, and Dr. Bong Sup Shim, and Dr. Jung Woo Lee were tremendously helpful in giving me scientific advices. I am especially thankful to my wonderful officemates, Peter Ho, Meghan Cuddihy, Dr. Daniel Lilly, Ashish Agarwal, and Christine Andres, for making our office a fun and enjoyable place to work at and for the many interesting and stimulating

discussions we had over the years whether they were scientific, philosophical, casual, or just random. I would to thank the undergraduate students who helped me with my experiments along the way, especially Vincent Husaini and Huey Shann Sue. I would also like to thank the administrative staff of the Chemical Engineering department, especially Rudy Sowards and Susan Hamlin, for making so many things easier and more convenient for graduate students.

I am very grateful for the many collaborators I was fortunate to work with during my Ph.D. studies. Specifically, I would like to thank Professor Yurii Gun'ko and Professor Yuri Volkov for mentoring my research project during my six-month stay at Trinity College Dublin. I also want to thank the many friends who helped me both in and outside of the laboratory while I was in Dublin. I want to express my gratitude to Professor David Martin for offering me the opportunity to work in his lab and start-up company, where I gained valuable knowledge about neural implants from Dr. Sarah Richardson-Burns and Dr. Jeffrey Hendricks.

Lastly, I would like to thank those who have shaped who I am. I would thank my parents and wife for their love and care. I would like to thank all my friends for the fun, companionship, inspirations, and supports they have provided me. I am grateful to all the volunteers of Tzu Chi Foundation from whom and with whom I have learned about compassion and selfless giving. I am most grateful to Venerable Dharma Master Cheng Yen whose teachings have lightened the path on becoming a better person for me.

PREFACE

This dissertation contains the following published articles and manuscript in preparation:

- **Jan, E.**; Byrne, S. J.; Cuddihy, M.; Davies, A. M.; Volkov, Y.; Gun'ko, Y. K.; Kotov, N. A. "High-content screening as a universal tool for fingerprinting of cytotoxicity of nanoparticles" *ACS Nano*, 2008, 2(5), 928-938.

- **Jan, E.**; Kotov, N. A. "Successful Differentiation of Mouse Neural Stem Cells on Layer-by-Layer Assembled Single-Walled Carbon Nanotube Composite." *Nano Letters*, 2007, 7(5), 1123-1128.

- Kam, N. W. S.; **Jan, E.**; Kotov, N. A. "Electrical Stimulation of Neural Stem Cells Mediated by Humanized Carbon Nanotube Composite Made with Extracellular Matrix Protein." *Nano Letters*, 2009, 9(1), 273-278.

- **Jan, E.**; Hendricks, J.L.; Husaini, V.; Richardson-Burns, S.M.; Sereno, A.; Martin, D.C.; Kotov, N. A. "Layered Carbon Nanotube-Polyelectrolyte Electrodes Outperform Traditional Neural Interface Materials." *Nano Letters*, 2009, 9(12), 4012-4018.

- **Jan, E.**; Pereira, F.N.; Kotov, N.A. "In-Situ Transfection and Neuronal Programming on Layered Carbon Nanotubes Nanocomposites." Submitted.

TABLE OF CONTENTS

LIST OF FIGURES

LIST OF TABLES

ABSTRACT

This dissertation investigates the utility of layer-by-layer (LBL) assembled carbon nanotube (CNT) composites as a neural interfacing material. The theoretical framework behind this research is based on the unique properties of CNTs and the ability of the LBL technique to impart multifunctionality into nanostructured thin films. The combination of CNTs and LBL assembly provides an opportunity to create materials with precisely controlled mechanical, electrochemical, and biological properties suitable for neural interfacing. In this dissertation, LBL assembled CNT-polyelectrolyte films were demonstrated to be biocompatible with neural cells using high-content screening methods. Moreover, these CNT composite films also supported the differentiation and electrical stimulation of neural stem cells, which hold promising therapeutic potentials. The electrochemical properties of LBL assembled CNT composites were established and found to outperform those of existing and emerging electrode materials. The incorporation of appropriate biological molecules into the CNT LBL films enabled the demonstration of enhanced neural stem cell differentiation and gene delivery that programmed multipotent cells into neurons. Finally, we purposed an in vitro 3D neural tissue model that can be used to facilitate the testing of electrode coatings designed to mitigate electrode-induced gliosis. The goal of this dissertation is to contribute to the development of next-generation neural electrode technologies, as well as to the fundamental understanding of both cellular response to nanomaterials and manipulation of cell behavior through nanostructured materials.

CHAPTER 1

Introduction

The development of nanotechnology has penetrated biology and medicine at a remarkable scale.[1] Nanotechnology has provided tools to measure and understand biosystems,[2-4] brought insights to challenges in biotechnology and biomedicine,[5-7] and offered building components for advanced biomaterials.[8-10] However, despite these advancements in biology and medicine, nanotechnology's applications to neuroscience are far behind applications to other disciplines of biomedicine.[11] The reason is multifold. The central nervous system (CNS) is highly complex in its anatomy, functional structuring, and information processing. Moreover, the CNS is difficult to access and consists of an extremely heterogeneous cellular and molecular environment. But recently we are beginning to see emerging progress in the application of nanotechnology in neuroscience.[12, 13] Armed with one of the most fascinating nanomaterials and an exceptionally versatile nanostructuring technique, we believe this research can make significant contributions to bridge the distance between nanotechnology and neuroscience, as well as provide novel solutions for better neural prosthetic devices.

1.1 Motivation

Diagnostic, therapeutic and treatment strategies for various neurological, sensory, and psychiatric conditions are increasingly relying on neural prosthetic devices. Deep brain stimulation and pace-makers are the two examples of this rapidly growing field of medical practice.[14-17] The employment of neural prosthetic devices has significantly improved the quality of life for those suffering from neurological disorders and injuries. The cochlear implant, as the most successful neural prosthetic device, has been in common clinical use for over two decades for restoration of hearing.[18] Chronic deep-brain stimulation with spike electrodes has proven to dramatically alleviate symptoms in patients of Alzheimer's and Parkinson's diseases.[19-23] Other devices have also allowed patients of ayomyotrophic lateral sclerosis and paralysis to regain their motor control and function.[24] Cuff electrodes around peripheral nerves are used for treatment of numerous disorders from pain and to incontinence, diabetes, depression, and arrhythmia.[25-35] All of these neural prosthetic devices are essential for restoring neurological functions, mobility of limbs and other parts of the body in case of injury or paralysis.[36]

Despite general success and proven medical importance, there are still multiple practical and fundamental challenges related to the utilization of neural electrodes. While most chronically implanted electrodes appear to be well tolerated initially, long-term viability of these electrodes remains a significant problem that is rooted in the lack of knowledge about neural interfacing and new materials. Some of the existing challenges include stability and charge injection safety of the electrode after prolonged use. Another

major issue is inflammatory responses brought about by a combination of factors, such as electrode size, mechanical mismatch between tissue and electrode, and poor integration of the electrode with surrounding tissue, leading to the formation of an insulating sheath encapsulating the electrode. Significant strides toward better and safer electrodes hinge on improvements of cellular interface, charge transport, mechanical compliance with the tissues, and chemical stability of the electrode materials.[14, 15, 17, 36-39]

Nanomaterials present an essential and largely untapped resource for the design of neural electrodes. The intrinsic properties of nanomaterials enable the engineering of cellular interface and nano/micro organization of the electrode which are essential to the physical, chemical and biological properties of the device.[40-46] For example, carbon nanotubes exhibit unique mechanical,[47], electrical,[48] and optical [49] properties that can be exceptionally useful for this application. Nanocomposites have been predominantly designed for a variety of high-end electronic and optical applications,[50-53] and the very same functions can be taken advantage of in designing neural electrodes.

This dissertation aims to develop a neural interfacing material based on layer-by-layer (LBL) assembled carbon nanotube (CNT) composite films that offers a more compliant and biocompatible interface, better charge transfer capability, and the ability to direct neuronal growth and deliver biological agents. The outcome of this research has both practical and scientific values. On the practical side, this research contributes to the development of a new generation of neural electrodes for electrical stimulation and recording of excitable cells. Scientifically, this research allows us to gain fundamental

understanding of both cellular response to nanomaterials and manipulation of cell behavior through nanostructured materials.

This dissertation is the convergence of several fields of study, including nanotechnology, materials engineering, biomedical engineering, tissue engineering, neuroscience, and stem cell biology. Therefore, this introductory chapter provides a review on a wide range of topics that are fundamental to this dissertation. We begin our review with the neural interface, which includes discussions on electrode materials, the issue of inflammatory reaction, and approaches to mitigate inflammatory reactions. This is followed by a discussion of the properties of carbon nanotubes (CNTs) and their applications in biomedicine and neural interfacing. Presented next is a review on the nanostructuring technique of layer-by-layer (LBL) assembly, with an emphasis on biomedical applications and LBL composites fabricated with CNTs. We then look at neural stem cells (NSCs), examining the significance of using these cells in this research and strategies that can be used to manipulate their behaviors. Lastly, we review the inverted colloidal crystal (ICC) scaffold design, which enables us to develop 3D neural tissue models to investigate electrode induced cellular reactions.

1.2 Neural Interface

Despite the variety of neural prosthetic devices and methods of their use, they all share a common purpose, which is to exchange information with the nervous system.[54] Neural interfaces are the connections that allow this exchange of information to take place, and thus neural interfaces are critically important to the efficacy of neural prosthetic devices. To initiate a response in the nervous system, information can be delivered by application of electrical signals to induce action potentials. On the other hand, information about the state of the nervous system can be extracted by recording the action potentials as electrical signals. The ability of a neural electrode to carry out its stimulation or recording function chronically is dependent on an array of factors, such as implantation techniques, geometry, mechanical properties, biocompatibility, and electrochemical properties. Among these, biocompatibility and electrochemical properties are perhaps the most important and of interest to this dissertation.

To maintain the exchange of information between a neural prosthetic device and the nervous system, the ideal neural interface must be able to integrate intimately with the surround neural tissue to ensure effective delivery or recording of electrical signals. Therefore, the material selection for the electrode is a critical determinant for this process. The ideal neural interfacing material must be biocompatible enough or encompass biofunctionalities to prevent or resolve inflammatory reactions and maintain stable connections with neurons. Inflammatory reactions caused by electrode implantation are often detrimental, resulting in loss of neuronal population and formation

of an insulating sheath that destroy the neural interface and render the electrode useless. In addition, the ideal neural interfacing material must also possess appropriate electrochemical properties necessary to carry out the intended functions. To achieve successful stimulation, the material must be able to deliver sufficient electrical charges to the interface with neurons without inducing chemical reactions that can damage the surrounding tissues. For recording purposes, the material must be able to record electrical signals at a high signal-to-noise ratio so that the signals can be successfully processed and interpreted. In this section, we will now review some of the conventionally used and emerging electrode materials, discuss the process of inflammatory reactions, and present strategies that have been used to control inflammatory reactions.

1.2.1 Neural Electrode Materials

The major types of neural electrode materials can be categorized as capacitive or faradaic, depending on the mechanism in which the electron flow in the electrode is transitioned into ion flow in the tissue.[55] Capacitive reactions are characterized by charging and discharging of the electrode-electrolyte double layer. Two of the mostly commonly used capacitive charge-injection materials are titanium nitride and tantalum/tantalum oxide.[56] In general such electrodes are highly desired as no chemical species are created or consumed during the process. Typically, for capacitive charge-injection materials, high charge-injection capacity is achieved through the employment of high dielectric constant coatings or the creation of a highly porous geometry that can provide large surface area accessible to ions.

Faradaic reactions result from the reduction and oxidation of surface-confined species at the electrode-electrolyte interface. Although faradaic reactions can provide large amount of charges for stimulation, these reactions often produce unwanted effects such as dissolution of the electrode and oxidization and reduction of water, all of which can be harmful to the surrounding tissues. Some of the most prevalent and established materials in this category are noble metals, such as Pt and PtIr alloys, and various forms of iridium oxide.[57, 58] Among these materials, iridium oxide is the material with the highest performance. Iridium oxide can be formed by electrochemical activation, or repeated oxidation and reduction, of iridium on a metal surface. Alternatively, iridium oxide can also e produced by reactive sputtering from iridium in an oxidizing plasma.[55] Although iridium oxide has been widely used in stimulation studies in the central nervous system and in clinical settings for acute and short-term studies,[59, 60] this material poses its own set of problems. Delamination and cracking of the iridium oxide coating have been reported under high charge density that resulted in the deposition of foreign materials in the surrounding tissues.[61, 62] Most importantly, this causes significant reduction of the charge injection capabilities over time because a layer of electrolytes sips between the conductive coating and the backing, causing multiple problems for effective electrical stimulation of the cells.[63]

Besides the ability to deliver sufficient charges without complications, the greatest hurdle for all conventionally used electrode materials is their capability to interface with neural tissues chronically. Mechanically, metal coatings are brittle and can only withstand limited number of flexural motions. Most importantly, these materials do

not encompass the ability to be surfaced modified for enhanced biocompatibility and biofunctionality that would enable long-term implantation in the body. Poly(ethylenedioxythiophene) (PEDOT) is a conducting polymer that has recently emerged as a promising material for this challenge. The biocompatibility of PEDOT has been successfully demonstrated in both cell culture and animal studies.[64-66] Remarkably, PEDOT has been shown to improve various aspects of the neural interface, including electrical properties, mechanical stability, neural attachment, and neurite outgrowth.[67] Most significantly, there is a wide array of ways in which biofunctionalities can be added. For example, nerve growth factor can be immobilized in PEDOT coatings and drugs can be loaded in PEDOT to allow controlled drug release.[68, 69] Despite the versatility and outstanding biocompatibility, PEDOT also suffers from cracking and delamination after repeated charge injections.[70]

Carbon nanotubes (CNTs) are another class of material that has emerged as an alternative to conventional electrode materials. They are a logical choice of material due to their exceptional mechanical and electrical properties, which are later discussed in this chapter. The goal of this dissertation is to establish layer-by-layer (LBL) assembled CNT composites as a suitable electrode material for neural interfacing. The combination of CNTs with LBL assembly is a promising and exciting platform, unmatched by any conventional materials, for creating a neural interface because of level of control in material properties that can be achieved, as well as the boundless possibilities of new functionalities that can be incorporated.

1.2.2 Inflammatory Reactions

The primary concern in the development of neural interfacing materials is the degradation of electrode performance over time due to inflammatory reactions. While the goal of every electrode implantation is to achieve a stable interface, characterized by minimal cellular changes in the surrounding tissue and sustained functioning of the implanted device, the placement and presence of the implanted electrode represents the greatest perturbation to the host tissue.

Generally, the implantation of an electrode induces a cascade of biological responses that are highly complex due to the dynamic environment in the neural tissue. The immediate injury caused by the implantation is the disruption of the blood brain barrier and neurovasculature, causing hypoxia and death of glial and neuronal cells at the implantation site.[71] The extent of trauma can be greatly exacerbated by the technique used to insert the electrode, the geometry of the electrode, and large mechanical mismatch between the electrode and the neural tissue.[72, 73] As a counter measure, the body initiates inflammatory and wound healing responses to remove the dead cells and repair the damaged tissue. An important part of this process is the activation of microglia, astrocytes, and infiltrated peripheral macrophages because these cells release both beneficial and harmful factors, including cytokines, chemokines, neurotransmitters, and reactive oxygen species, that can affect the severity and length of the inflammatory reactions.[71] Typically, acute inflammatory reactions lead to the displacement of neuronal

bodies due to swelling in the implantation site, resulting in an increase in the impedance values.[65]

Chronic inflammatory reactions are destructive and the main reason why advanced electrode designs are needed. Chronic inflammatory responses at the implantation site are characterized by the activation of astrocytes and the attachment and invasion of activated microglia on the neural interface. Activated microglia cells secrete lytic enzymes and reactive oxygen species in attempts to degrade and remove the foreign object and release cytokines that result in astrocyte activation.[74, 75] Once activated, astrocytes produce inhibitory molecules that lead to the formation of a dense insulting sheath around the implant known as glial scarring.[76] The encapsulating sheath not only pushes neuronal bodies away from the surface of the electrode but also causes neurons to degenerate over time. The consequence can be severe, as more charges must be delivered to produce a stimulatory response, if any is still inducible. In addition, the increase in impedance can potentially render the recorded signals and noises to be indistinguishable from each other, and thus bring about the loss of recording capabilities.

1.2.3 Approaches to Reducing Inflammatory Reactions

Various strategies have been explored to mitigate inflammatory reactions induced by the implantation of neural electrodes and to maintain a stable neural interface. Generally, these strategies can be categorized into four main approaches. They include engineering of the mechanical properties of the interface, tailoring the geometry of the electrode, controlling of inflammatory response, and maintaining a healthy neuronal

population at the electrode interface. We have to point out that while acute inflammatory responses are primarily the result of mechanical injuries than inadequate biocompatibility, they can often develop into chronic problems if the inflammation persists.

Mechanical properties of electrodes are an important parameter since mechanical stress can activate reactive astrocytes.[73, 77-79] The large mismatch between the hardness of neural tissue and conventional electrodes is considered to be the main contributor of mechanical stress and micromotions.[72, 73] Therefore, fabrication of soft conductive materials, such as poly(pyrrole) or PEDOT, that could match the stiffness of the neural tissuesmay be a promising solution to attaining a more compliant interface.[72, 80-87] The geometry or physical dimension of neural electrodes is also an important parameter for reducing tissue encapsulation.[88] Studies have shown that subcellular-sized features can reduce adhesion of macrophages and decrease capsular thickness.[89, 90] In addition, physical dimensions of surface features were found to affect mechanotrunsduction, adhesion, and apoptosis.[91-93]

Another approach to reduce tissue reactions is to manage the inflammatory responses. One solution is to deliver anti-inflammatory drugs by local or systemic routes.[94-97] However, with advancement in surface modification technologies, a simpler and more elegant solution is to incorporate special anti-inflammatory coatings to the electrode surface.[98-102] With this method, it is possible to fabricate an inherently anti-inflammatory surface by immobilization of biomolecules that can modulate the

expression of inflammatory cytokines.[98] The last approach to maintaining a stable neural interface is to ensure an effective neuronal population is available for delivery or recording of electrical signals. This can be achieved by attracting neurons to migrate toward the implantation site and encourage the development of neural processes. Many studies have successfully demonstrated this concept by incorporation of various biomolecules, such as proteins and growth factors.[85, 95, 103-107] As adult neurons in the central nervous system are fragile and do not proliferate, an alternative solution is to generate neurons from neural stem cells or other multipotent cells that are already present in the nervous system or introduced externally. This is indeed the approach that we will explore in this dissertation. Specifically, we will investigate the feasibility to enhance neuronal differentiation of neural stem cells and program multipotent cells into neurons by tailoring the biological properties of layer-by-layer (LBL) assembled carbon nanotube (CNT) composites.

1.3 Carbon Nanotubes

Carbon nanotubes (CNT) are a special class of nanomaterials. CNTs are tubular in structure with nanometer range diameters and micrometer range lengths. Discovered by Iijima in 1991,[108] multi-walled carbon nanotubes (MWNTs) were the earliest observed CNT structures and can be described as sheets of graphite arranged in concentric cylinders. Quickly after the discovery of MWNTs, single-walled carbon nanotubes (SWNTs) were synthesized in 1993 using arc-discharge methods with transition metal

catalysts.[109, 110] The structure of SWNTs sets them apart from any other materials and is the source of their amazing features and properties, which have attracted scientists and engineers from all disciplines.

1.3.1 Electrical Properties and Applications

The structure of a single SWNT can be described as a single, one-atom-thick, layer of graphite, known as a graphene sheet (Figure 1.1 a), rolled up into a seamless cylinder with a diameter close to 1 nm and length that can be thousand of times larger (Figure 1.1 e). The way the graphene sheet is wrapped specifies the lattice of a SWNT to be armchair, zigzag, or chiral (Figure 1.1 b, c, d) and give rise to different electronic structures and properties.[111] The unique electrical properties of SWNTs are contributed by the peculiar electronic structure of graphene and the one dimensional structure of SWNTs. The symmetry and unique electronic structure of graphene allow electrons move freely as in metals in some configurations while behave like semiconductors in others[112]. As a consequence, all SWNTs are semiconducting except those with the armchair configuration which are metallic. The one-dimensional (1D) structure of SWNTs confines electrons to motion along the tube axis, reducing the phase space for the scattering processes that are responsible for the electrical resistance of the metallic SWNTs.[112, 113] For this reason, metallic CNTs are highly conductive and can carry enormous current densities up to 10^9 A/cm^2, which are 2 to 3 orders of magnitude higher than the threshold in metals such as aluminum and copper.[112, 114] Because of their 1D, high aspect ratio nanoscale structure and unique electrical properties, SWNTs have been

heavily explore for applications in nanoelectronic devices,[115-117] sensors,[118-120] field-emission electron sources,[121, 122] displays and lighting elements,[123] and scanning probe tips.[124] For this research, we would like to exploit SWNTs' excellent electrical conductivity for the fabrication of a biocompatible and multifunctional neural interface that is capable of delivering electrical stimulation and recording signals from neural activities.

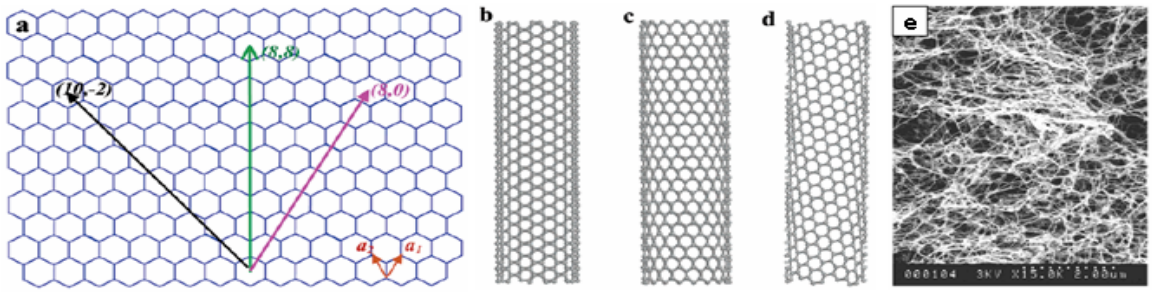

Figure 1.1 (**a**) Schematic honeycomb structure of a graphene sheet. SWNTs can be formed by folding the sheet along lattice vectors. Folding of different vectors lead to armchair (**b**), zigzag (**c**), and chiral (**d**) carbon nanotubes.[125] (**e**) A scanning electron microscopy image of single-walled carbon nanotubes (SWNTs).[126]

1.3.2 Mechanical Properties and Applications

Like the electrical properties, the mechanical properties of SWNTs have their origin in the structure of SWNTs. Their remarkable strength is a product of the extremely strong covalent sp^2 bonds between individual carbon atoms in the graphene sheet. Experiments[127-129] and calculations[130-133] have shown that the Young's modulus of

isolated SWNTs has a value of approximately 1 TPa, while the tensile strength has been measured to be between 13 and 50 GPa.[129, 134] In addition, SWNTs also demonstrate high flexibility, toughness, and capacity for reversible deformation as atomic force microscopy (AFM) measurements have indicated that SWNTs can bend into loops without breaking.[135] It has been proposed that SWNTs accommodate large strains by diatomic rotation to unlock the pristine nanotube wall through the formation of a dislocations dipole with the pentagon-heptagon cores.[136]

The exceptional mechanical properties of SWNTs have led to a new generation of CNT-based composite materials with extraordinary strength and lightweight. Most of them are fabricated by microscale blending of CNTs with polymers, metals, or ceramics through processes such as melt mixing, film casting, spin coating, polymerization, and fiber spinning.[137-140] For biomedical devices, qualities such as durability, material stability, and flexibility are critical to the biocompatibility and longevity of the devices. In this research, the design and fabrication of novel neural interfacing materials are based on the layer-by-layer (LBL) assembly of CNTs. The method of LBL assembly is an emerging and versatile nanostructuring technique for fabricating CNT-based composites that are mechanically strong and flexible.[141] We believe we can create advanced and multifunctional neural interfaces by taking advantage of the excellent mechanical properties, as well as many other exciting properties, afforded by LBL assembly of CNTs.

1.3.3 Functionalization and Biomedical Applications

In order to exploit the amazing properties of SWNTs for biomedical applications, functionalization of SWNTs is essential and requires the understanding and mastery of CNT chemistry.[142] Since chemistry normally occurs in solution, dissolution of SWNTs is crucial[126] and allows further functionalization of SWNTs to be achieved. SWNTs without any functionalization are chemically inert. They are also extremely resistant to wetting[143] and typically exist as ropes or bundles 10 to 25 nm in diameter and a few micrometers long.[126] Functionalizations are made possible through covalent and non-covalent means.

Covalent chemistry of SWNTs is possible at both the end caps and sidewall of SWNTs.[126, 144-146] The end caps of SWNTs are more reactive then the sidewall because of the strain induced from the curvature of the hemispherical caps. Oxidization[147-149] of the end caps to carboxylic acid and other weakly acidic functionalities by treatment with nitric acid[147, 150] allows dissolution of SWNTs in amide-type organic solvents and introduces chemical functionalities for subsequent elaborations. The less reactive sidewall is also susceptible to reaction because of the strain from π-orbital misalignment. It's important to note that covalent functionalizations at the end caps and sidewall typically disrupt the aromatic ring system of SWNTs and result in reduction of tube length and loss of electrical and mechanical properties.[125, 126] Non-covalent methods allow the preservation of SWNTs' important properties. SWNTs can be dispersed and functionalized effectively by polymer wrapping[151-154] and adsorption of amines and molecules with large π-systems.[155, 156]

Functionalization of SWNTs has lead to an explosion of biomedical applications. Utilizing the scheme of π-stacking, Chen et al. have immobilized a wide range of biomolecules, such as ferritin, streptavidin, and biotin-PEO-amine, on the sidewalls of SWNTs with high efficiency.[155] Gheith et al. have created biocompatible CNT-based composites using polymer-wrapped SWNTs together with LBL assembly.[157] Other researchers have also functionalized SWNTs with bioactive groups such as peptides,[158, 159] proteins,[160] and DNA[161] and utilized them as sensing materials for DNA[162], glucose,[163, 164] peptides,[165] and proteins.[166-168] The development of a smart SWNT-based biomaterial for neural interfacing will rely in part on non-covalent functionalization of SWNTs. The other part will rely on appropriate selection of components for LBL assembly, which will be discussed below.

1.3.4 Neural Prosthetic Applications

Biocompatibility is essential to the development of biomedical applications. It is always the first and essential step in establishing the applicability of a new material for medical applications. So far, cellular behavior with and on CNTs have been tested with various types of cells.[169-176] In the case of neural cells, biocompatibility of CNT-based materials has been demonstrated by several research groups using adult primary neural cells.[177, 178] In addition, carbon nanofiber reinforced composites were shown to increase neuronal cell functions while providing a mechanically strong and electrically conductive substrate.[179] Patterned CNTs were utilized to guide neural cell growth, and preferential

cell attachment on CNTs was demonstrated.[180, 181] Neural signal transmission efficacy was reported to increase on CNT-coated substrates.[182]

These recent studies show that long-term CNT-based implants are a realistic target. However, none of the materials employed in these studies can be practically used for such a purpose. CNT-based thin films and coatings produced by drying,[179, 183] spraying and evaporation,[177, 178, 182, 184] and chemical vapor deposition on silicon substrates[180, 181] are either not stable or durable enough for chronic implantation in physiological conditions or limited to fabrication on silicon substrates. In addition, films and coatings fabricated in such ways cannot be controlled or modified at the molecular level. This limitation significantly diminishes the excellent electrical and mechanical properties that could be brought about by the nanoscale building blocks through nanostructuring techniques such as LBL assembly.

Up to this date, very few stem cell cultures have been investigated in conjunction with nanomaterials. As demonstrated in this research, we see strong possibilities, fundamental importance, and practical need to use neural stem cells (NSCs)[185, 186] rather than adult cells in the studies of SWNT-based materials for neural tissue engineering. Adult cells have limited capacities for extracellular matrix remodeling, axonal extension, and interfacing with implants.[187-189] Successful implantation and long-term performance of a neural implant and prosthetic device may require a durable interface as well as potent stem cells to revitalize the targeted tissue.

1.4 Layer-by-Layer Assembly

The usefulness of nanomaterials is heavily dependent on the ability to assemble them into bulk materials by manipulating them at the molecular level. This is especially the case for creating and designing biomaterials. For a long time, Langmuir-Blodgett deposition, invented by Langmuir[190] and Blodgett,[191] and self-assembled monolayers (SAMs), developed by Nuzzo,[192] Allara,[192] and Whiteside,[193] remained the primary methods for fabricating sold thin films from molecular components. As pointed out by Tang et al,[194] although numerous applications have been developed for tissue engineering and drug delivery using these techniques, Langmuir-Blodgett deposition and SAMs suffer from significant drawbacks. Langmuir-Blodgett films are unstable, time consuming to produce, limited to components with amphiphilic property, and require expensive instrumentations. SAMs are low in loading of biological components due to their monolayer nature. They are also limited to a few substrate types because of the chemistry involved and are relatively unstable under ambient and physiological conditions.

The layer-by-layer (LBL) assembly technique, introduced by Decher[195] in 1992, is free of the problems associated with Langmuir-Blodgett deposition and SAMs. The LBL assembly technique is based on alternating adsorption of monolayers of individual molecular components, such as polyelectrolytes, attracted to each other by a combination of interactions: electrostatic,[196, 197] hydrophobic,[198] hydrogen bonding,[199] charge-transfer,[200] biological recognition,[201] and others (Figure 1.2). The adsorption process is

cyclically repeated on substrates until desirable structures, thicknesses, and loadings of interested species are obtained. Since thin films are assembled one monolayer at a time, LBL assembly affords nanometer level control of the film thickness and composition.[196] It must be emphasized that the individual layers in the thin film are not discrete and segregated. In contract, as shown in Figure 2.1, the structure of the assembled material consists of interpenetrating layers that result in high homogeneity of the individual components which is important for achieving outstanding material properties. Thin films produced in this manner are also considerably stable in physiological conditions due to the cooperative effects of multiple interactions among the film components.

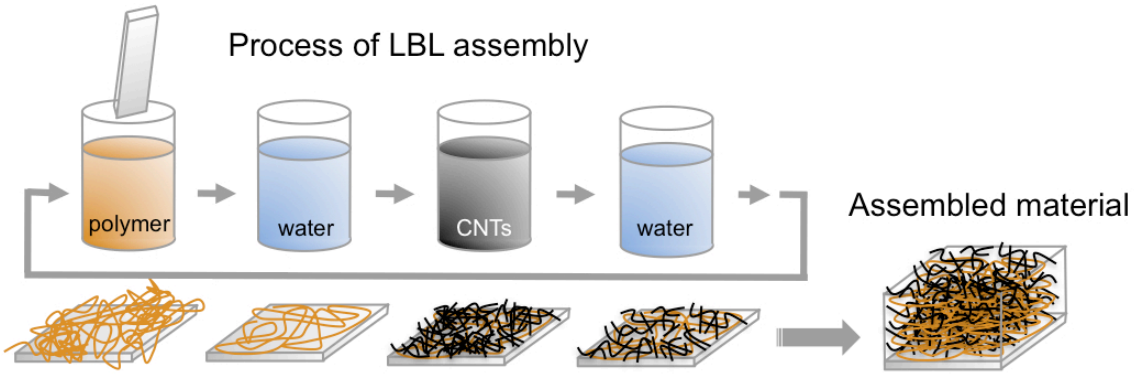

Figure 1.2 Schematics of layer-by-layer (LBL) assembly. LBL assembly is characterized by the sequential deposition of complementary species onto a substrate. Here, the LBL assembly of carbon nanotube (CNT) with polymer is depicted. The assembled composite material consists of interpenetrating layers of polymer and CNTs.

The simple and efficient technique of LBL assembly can be preformed on a variety of novel and unique geometries to create multilayer thin films and coatings using templating and patterning techniques.[202, 203] This capability is a powerful advantage for medical devices such as implantable chips, probes, and scaffolds that have small dimensions, irregular shapes, lithographically patterned elements, and surface engineered components. Furthermore, LBL assembly can be performed with to a wide range of inorganic and biologically active materials including as nanoparticles,[204] nanotubes,[141] nanoplates,[205] organic dyes,[206] dendrimers,[207] polypeptides,[208] DNA,[209] and proteins.[210, 211]

1.4.1 Biomedical Applications

As discussed above, LBL assembly has demonstrated itself as a simple, fast, and versatile technique for fabricating solid thin films. LBL films are physiologically stable and can be fabricated on essentially any type and shape of substrates. Its ability to incorporate a vast variety of biologically interesting species at high loading has led to numerous biomedical applications.

LBL assembled thin films have been developed into biosensors and drug delivery agents. By incorporation of inorganic particles, enzymes, antigens, antibodies, proteins, nucleic acids, and DNA, a variety of biosensors have been created to detect oxygen, glucose, DNA binding, toxic chemicals, insulin, pH changes, and many other chemicals. Detection can be achieved by measuring the electrochemical, gravitational, optical, and mechanical properties of the films.[194] In the case of drug delivery, LBL assembled films

offer the ability to control the dosage and kinetics by varying the thickness and composition of assembled multilayers. The release of a component typically depends on its permeability and the breakdown of the polymer multilayer matrix, which can be stimulated by changes in the pH, temperature, or ionic strength of the solution, application of an external electrical field, exposure to UV light, or by the incorporation of a hydrolytically-, enzymatically-, or self-degradable macromolecular matrix.[194]

LBL films have also been engineered to mediate cellular functions by incorporating various growth factors and polymers. Poly(ethyleneimine) (PEI), poly(allylamine hydrochloride) (PAH), poly(styrene sulfonate) (PSS), poly(D-lysine) (PDL), and poly(L-lysine) (PLL) have been utilized to manipulate cell adhesion, proliferation, and differentiation. Higher endothelial cell viability was demonstrated on PDL and PAH multilayers.[194] Enhanced turmor cell adhesion and secretion of chemokines were shown on PAH and PLL ending polyelectrolyte films.[212] The integration of fibroblast growth factor into multilayer PEI films increased fibroblast proliferation and secretion of type 1 collagen and interleukin-6.[213] For this research, we are interested in species that can enhance the adhesion, proliferation, and differentiation of neural cells and neural stem cells.

Lastly, LBL assembled films have been fabricated to yield anti-biofouling properties. Resistance against blood coagulation is critical to implantable materials and has been demonstrated by the incorporation of serum albumin, heparin, dextran, and chitosan into LBL assembled thin films.[194] Anti-inflammatory response is especially

important to neural prosthetic devices and has been demonstrated on LBL coatings containing anti-inflammatory agents and polypeptides.[214, 215] Anti-bacterial properties have also been realized by the incorporation of antimicrobial peptides[216] and silver nanoparticles.[217]

1.4.2 Layer-by-Layer Assembled Carbon Nanotube Composites

LBL assembled SWNT-polyelectrolyte multilayers are a class of novel composite materials with extraordinary properties. The versatile architectures of SWNT-polyelectrolyte thin films can be engineered at the nanoscale level to attain desirable mechanical, structural, and electrical properties. The immobilization of macromolecular species and strong interdigitation of the nanometer-thick film result in close-to-perfect molecular blending of the components (Figure 1.2, Figure 1.3 a, b), giving rise an impressive tensile strength of 220±40 MPa,[141] which is more than sufficient for any biomedical implants. SWNT-polyelectrolyte thin films are also mechanically flexible due to the homogeneous distribution of polymer chains in the nanostructured material. This property is very important for neural prosthetic applications since neural electrodes should be mechanically compliant and conformal to reduce mechanical injuries and micromotions. SWNT composites also have electrical conductivity of at least 4.15×10^4 S/cm,[218] which exceeds the requirements of successful excitation of neurons. We believe the combination of strength, flexibility, stability, fast charge transport, and a variety of necessary geometries and patterns,[202, 203, 219] including free-standing films (Figure 1.3 c),

available for LBL films demonstrates LBL assembled SWNT composites as the choice of material for neural tissue engineering applications.

Besides the bulk properties, LBL assembled SWNT films also have very interesting topological features. The manifold of forces involved in the formation of the films make them especially appropriate for the interactions with the cellular membranes. The topology of the LBL SWNT composite (Figure 1.3 a, b) resembles very closely the nanoscale features of collagen fibers in the extracellular matrix,[169, 175, 220, 221] which serves as growth and differentiation environment for neurons. The cytoskeleton of neural cells consists of microtubules, neurofilaments, and actin microfilaments that range from 7 to 25 nm in diameter.[222] We believe these filamentous structures, which are responsible for important functions such as the remodeling of processes and the motility of growth cones, can associate with SWNTs to form a biologically cohesive interface for promoting stem cell proliferation and differentiation.

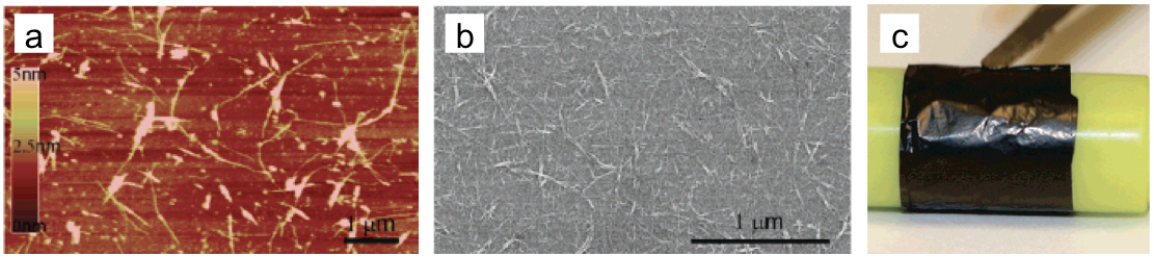

Figure 1.3 (**a**) An atomic force microscopy (AFM) image of $(PVA/SWNT\text{-}PSS)_1$ on silicon substrate. (**b**) A scanning electron microscopy (SEM) image of $(PVA/SWNT\text{-}PSS)_3$ on silicon substrate. (**c**) Demonstration of the flexibility of a piece of $(PVA/SWNT\text{-}PSS)_{200}$ free-standing LBL composite film.[218]

In a previously reported study, using a murine neuroblastoma × glioma hybrid cell line, we demonstrated for the first time neuronal cell attachment and differentiation on LBL assembled SWNT-polyelectrolyte coatings and freestanding thin films.[157] Although this very preliminary study indicates that LBL prepared SWNT composites, which encompass the versatility of LBL assembly and novelty of SWNTs, may be well qualified for neural interfacing applications, there is tremendous work to be carried out to transform this concept into a platform technology. The purpose of this research is exactly to accomplish this, by demonstrating SWNT LBL film's utilities, in terms of biocompatibility and electrochemical properties, and developing new functionalities that will enhance integration of the artificial interface with neural tissues.

1.5 Neural Stem Cells

One key focus of this dissertation is the interaction of nanostructured carbon nanotube (CNT) materials with neural stem cells (NSCs). This is an area that has not yet been explored by researchers and therefore deserves to be investigated in this research. NSCs are cells that can generate neural tissues or are cells derived from the nervous system with some capacity for self-renewal and ability to give rise to cells other than themselves through asymmetric cell divisions[223] (Figure 1.4). Ever since their discovery,[185, 186] NSCs have been extensively studied to understand their niche in the CNS[224] and demonstrate their potential therapeutic values in replacing damaged and lost cells in the CNS.[225, 226] Neural progenitor or precursor cells (NPCs) are a subset of NSCs

but with a more limited self-renewal potential and are sometimes used interchangeably with NSCs in the literature.

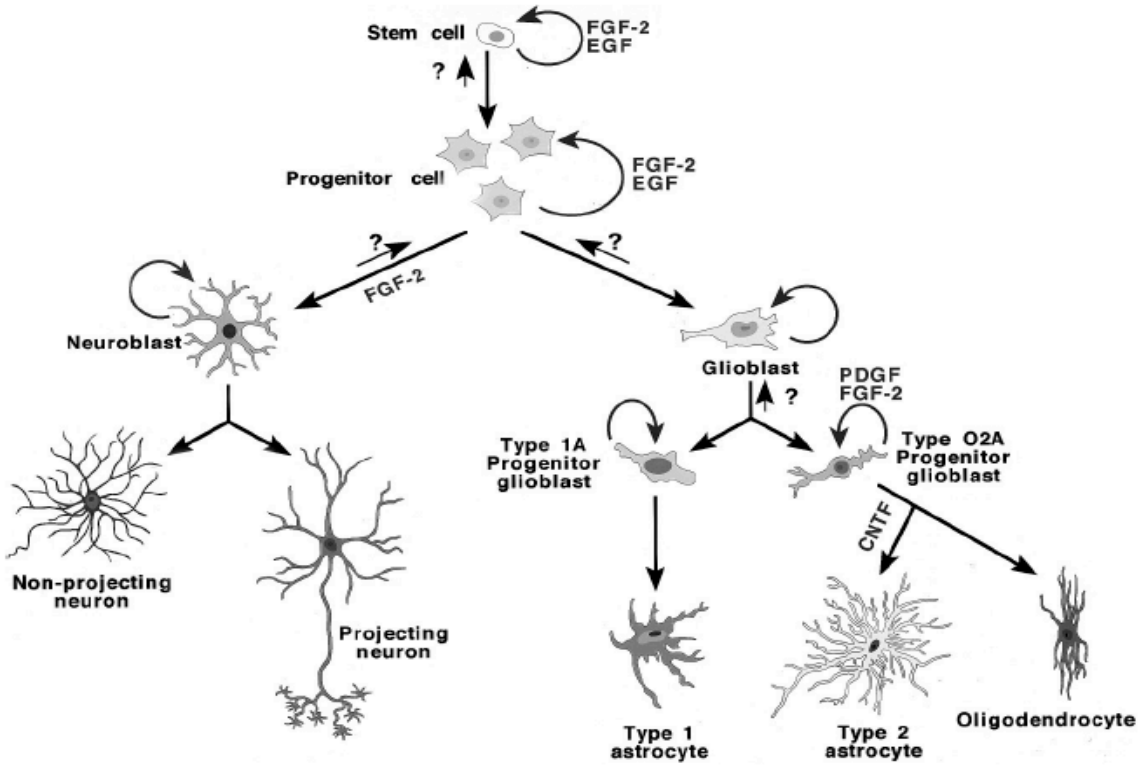

Figure 1.4 Schematic of neural cell lineages. A self-renewing population of undifferentiated stem cells ultimately give rise to all of the diverse cell types that are present within the adult CNS.[227]

NSCs for in vitro studies are isolated by dissecting out a region of the fetal or adult brain that has been demonstrated to contain dividing cells.[223] The tissue is then dissociated and exposed to a high concentration of mitogen such as fibroblast growth

factor-2 (FGF-2)[228] or epidermal growth factor (EGF)[229] for proliferation. NSCs are typically expanded as floating aggregates called neurospheres and differentiated as dissociated single cells or whole neurospheres on coated substrates to provide adhesion.[230] Differentiation of the cells is induced by either withdrawing the mitogens or by exposing the cells to factors that induce differentiation into specific lineages. NSCs are capable of generating the three principal cell types of the central nervous system – neurons, astrocytes, and oligodendrocytes (Figure 1.4). The differentiated cellular phenotypes are most commonly analyzed by immunohistochemical and immunocytochemical techniques.[223] Cell functionality is demonstrated by staining of functional synaptic connections[231] or by employing electrophysiological techniques to obtain current- and voltage-clamp recordings.[232]

Recently, a number of researchers have begun to explore the behavior of NSCs on engineered materials. Young and his colleagues have done extensive work in this area, especially with polymeric and biomimetic substrates.[233-235] Silva and Stupp have studied the differentiation of NPCs in peptide nanofiber matrices.[236] However, very little is known regarding the behavior of NSCs on CNT-based materials. Because of NSC's potential in reducing inflammation, providing trophic support, replacing dead neurons, and reforming neural circuitry,[237] we find it important to establish their biocompatibility with LBL assembled SWNT composites in this research. To fully utilize NSC's therapeutic values, equally important is the ability to manipulate their cellular behaviors, such as differentiation, neurite outgrowth, and excitation, which are also demonstrated in this research.

1.5.1 Manipulation of Neural Stem Cells

The cellular behavior of neural stem cells (NSCs) is mediated by a wide range of biomolecules. Jacques et al. found that ECM molecules fibronectin and laminin produced a 2-fold increase in mouse neurospheres cell proliferation compared to a non-specific adhesive poly-D-lysine substratum, while the soluble peptide P3 (VSWFSRHRYSPFAVS) stimulated chain migration by over 300%[238]. Their study also demonstrated that cell proliferation and migration are regulated by distinct integrins. Consistently, Flanagan and coworkers confirmed the role for integrins in laminin-dependent migrations[239]. They found laminin to enhance human NSC migration, expansion, differentiation into neurons and astrocytes, and elongation of neurites from neurons. Axon guidance molecules have also been identified by genetic and biochemical studies. Guidance cues, such as netrins, slits, semaphorins, and epherins, guide axons by repelling or attracting the highly motile and sensitive structure of growth cone[240].

The fate of NSCs is in part regulated by environmental signals. In their study of NSCs, Takahashi et al. discovered retinoic acid (RA)'s role in promoting acquisition of a neuronal fate and neurotrophins (NTs)' role in enhancing maturation of neuronal phenotypes[241]. The combination of RA and NTs effectively stimulated NSCs to differentiate into neurons of a various phenotypes. NSCs can also adopt a glial fate if exposed to ciliary neurotrophic factor (CNTF), leukocyte inhibitory factor (LIF), and morphogentic protein 4 (BMP4)[242]. Recently, Davies et al found that transplantation of astrocytes pre-differentiated from embryonic NPCs not only promoted growth of axons

and induced realignment of injured tissue in rats but also suppressed scarring[243]. Surprisingly, transplantation of undifferentiated NPCs failed to provide any beneficial effects. Potentially layer-by-layer (LBL) assembled carbon nanotube (CNT) composites can be engineered to allow controlled pre-differentiation of NSCs and potentially create a novel strategy for repairing neural injuries.

Besides actively participating in the repair process, NSCs can also provide therapeutic effects by producing essential enzymes and neural transmitters.[227] By exposing NPCs to basic fibroblast growth factor 2 (FGF2) and glial cell conditioned media, Daadi and Weiss were able to derive neurons that produce tyrosine hydroxylase, an important rate-limiting enzyme in the synthesis of dopamine which patients of Parkinson's disease lack[244]. The enzyme tyrosine hydroxylase is found in the cytosol of all cells containing the neural transmitter catacholamine. The possibility of differentiating neural progenitor cells toward a catecholamine phenotype was demonstrated by treatment with FGF2 and neural growth factors[227]. Some work has also been done to convert NPCs into a cholinergic phenotype by treatment with LIF as a way to replenish the level of the vital neurotransmitter acetylcholine in the damaged sites[227]. Acetylcholine is hypothesized to be deficient in patients suffering from Alzheimer's disease.

1.6 Inverted Colloidal Crystal Hydrogel Scaffolds

Considerable effort has been made to develop biocompatible scaffolds for tissue engineering as they are needed to guide cells to grow, synthesize extracellular matrix, and form functional tissues.[245, 246] As biology's demand for quantitative analysis increases, scientists are also looking for a three-dimensional (3D) culture system that can authentically represent a cell's environment in a living organism.[247, 248] A properly designed 3D scaffold can satisfy the needs in tissue engineering and biomedicine to provide better solutions for tissue repair and regeneration and to facilitate the study of biological systems.

The first design criterion for a scaffold is biocompatibility. Cells must be able to attach and survive on the scaffold in order to form a functional structure. Secondly, the scaffold should have high porosity and proper pore size. This will ensure an adequate geometry for cell penetration, a high surface area for cell attachment, and interconnected space for intercellular interactions. Thirdly, the scaffold should be mechanically strong enough to support the tissue structure. Lastly and very importantly, the scaffold should positively interact with cells to enhance adhesion, proliferation, migration, differentiation, and functionality.[246 249]

Scaffolds prepared from colloidal crystal templates can meet all of the listed criteria.[250-252] To fabricate these scaffolds, colloidal particles are assembled into 3D crystals with hexagonally packed structure (Figure 1.4 a-c) and subsequently infiltrated with sol-gel or hydrogel solutions. After solidification or polymerization, the colloidal

crystal templates are dissolved to yield scaffolds with high porosity and inverted colloidal crystal (ICC) geometry (Figure 1.4 d-f). The ICC geometry can be described as highly organized spherical pores with interconnecting channels. This arrangement gives a maximum theoretic porosity of 74%, providing large void volume for cell growth while preserving structural integrity of the scaffolds. Desirable pore size and channel size can be tightly controlled by adjusting the size of colloidal particles used to fabricate the templates and by changing the assembly conditions. For this reason, the geometry of ICC scaffolds is well-ordered, easily characterized, and highly reproducible. This translates into good control over tissue structure, making ICC scaffolds an excellent system for tissue engineering and research in cell biology.

The biocompatibility of ICC Na_2SiO_3 gel[251, 252] and poly(acryalamide) hydrogel[250] ICC scaffolds have been demonstrated for liver cell,[253] bone cell,[254] thymic stromal cell,[255] and hematopoietic stem cell cultures.[256] Diffusion[257] and cell distribution[258] in ICC scaffolds have also been studied experimentally and computationally. Combined with LBL assembly, ICC scaffolds are well suited for investigations of cell-cell and cell-matrix interactions, cell migration and differentiation, and tissue formation. We have shown that LBL modification of scaffolds with collagen, fibronectin, and clay can significantly increases biocompatibility.[255, 256, 259]

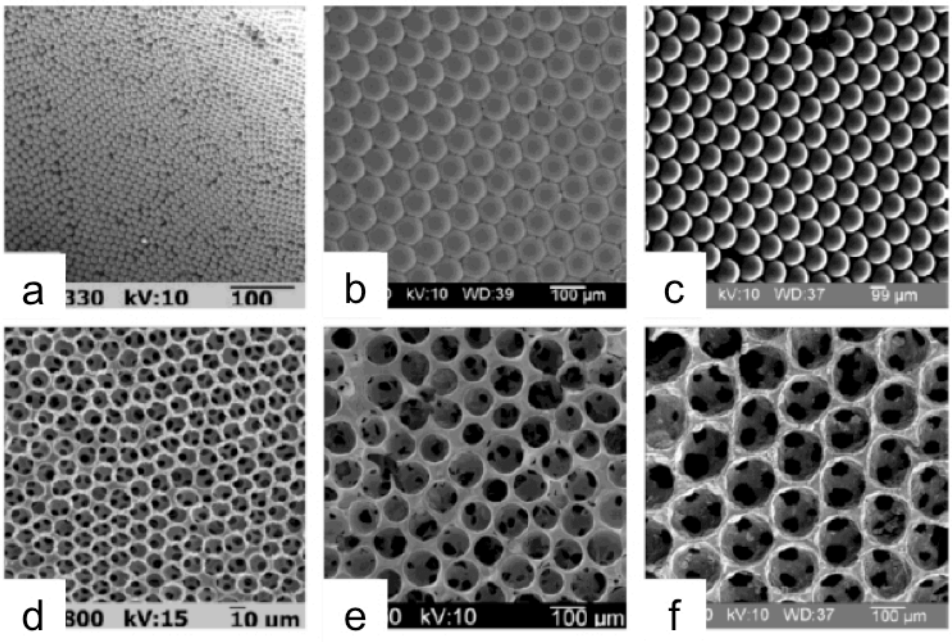

Figure 1.4 SEM images of colloidal crystals (**a-c**) and their inverted replicas (**d-f**) fabricated from 10-µm (**a, d**), 75-µm (**b, e**), and 160-µm (**c, f**) spheres.[252]

We devote part of this research to the development of an in vitro 3D neural tissue model to study neural electrode induced cellular responses. It has been reported recently that a 3D spheroid liver tissue spheroid model can be created from ICC hydrogel scaffolds for in vitro assay applications.[260] The study, which explored the toxicity of nanoparticles, showed dramatic differences between 2D and 3D spheroid cultures that resulted from morphologic and phenotypic changes. Similarly, by developing a 3D neural tissue model, we aim to improve the predictive power of in vitro assays for neural inflammatory responses.

1.7 Overview

The theoretical framework of this dissertation lies in the unique properties of CNTs and versatility of the nanostructuring technique of LBL assembly. The combination of excellent mechanical stability and high conductivity required for the ideal neural electrode design makes CNTs the perfect candidate for interfacing with the neural system. As discussed above, CNTs have an exceptional current carrying capacity, tensile strength, and Young's modulus, as well as a wealth of available chemical modification techniques to impart them specific functionalities. The technique of LBL assembly, which enables complementary molecular species, such as polyelectrolytes, nanoparticles, and biomolecules, to be constructed into a composite film one monolayer at a time, allows precise control over the film structure and composition, and therefore fine-tuning of the film properties. By combining CNTs with LBL assembly, we envision the ability to fabricate neural interfaces of specifically designed mechanical, electrochemical, and biological properties that can evolve into a platform technology for next-generation neural electrodes and help us gain better understanding of the nano-bio interface.

This dissertation is a collection of work that aims to realize this vision and can be divided into four parts. The first part consists of studies designed to establish the biocompatibility of LBL assembled CNT films. **Chapter 2** examines the cytotoxicity of CNT LBL films, dispersed CNTs, and other nanoparticles using the technology of high-content screening. **Chapter 3** demonstrates the biocompatibility of CNT LBL films with neural stem cells (NSCs). The incorporation of NSCs represents a very important venue

for establishing an effective tissue-electrode interface as they can potentially reduce inflammatory response and develop into mature functional neurons. The second part of this dissertation is contained in **Chapter 4**, which aims to establish the electrochemical properties of electrodes made from LBL assembled CNT composites. Measurements such as impedance, charge storage capacity, voltage excursion, and electrochemical stability are reported here, and a side-by-side comparison with well-established and emerging electrode materials is presented. The third part of this dissertation consists of two studies exploring methods for controlling cell differentiation on LBL assembled CNT films. **Chapter 5** demonstrates that LBL films fabricated from the assembly of CNTs with laminin can enhance the differentiation of NSCs and can be used to electrically stimulate differentiated NSCs. In **Chapter 6**, we describe the delivery of genes through CNT LBL composite films and demonstrate that multipotent cells can be programmed into neuronal cells. The last part of the dissertation, which is encompassed in **Chapter 7**, describes the development of an in vitro three-dimensional neural tissue model for the purpose of investigating cellular response induced by electrodes. Such a system can be utilized for rapid and inexpensive screening of the numerous electrode interfaces that can be designed and produced using the platform of LBL assembled CNTs.

1.8 References

1. Roco, M. C., Nanotechnology: convergence with modern biology and medicine. *Current Opinion in Biotechnology* **2003,** *14* (3), 337-346.

2. Dubertret, B.; Skourides, P.; Norris, D. J.; Noireaux, V.; Brivanlou, A. H.; Libchaber, A., In Vivo Imaging of Quantum Dots Encapsulated in Phospholipid Micelles. *Science* **2002,** *298* (5599), 1759-1762.

3. Muller, D. J.; Janovjak, H.; Lehto, T.; Kuerschner, L.; Anderson, K., Observing structure, function and assembly of single proteins by AFM. *Progress in Biophysics and Molecular Biology* **2002,** *79* (1-3), 1-43.

4. Ishijima, A.; Yanagida, T., Single molecule nanobioscience. *Trends in Biochemical Sciences* **2001,** *26* (7), 438-444.

5. Curtis, A.; Wilkinson, C., Nantotechniques and approaches in biotechnology. *Trends in Biotechnology* **2001,** *19* (3), 97-101.

6. Patri, A. K.; Majoros, I. J.; Baker, J. J. R., Dendritic polymer macromolecular carriers for drug delivery. *Current Opinion in Chemical Biology* **2002,** *6* (4), 466-471.

7. Bogunia-Kubik, K.; Sugisaka, M., From molecular biology to nanotechnology and nanomedicine. *Biosystems* **2002,** *65* (2-3), 123-138.

8. Seeman, N. C.; Belcher, A. M., Emulating biology: Building nanostructures from the bottom up. *PNAS* **2002,** *99* (90002), 6451-6455.

9. Whitesides, G. M.; Boncheva, M., Supramolecular Chemistry And Self-assembly Special Feature: Beyond molecules: Self-assembly of mesoscopic and macroscopic components. *PNAS* **2002,** *99* (8), 4769-4774.

10. Stevens, M. M.; George, J. H., Exploring and Engineering the Cell Surface Interface. *Science* **2005,** *310* (5751), 1135-1138.

11. Silva, G. A., Nanotechnology approaches for the regeneration and neuroprotection of the central nervous system. *Surgical Neurology* **2005,** *63* (4), 301-306.

12. Silva, G. A., Small neuroscience: the nanostructure of the central nervous system and emerging nanotechnology applications. *Current Nanoscience* **2005,** *1*, 225-236.

13. Silva, G. A., Neuroscience nanotechnology: progress, opportunities and challenges. *Nat Rev Neurosci* **2006,** *7* (1), 65-74.

14. Bradley, The technology: The anatomy of a spinal cord and nerve root stimulation: the lead and the power source. *Pain Medicine* **2006,** *7*, S27-S34.

15. Harnack, D.; Winter, C.; Meissner, W.; Reum, T.; Kupsch, A.; Morgenstern, R., The effects of electrode material, charge density and stimulation duration on the safety of high-frequency stimulation of the subthalamic nucleus in rats. *Journal of Neuroscience Methods* **2004,** *138* (1-2), 207-216.

16. Kerns, J. M.; Fakhouri, A. J.; Weinrib, H. P.; Freeman, J. A., Electrical-Stimulation of Nerve Regeneration in the Rat - the Early Effects Evaluated by a Vibrating Probe and Electron-Microscopy. *Neuroscience* **1991,** *40* (1), 93-107.

17. Merrill, D. R.; Bikson, M.; Jefferys, J. G. R., Electrical stimulation of excitable tissue: design of efficacious and safe protocols. *Journal of Neuroscience Methods* **2005,** *141* (2), 171-198.

18. Middlebrooks, J. C.; Bierer, J. A.; Snyder, R. L., Cochlear implants: the view from the brain. *Current Opinion in Neurobiology* **2005,** *15* (4), 488-493.

19. Benabid, A. L., Deep brain stimulation for Parkinson's disease. *Current Opinion in Neurobiology* **2003,** *13* (6), 696-706.

20. Haberler, C.; Alesch, F.; Mazal, P. R.; Pilz, P.; Jellinger, K.; Pinter, M. M.; Hainfellner, J. A.; Budka, H., No tissue damage by chronic deep brain stimulation in Parkinson's disease. *Annals of Neurology* **2000,** *48* (3), 372-376.

21. Vitek, J. L.; Hashimoto, T.; Peoples, J.; DeLong, M. R.; Bakay, R. A. E., Acute stimulation in the external segment of the globus pallidus improves parkinsonian motor signs. *Movement Disorders* **2004,** *19* (8), 907-915.

22. Chang, J.-Y., Brain stimulation for neurological and psychiatric disorders, current status and future direction. *J. Pharmacol. Exp. Ther.* **2004,** *309* (1), 1-7.

23. Hamani, C.; McAndrews, M. P.; Cohn, M.; Oh, M.; Zumsteg, D.; Shapiro, C. M.; Wennberg, R. A.; Lozano, A. M., Memory enhancement induced by hypothalamic/fornix deep brain stimulation. *Annals of Neurology* **2008,** *63* (1), 119-123.

24. Donoghue, J. P., Connecting cortex to machines: recent advances in brain interfaces. *Nat Neurosci* **2002,** (5), 1085-1088.

25. Keith, M. W., Neuroprostheses for the upper extremity. *Microsurgery* **2001,** *21* (6), 256-63.

26. Matzel, K. E.; Stadelmaier, U.; Hohenfellner, M.; Hohenberger, W., Chronic sacral spinal nerve stimulation for fecal incontinence: long-term results with foramen and cuff electrodes. *Dis Colon Rectum* **2001,** *44* (1), 59-66.

27. Rozman, J.; Zorko, B.; Bunc, M.; Zitko, M., Stimulation of nerves innervating the dog's pancreas. *Artif Organs FIELD Full Journal Title:Artificial organs* **2002,** *26* (3), 241-3.

28. Andrews Russell, J., Neuroprotection trek--the next generation: neuromodulation I. Techniques--deep brain stimulation, vagus nerve stimulation, and transcranial magnetic stimulation. *Ann N Y Acad Sci* **2003,** *993*, 1-13; discussion 48-53.

29. Goodnick, P. J.; Rush, A. J.; George, M. S.; Marangell, L. B.; Sackeim, H. A., Vagus nerve stimulation in depression. *Expert Opin Pharmacother* **2001,** *2* (7), 1061-3.

30. Holtzheimer Paul, E., 3rd; Nemeroff Charles, B., Emerging treatments for depression. *Expert Opin Pharmacother* **2006,** *7* (17), 2323-39.

31. Matsumoto, T.; Kanno, T., Potentiation of cholecystokinin-induced exocrine secretion by either electrical stimulation of the vagus nerve or exogenous VIP administration in the guinea pig pancreas. *Peptides* **1984,** *5* (2), 285-9.

32. Osadchii, O. E.; Pokrovskii, V. M.; Kompaniets, O. G.; Kurzanov, A. N., Effect of neurotensin and epinephrine on sinus arrhythmia caused by burst stimulation of the vagus nerve. *Bull. Exp. Biol. Med.* **1997,** *123* (5), 427-430.

33. Yamazaki, M.; Sakaguchi, T., Pancreatic vagal functional distribution in the secretion of insulin evoked by portal infusion of D-glucose. *Brain Res.* **1989,** *484* (1-2), 357-60.

34. Yoshizaki, A.; Takagi, Y.; Kanno, T., Vagal component of enhanced secretory responses of exocrine pancreas to combined stimulation with CCK-8 and secretin in anesthetized rats. *Biomed. Res.* **1992,** *13* (4), 303-8.

35. Ziyatdinova, N. I.; Gainullin, A. A.; Ziganshin, A. U.; Zefirov, T. L., Stimulation of Vagus Nerve Modifies Negative Chronotropic and Hypotensive Effects of Adenosine. *Bull. Exp. Biol. Med.* **2004,** *137* (5), 425-427.

36. Stieglitz, T.; Meyer, J.-U., Neural implants in clinical practice: interfacing neurons for neuro-modulation, limb control, and to restore vision-part I. *Microsystems* **2007,** *16* (BioMEMS), 41-70.

37. Gimsa, J.; Habel, B.; Schreiber, U.; Rienen, U. v.; Strauss, U.; Gimsa, U., Choosing electrodes for deep brain stimulation experiments-electrochemical considerations. *Journal of Neuroscience Methods* **2005,** *142* (2), 251-265.

38. McCreery, D. B.; Agnew, W. F.; Yuen, T. G. H.; Bullara, L., Charge density and charge per phase as cofactors in neural injury induced by electrical stimulation. *IEEE Transactions on Biomedical Engineering* **1990,** *37*, 996-1001.

39. Foreman, R. D.; Linderoth, B.; Ardell, J. L.; Barron, K. W.; Chandler, M. J.; Hull, S. S.; TerHorst, G. J.; DeJongste, M. J. L.; Armour, J. A., Modulation of intrinsic cardiac neurons by spinal cord stimulation: implications for its therapeutic use in angina pectoris. *Cardiovasc. Res.* **2000,** *47* (2), 367-375.

40. Bianco, A.; Kostarelos, K.; Partidos, C. D.; Prato, M., Biomedical applications of functionalised carbon nanotubes. *Chem. Comm.* **2005,** *5*, 571-577.

41. Gheith, M. K.; Pappas, T. C.; Liopo, A. V.; Sinani, V. A.; Shim, B. S.; Motamedi, M.; Wicksted, J. P.; Kotov, N. A., Stimulation of Neural Cells by Lateral Currents in Conductive LBL Films of Single-Walled Carbon Nanotubes. *Adv. Mat.* **2006,** *18*, 2975-2979.

42. Patolsky, F.; Timko, B. P.; Yu, G.; Fang, Y.; Greytak, A. B.; Zheng, G.; Lieber, C. M., Detection, Stimulation, and Inhibition of Neuronal Signals with High-Density Nanowire Transistor Arrays. *Science* **2006,** *313* (5790), 1100-1104.

43. Silva, G. A., Neuroscience nanotechnology: progress, opportunities and challenges. *Nat Rev Neurosci* **2006,** *7* (1), 65.

44. Wang, K.; Fishman, H. A.; Dai, H.; Harris, J. S., Neural Stimulation with a Carbon Nanotube Microelectrode Array. *Nano Lett.* **2006,** *6* (9), 2043-2048.

45. Webster, A. T. J.; Waid, A. M. C.; McKenzie, A. J. L.; Price, A. R. L.; Ejiofor, A. J. U., Nano-biotechnology: carbon nanofibres as improved neural and orthopaedic implants. *Nanotechnology* **2004,** *15*, 48-54.

46. Gheith, M. K.; Sinani, V. A.; Wicksted, J. P.; Matts, R. L.; Kotov, N. A., Single-walled carbon nanotube polyelectrolyte multilayers and freestanding films as a biocompatible platform for neuroprosthetic implants. *Adv. Mat.* **2005,** *17*, 2663-2670.

47. Treacy, M. M. J., Ebbesen, T. W. and Gibson, J. M., Exceptionally high young's modulus observed for individual carbon nanotubes. *Nature* **1996,** *381*, 678-680.

48. Yao, Z., Kane, C. L. and Dekker, C., High-field electrical transport in single-wall carbon nanotubes. *Physical Review Letters* **2000,** *84*, 2941.

49. O'Connell, M. J.; Bachilo, S. M.; Huffman, C. B.; Moore, V. C.; Strano, M. S.; Haroz, E. H.; Rialon, K. L.; Boul, P. J.; Noon, W. H.; Kittrell, C.; Ma, J. P.; Hauge, R. H.; Weisman, R. B.; Smalley, R. E., Band gap fluorescence from individual single-walled carbon nanotubes. *Science* **2002,** *297*, 593-6.

50. Dai, H., Carbon nanotubes: synthesis, integration, and properties. *Acc. Chem. Res.* **2002,** *35*, 1035-1044.

51. Kim, Y. J.; Kim, Y. A.; Chino, T.; Suezaki, H.; Endo, M.; Dresselhaus, M. S., Chemically modified multiwalled carbon nanotubes as an additive for supercapacitors. *Small* **2006,** *2* (3), 339-345.

52. Saito, R., Dresselhaus, G. and Dresselhaus, M. S., *Physical properties of carbon nanotubes*. Imperial College Press: 1998.

53. Iijima, Helical microtubules of graphitic carbon. *Nature* **1991,** *354*, 56-58.

54. Grill, W. M.; Norman, S. E.; Bellamkonda, R. V., Implanted Neural Interfaces: Biochallenges and Engineered Solutions. *Annu. Rev. Biomed. Eng.* **2009,** *11*, 1-24.

55. Cogan, S. F., Neural stimulation and recording electrodes. *Annu. Rev. Biomed. Eng.* **2008,** *10*, 275-309.

56. Rose, T. L.; Kelliher, E. M.; Robblee, L. S., Assessment of capacitor electrodes for intracortical neural stimulation. *Journal of Neuroscience Methods* **1985,** *12* (3), 181-193.

57. Cogan, S. F.; Troyk, P. R.; Ehrlich, J.; Plante, T. D., In vitro comparison of the charge-injection limits of activated iridium oxide (AIROF) and platinum-iridium microelectrodes. *Biomedical Engineering, IEEE Transactions on* **2005,** *52* (9), 1612-1614.

58. Rose, T. L.; Robblee, L. S., Electrical stimulation with Pt electrodes. VIII. Electrochemically safe charge injection limits with 0.2 ms pulses (neuronal application). *Biomedical Engineering, IEEE Transactions on* **1990,** *37* (11), 1118-1120.

59. Schmidt, E. M.; Bak, M. J.; Hambrecht, F. T.; Kufta, C. V.; O'Rourke, D. K.; Vallabhanath, P., Feasibility of a visual prosthesis for the blind based on intracortical micro stimulation of the visual cortex. *Brain* **1996,** *119* (2), 507-522.

60. McCreery, D. B.; Bullara, L. A.; Agnew, W. F., Neuronal activity evoked by chronically implanted intracortical microelectrodes. *Exp. Neurol.* **1986,** *92* (1), 147-161.

61. Cogan, S. F.; Guzelian, A. A.; Agnew, W. F.; Yuen, T. G. H.; McCreery, D. B., Over-pulsing degrades activated iridium oxide films used for intracortical neural stimulation. *Journal of Neuroscience Methods* **2004,** *137* (2), 141-150.

62. Specht, H.; Krueger, F.; Wachter, H. J.; Keitel, O.; Leitold, C.; Frericks, M., Electrochemical properties and stability of PVD coatings for the application in cardiac

and neurological stimulation. *Med. Device Mater. III, Proc. Mater. Processes Med. Devices Conf., 3rd* **2006**, 169-173.

63. Twardoch, U. M., Integrity of ultramicro-stimulation electrodes determined from electrochemical measurements. *J. Appl. Electrochem.* **1994,** *24* (9), 835-57.

64. Yang, J.; Kim, D. H.; Hendricks, J. L.; Leach, M.; Northey, R.; Martin, D. C., Ordered surfactant-templated poly(3,4-ethylenedioxythiophene) (PEDOT) conducting polymer on microfabricated neural probes. *Acta Biomaterialia* **2005,** *1* (1), 125-136.

65. Ludwig, K. A.; Uram, J. D.; Yang, J. Y.; Martin, D. C.; Kipke, D. R., Chronic neural recordings using silicon microelectrode arrays electrochemically deposited with a poly(3,4-ethylenedioxythiophene) (PEDOT) film. *Journal of Neural Engineering* **2006,** *3* (1), 59-70.

66. Abidian, M. R.; Ludwig, K. A.; Marzullo, T. C.; Martin, D. C.; Kipke, D. R., Interfacing Conducting Polymer Nanotubes with the Central Nervous System: Chronic Neural Recording using Poly(3,4-ethylenedioxythiophene) Nanotubes. *Advanced Materials* **2009,** *21* (37), 3764-3770.

67. Abidian, M. R.; Corey, J. M.; Kipke, D. R.; Martin, D. C., Conducting-Polymer Nanotubes Improve Electrical Properties, Mechanical Adhesion, Neural Attachment, and Neurite Outgrowth of Neural Electrodes. *Small 6* (3), 421-429.

68. Kim, D.-H.; Richardson-Burns, S. M.; Hendricks, J. L.; Sequera, C.; Martin, D. C., Effect of Immobilized Nerve Growth Factor on Conductive Polymers: Electrical Properties and Cellular Response. *Advanced Functional Materials* **2007,** *17* (1), 79-86.

69. Abidian, M. R.; Kim, D.-H.; Martin, D. C., Conducting-Polymer Nanotubes for Controlled Drug Release. *Advanced Materials* **2006,** *18* (4), 405-409.

70. Cul, X. T.; Zhou, D. D., Poly (3,4-ethylenedioxythiophene) for chronic neural stimulation. *IEEE Transactions on Neural Systems and Rehabilitation Engineering* **2007,** *15* (4), 502-508.

71. Leach, J. B.; Achyuta, A. K. H.; Murthy, S. K., Bridging the divide between neuroprosthetic design, tissue engineering and neurobiology. *Frontiers in Neuroengineering* **2009,** *2*.

72. Keohan, F.; Wei, X. F.; Wongsarnpigoon, A.; Lazaro, E.; Darga, J. E.; Grill, W. M., Fabrication and evaluation of conductive elastomer electrodes for neural stimulation. *J. Biomater. Sci., Polym. Ed.* **2007,** *18* (8), 1057-1073.

73. Subbaroyan, J.; Martin David, C.; Kipke Daryl, R., A finite-element model of the mechanical effects of implantable microelectrodes in the cerebral cortex. *J Neural Eng.* **2005,** *2* (4), 103-13.

74. Takeuchi, A.; Miyaishi, O.; Kiuchi, K.; Isobe, K.-i., Macrophage colony-stimulating factor is expressed in neuron and microglia after focal brain injury. *Journal of Neuroscience Research* **2001,** *65* (1), 38-44.

75. John, G. R.; Lee, S. C.; Song, X.; Rivieccio, M.; Brosnan, C. F., IL-1-regulated responses in astrocytes: Relevance to injury and recovery. *Glia* **2005,** *49* (2), 161-176.

76. Szarowski, D. H.; Andersen, M. D.; Retterer, S.; Spence, A. J.; Isaacson, M.; Craighead, H. G.; Turner, J. N.; Shain, W., Brain responses to micro-machined silicon devices. *Brain Research* **2003,** *983* (1-2), 23-35.

77. Biran, R.; Martin, D. C.; Tresco, P. A., The brain tissue response to implanted silicon microelectrode arrays is increased when the device is tethered to the skull. *J. Biomed. Mater. Res., Part A* **2007,** *82A* (1), 169-178.

78. Kim, Y.-T.; Hitchcock, R. W.; Bridge, M. J.; Tresco, P. A., Chronic response of adult rat brain tissue to implants anchored to the skull. *Biomaterials* **2004,** *25* (12), 2229-2237.

79. Seymour, J. P.; Kipke, D. R., Neural probe design for reduced tissue encapsulation in CNS. *Biomaterials* **2007,** *28* (25), 3594-3607.

80. Abidian, M. R.; Martin, D. C., Experimental and theoretical characterization of implantable neural microelectrodes modified with conducting polymer nanotubes. *Biomaterials* **2008,** *29* (9), 1273-1283.

81. Foos, J. S.; Erker, S. M., Conductive polymer electrodes for neural prosthetic applications. *Mater. Res. Soc. Symp. Proc.* **1986,** *55* (Biomed. Mater.), 281-6.

82. Li, M.-y.; Bidez, P.; Guterman-Tretter, E.; Guo, Y.; MacDiarmid, A. G.; Lelkes, P. I.; Yuan, X.-b.; Yuan, X.-y.; Sheng, J.; Li, H.; Song, C.-x.; Wei, Y., Electroactive and nanostructured polymers as scaffold materials for neuronal and cardiac tissue engineering. *Chin. J. Polym. Sci.* **2007,** *25* (4), 331-339.

83. Nyberg, T.; Shimada, A.; Torimitsu, K., Ion conducting polymer microelectrodes for interfacing with neural networks. *J. Neurosci. Methods* **2007,** *160* (1), 16-25.

84. Stauffer, W. R.; Cui, X. T., Polypyrrole doped with 2 peptide sequences from laminin. *Biomaterials* **2006,** *27* (11), 2405-2413.

85. Gomez, N.; Schmidt, C. E., Nerve growth factor-immobilized polypyrrole: bioactive electrically conducting polymer for enhanced neurite extension. *J. Biomed. Mater. Res., Part A* **2007,** *81A* (1), 135-149.

86. Zhang, Z.; Rouabhia, M.; Wang, Z.; Roberge, C.; Shi, G.; Roche, P.; Li, J.; Dao, L. H., Electrically conductive biodegradable polymer composite for nerve regeneration: electricity-stimulated neurite outgrowth and axon regeneration. *Artif. Organs* **2007,** *31* (1), 13-22.

87. Schmidt, C. E.; Shastri, V. R.; Vacanti, J. P.; Langer, R., Stimulation of neurite outgrowth using an electrically conducting polymer. *Proc. Natl. Acad. Sci. U. S. A.* **1997,** *94* (17), 8948-8953.

88. Seymour, J. P.; Kipke, D. R., Neural probe design for reduced tissue encapsulation in CNS. *Biomaterials* **2007,** *28* (25), 3594-3607.

89. Bernatchez, S. F.; Parks, P. J.; Gibbons, D. F., Interaction of macrophages with fibrous materials in vitro. *Biomaterials* **1996,** *17* (21), 2077-2086.

90. Sanders, J. E.; Stiles, C. E.; Hayes, C. L., Tissue response to single-polymer fibers of varying diameters: Evaluation of fibrous encapsulation and macrophage density. *Journal of Biomedical Materials Research* **2000,** *52* (1), 231-237.

91. Turner, A. M.; Dowell, N.; Turner, S. W.; Kam, L.; Isaacson, M.; Turner, J. N.; ., e. a., Attachment of astroglial cells to microfabricated pillar arrays of different geometries. *J. Biomed. Mater. Res.* **2000,** *51* (3), 430-41.

92. Chen, C. S.; Tan, J.; Tien, J., Mechanotransduction at cell-matrix and cell-cell contacts. . *J. Annu Rev Biomed Eng* **2004,** *6*, 275-302.

93. Chen, C. S.; Mrksich, M.; Huang, S.; Whitesides, G. M.; Ingber, D. E., Geometric control of cell life and death. *Science* **1997,** *276* (5317), 1425-8.

94. Meilander, N. J.; Yu, X.; Ziats, N. P.; Bellamkonda, R. V., Lipid-based microtubular drug delivery vehicles. *Journal of Controlled Release* **2001,** *71* (1), 141-152.

95. Zhong, Y. H.; Yu, X. J.; Gilbert, R.; Bellamkonda, R. V., Stabilizing electrode-host interfaces: A tissue engineering approach. *Journal of Rehabilitation Research and Development* **2001,** *38* (6), 627-632.

96. Manna, S. K.; Aggarwal, B. B., alpha-melanocyte-stimulating hormone inhibits the nuclear transcription factor NF-kappa B activation induced by various inflammatory agents. *Journal of Immunology* **1998,** *161* (6), 2873-2880.

97. Shain, W.; Spataro, L.; Dilgen, J.; Haverstick, K.; Retterer, S.; Isaacson, M.; Saltzman, M.; Turner, J. N., Controlling cellular reactive responses around neural prosthetic devices using peripheral and local intervention strategies. *Neural Systems and Rehabilitation Engineering, IEEE Transactions on [see also IEEE Trans. on Rehabilitation Engineering]* **2003,** *11* (2), 186-188.

98. Zhong, Y.; Bellamkonda, R. V., Controlled release of anti-inflammatory agent [alpha]-MSH from neural implants. *Journal of Controlled Release* **2005,** *106* (3), 309-318.

99. Chvatal, S. A.; Kim, Y.-T.; Bratt-Leal, A. M.; Lee, H.; Bellamkonda, R. V., Spatial distribution and acute anti-inflammatory effects of Methylprednisolone after sustained local delivery to the contused spinal cord. *Biomaterials* **2008,** *29* (12), 1967-1975.

100. He, W.; McConnell, G. C.; Schneider, T. M.; Bellamkonda, R. V., A novel anti-inflammatory surface for neural electrodes. *Adv. Mater.* **2007,** *19* (21), 3529-3533.

101. Zhong, Y.; Bellamkonda, R. V., Controlled release of anti-inflammatory agent alpha -MSH from neural implants. *J. Controlled Release.* **2005,** *106* (3), 309-318.

102. Zhong, Y.; Bellamkonda, R. V., Dexamethasone-coated neural probes elicit attenuated inflammatory response and neuronal loss compared to uncoated neural probes. *Brain Res.* **2007,** *1148*, 15-27.

103. Cui, X. Y.; Lee, V. A.; Raphael, Y.; Wiler, J. A.; Hetke, J. F.; Anderson, D. J.; Martin, D. C., Surface modification of neural recording electrodes with conducting polymer/biomolecule blends. *Journal of Biomedical Materials Research* **2001,** *56* (2), 261-272.

104. Wei, H.; George, C. M.; Ravi, V. B., Nanoscale laminin coating modulates cortical scarring response around implanted silicon microelectrode arrays. *Journal of Neural Engineering* **2006,** (4), 316.

105. Winter, J. O.; Cogan, S. F.; Rizzo, J. F., III, Neurotrophin-eluting hydrogel coatings for neural stimulating electrodes. *J. Biomed. Mater. Res., Part B* **2007,** *81B* (2), 551-563.

106. Burdick, J. A.; Ward, M.; Liang, E.; Young, M. J.; Langer, R., Stimulation of neurite outgrowth by neurotrophins delivered from degradable hydrogels. *Biomaterials* **2006,** *27* (3), 452-459.

107. Yu, X.; Dillon, G. P.; Bellamkonda, R. V., A laminin and nerve growth factor-laden three-dimensional scaffold for enhanced neurite extension. *Tissue Eng.* **1999,** *5* (4), 291-304.

108. Iijima, S., Helical microtubules of graphitic carbon. *Nature* **1991,** *354* (6348), 56-58.

109. Iijima, S.; Ichihashi, T., Single-shell carbon nanotubes of 1-nm diameter. *Nature* **1993,** *363* (6430), 603-605.

110. Bethune, D. S.; Klang, C. H.; de Vries, M. S.; Gorman, G.; Savoy, R.; Vazquez, J.; Beyers, R., Cobalt-catalysed growth of carbon nanotubes with single-atomic-layer walls. *Nature* **1993,** *363* (6430), 605-607.

111. Dresselhaus, M. S.; Dresselhaus, G.; Jorio, A., UNUSUAL PROPERTIES AND STRUCTURE OF CARBON NANOTUBES. *Annual Review of Materials Research* **2004,** *34* (1), 247-278.

112. Avouris, P., Molecular Electronics with Carbon Nanotubes. *Acc. Chem. Res.* **2002,** *35* (12), 1026-1034.

113. Appenzeller, J.; Martel, R.; Avouris, P.; Stahl, H.; Lengeler, B., Optimized contact configuration for the study of transport phenomena in ropes of single-wall carbon nanotubes. *Applied Physics Letters* **2001,** *78* (21), 3313-3315.

114. Frank, S.; Poncharal, P.; Wang, Z. L.; Heer, W. A.; nbsp; de, Carbon Nanotube Quantum Resistors. *Science* **1998,** *280* (5370), 1744-1746.

115. Rueckes, T.; Kim, K.; Joselevich, E.; Tseng, G. Y.; Cheung, C.-L.; Lieber, C. M., Carbon Nanotube-Based Nonvolatile Random Access Memory for Molecular Computing. *Science* **2000,** *289* (5476), 94-97.

116. Baughman, R. H.; Cui, C.; Zakhidov, A. A.; Iqbal, Z.; Barisci, J. N.; Spinks, G. M.; Wallace, G. G.; Mazzoldi, A.; De Rossi, D.; Rinzler, A. G.; Jaschinski, O.; Roth, S.; Kertesz, M., Carbon Nanotube Actuators. *Science* **1999,** *284* (5418), 1340-1344.

117. Martel, R.; Schmidt, T.; Shea, H. R.; Hertel, T.; Avouris , P., Single- and multi-wall carbon nanotube field-effect transistors. *Applied Physics Letters* **1998,** *73* (17), 2447-2449.

118. Chopra, S.; McGuire, K.; Gothard, N.; Rao, A. M.; Pham, A., Selective gas detection using a carbon nanotube sensor. *Applied Physics Letters* **2003,** *83* (11), 2280-2282.

119. Kong, J.; Franklin, N. R.; Zhou, C.; Chapline, M. G.; Peng, S.; Cho, K.; Dai, H., Nanotube Molecular Wires as Chemical Sensors. *Science* **2000,** *287* (5453), 622-625.

120. Bradley, K.; Gabriel, J. C. P.; Star, A.; Gruner, G., Short-channel effects in contact-passivated nanotube chemical sensors. *Applied Physics Letters* **2003,** *83* (18), 3821-3823.

121. de Heer, W. A.; Chatelain, A.; Ugarte, D., A Carbon Nanotube Field-Emission Electron Source. *Science* **1995,** *270* (5239), 1179-1180.

122. Rinzler, A. G.; Hafner, J. H.; Nikolaev, P.; Nordlander, P.; Colbert, D. T.; Smalley, R. E.; Lou, L.; Kim, S. G.; Tomanek, D., Unraveling Nanotubes: Field Emission from an Atomic Wire. *Science* **1995,** *269* (5230), 1550-1553.

123. Saito, Y.; Uemura, S., Field emission from carbon nanotubes and its application to electron sources. *Carbon* **2000,** *38* (2), 169-182.

124. Hafner, J. H.; Cheung, C. L.; Lieber, C. M., Direct Growth of Single-Walled Carbon Nanotube Scanning Probe Microscopy Tips. *J. Am. Chem. Soc.* **1999,** *121* (41), 9750-9751.

125. Dai, H., Carbon Nanotubes: Synthesis, Integration, and Properties. *Acc. Chem. Res.* **2002,** *35* (12), 1035-1044.

126. Niyogi, S.; Hamon, M. A.; Hu, H.; Zhao, B.; Bhowmik, P.; Sen, R.; Itkis, M. E.; Haddon, R. C., Chemistry of Single-Walled Carbon Nanotubes. *Acc. Chem. Res.* **2002,** *35* (12), 1105-1113.

127. Wong, E. W.; Sheehan, P. E.; Lieber, C. M., Nanobeam Mechanics: Elasticity, Strength, and Toughness of Nanorods and Nanotubes. *Science* **1997,** *277* (5334), 1971-1975.

128. Treacy, M. M. J.; Ebbesen, T. W.; Gibson, J. M., Exceptionally high Young's modulus observed for individual carbon nanotubes. *Nature* **1996,** *381* (6584), 678-680.

129. Yu, M. F.; Files, B. S.; Arepalli, S.; Ruoff, R. S., Tensile loading of ropes of single wall carbon nanotubes and their mechanical properties. *Physical Review Letters* **2000,** *84* (24), 5552-5555.

130. Gao, G. H.; Cagin, T.; Goddard, W. A., Energetics, structure, mechanical and vibrational properties of single-walled carbon nanotubes. *Nanotechnology* **1998,** *9* (3), 184-191.

131. Yao, N.; Lordi, V., Young's modulus of single-walled carbon nanotubes. *Journal of Applied Physics* **1998,** *84* (4), 1939-1943.

132. Ruoff, R. S.; Lorents, D. C., Mechanical and Thermal-Properties of Carbon Nanotubes. *Carbon* **1995,** *33* (7), 925-930.

133. Robertson, D. H.; Brenner, D. W.; Mintmire, J. W., Energetics of Nanoscale Graphitic Tubules. *Physical Review B* **1992,** *45* (21), 12592-12595.

134. Li, F.; Cheng, H. M.; Bai, S.; Su, G.; Dresselhaus, M. S., Tensile strength of single-walled carbon nanotubes directly measured from their macroscopic ropes. *Applied Physics Letters* **2000,** *77* (20), 3161-3163.

135. Falvo, M. R.; Clary, G. J.; Taylor, R. M.; Chi, V.; Brooks, F. P.; Washburn, S.; Superfine, R., Bending and buckling of carbon nanotubes under large strain. *Nature* **1997,** *389* (6651), 582-584.

136. Yakobson, B. I., Mechanical relaxation and "intramolecular plasticity" in carbon nanotubes. *Applied Physics Letters* **1998,** *72* (8), 918-920.

137. Thostenson, E. T.; Ren, Z.; Chou, T.-W., Advances in the science and technology of carbon nanotubes and their composites: a review. *Composites Science and Technology* **2001,** *61*, 1899-1912.

138. Coleman, J.; Khan, U.; Gun'ko, Y., Mechanical Reinforcement of Polymers Using Carbon Nanotubes. *Advanced Materials* **2006,** *18* (6), 689-706.

139. Lau, A. K.-T.; Hui, D., The revolutionary creation of new advanced materials--carbon nanotube composites. *Composites Part B: Engineering* **2002,** *33* (4), 263-277.

140. Breuer, O.; Sundararaj, U., Big returns from small fibers: A review of polymer/carbon nanotube composites. *Polym. Compos.* **2004,** *25* (6), 630-645.

141. Mamedov, A. A. K., Nicholas A.; Prato, Maurizio; Guldi, Dirk M.; Wicksted, James P.; Hirsch, Andreas., Molecular design of strong single-wall carbon nanotube/polyelectrolyte multilayer composites. *Nature Materials* **2002,** *1*, 190-194.

142. Haddon, R. C., Carbon Nanotubes. *Acc. Chem. Res.* **2002,** *35* (12), 997-997.

143. Dujardin, E.; Ebbesen, T. W.; Krishnan, A.; Treacy, M. M. J., Wetting of Single Shell Carbon Nanotubes. *Advanced Materials* **1998,** *10* (17), 1472-1475.

144. Bahr, J. L.; Tour, J. M., Covalent chemistry of single-wall carbon nanotubes. *Journal of Materials Chemistry* **2002,** *12*, 1952-1958.

145. Dyke, C. A.; Tour, J. M., Covalent Functionalization of Single-Walled Carbon Nanotubes for Materials Applications. *J. Phys. Chem. A* **2004,** *108* (51), 11151-11159.

146. Banerjee, S.; Kahn, M. G. C.; Wong, S. S., Rational Chemical Strategies for Carbon Nanotube Functionalization. *Chemistry - A European Journal* **2003,** *9* (9), 1898-1908.

147. Liu, J.; Rinzler, A. G.; Dai, H.; Hafner, J. H.; Bradley, R. K.; Boul, P. J.; Lu, A.; Iverson, T.; Shelimov, K.; Huffman, C. B.; Rodriguez-Macias, F.; Shon, Y.-S.; Lee, T. R.; Colbert, D. T.; Smalley, R. E., Fullerene Pipes. *Science* **1998,** *280* (5367), 1253-1256.

148. Mawhinney, D. B.; Naumenko, V.; Kuznetsova, A.; Yates Jr, J. T.; Liu, J.; Smalley, R. E., Surface defect site density on single walled carbon nanotubes by titration. *Chemical Physics Letters* **2000,** *324* (1-3), 213-216.

149. Hu, H.; Bhowmik, P.; Zhao, B.; Hamon, M. A.; Itkis, M. E.; Haddon, R. C., Determination of the acidic sites of purified single-walled carbon nanotubes by acid-base titration. *Chemical Physics Letters* **2001,** *345* (1-2), 25-28.

150. Ebbesen, T. W., Cones and Tubes: Geometry in the Chemistry of Carbon. *Acc. Chem. Res.* **1998,** *31* (9), 558-566.

151. Star, A.; Stoddart, J. F.; Steuerman, D.; Diehl, M.; Boukai, A.; Wong, E. W.; Yang, X.; Chung, S.-W.; Choi, H.; Heath, J. R., Preparation and Properties of Polymer-Wrapped Single-Walled Carbon Nanotubes. *Angewandte Chemie* **2001,** *113* (9), 1771-1775.

152. O'Connell, M. J.; Boul, P.; Ericson, L. M.; Huffman, C.; Wang, Y.; Haroz, E.; Kuper, C.; Tour, J.; Ausman, K. D.; Smalley, R. E., Reversible water-solubilization of single-walled carbon nanotubes by polymer wrapping. *Chemical Physics Letters* **2001,** *342* (3-4), 265-271.

153. Shim, M.; Javey, A.; Shi Kam, N. W.; Dai, H., Polymer Functionalization for Air-Stable n-Type Carbon Nanotube Field-Effect Transistors. *J. Am. Chem. Soc.* **2001,** *123* (46), 11512-11513.

154. Tang, B. Z.; Xu, H., Preparation, Alignment, and Optical Properties of Soluble Poly(phenylacetylene)-Wrapped Carbon Nanotubes. *Macromolecules* **1999,** *32* (8), 2569-2576.

155. Chen, R. J.; Zhang, Y.; Wang, D.; Dai, H., Noncovalent Sidewall Functionalization of Single-Walled Carbon Nanotubes for Protein Immobilization. *J. Am. Chem. Soc.* **2001,** *123* (16), 3838-3839.

156. Kong, J.; Dai, H., Full and Modulated Chemical Gating of Individual Carbon Nanotubes by Organic Amine Compounds. *J. Phys. Chem. B* **2001,** *105* (15), 2890-2893.

157. Gheith, M. S., V.; Wicksted, J.; Matts, R.; Kotov, N., Single-Walled Carbon Nanotube Polyelectrolyte Multilayers and Freestanding Films as a Biocompatible Platform for Neuroprosthetic Implants. *Advanced Materials* **2005,** *17* (22), 2663-2670.

158. Dieckmann, G. R.; Dalton, A. B.; Johnson, P. A.; Razal, J.; Chen, J.; Giordano, G. M.; Munoz, E.; Musselman, I. H.; Baughman, R. H.; Draper, R. K., Controlled Assembly of Carbon Nanotubes by Designed Amphiphilic Peptide Helices. *J. Am. Chem. Soc.* **2003,** *125* (7), 1770-1777.

159. Zorbas, V.; Ortiz-Acevedo, A.; Dalton, A. B.; Yoshida, M. M.; Dieckmann, G. R.; Draper, R. K.; Baughman, R. H.; Jose-Yacaman, M.; Musselman, I. H., Preparation and Characterization of Individual Peptide-Wrapped Single-Walled Carbon Nanotubes. *J. Am. Chem. Soc.* **2004,** *126* (23), 7222-7227.

160. Shim, M.; Shi Kam, N. W.; Chen, R. J.; Li, Y.; Dai, H., Functionalization of Carbon Nanotubes for Biocompatibility and Biomolecular Recognition. *Nano Lett.* **2002,** *2* (4), 285-288.

161. Zheng, H. P.; Berg, M. C.; Rubner, M. F.; Hammond, P. T., Controlling cell attachment selectively onto biological polymer-colloid templates using polymer-on-polymer stamping. *Langmuir* **2004,** *20* (17), 7215-7222.

162. Cai, H.; Cao, X.; Jiang, Y.; He, P.; Fang, Y., Carbon nanotube-enhanced electrochemical DNA biosensor for DNA hybridization detection. *Analytical and Bioanalytical Chemistry* **2003,** *375* (2), 287-293.

163. Davis, J. J.; Coleman, K. S.; Azamian, B. R.; Bagshaw, C. B.; Green, M. L. H., Chemical and Biochemical Sensing with Modified Single Walled Carbon Nanotubes. *Chemistry - A European Journal* **2003,** *9* (16), 3732-3739.

164. Besteman, K.; Lee, J. O.; Wiertz, F. G. M.; Heering, H. A.; Dekker, C., Enzyme-Coated Carbon Nanotubes as Single-Molecule Biosensors. *Nano Lett.* **2003,** *3* (6), 727-730.

165. Bianco, A.; Prato, M., Can Carbon Nanotubes be Considered Useful Tools for Biological Applications? *Advanced Materials* **2003,** *15* (20), 1765-1768.

166. Star, A.; Gabriel, J. C. P.; Bradley, K.; Gruner, G., Electronic Detection of Specific Protein Binding Using Nanotube FET Devices. *Nano Lett.* **2003,** *3* (4), 459-463.

167. Chen, R. J.; Choi, H. C.; Bangsaruntip, S.; Yenilmez, E.; Tang, X.; Wang, Q.; Chang, Y. L.; Dai, H., An Investigation of the Mechanisms of Electronic Sensing of Protein Adsorption on Carbon Nanotube Devices. *J. Am. Chem. Soc.* **2004,** *126* (5), 1563-1568.

168. Bradley, K.; Briman, M.; Star, A.; Gruner, G., Charge Transfer from Adsorbed Proteins. *Nano Lett.* **2004,** *4* (2), 253-256.

169. MacDonald, R. A.; Laurenzi, B. F.; Viswanathan, G.; Ajayan, P. M.; Stegemann, J. P., Collagen-carbon nanotube composite materials as scaffolds in tissue engineering. *Journal of Biomedical Materials Research Part A* **2005,** *74A* (3), 489-496.

170. Zanello, L. P.; Zhao, B.; Hu, H.; Haddon, R. C., Bone Cell Proliferation on Carbon Nanotubes. *Nano Lett.* **2006,** *6* (3), 562-567.

171. Shi Kam, N. W.; O'Connell, M.; Wisdom, J. A.; Dai, H., Carbon nanotubes as multifunctional biological transporters and near-infrared agents for selective cancer cell destruction. *PNAS* **2005,** *102* (33), 11600-11605.

172. ShiKam, N. W.; Jessop, T. C.; Wender, P. A.; Dai, H., Nanotube Molecular Transporters: Internalization of Carbon Nanotube-Protein Conjugates into Mammalian Cells. *J. Am. Chem. Soc.* **2004,** *126* (22), 6850-6851.

173. Kam, N. W. S.; Liu, Z.; Dai, H., Carbon Nanotubes as Intracellular Transporters for Proteins and DNA: An Investigation of the Uptake Mechanism and Pathway. *Angewandte Chemie International Edition* **2006,** *45* (4), 577-581.

174. Correa-Duarte, M. A.; Wagner, N.; Rojas-Chapana, J.; Morsczeck, C.; Thie, M.; Giersig, M., Fabrication and biocompatibility of carbon nanotube-based 3D networks as scaffolds for cell seeding and growth. *Nano Letters* **2004,** *4* (11), 2233-2236.

175. George, J. H.; Shaffer, M. S.; Stevens, M. M., Investigating the cellular response to nanofibrous materials by use of a multi-walled carbon nanotube model. *Journal of Experimental Nanoscience* **2006,** *1* (1), 1-12.

176. Elias, K. L.; Price, R. L.; Webster, T. J., Enhanced functions of osteoblasts on nanometer diameter carbon fibers. *Biomaterials* **2002,** *23* (15), 3279-3287.

177. Mattson, M. P. H., Robert C.; Rao, Apparao M., Molecular Functionalization of Carbon Nanotubes and Use as Substrates for Neuronal Growth. *Journal of Molecular Neuroscience* **2000,** *14*, 175.

178. Hu, H.; Ni, Y.; Montana, V.; Haddon, R. C.; Parpura, V., Chemically Functionalized Carbon Nanotubes as Substrates for Neuronal Growth. *Nano Lett.* **2004,** *4* (3), 507-511.

179. Waid, M. C.; McKenzie, J. L.; Price, R. L.; Ejiofor, J. U.; Webster, T. J., Nano-biotechnology: carbon nanofibres as improved neural and orthopaedic implants. *Nanotechnology* **2004,** *15*, 48-54.

180. Zhang, X.; Prasad, S.; Niyogi, S.; Morgan, A.; Ozkan, M.; Ozkan, C. S., Guided neurite growth on patterned carbon nanotubes. *Sensors and Actuators B: Chemical* **2005,** *106* (2), 843-850.

181. Gabay, T.; Jakobs, E.; Ben-Jacob, E.; Hanein, Y., Engineered self-organization of neural networks using carbon nanotube clusters. *Physica A: Statistical and Theoretical Physics* **2005,** *350* (2-4), 611-621.

182. Lovat, V.; Pantarotto, D.; Lagostena, L.; Cacciari, B.; Grandolfo, M.; Righi, M.; Spalluto, G.; Prato, M.; Ballerini, L., Carbon Nanotube Substrates Boost Neuronal Electrical Signaling. *Nano Lett.* **2005,** *5* (6), 1107-1110.

183. McKenzie, J. L.; Waid, M. C.; Shi, R.; Webster, T. J., Decreased functions of astrocytes on carbon nanofiber materials. *Biomaterials* **2004,** *25* (7-8), 1309-1317.

184. Hu, H.; Ni, Y.; Mandal, S. K.; Montana, V.; Zhao, B.; Haddon, R. C.; Parpura, V., Polyethyleneimine Functionalized Single-Walled Carbon Nanotubes as a Substrate for Neuronal Growth. *J. Phys. Chem. B* **2005,** *109* (10), 4285-4289.

185. Reynolds, B. A.; Weiss, S., Generation of neurons and astrocytes from isolated cells of the adult mammalian central nervous system. *Science* **1992,** *255*, 1707-1710.

186. Cattaneo, E.; McKay, R., Proliferation and differentiation of neuronal stem cells regulated by nerve growth factor. *Nature* **1990,** *347*, 762-765.

187. Fawcett, J. W.; Asher, R. A., The glial scar and central nervous system repair. *Brain Research Bulletin* **1999,** *49* (6), 377-391.

188. Chen, D. F. T., Susumu, Why do mature CNS neurons of mammals fail to re-establish connections following injury-functions of Bcl-2. *Cell Death & Differentiation* **1998,** *5*, 816-822.

189. Stichel, C. C.; Muller, H. W., The CNS lesion scar: new vistas on an old regeneration barrier. *Cell and Tissue Research* **1998,** *294* (1), 1-9.

190. Langmuir, I.; Schaefer, V. J., Monolayers and Multilayers of Chlorophyll *Journal of the American Chemical Society* **1937,** *59* (10), 2075-2076.

191. Blodgett, K. B., Films Built by Depositing Successive Monomolecular Layers on a Solid Surface *Journal of the American Chemical Society* **1935,** *57* (6), 1007-1022.

192. Nuzzo, R. G.; Allara, D. L., Adsorption of bifunctional organic disulfides on gold surfaces. *Journal of the American Chemical Society* **1983,** *105* (13), 4481-4483.

193. Bain, C. D.; Whitesides, G. M., Formation of monolayers by the coadsorption of thiols on gold: variation in the length of the alkyl chain. *Journal of the American Chemical Society* **1989,** *111* (18), 7164-7175.

194. Tang, Z.; Wang, Y.; Podsiadlo, P.; Kotov, N. A., Biomedical Applications of Layer-by-Layer Assembly: From Biomimetics to Tissue Engineering. *Advanced Materials* **2006,** *18* (24), 3203-3224.

195. Decher, G.; Hong, J. D.; Schmitt, J., Buildup of ultrathin multilayer films by a self-assembly process: III. Consecutively alternating adsorption of anionic and cationic polyelectrolytes on charged surfaces. *Thin Solid Films* **1992,** *210-211* (Part 2), 831-835.

196. Decher, G., Fuzzy Nanoassemblies: Toward Layered Polymeric Multicomposites. *Science* **1997,** *277* (5330), 1232-1237.

197. Cheung, J. H.; Stockton, W. B.; Rubner, M. F., Molecular-Level Processing of Conjugated Polymers. 3. Layer-by-Layer Manipulation of Polyaniline via Electrostatic Interactions. *Macromolecules* **1997,** *30* (9), 2712-2716.

198. Lojou, E.; Bianco, P., Buildup of Polyelectrolyte-Protein Multilayer Assemblies on Gold Electrodes. Role of the Hydrophobic Effect. *Langmuir* **2004,** *20* (3), 748-755.

199. Stockton, W. B.; Rubner, M. F., Molecular-Level Processing of Conjugated Polymers. 4. Layer-by-Layer Manipulation of Polyaniline via Hydrogen-Bonding Interactions. *Macromolecules* **1997,** *30* (9), 2717-2725.

200. Shimazaki, Y.; Mitsuishi, M.; Ito, S.; Yamamoto, M., Preparation of the Layer-by-Layer Deposited Ultrathin Film Based on the Charge-Transfer Interaction. *Langmuir* **1997,** *13* (6), 1385-1387.

201. Anzai, J. i.; Kobayashi, Y.; Nakamura, N.; Nishimura, M.; Hoshi, T., Layer-by-Layer Construction of Multilayer Thin Films Composed of Avidin and Biotin-Labeled Poly(amine)s. *Langmuir* **1999,** *15* (1), 221-226.

202. Crisp, M. T.; Kotov, N. A., Preparation of Nanoparticle Coatings on Surfaces of Complex Geometry. *Nano Lett.* **2003,** *3* (2), 173-177.

203. Hammond, P. T., Form and function in multilayer assembly: New applications at the nanoscale. *Advanced Materials* **2004,** *16* (15), 1271-1293.

204. Kotov, N. A.; Zavala, G.; Fendler, J. H., Langmuir-Blodgett-Films Prepared from Ferroelectric Lead Zirconium Titanate Particles. *Journal of Physical Chemistry* **1995,** *99* (33), 12375-12378.

205. Tang, Z. Y.; Kotov, N. A.; Magonov, S.; Ozturk, B., Nanostructured artificial nacre. *Nature Materials* **2003,** *2* (6), 413-U8.

206. Cooper, T. M.; Campbell, A. L.; Crane, R. L., Formation of Polypeptide-Dye Multilayers by an Electrostatic Self-Assembly Technique. *Langmuir* **1995,** *11* (7), 2713-2718.

207. He, J. A.; Valluzzi, R.; Yang, K.; Dolukhanyan, T.; Sung, C.; Kumar, J.; Tripathy, S. K.; Samuelson, L.; Balogh, L.; Tomalia, D. A., Electrostatic Multilayer Deposition of a Gold-Dendrimer Nanocomposite. *Chem. Mater.* **1999,** *11* (11), 3268-3274.

208. Boulmedais, F.; Ball, V.; Schwinte, P.; Frisch, B.; Schaaf, P.; Voegel, J. C., Buildup of Exponentially Growing Multilayer Polypeptide Films with Internal Secondary Structure. *Langmuir* **2003,** *19* (2), 440-445.

209. Lvov, Y.; Decher, G.; Sukhorukov, G., Assembly of Thin-Films by Means of Successive Deposition of Alternate Layers of DNA and Poly(Allylamine). *Macromolecules* **1993,** *26* (20), 5396-5399.

210. Lvov, Y.; Ariga, K.; Ichinose, I.; Kunitake, T., Assembly of Multicomponent Protein Films by Means of Electrostatic Layer-by-Layer Adsorption. *Journal of the American Chemical Society* **1995,** *117* (22), 6117-6123.

211. Lvov, Y.; Ariga, K.; Kunitake, T., Layer-by-Layer Assembly of Alternate Protein Polyion Ultrathin Films. *Chemistry Letters* **1994,** (12), 2323-2326.

212. Vautier, D.; Karsten, V.; Egles, C.; Chluba, J.; Schaaf, P.; Voegel, J.-C.; Ogier, J., Polyelectrolyte multilayer films modulate cytoskeletal organization in chondrosarcoma cells. *Journal of Biomaterials Science, Polymer Edition* **2002,** *13* (6), 712-731.

213. Mao, Z.; Ma, L.; Zhou, J.; Gao, C.; Shen, J., Bioactive Thin Film of Acidic Fibroblast Growth Factor Fabricated by Layer-by-Layer Assembly. *Bioconjugate Chem.* **2005,** *16* (5), 1316-1322.

214. Benkirane-Jessel, N.; Lavalle, P.; Meyer, F.; Audouin, F.; Frisch, B.; Schaaf, P.; Ogier, J.; Decher, G.; Voegel, J. C., Control of Monocyte Morphology on and Response to Model Surfaces for Implants Equipped with Anti-Inflammatory Agent. *Advanced Materials* **2004,** *16* (17), 1507-1511.

215. N. Benkirane-Jessel; Schwint, P.; Falvey, P.; Darcy, R.; Haikel, Y.; Schaaf, P.; Voegel, J. C.; Ogier, J., Build-up of Polypeptide Multilayer Coatings with Anti-Inflammatory Properties Based on the Embedding of Piroxicam-Cyclodextrin Complexes. *Advanced Functional Materials* **2004,** *14* (2), 174-182.

216. Etienne, O.; Gasnier, C.; Taddei, C.; Voegel, J.-C.; Aunis, D.; Schaaf, P.; Metz-Boutigue, M.-H.; Bolcato-Bellemin, A.-L.; Egles, C., Antifungal coating by biofunctionalized polyelectrolyte multilayered films. *Biomaterials* **2005,** *26* (33), 6704-6712.

217. Podsiadlo, P.; Paternel, S.; Rouillard, J. M.; Zhang, Z.; Lee, J.; Lee, J. W.; Gulari, E.; Kotov, N. A., Layer-by-Layer Assembly of Nacre-like Nanostructured Composites with Antimicrobial Properties. *Langmuir* **2005,** *21* (25), 11915-11921.

218. Shim, B. S.; Tang, Z. Y.; Morabito, M. P.; Agarwal, A.; Hong, H. P.; Kotov, N. A., Integration of conductivity transparency, and mechanical strength into highly homogeneous layer-by-layer composites of single-walled carbon nanotubes for optoelectronics. *Chemistry of Materials* **2007,** *19* (23), 5467-5474.

219. Firkowska, I.; Olek, M.; Pazos-Perez, N.; Rojas-Chapana, J.; Giersig, M., Highly Ordered MWNT-Based Matrixes: Topography at the Nanoscale Conceived for Tissue Engineering. *Langmuir* **2006,** *22* (12), 5427-5434.

220. Ma, Z.; Kotaki, M.; Inai, R.; Ramakrishna, S., Potential of Nanofiber Matrix as Tissue-Engineering Scaffolds. *Tissue Engineering* **2005,** *11* (1-2), 101-109.

221. Ma, P. X.; Zhang, R., Synthetic nano-scale fibrous extracellular matrix. *Journal of Biomedical Materials Research* **1999,** *46* (1), 60-72.

222. Kandel, E. R. S., James H.; Jessell, Thomas M. , *Principles of Neural Science*. 4th ed. ed.; McGraw-Hill: New York, 2000.

223. Gage, F. H., Mammalian Neural Stem Cells. *Science* **2000,** *287* (5457), 1433-1438.

224. Doetsch, F., A niche for adult neural stem cells. *Current Opinion in Genetics & Development* **2003,** *13* (5), 543-550.

225. Martino, G.; Pluchino, S., The therapeutic potential of neural stem cells. *Nat Rev Neurosci* **2006,** *7* (5), 395-406.

226. Muller, F.-J.; Snyder, E. Y.; Loring, J. F., Gene therapy: can neural stem cells deliver? *Nat Rev Neurosci* **2006,** *7* (1), 75-84.

227. Fisher, L. J., Neural Precursor Cells: Applications for the Study and Repair of the Central Nervous System. *Neurobiology of Disease* **1997,** *4* (1), 1-22.

228. Davis, A. A.; Temple, S., A self-renewing multipotential stem cell in embryonic rat cerebral cortex. *Nature* **1994,** *372* (6503), 263-266.

229. Reynolds, B. A.; Tetzlaff, W.; Weiss, S., A multipotent EGF-responsive striatal embryonic progenitor cell produces neurons and astrocytes. *J. Neurosci.* **1992,** *12* (11), 4565-4574.

230. Svendsen, C. N.; ter Borg, M. G.; Armstrong, R. J. E.; Rosser, A. E.; Chandran, S.; Ostenfeld, T.; Caldwell, M. A., A new method for the rapid and long term growth of human neural precursor cells. *Journal of Neuroscience Methods* **1998,** *85* (2), 141-152.

231. Holmes, T. C.; de Lacalle, S.; Su, X.; Liu, G.; Rich, A.; Zhang, S., Extensive neurite outgrowth and active synapse formation on self-assembling peptide scaffolds. *PNAS* **2000,** *97* (12), 6728-6733.

232. Westerlund, U.; Moe, M. C.; Varghese, M.; Berg-Johnsen, J.; Ohlsson, M.; Langmoen, I. A.; Svensson, M., Stem cells from the adult human brain develop into functional neurons in culture. *Experimental Cell Research* **2003,** *289* (2), 378-383.

233. Young, T.-H.; Hung, C.-H., Behavior of embryonic rat cerebral cortical stem cells on the PVA and EVAL substrates. *Biomaterials* **2005,** *26* (20), 4291-4299.

234. Wang, J.-H.; Hung, C.-H.; Young, T.-H., Proliferation and differentiation of neural stem cells on lysine-alanine sequential polymer substrates. *Biomaterials* **2006,** *27* (18), 3441-3450.

235. Hung, C.-H.; Lin, Y.-L.; Young, T.-H., The effect of chitosan and PVDF substrates on the behavior of embryonic rat cerebral cortical stem cells. *Biomaterials* **2006,** *27* (25), 4461-4469.

236. Silva, G. A.; Czeisler, C.; Niece, K. L.; Beniash, E.; Harrington, D. A.; Kessler, J. A.; Stupp, S. I., Selective Differentiation of Neural Progenitor Cells by High-Epitope Density Nanofibers. *Science* **2004,** *303* (5662), 1352-1355.

237. Englund, U.; Bjorklund, A.; Wictorin, K.; Lindvall, O.; Kokaia, M., Grafted neural stem cells develop into functional pyramidal neurons and integrate into host cortical circuitry. *Proceedings of the National Academy of Sciences of the United States of America* **2002,** *99* (26), 17089-17094.

238. Jacques, T. S.; Relvas, J. B.; Nishimura, S.; Pytela, R.; Edwards, G. M.; Streuli, C. H.; ffrench-Constant, C., Neural precursor cell chain migration and division are regulated through different beta1 integrins. *Development* **1998,** *125* (16), 3167-3177.

239. Flanagan, L. A.; Rebaza, L. M.; Derzic, S.; Schwartz, P. H.; Monuki, E. S., Regulation of human neural precursor cells by laminin and integrins. *Journal of Neuroscience Research* **2006,** *83* (5), 845-856.

240. Dickson, B. J., Molecular Mechanisms of Axon Guidance. *Science* **2002,** *298* (5600), 1959-1964.

241. Takahashi, J.; Palmer, T. D.; Gage, F. H., Retinoic acid and neurotrophins collaborate to regulate neurogenesis in adult-derived neural stem cell cultures. *Journal of Neurobiology* **1999,** *38* (1), 65-81.

242. Lillien, L., Neural progenitors and stem cells: mechanisms of progenitor heterogeneity. *Current Opinion in Neurobiology* **1998,** *8* (1), 37-44.

243. Davies, J.; Huang, C.; Proschel, C.; Noble, M.; Mayer-Proschel, M.; Davies, S., Astrocytes derived from glial-restricted precursors promote spinal cord repair. *Journal of Biology* **2006,** *5* (3), 7.

244. Daadi, M. M.; Weiss, S., Generation of Tyrosine Hydroxylase-Producing Neurons from Precursors of the Embryonic and Adult Forebrain. *J. Neurosci.* **1999,** *19* (11), 4484-4497.

245. Drury, J. L.; Mooney, D. J., Hydrogels for tissue engineering: scaffold design variables and applications. *Biomaterials* **2003,** *24* (24), 4337-4351.

246. Ma, P. X., Scaffolds for tissue fabrication. *Materials Today* **2004,** *7* (5), 30-40.

247. Lee, J.; Cuddihy, M. J.; Kotov, N. A., Three-dimensional cell culture matrices: State of the art. *Tissue Engineering Part B-Reviews* **2008,** *14* (1), 61-86.

248. Zhang, S., Beyond the Petri dish. *Nat Biotech* **2004,** *22* (2), 151-152.

249. Peppas, N. A.; Hilt, J. Z.; Khademhosseini, A.; Langer, R., Hydrogels in Biology and Medicine: From Molecular Principles to Bionanotechnology. *Advanced Materials* **2006,** *18* (11), 1345-1360.

250. Zhang, Y.; Wang, S.; Eghtedari, M.; Motamedi, M.; Kotov, N., Inverted-Colloidal-Crystal Hydrogel Matrices as Three-Dimensional Cell Scaffolds. *Advanced Functional Materials* **2005,** *15* (5), 725-731.

251. Liu, Y. F.; Wang, S. P.; Lee, J. W.; Kotov, N. A., A floating self-assembly route to colloidal crystal templates for 3D cell scaffolds. *Chemistry of Materials* **2005,** *17* (20), 4918-4924.

252. Kotov, N. A.; Liu, Y. F.; Wang, S. P.; Cumming, C.; Eghtedari, M.; Vargas, G.; Motamedi, M.; Nichols, J.; Cortiella, J., Inverted colloidal crystals as three-dimensional cell scaffolds. *Langmuir* **2004,** *20* (19), 7887-7892.

253. Lee, J.; Cuddihy, M. J.; Cater, G. M.; Kotov, N. A., Engineering liver tissue spheroids with inverted colloidal crystal scaffolds. *Biomaterials* **2009,** *30* (27), 4687-4694.

254. Cuddihy, M. J.; Kotov, N. A., Poly(lactic-co-glycolic acid) Bone Scaffolds with Inverted Colloidal Crystal Geometry. *Tissue Engineering Part A* **2008,** *14* (10), 1639-1649.

255. Lee, J.; Kotov, N. A., Notch Ligand Presenting Acellular 3D Microenvironments for ex vivo Human Hematopoietic Stem-Cell Culture made by Layer-By-Layer Assembly. *Small* **2009,** *5* (9), 1008-1013.

256. Nichols, J. E.; Cortiella, J. Q.; Lee, J.; Niles, J. A.; Cuddihy, M.; Wang, S. P.; Bielitzki, J.; Cantu, A.; Mlcak, R.; Valdivia, E.; Yancy, R.; McClure, M. L.; Kotov, N. A., In vitro analog of human bone marrow from 3D scaffolds with biomimetic inverted colloidal crystal geometry. *Biomaterials* **2009,** *30* (6), 1071-1079.

257. Shanbhag, S.; Woo Lee, J.; Kotov, N., Diffusion in three-dimensionally ordered scaffolds with inverted colloidal crystal geometry. *Biomaterials* **2005,** *26* (27), 5581-5585.

258. Shanbhag, S.; Wang, S. P.; Kotov, N. A., Cell distribution profiles in three-dimensional scaffolds with inverted-colloidal-crystal geometry: Modeling and experimental investigations. *Small* **2005,** *1* (12), 1208-1214.

259. Liu, Y. F.; Wang, S. P.; Kotov, N. A.; Cumming, C.; Motamedi, M.; Nichols, J. E.; Cortiella, J., Preparation of ordered 3D cell scaffolds with LBL surface modification. *Abstracts of Papers of the American Chemical Society* **2004,** *227*, U529-U529.

260. Lee, J.; Lilly, G. D.; Doty, R. C.; Podsiadlo, P.; Kotov, N. A., In vitro Toxicity Testing of Nanoparticles in 3D Cell Culture. *Small* **2009,** *5* (10), 1213-1221.

CHAPTER 2

Cytotoxicity Profiling of Nanomaterials Using High Content Screening Assays

2.1 Abstract

Recent advances and progress in nanobiotechnology have demonstrated many nanomaterials as potential and novel drug delivery vehicles, therapeutic agents, and contrast agents and luminescent biological labels for bioimaging. The emergence of new biomedical applications based on nanomaterials signifies the need to understand, compare, and manage their cytotoxicity. In this study, we demonstrated the use of high content screening assay (HCA) as a universal tool to probe the cytotoxicity of NPs and specifically cadmium telluride quantum dots (CdTe QDs) and gold NPs (Au NPs) in NG108-15 murine neuroblastoma cells and HepG2 human hepatocellular carcinoma cells. In addition, we also compared the cytotoxic effects of carbon nanotube (CNT) dispersions and thin films in the NG108-15 neural cells. Neural cells represent special interest for NP and CNT induced cytotoxicity because of the optical and electrical functionalities of materials necessary for neural imaging and interfacing are matched well with the properties of these nanomaterials. Moreover, the cellular morphology of neurons

is particularly suitable for automated high content screening. HepG2 cells represent a good model for high content screening studies since they are commonly used as a surrogate for human hepatocytes in pharmaceutical studies. We found the CdTe QDs to induce primarily apoptotic response in a time- and dosage-dependent manner and produce different toxicological profiles and responses in undifferentiated and differentiated neural cells. Au NPs were found to inhibit the proliferation and intracellular calcium release of HepG2 cells. Layer-by-layer (LBL) assembled single-walled carbon nanotube (SWNT) thin films displayed minimal cytotoxicity while the cytotoxic effect of dispersed SWNTs increased with concentration.

2.2 Introduction

Research on nanomaterials has generated numerous biological applications in the past decade. With continuing progress of nanoscale synthesis and biological applications of nanomaterials, such as nanoparticles (NPs) and carbon nanotubes (CNTs), one needs to develop a quick and fairly standard assessment tool to evaluate their cytotoxicity. Since many structural and physical properties of nanomaterials have clear similarities with those of proteins,[1-3] it is not surprising that nanomaterials may exhibit cytotoxicity or, in more general terms, biological activity that is specific to NPs and CNTs and affects cell signaling mechanism differently from that observed for ionic, polymeric systems and small molecules. The detrimental effects of such biological activity can be captured by

the term nanotoxicity,[4-6] which is probably the most critical from a health safety perspective.[7]

The purpose of this study is to make the first step toward the development both fast and fairly comprehensive method of screening of biological activity and cytotoxicity of NPs and CNTs. We see two important factors that necessitate the development of such protocol(s). (1) Since the synthesis of NPs and CNTs is much simpler than the synthesis of proteins and other drugs, minor changes in the synthetic protocol are likely to affect their interactions with cells. So, one can expect to see a tremendous surge of potential candidates for toxicity/biological activity screening. Taking II-VI semiconductor quantum dots (QDs) as an example, beside the release of heavy metal elements from the core which can lead to cell poisoning,[8] studies have shown that the cytotoxicity of these QDs is highly dependent on their processing parameters,[9] surface modifications,[8-10] as well as a number of physicochemical and environmental factors, such as size, charge, concentration, and stability.[11] Such amounts will be difficult to analyze using conventional approaches. (2) Considering the diversity of NPs and CNTs being synthesized, one needs a unified approach for screening nanomaterials. Such a systematic approach is not only fundamental to the construction of a unified database for biological and cytotoxic effects of nanomaterials but will also enable scientists to synthesize safer and more efficacious nanostructures at an ever-more efficient rate. We can expect the engineering of biologically functional nanostructures to follow the path of synthetic pharmaceuticals in drug discovery. In the near future, panels of nanomaterials with

slightly varying properties and structures will be synthesized and evaluated for cytotoxicity before qualified candidates are designated subsequent developments.

In this study, we are motivated to explore the possibility of building a high-content, high-throughput cytotoxicity assay platform based on high-content screening (HCS) technology to meet future's demand for nanotoxicity studies. HCS is a recent advance in the integration and automation of quantitative fluorescence microscopy and image analysis, and it has already started to generate impact in pharmaceutical and biotechnology industries.[12, 13] Zhang et al. were the first to employ high-content image analysis, in conjunction with high-throughput analysis, to study the cytotoxicity of QDs.[14] They investigated the cellular and molecular effect of high doses of poly(ethylene glycol) silanized QDs (PEG-silane-QDs) on human lung and skin epithelial cells, and reported PEG-silane-QDs to induce minimal cytotoxicity even at high dosages. While the use of HCS analysis in their study is confined to cell counting, quantification of apoptotic and necrotic cell population, and generation of cell cycle profiles, our current study extends the application of HCS technology to the evaluation of cell function, specifically neurite outgrowth, and the development of a multiplexed cytotoxicity assay that may serve as the basis of a standardized nanotoxicity assay and facilitate the formation of a unified nanotoxicology database.

Semiconductor QDs are most well known for their potential applications in biosensing, ex vivo live cell imaging and in vivo animal targeting,[15-18] while Au NPs have demonstrated promising capabilities as novel drug delivery vehicles,[19] near-infrared

agents for thermal therapy,[20] and contrast agents for biomedical imaging.[21-23] More recently in search of new neurotherapeutic, neuroprosthetic, and neuroimaging strategies, many researchers have explored the use of NPs to manipulate and create active cellular interfaces with nerve cells.[24, 25] Vu et al. utilized peptide conjugated QDs to initiate neuronal differentiation[26] while Dahan et al. used antibody functionalized QDs to track the diffusion of glycine receptors in neurons.[27] Jackson and colleagues demonstrated that QDs can improve identification and visualization of brain tumors.[28] At the neural interface, Winter et al. investigated the possibility to build a bioelectronic interface by both culturing nerve cells on tethered QD thin films[29] and attaching QDs directly to nerve cells via biological recognition molecules.[30] Most recently, Kotov and colleagues demonstrated, for the first time, the excitation of neural cells through a sequence of photochemical and charge-transfer reactions on layer-by-layer assembled NP-polyelectrolyte composite films.[31] In the case of CNTs, due to their unique physical and electrical properties, many studies have investigated their potential as therapeutic agents and neural interfacing materials.[32] CNTs have been shown to promote neuron differentiation from embryonic stem cells.[33] Substrates fabricated from CNTs have also been demonstrated to support neural differentiation[34] and promote neural electrical activity.[35]

Our study began with a comprehensive investigation of cadmium telluride (CdTe) QD induced cytotoxicity in NG108-15 murine neuroblastoma cells using various HCS assays. We then extended the application of our multiplexed cytotoxicity assay to study the cytotoxic effect of gold NPs (Au NPs) on the HepG2 human hepatocellular carcinoma

cells. Finally, using the same multiplexed cytotoxicity assay, a comparison of cytotoxicity induced by dispersed CNTs and CNT thin films were made using NG108-15 neuralblastoma cells.

2.3 Methods

2.3.1 Synthesis of CdTe Quantum Dots

Millipore water (120 mL) was degassed by bubbling argon for approximately 1 h. $Cd(ClO_4)_2 \cdot 6H_2O$ (3.22 g, 7.68 mmol), TGA stabilizer (1.24 g, 13.46 mmol, 1.75 molar equivalents) were added and the pH was adjusted to 11.2–11.3 by the addition of NaOH solution (2M). For gelatin-containing samples, gelatin (0.3 g) was dissolved in water (10 mL) by heating gently and added to the reaction mixture. Gaseous H2Te, generated from Al_2Te_3 (0.56 g, 0.128 mmol) by dropwise addition of H_2SO_4 solution (0.5m) was bubbled through the cadmium/thiol/gelatin solution under a slow argon flow for approximately 10 min. The resultant nonluminescent solution was then heated to reflux. Fractions were precipitated by the addition of isopropanol and were stored at 4°C.

2.3.2 Synthesis of Gold Nanoparticles

Gold chloride solution (0.01g HAuCl4 in 100ml water) was first brought to boil, followed by addition of 2ml 1% sodium citrate solution (0.02g trisodium citrate in 2ml water). The gold nanoparticle solution was stirred for 10min and allowed to cool to room

temperature. Stabilizer was introduced by adding 102μL of cysteine solution (0.01g l-cysteine in 1ml water) to the gold nanoparticle solution with stirring. The final gold nanoparticle solution was filtered through a 0.22μm filter for sterility and stored at room temperature.

2.3.3 Preparation of Carbon Nanotube Dispersion and Thin Films

Single-walled carbon nanotubes (SWNTs) were dispersed at 0.5 mg/ml in 0.1 wt% poly(sodium 4-styrene-sulfonate) (PSS; MW 1000k) solution by ultra-sonication. Thin films of SWNTs were prepared in 96-well tissue culture plates using the technique of layer-by-layer (LBL) assembly. Specifically, SWNT thin films were formed by alternating deposition of 1 wt% poly(vinyl alcohol) (PVA; MW 70k, pH 2, 6 or 10) with the SWNT dispersion. For each deposition, the bottom of each well was covered with the corresponding solution for 5 min, followed by rinsing with deionized water and drying with an air jet. The resulting thin film of coating was designated as $(PVA/SWNT)_n$ where n is the number of bilayers.

2.3.4 Cell Culture

NG108-15 murine neuroblastoma×glioma hybrid cells and HepG2 Human hepatocyte carcinoma cells were obtained from the European Collection of Cell Cultures.

NG108-15 cells were grown in high-glucose Dulbecco's modified Eagle's medium, supplemented with 10% (v/v) of fetal calf serum, 0.1 mM hypoxanthine, 1 μM aminopterin, and 16 μM thymidine. To induce differentiation, the amount of serum was lowered to 1% (v/v). HepG2 cells were cultured in Eagel minimum essential medium supplemented with 10% (v/v) fetal bovine serum.

2.3.5 Apoptosis/Necrosis Assay

Cells were seeded in 96-well tissue culture plate (Nunc) and allowed to adhere overnight. At the indicated time point (1.5h, 6h, 24h) following treatment with TGA-QDs or Gelatin-QDs, cells were stained with propidium iodide (1 μg/ml) and Hoechst 33342 (2 μg/ml) for 10 min at room temperature and imaged using the IN Cell Analyzer 1000 HCS system (GE Healthcare). The HCS system scans through the bottom the plate, focuses on individual fields of cells, and acquires images at each selected fluorescence channel. Hoechst was visualized in the blue channel and propidium iodide in the red channel. The experiment was conducted in 3 independent runs. For each run, 5 independent fields from each well were imaged using a 20X objective. Cells were classified as either healthy, apopotic, or necrotic using the supervised classification function of the IN Cell Investigator image analysis software (GE Healthcare).

2.3.6 Neurite Outgrowth Assay

Cells were seeded in 96-well tissue culture plate and allowed to adhere overnight. After treatment with TGA-QDs or Gelatin-QDs for 6h, cells were gently washed with

fresh medium and cultured with reduced serum supplementation to induce neuronal differentiation. No supplementary growth factor was added. After 4 days of differentiation, cells were fixed in 2% paraformaldehyde, permeabilized in 0.1% Triton X-100 in 1% BSA, and stained using mouse anti-β-tubulin III (1:800 in 1% BSA; overnight at 4 ºC) followed by Alexa Fluor 488 conjugated goat anti-mouse IgG (1:200; 1h at 37 ºC). The experiment was carried out in triplicates. For each well, 4 independent fields were imaged using a 10X objective and analyzed using the Neurite Outgrowth Analysis Module of the IN Cell Investigator software. The analysis module reports population-averaged measurements for a range of cell parameters, including neurite length and neurite count.

2.3.7 Multiplexed Cytotoxicity Assay

Cells were seeded in 96-well plate and allowed to adhere overnight. Following treatment with either CdTe QDs, Au NPs, or CNTs, cells were very gently washed with pre-warmed fresh medium and simultaneously loaded with 1 μM Hoechst 33342, 20 nM TMRM (tetramethyl rhodamine methyl ester perchlorate), and 1 μM Fluo-4 (fluo-4 acetoxymethyl ester). Cells were loaded in the corresponding culture media for 30min at 37 °C and then imaged using the IN Cell Analyzer 1000 HCS system. Hoechst was visualized in the blue channel while TMRM and Fluo-4 were visualized in the red and green channels, respectively. The following data were collected and analyzed using the Dual Area Object Analysis Module of the IN Cell Investigator software. The module allows simultaneous quantification of sub-cellular inclusions that are marked by different

fluorescent probes and measures fluorescence intensity associated with predefined nuclear and cytoplasmic compartments. The following data were collected. Cell count was generated from the number of Hoechst 33342 stained nuclei. Nuclear size was defined as the mean object area of Hoechst 33342. Cellular mitochondrial membrane potential was measured by the TMRM fluorescence intensity in punctuate cytosolic regions (cellular inclusions) around the nucleus. Intracellular free calcium concentration was measured by the fluorescence intensity of Fluo-4 in an intracellular circular region (cellular compartment) centered at the nucleus.

2.4 Results and Discussion

2.4.1 CdTe Quantum Dots

One question we would like to answer in our exploration of HCS technology and assays is how undifferentiated and differentiated cells respond to treatment with NPs. This is an important question because target cells at various stages of differentiation and maturation respond to therapeutic interventions in different ways. To answer this, we investigated the cellular response of the NG108-15 murine neuroblastoma cells to two types of CdTe QDs. The first is a thioglycolic acid (TGA)-capped CdTe QD (TGA-QD), and the other is a TGA-capped CdTe QD produced in the presence of gelatin (Gelatin-QD). Both of these QDs have a diameter of 3nm and emits in the green-yellow region of the spectrum (~560nm). Some of us recently published the synthesis and characterization

of this Gelatin-NP nanocomposite along with a preliminary cytotoxicity study that demonstrated reduced cytotoxicity of Gelatin-QDs in THP-1 human monocytic cells.[36] It has been suggested that gelatin enables the QDs to grow more discretely (blue shifted) and serve as a co-capping agent for stabilization of QDs and encapsulation of the toxic heavy metal core. While poly(ethylene glycol) (PEG) remains the most promising coating material for reducing cytotoxicity to this date, we believe naturally occurring biopolymers, such as gelatin, may provide additional biological functionalities in addition to their protective property. We chose to work with the NG108-15 murine neuroblastoma cells because they possess neuron-like properties and can be differentiated relatively easily and quickly.

The first HCS assay we employed was an apoptosis/necrosis assay for the quantification of healthy, apoptotic, and necrotic cells. At the indicated time point (1.5h, 6h, 24h) following treatment with TGA-QDs or Gelatin-QDs, cells were stained with propidium iodide (1 μg/ml) and Hoechst 33342 (2 μg/ml) for 10 min at room temperature and imaged using the IN Cell Analyzer 1000 HCS system (GE Healthcare). Cells in each category were classified using the supervised classification function of the IN Cell Investigator image analysis software (GE Healthcare), which analyzed the fluorescence quantitatively on a cell-by-cell basis. Figure 2.1 illustrates representative images of healthy, apoptotic, and necrotic cells. The plasma membranes of necrotic cells are permeable to propidium iodide, so necrotic cells were identified by their intense red fluorescence. Apoptotic cells were identified as being impermeable to propidium iodide but showing condensed and fragmented nuclei from the Hoechst 33342 stain. Healthy

cells were stained by Hoechst 33342 only and displayed intact and homogeneously stained nuclei. The experiment was carried out in triplicates in 96-well plates, which helps to increase throughput and reduce consumption of cell culture and assay reagents and ensures reproducibility at the large cell population scale.

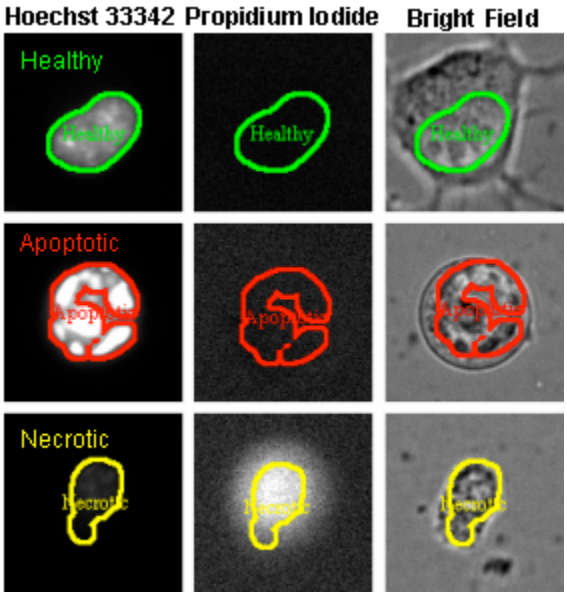

Figure 2.1 Representative fluorescence and bright field images of a healthy (green outline), an apoptotic (red outline), and a necrotic (yellow outline) cell. Outline and classification of cells were generated by the IN Cell Investigator image analysis software using the supervised classification capability.

Figure 2.2 shows the average result from 3 independent runs. For each run, 5 independent fields from each well were imaged using a 20X objective. The entire experiment, including all concentrations and time points, is an assessment of as many as

25,000 individually analyzed cells and demonstrates the robustness of HCS assays. For both undifferentiated and differentiated cells, treatment with QDs induced predominantly an increase in apoptotic cell population, as the number of necrotic cells remained relatively constant regardless of QD dosage or treatment time. This finding is corroborated by published results from Chan et al., who demonstrated that CdSe-core QDs induce apoptotic biochemical changes in human neuroblastoma cells via mitochondrial-dependent pathways and inhibition of survival signals.[37] In addition, our study also found undifferentiated and differentiated cells to respond differently to treatment with QDs. This is an important finding because the human is composed of cells and tissue at different levels of maturity and differentiation. For undifferentiated NG108-15 cells, the number of apoptotic cells remained constant between 1.5h and 6h of incubation with QDs and increased sharply after 24h. We suspect the delayed cytotoxic response is a buffering effect owing to the proliferating potential of undifferentiated cells. For differentiated cells, an incremental increase in apoptotic population was observed between the three time points, indicating differentiated cells to be more sensitive and vulnerable to QD treatment.

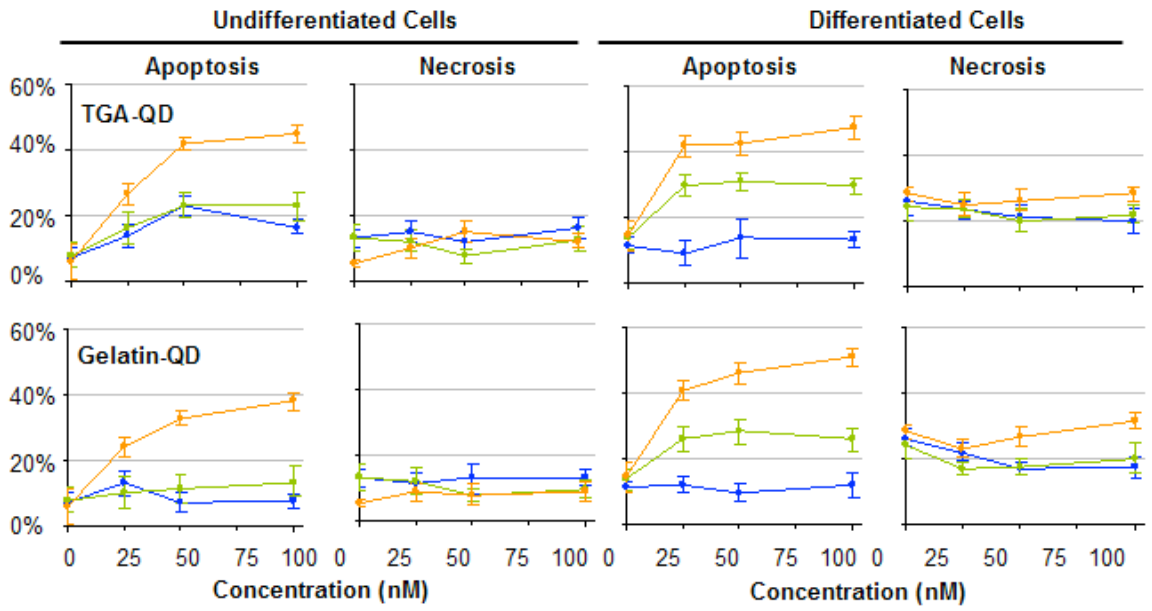

Figure 2.2 Effect of QD treatment on NG108-15 cells. Undifferentiated and differentiated NG108-15 cells were incubated with various concentrations of TGA-QDs and Gelatin-QDs for 1.5 h (blue), 6 h (green), and 24 h (orange). Percentages of apoptosis and necrosis were determined by staining the cells with propidium iodide and Hoechst 33342, followed by image acquisition and analysis using a HCS system.

It should be emphasized that although TGA-QDs and Gelatin-QDs produced similar cellular response in NG108-15 cells, in HCS assays even a 5-15% difference represents a consistent and significant response at the cell population level and is likely to include moderate and below average response typical of the *in vivo* physiological situations. The most obvious difference between the two QDs is seen in the apoptotic population of the undifferentiated cells. While the apoptotic population of TGA-QD treated cells increased with QD concentration at 1.5h and 6h, the apoptotic population of Gelatin-QD treated cells remained unchanged. In addition, TGA-QD treated cells also

displayed a more drastic increase in apoptotic population after 24h compared to Gelatin-QD treated cells, indicating somewhat lower cytotoxicity in the Gelatin-QDs. Generalizing the results, it is important to make three points here. (1) HCS allows one to reliably identify these differences in cellular response to NPs and use it for comparison of their (bio)medical prospects, which provides a substantial advantage over less systematic techniques used now. (2) We used here a version of analysis with fairly wide concentration step and finer profiles could be obtained to highlight even smaller effects for more advanced fingerprinting. (3) Greater number of labels in the panel will further improve differentiation of the effect of one NPs versus the other or one cell type versus the other, which will be demonstrated below.

To further investigate the difference between TGA-QDs and Gelatin-QDs, we conducted a neurite outgrowth assay to investigate the effect of QD treatment on neuronal differentiation. One day following cell seeding, NG108-15 cells were incubated with either type of QDs for 6 hours, after which the cells were washed with fresh medium and cultured in medium with reduced amount of serum to induce differentiation. No supplementary growth factor was added in order to avoid interference or counteracting effect. After 4 days of differentiation, cells were stained and imaged using the IN Cell Analyzer 1000 HCS system. Cells were first fixed in 2% paraformaldehyde and permeabilized in 0.1% Triton X-100 in 1% BSA. Neurites were stained using mouse anti-β-tubulin III (1:800 in 1% BSA; overnight at 4 ºC) followed by Alexa Fluor 488 conjugated goat anti-mouse IgG (1:200; 1h at 37 ºC). The experiment was carried out in

triplicates. For each well, 4 independent fields were imaged using a 10X objective and analyzed using the IN Cell Investigator software.

Figure 2.3 shows representative images acquired by the robotic imaging system at different treatment conditions. The measurement of neurite outgrowth is traditionally a time-consuming and tedious job, but the work is greatly simplified with the aid of a HCS system. An analysis of the total neurite length with respect to the untreated control is presented in Figure 2.4. A 6h treatment with 25nM of TGA-QDs prior to neuronal differentiation reduced the total neurite length by approximately 50%, primarily due to a decrease in cell number as illustrated in Figure 2.3. However, treatment with 25nM of Gelatin-QDs led to a slight increase in total neurite length. We suspect this contradicting effect at low dose could be a hormetic response as hormesis is frequently observed as a result of low dose stimulation in toxicological studies.[38, 39] The mechanisms involved in countering the cytotoxic effect of a short, non-lethal low dose treatment might have stimulated the formation of neurites. The difference between the two QDs is most evident at the 50nM concentration, where all TGA-QD treated cells were killed while Gelatin-QD treated cells still exhibited some viability and a moderate level of neurite outgrowth. A 100nM treatment with either type of QDs appeared to be too toxic for any cells to survive.

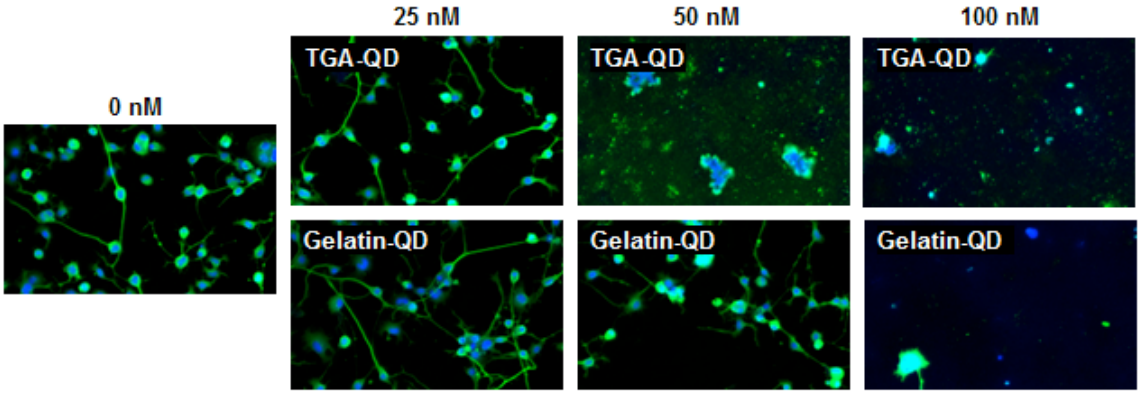

Figure 2.3 Effect of QD treatment on neurite outgrowth of NG108-15 cells. Cell were incubated with TGA-QDs and Gelatin-QDs at various concentrations for 6 h and induced to differentiate for 4 additional days in low-serum medium. Cells were stained for β-tubulin III (green) and nuclei (blue) and imaged using a HCS system.

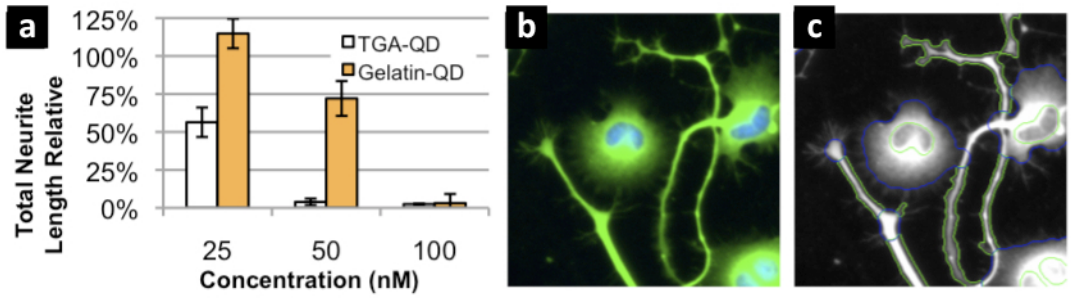

Figure 2.4 Neurite outgrowth was assessed in terms of total neurite length per field. The result is the average of 3 independent experiments (4 independent fields each) and is expressed as percentage relative to the total neurite length per field of the untreated control (**a**). A false-colored composite fluorescent image of neurite outgrowth is shown here (**b**). During image analysis, the software's image processing algorithm allows system to identify of neurites (green outlines) and make quantitative measurements (**c**).

The apoptosis/necrosis assay and neurite outgrowth assay prompted us to further investigate the cellular response of neural cells to QD treatments. The apoptosis/necrosis assay measures only late-stage toxicity and cellular events associated with a lethal apoptotic or necrotic effect. This assay is important but needs to be augmented with other assays for detailed toxicology fingerprinting, because it provides little mechanistic understanding of toxicological effects. The neurite outgrowth assay clearly revealed the toxicological difference between the two QDs and demonstrated the importance of a functionality assay in cytotoxicity studies. Since our motivation is to explore the use of HCS assays for the study of nanotoxicity, we subsequently employed another kind of assay, this time an assay that would detect sublethal cytotoxicity in a multiparameter format to give us more information and sensitivity regarding the cytotoxicity of a given nanocolloid.

Although the success and advantages of a sublethal, multiplexed cytotoxicty assay has been demonstrated by O'Brien and his colleagues in the study of hepatotoxicity,[39, 40] it has never been utilized in the context of nanotoxicity. Such an assay evaluates specific toxicological mechanisms in cells prior to the onset of the late stages of non-specific degeneration and apoptotic or necrotic death, providing greater predictive power and extrapolatability across models and species.[40] The multiparametric nature of the assay originates from the multiple fluorescent probes that simultaneously and coherently monitor different cellular functions in vitro and is made possible by recent advances in fluorescent probe technology.[41]

In this study, undifferentiated and differentiated NG108-15 cells were treated with QDs at various concentrations for 24h, after which the medium was removed and the cells were incubated with a cocktail of fluorescent probes for 30 min before they were imaged using the IN Cell Analyzer 1000 HCS system. The cocktail of fluorescent probes was prepared in fresh medium and consisted of 1μM Hoechst 33342, 20nM TMRM, and 1μM Fluo-4. These fluorescent probes were selected for specific reasons. First of all, these fluorescent probes can be used concurrently and are readily internalized by live cells without posing substantial harm. Hoechst 33342 allows identification of individual cell nuclei, which permits the measurement of cell count and nuclear area and allows subsequent analysis on the complementary stains to be conducted. A decrease in cell number indicates cell death and/or decreased cell proliferation, while nuclear shrinkage is typically a consequence of chromatin condensation and a sign of apoptotic cell death. TMRM and Fluo-4 allow the assessment of mitochondrial membrane potential and intracellular free calcium concentration, respectively. The mitochondrion is central to the functioning and survival of nerve cells.[42] It is responsible for ATP generation, Ca^{2+} uptake and storage, and the generation of detoxification of reactive oxygen species.[43] A drop in the electrochemical gradient across the mitochondrial membrane therefore signals weakened cellular respiratory capacity and energetics. Intracellular Ca^{2+} is a chief regulator of a variety of biological processes.[44] For this reason, pharmaceutical companies have long adopted the measurement of intracellular Ca^{2+} for high-throughput screening.[45] Intracellular Ca^{2+} is especially important in neural cells since it regulates neurite outgrowth and synaptogenesis, synaptic transmission and plasticity, and cell

survival.[46, 47] A dramatic increase in intracellular Ca^{2+} is an early event in the development of cell injury due to cytotoxicity.[48]

The concentration response of cells was measured using the IN Cell Investigator software and evaluated in terms of cell number, nuclear area, mitochondrial function, and intracellular calcium homeostatsis. Cell count was generated from the number of Hoechst 33342 stained nuclei. Nuclear size was defined as the area of Hoechst 33342 fluorescence (Figure 2.5, inner blue circle). Cellular mitochondrial membrane potential was defined as the TMRM fluorescence intensity in punctuate cytosolic regions around the nucleus (Figure 2.5, yellow inclusions), while intracellular free calcium concentration was measured by the fluorescence intensity of Fluo-4 in a large intracellular circular region centered at the nucleus (Figure 2.5, outer green circle). Since the HCS platform is based on the acquisition, processing, and analysis of fluorescence images, we made sure the NG108-15 cells do not uptake significant amount of QDs to interfere with our multiplexed cytotoxicity assay (data not included). The level of fluorescence signal from QDs was constant regardless of concentration and was well below the basal fluorescence level of TMRM and Fluo-4. This was not a problem in the apoptosis/necrosis and neurite outgrowth assays because the emission spectrum of the QDs does not coincide with Hoechst 33342 and propidium iodide and immunological staining is much more specific and intense than nonspecific uptake and adsorption of the QDs.

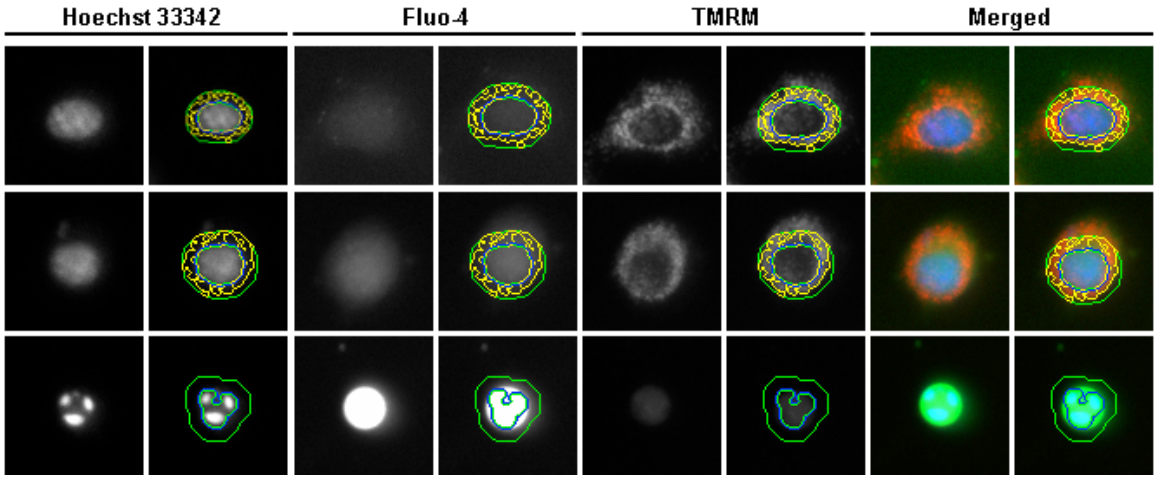

Figure 2.5 Representative fluorescence images of a healthy (first row), an impaired (middle row), and a dying (last row) cells acquired and processed by the IN Cell HCS system. The nucleus, stained by Hoechst 3342, is outlined by a blue circle. The cell body or the intracellular region is enclosed by a green circle, within which the intensity of Fluo-4 fluorescence is measured. The punctuate, TMRM-bound mitochondrial organelles in the cytosol are identified by the yellow inclusions. In the merged images, Hoechst 3342, Fluo-4, and TMRM stains are shown in blue, green, and red, respectively. As the health condition of cells deteriorates, the nucleus shrinks and becomes fragmented, the Fluo-4 stain intensifies and signal a sharp increase in intracellular free calcium concentration, and the TMRM stain diminishes as a result of reduction in mitochondrial membrane potential.

Figure 2.6 shows the average result of our multiplexed cytotoxicity fingerprinting. Overall, cell count appears to be the most sensitive indicator of cytotoxicity, as significant changes in cell count tend to occur at a much lower QD concentration than the other parameters. In addition, the largest difference between the toxicity profiles of TGA-QDs and Gelatin-QDs treated cells is observed in this fluorescence parameter. For Gelatin-QD and TGA-QD treated cells, the cell count falls below 70% at 12.5nM and 1.56nM respectively in undifferentiated cells and at 1.56nM and 0.39nM respectively in

differentiated cells. Similar findings are observed in the other parameters, where the onset of change in fluorescence parameters (except nuclear area) consistently occurs at a lower QD concentration in TGA-QD treated cells and in differentiated cells. These differences are summarized in Table 2.1 and have two implications. (1) It is confirmed that the Gelatin-QDs are less cytotoxic and more biocompatible than the TGA-QDs. The gelatin-CdTe nanocomposite reduced the sublethal concentration (>30% cell death) of CdTe QDs by at least 4 times in both undifferentiated and differentiated cells (Table 2.1). This outcome validates our rationale behind the incorporation of biological molecules in the synthesis of NPs as a mean to achieve better stability and biocompatibility. We have to keep in mind that the toxic effect of CdTe made in a general synthetic rout described here can never be eliminated but modified or reduced and we use these NPs here as a model system. We also have to reiterate that although some of the observed differences between the two QDs could potentially be interpreted as marginal, the fact is that in systems implementing HCS principles a 5-15% difference represents a consistent and significant response because of the large cell population being analyzed. The close resemblance between the toxicity profiles of TGA-QDs and Gelatin-QDs also indicates that their toxicity share a common source, which most likely comes from the leakage of cadmium from the core of the NPs. (2) As already indicated by the apoptosis/necrosis assay, is that differentiated cells are more sensitive and vulnerable to QD-induced cytotoxicity, which is somewhat surprising because they are generally regarded as more sensitive to the environment. The large number of fragmented nuclei (Figure 2.5, last row) observed at high QD concentrations again confirms apoptosis as the primary cellular response to the

QD-induced cytotoxicity. Beside the larger scale of decrease in cell count and mitochondrial membrane potential observed in differentiated cells, the hormetic response in the nuclear area observed in undifferentiated cells is absent in differentiated cells and is replaced by marginal reduction. While the mitochondrial membrane potential of undifferentiated cells follows an inverse decay, the same parameter appears to decay exponentially in differentiated cells and could possibly explain their vulnerability to QD-induced apoptosis. We suspect these differences in cellular response arise from changes in biological machinery as cells differentiate.[49] Changes involving mitochondria, membrane structures, and protein modifications may account for the higher sensitivity of differentiated neurons to cytotoxic substances.[50]

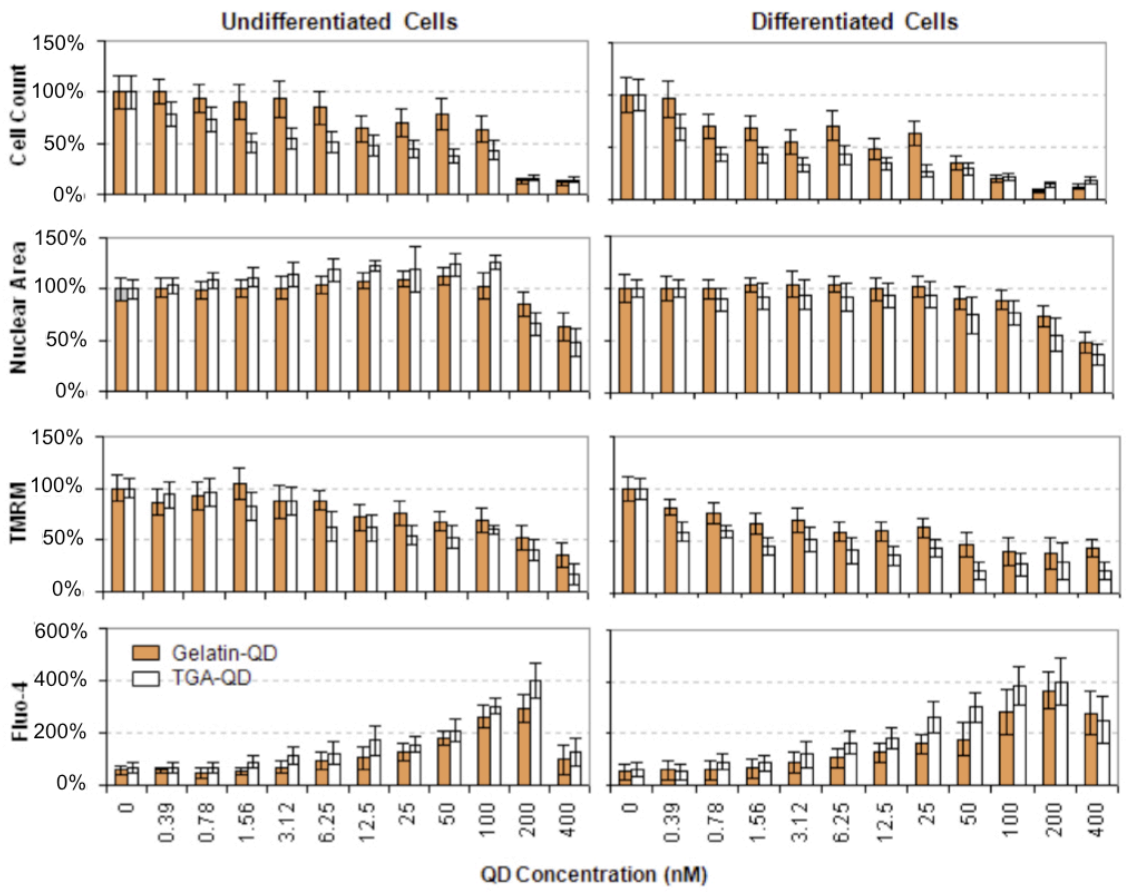

Figure 2.6 Cytotoxic effects of TGA-QDs (white bars) and Gelatin-QDs (gray bars) in NG108-15 cells. Undifferentiated (left half) and differentiated (right half) cells were treated with QDs for 24 h and assayed for cell number (Hoechst 33342; top), nuclear area (Hoechst 33342; second from top), mitochondrial membrane potential (TMRM; third from top), and intracellular ionized Ca (Fluo-4; bottom). At each concentration, 5 independent fields were imaged and analyzed. Data is expressed as average of 3 independent runs.

	Onset of Change			
	Undifferentiated		Differentiated	
Fluorescence Parameters	***Gelatin-QD***	***TGA-QD***	***Gelatin-QD***	***TGA-QD***
Cell Count (below 70%)	12.5nM	1.56nM	1.56nM	0.39nM
Nuclear Area (10% deviation)	25nM	1.56nM	100nM	50nM
TMRM (below 70%)	50nM	6.26nM	6.25nM	0.39nM
Fluo-4 (above 30%)	25nM	6.25nM	12.6nM	3.12nM

Table 2.1 A summary of the onset of change in each of the 4 fluorescence parameters.

2.4.2 Gold Nanoparticles

As an extension to the CdTe QD study, we employed the multiplexed cytotoxicity assay to study the effect of gold NPs (Au NPs) on HepG2 human hepatocellular carcinoma cells. We have recently demonstrated the use of gold NPs for early detection of cancerous tumors and inflammatory responses by photoacoustic imaging.[22, 51] Considering the numerous functionalization strategies available for Au NPs, the ability to characterize toxicity using a HCS platform will be immensely valuable for the development of biomedical applications. We chose the HepG2 cells because they are one of the most commonly used cell types for HCS studies and have implications for metal poisoning associated with hepatic toxicities.

Our study with Au NPs differs from those with CdTe QDs in a couple ways. In addition to the use of a different cell line, the Au NP study aims to determine the effect of exposure duration to the NPs, as well as post-exposure changes in cell physiology, while

the previous studies focus on the concentration-dependent effect of NPs. To investigate these effects, we treated HepG2 cells with Au NPs for various lengths of time (0, 1, 2, 4, and 6 h). Following the Au NP treatment, cells were washed with PBS and allowed to grow in fresh medium for an additional period of time (1, 2, and 4 days). Similar to the previous studies on NG108-15 cells, HepG2 cells were analyzed for nuclei count, nuclear area, mitochondrial membrane potential, and intracellular free calcium concentration by incubating with a cocktail of dye solutions and imaging with the IN Cell Analyzer 1000 HCS system to achieve complete fingerprinting of cellular response.

Our data suggests that Au NPs inhibited the proliferation of HepG2 cells. Figure 7 shows that although cell number appears to be relatively constant across different treatment times on day 1 and day 2 following Au NP treatment, it becomes inversely proportional to treatment time on day 4. Stronger inhibitory effect was observed with increasing exposure time to Au NPs. The inhibition of proliferation by Au NPs has been reported in other cells including endothelial cells and multiple myeloma cells.[52-54] Au NPs have been found to bind to and block the function of proteins that are essential for cell proliferation. In addition, Au NPs can also block and disrupt certain cellular signaling pathways that required for growth and survival. In our study, this inhibitory effect was also accompanied by enlargement in the nuclear area. Cells having the longest exposure to Au NPs had an average nuclear area that was 13% larger than the untreated cells on day 4 after treatment. The concentration and exposure times of Au NPs employed in this study were shown to be only mildly cytotoxic to the HepG2 cells. Changes in the cellular mitochondrial membrane potential and intracellular free calcium

concentration never deviated more than 10% from the untreated control. Treatment with Au NP reduced the mitochondrial membrane potential, which is a typical cellular response to cytotoxic material. The reduction was only apparent after 4 days following treatment and increased slightly with increasing exposure time. While cytotoxic stimulation typically leads to an increase in intracellular free calcium concentration, we unexpectedly observed a decrease in intracellular free calcium concentration 1 day following the Au NP treatment. The decrease appeared to be proportional to the exposure time, reaching approximately 10% for the longest exposed cells (6h). Interestingly, the drop in intracellular free calcium concentration recovered by itself to the normal level as the culture time increased. The rate of recovery was inversely proportional to the exposure time, with the cells having the shortest exposure to Au NPs (1h) making the quickest recovery. These findings indicate that the Au NPs inhibited intracellular calcium release in the HepG2 cells. Similar findings have also been reported for endothelial cells.[54] In our study, we also found this inhibitory effect by Au NPs to be reversible once the Au NPs are removed and the cells are allowed to recuperate in fresh medium.

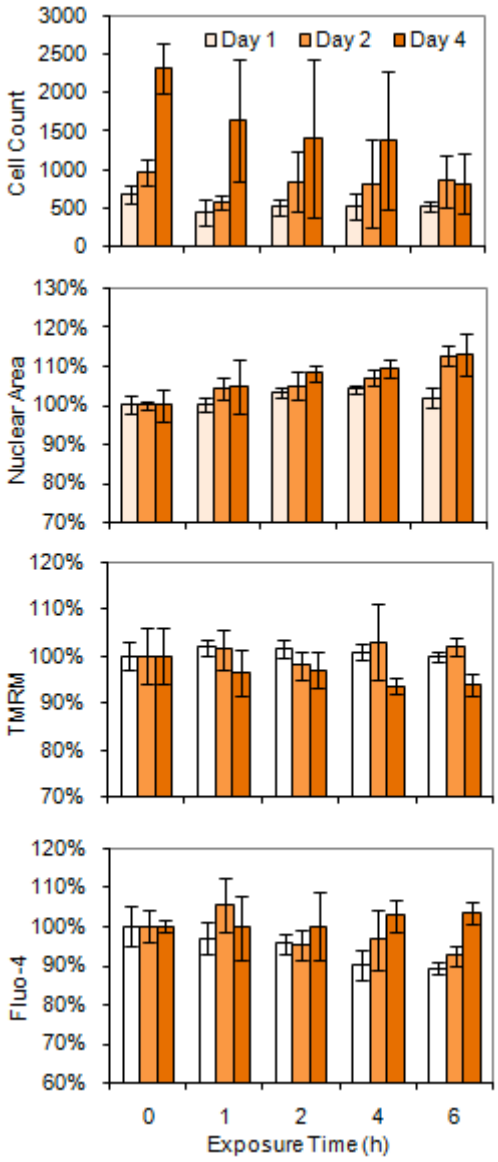

Figure 2.7 Cytotoxic effects of gold NPs in HepG2 cells. HepG2 cells were treated with gold NPs for 0, 1, 2, 4, and 6h and assayed for cell number (Hoechst 33342; top), nuclear area (Hoechst 33342; second from top), mitochondrial membrane potential (TMRM; third from top), and intracellular ionized Ca (Fluo-4; bottom) 1, 2, and 4 days after treatment. Data is expressed as average of 4 independent runs.

2.4.3 Dispersed Carbon Nanotubes and Carbon Nanotube Thin Films

As a final demonstration, we again employed the multiplexed cytotoxicity assay to study the effect of carbon nanotubes (CNTs) on NG108-15 murine neuroblastoma cells. We are interested in the cytotoxicity of CNTs in two different modes: free CNTs in the dispersed form and immobilized CNTs as thin films. Although there have been intensive research efforts exploring biological applications of CNTs,[55, 56] studies investigating the cytotoxicity of CNTs have generated conflicting results. While researchers have found dispersed CNTs to exert a wide range of effects, ranging from indirect and minimal to severely cytotoxic,[57, 58] studies have found immobilized CNT matrixes and substrates to produce little to no cytotoxicity and in some cases even enhanced cellular functions.[59, 60] As these studies were motivated by vastly different goals and employed different experimental methods, the development of a universal assay for evaluating the cytotoxic effects of dispersed and immobilized CNTs can provide a more objective viewpoint on the cytotoxicity of CNT-based nanostructures and create a model platform for future studies of functionalized CNTs and CNT-based substrates.

In this study, NG108-15 cells were treated with culture medium containing various concentrations of single-walled carbon nanotubes (SWNTs) dispersed with poly(sodium 4-styrene-sulfonate) (PSS). To eliminate any differences caused by the presence of dispersing reagent,[61] all treatments, including the control, were prepared with the same concentration of PSS. In addition, cells were also cultured on polystyrene culture plate coated with SWNT thin films fabricated from the layer-by-layer (LBL)

assembly of poly(vinyl alcohol) (PVA) with PSS-dispersed SWNTs (SWNT-PSS). Thin films of SWNTs were assembled with PVA solutions at a pH value of 2, 6 or 10 and fabricated to a total of 2 or 6 bilayers of PVA/SWNT-PSS. Following 48 hours of treatment, cells were washed with PBS, incubated with a cocktail of dye solutions, and imaged with the IN Cell Analyzer 1000 HCS system to analyze for nuclei count, nuclear area, mitochondrial membrane potential, and intercellular free calcium.

Our data shows that all of the SWNT LBL films we tested displayed minimal degree of cytotoxicity regardless of the number of bilayers and the pH of the PVA solution used to assemble the films. As illustrated by Figure 2.8, for cells cultured on the SWNT thin films, the four parameters examined by the assay remained relatively constant and close to the level exhibited by the untreated control group, indicating that the SWNT LBL films are inert and behave like the polystyrene cell culture plate. Figure 2.8 shows a small drop in the nuclear area for cells cultured on SWNT LBL films with a thickness of 6 bilayers. However, this effect is absent for cells on the 2-bilayer films. We suspect this is an artifact from the automated HCS imaging system caused by the opaqueness of SWNTs in the thicker 6-bilayer films. The slight loss of transparency was an issue for measurements relying on the area and intensity of the fluorescence staining, but not so much for the measurement of cell count, which tallies the total number of stained cell nuclei. We were able to correct the fluorescence intensity measurements of TMRM and Fluo-4 using a reference culture plate to reflect the true values. However, without a simple and reliable fix, the nuclear area measurements were not adjusted, and therefore the data presented here does not account for the reduction in software-

determined nuclear area as a result of decreased transparency of the culture substrates. Nevertheless, with the reduced nuclear area measurements at above 80%, and along with the data from the other parameters, the outcome still indicates a very healthy cell culture on the SWNT LBL films, demonstrating their potential as a biocompatible material for neural cells.

For cells treated with dispersed SWNTs, cytotoxicity was observed to increase with SWNT concentration. Mitochondrial membrane potential, which was probed with TMRM, was the most sensitive indicator of cytotoxicity. While, a SWNT concentration of just 0.8 μg/ml caused the fluorescence intensity of TMRM to fall below 80%, all other parameters were unchanged. Another noticeable difference in the cytotoxicity profiles is the change in intracellular free calcium concentration with respect to SWNT concentration. While the profiles for cell count, nuclear area, and mitochondrial membrane potential followed similar pattern as those obtained in the CdTe QD study, here the intracellular free calcium concentration did not increase with raising SWNT concentration but instead remained largely unchanged. This could be an indication that a different mechanism might be at play in generating cytotoxicity in response to the SWNT treatment. In this study, we found that a relatively high concentration of SWNTs (>25 μg/ml) was required to inhibit cell proliferation or cause significant cell death. At the same time, low concentrations of SWNTs were sufficient to disrupt the mitochondrial membrane potential considerably, which has been reported previously.[62] Judging from this result, it's likely that prolong exposure with SWNTs could elicit more enhanced level of cytotoxicity at lower concentrations.

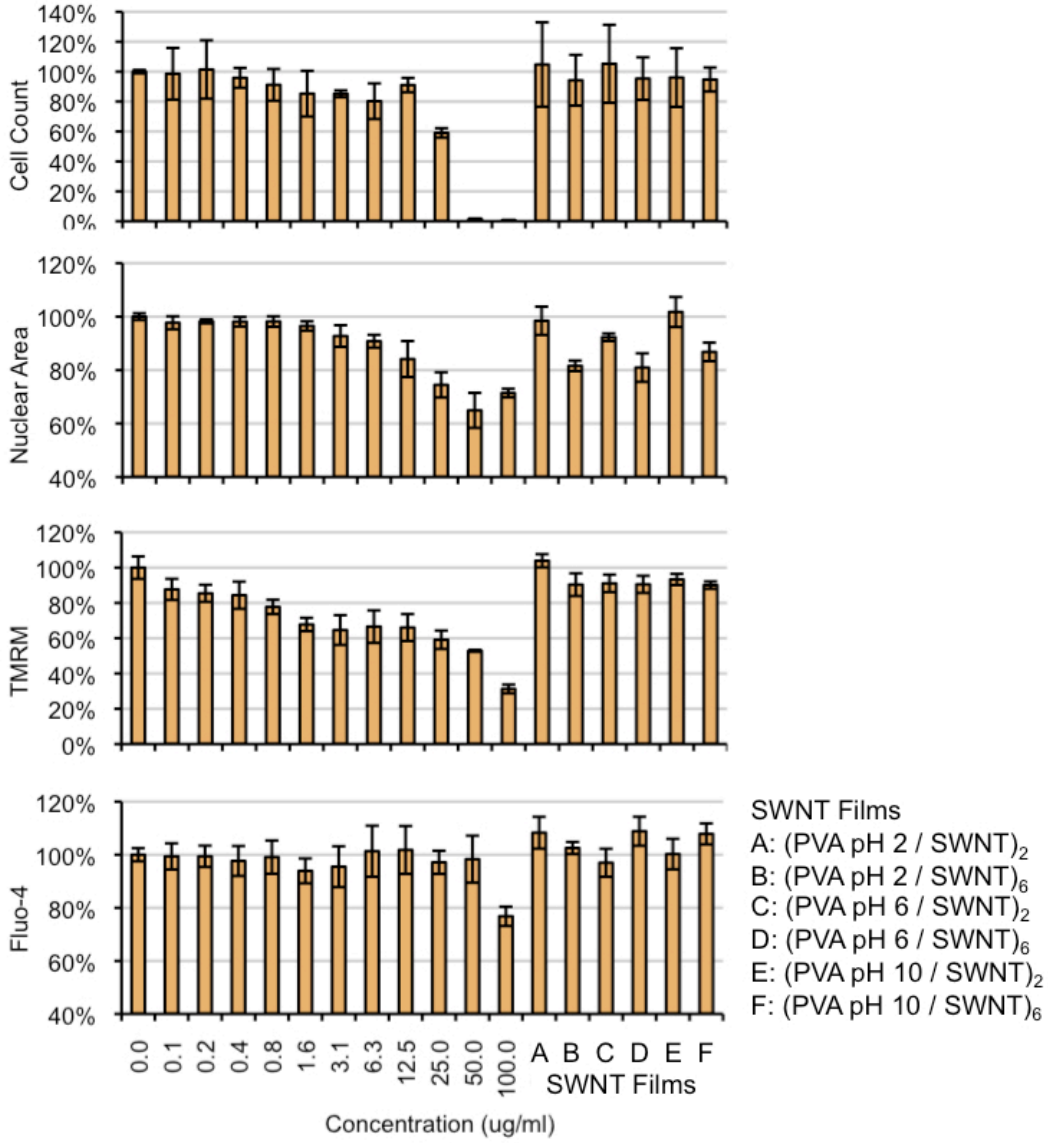

Figure 2.8 Cytotoxic effects of dispersed SWNTs and SWNT LBL films in NG108-15 cells. NG108-15 neuroblastoma cells were seeded on SWNT LBL films or treated with dispersed SWNTs for 48h and assayed for cell number (Hoechst 33342; top), nuclear area (Hoechst 33342; second from top), mitochondrial membrane potential (TMRM; third from top), and intracellular ionized Ca (Fluo-4; bottom). At each treatment, five independent fields were imaged and analyzed. Data is expressed as average of 3 independent runs.

2.5 Conclusions

In summary, we have demonstrated the use of various HCS assays to study the cytotoxicity of CdTe QDs, Au NPs, CNTs, and LBL films of CNTs in NG108-15 neuroblastoma cells and HepG2 human hepatocellular carcinoma cells. We found the neurite outgrowth assay, which assesses the functionality of differentiated neural cells, to be particularly important and the multiplexed cytotoxicity assay as a sensitive and informative assessment of toxicological mechanisms. The versatility of the multiplexed cytotoxicity assay was demonstrated across the different nanomaterials tested in this study. The assays were capable of distinguishing the subtle differences in the cytotoxicity generated by TGA-QDs and Gelatin-QDs. The Gelatin-NPs, which were synthesized in the presence of gelatin, provided insight for surface modification and bio-functionalization of NPs. Most importantly, we demonstrated that undifferentiated and differentiated NG108-15 neuroblastoma cells respond differently to CdTe QD-induced cytotoxicity. Specifically, the differentiated cells are more sensitive and vulnerable to QD treatment, which can be understood as the demonstration of adaptability of cells in undifferentiated state. This difference should be taken into account in the establishment of treatment dosage for any NP-based biological studies or therapies. Using the multiplexed cytotoxicity assay, we were able to uncover the inhibitory effect of Au NPs on cell growth and release of intracellular free calcium in HepG2 cells. In addition, we were also able to examine the cytotoxic effects of dispersed CNTs and CNT LBL films, demonstrating that free CNTs induced a drop in mitochondrial membrane potential while the CNT LBL films appeared to be biocompatible.

The cytotoxicity profiles generated from the multiplexed cytotoxicity assay can be regarded as the "fingerprints" of the corresponding nanomaterials. The multiparametric nature of these profiles will allow cytotoxicity analyses to be conducted at much higher throughput and accuracy in the future. Importantly, we demonstrate here that the application of HCS technology in the study of nanomaterials is not limited to the cytotoxicity of colloidal NPs, but is also suitable for the assessment of biocompatibility of multilayer thin films produced from LBL assembly. We believe HCS technology can also be extremely useful for the study of the transport and localization of engineered NPs and CNTs in living cells. Such an endeavor could shed light on the development of new drugs and drug delivery strategies based on nanomaterials.

We also consider it essential to mention here that the presented modality of the technique also has a significant limitation that needs to be addressed. It is related to the two-dimensional nature of cell cultures currently used in HCA most often. Cellular response in 2D cell cultures was shown to be different than cells in the natural tissue environment. More adequate 3D cell cultures techniques need to be developed. HCA does afford analysis of 3D images in a similar way as we presented here; however, the 3D approach will indeed require development of appropriate 3D matrixes (scaffolds), cell culture techniques, and refinement of software algorithms for image analysis. A suitable matrix must be transparent, mechanically robust, very biocompatible, and exceptionally standardized. Hydrogel matrixes made with geometry of inverted colloidal crystals[63, 64] and potentially some other sharing the properties[65, 66] mentioned above can be successfully used for this task.

2.6 References

1. Zhang, Z. L.; Tang, Z. Y.; Kotov, N. A.; Glotzer, S. C., Simulations and Analysis of Self-Assembly of CdTe Nanoparticles into Wires and Sheets. *Nano Lett.* **2007,** *7* (6), 1670-1675.

2. Sarikaya, M.; Tamerler, C.; Jen, A. K. Y.; Schulten, K.; Baneyx, F., Molecular biomimetics: nanotechnology through biology. *Nat Mater* **2003,** *2* (9), 577-585.

3. Tang, Z.; Zhang, Z.; Wang, Y.; Glotzer, S. C.; Kotov, N. A., Self-Assembly of CdTe Nanocrystals into Free-Floating Sheets. *Science* **2006,** *314* (5797), 274-278.

4. Oberdorster, G.; Oberdorster, E.; Oberdorster, J., Nanotoxicology: An emerging discipline evolving from studies of ultrafine particles. *Environmental Health Perspectives* **2005,** *113* (7), 823-839.

5. Stone, V.; Donaldson, K., Nanotoxicology - Signs of stress. *Nature Nanotechnology* **2006,** *1* (1), 23-24.

6. Donaldson, K.; Stone, V.; Tran, C. L.; Kreyling, W.; Borm, P. J. A., Nanotoxicology. *Occup Environ Med* **2004,** *61* (9), 727-728.

7. Klostranec, J. M.; Chan, W. C. W., Quantum dots in biological and biomedical research: Recent progress and present challenges. *Advanced Materials* **2006,** *18* (15), 1953-1964.

8. Kirchner, C.; Liedl, T.; Kudera, S.; Pellegrino, T.; Javier, A. M.; Gaub, H. E.; Stolzle, S.; Fertig, N.; Parak, W. J., Cytotoxicity of colloidal CdSe and CdSe/ZnS nanoparticles. *Nano Letters* **2005,** *5* (2), 331-338.

9. Derfus, A. M.; Chan, W. C. W.; Bhatia, S. N., Probing the cytotoxicity of semiconductor quantum dots. *Nano Letters* **2004,** *4* (1), 11-18.

10. Hoshino, A.; Fujioka, K.; Oku, T.; Suga, M.; Sasaki, Y. F.; Ohta, T.; Yasuhara, M.; Suzuki, K.; Yamamoto, K., Physicochemical properties and cellular toxicity of nanocrystal quantum dots depend on their surface modification. *Nano Letters* **2004,** *4* (11), 2163-2169.

11. Hardman, R., A toxicologic review of quantum dots: Toxicity depends on physicochemical and environmental factors. *Environmental Health Perspectives* **2006,** *114* (2), 165-172.

12. Giuliano, K. A.; Haskins, J. R.; Taylor, D. L., Advances in High Content Screening for Drug Discovery. *ASSAY and Drug Development Technologies* **2003,** *1* (4), 565-577.

13. Comley, J., High Content Screening - Emerging Importance of Novel Reagents/Probes and Pathway Analysis. *Drug Disc. World* **Summer 2005**, 31-53.

14. Zhang, T. T.; Stilwell, J. L.; Gerion, D.; Ding, L. H.; Elboudwarej, O.; Cooke, P. A.; Gray, J. W.; Alivisatos, A. P.; Chen, F. F., Cellular effect of high doses of silica-coated quantum dot profiled with high throughput gene expression analysis and high content cellomics measurements. *Nano Letters* **2006,** *6* (4), 800-808.

15. Michalet, X.; Pinaud, F. F.; Bentolila, L. A.; Tsay, J. M.; Doose, S.; Li, J. J.; Sundaresan, G.; Wu, A. M.; Gambhir, S. S.; Weiss, S., Quantum dots for live cells, in vivo imaging, and diagnostics. *Science* **2005,** *307* (5709), 538-544.

16. Jaiswal, J. K.; Mattoussi, H.; Mauro, J. M.; Simon, S. M., Long-term multiple color imaging of live cells using quantum dot bioconjugates. *Nature Biotechnology* **2003,** *21* (1), 47-51.

17. Parak, W. J.; Gerion, D.; Pellegrino, T.; Zanchet, D.; Micheel, C.; Williams, S. C.; Boudreau, R.; Le Gros, M. A.; Larabell, C. A.; Alivisatos, A. P., Biological applications of colloidal nanocrystals. *Nanotechnology* **2003,** *14* (7), R15-R27.

18. Medintz, I. L.; Uyeda, H. T.; Goldman, E. R.; Mattoussi, H., Quantum dot bioconjugates for imaging, labelling and sensing. *Nature Materials* **2005,** *4* (6), 435-446.

19. Thomas, M.; Klibanov, A. M., Conjugation to gold nanoparticles enhances polyethylenimine's transfer of plasmid DNA into mammalian cells. *Proceedings of the National Academy of Sciences* **2003,** *100* (16), 9138-9143.

20. Hirsch, L. R.; Stafford, R. J.; Bankson, J. A.; Sershen, S. R.; Rivera, B.; Price, R. E.; Hazle, J. D.; Halas, N. J.; West, J. L., Nanoshell-mediated near-infrared thermal therapy of tumors under magnetic resonance guidance. *Proceedings of the National Academy of Sciences* **2003,** *100* (23), 13549-13554.

21. Chen, J.; Wiley, B.; Li, Z. Y.; Campbell, D.; Saeki, F.; Cang, H.; Au, L.; Lee, J.; Li, X.; Xia, Y., Gold Nanocages: Engineering Their Structure for Biomedical Applications. *Advanced Materials* **2005,** *17* (18), 2255-2261.

22. Eghtedari, M.; Oraevsky, A.; Copland, J. A.; Kotov, N. A.; Conjusteau, A.; Motamedi, M., High Sensitivity of In Vivo Detection of Gold Nanorods Using a Laser Optoacoustic Imaging System. *Nano Lett.* **2007,** *7* (7), 1914-1918.

23. Copland, J. A.; Eghtedari, M.; Popov, V. L.; Kotov, N.; Mamedova, N.; Motamedi, M.; Oraevsky, A. A., Bioconjugated gold nanoparticles as a molecular based contrast agent: Implications for imaging of deep tumors using optoacoustic tomography. *Molecular Imaging and Biology* **2004,** *6* (5), 341-349.

24. Gomez, N.; Winter, J. O.; Shieh, F.; Saunders, A. E.; Korgel, B. A.; Schmidt, C. E., Challenges in quantum dot-neuron active interfacing. *Talanta* **2005,** *67* (3), 462-471.

25. Pathak, S.; Cao, E.; Davidson, M. C.; Jin, S. H.; Silva, G. A., Quantum dot applications to neuroscience: New tools for probing neurons and glia. *Journal of Neuroscience* **2006,** *26* (7), 1893-1895.

26. Vu, T. Q.; Maddipati, R.; Blute, T. A.; Nehilla, B. J.; Nusblat, L.; Desai, T. A., Peptide-conjugated quantum dots activate neuronal receptors and initiate downstream signaling of neurite growth. *Nano Letters* **2005,** *5* (4), 603-607.

27. Dahan, M.; Levi, S.; Luccardini, C.; Rostaing, P.; Riveau, B.; Triller, A., Diffusion dynamics of glycine receptors revealed by single-quantum dot tracking. *Science* **2003,** *302* (5644), 442-445.

28. Jackson, H.; Muhammad, O.; Daneshvar, H.; Nelms, J.; Popescu, A.; Vogelbaum, M. A.; Bruchez, M.; Toms, S. A., Quantum dots are phagocytized by macrophages and colocalize with experimental gliomas. *Neurosurgery* **2007,** *60* (3), 524-529.

29. Winter, J. O.; Gomez, N.; Korgel, B. A.; Schmidt, C. E. In *Quantum dots for electrical stimulation of neural cells*, Nanobiophotonics and Biomedical Applications II, San Jose, CA, USA, SPIE: San Jose, CA, USA, 2005; pp 235-246.

30. Winter, J. O.; Liu, T. Y.; Korgel, B. A.; Schmidt, C. E., Recognition molecule directed interfacing between semiconductor quantum dots and nerve cells. *Advanced Materials* **2001,** *13* (22), 1673-1677.

31. Pappas, T. C.; Wickramanyake, W. M. S.; Jan, E.; Motamedi, M.; Brodwick, M.; Kotov, N. A., Nanoscale engineering of a cellular interface with semiconductor nanoparticle films for photoelectric stimulation of neurons. *Nano Letters* **2007,** *7* (2), 513-519.

32. Tran, P. A.; Zhang, L. J.; Webster, T. J., Carbon nanofibers and carbon nanotubes in regenerative medicine. *Advanced Drug Delivery Reviews* **2009,** *61* (12), 1097-1114.

33. Chao, T. I.; Xiang, S. H.; Chen, C. S.; Chin, W. C.; Nelson, A. J.; Wang, C. C.; Lu, J., Carbon nanotubes promote neuron differentiation from human embryonic stem cells. *Biochemical and Biophysical Research Communications* **2009,** *384* (4), 426-430.

34. Jan, E.; Kotov, N. A., Successful differentiation of mouse neural stem cells on layer-by-layer assembled single-walled carbon nanotube composite. *Nano Letters* **2007,** *7* (5), 1123-1128.

35. Cellot, G.; Cilia, E.; Cipollone, S.; Rancic, V.; Sucapane, A.; Giordani, S.; Gambazzi, L.; Markram, H.; Grandolfo, M.; Scaini, D.; Gelain, F.; Casalis, L.; Prato, M.; Giugliano, M.; Ballerini, L., Carbon nanotubes might improve neuronal performance by favouring electrical shortcuts. *Nature Nanotechnology* **2009,** *4* (2), 126-133.

36. Stephen J. Byrne; Williams, Y.; Davies, A.; Corr, Serena A.; Rakovich, A.; Gun'ko, Yurii K.; Rakovich, Yury P.; Donegan, John F.; Volkov, Y., "Jelly Dots": Synthesis and Cytotoxicity Studies of CdTe Quantum Dot-Gelatin Nanocomposites. *Small* **2007,** *3* (7), 1152-1156.

37. Chan, W. H.; Shiao, N. H.; Lu, P. Z., CdSe quantum dots induce apoptosis in human neuroblastoma cells via mitochondrial-dependent pathways and inhibition of survival signals. *Toxicology Letters* **2006,** *167* (3), 191-200.

38. Calabrese, E. J.; Baldwin, L. A., Applications of hormesis in toxicology, risk assessment and chemotherapeutics. *Trends in Pharmacological Sciences* **2002,** *23*, 331-337.

39. O'Brien, P. J.; Irwin, W.; Diaz, D.; Howard-Cofield, E.; Krejsa, C. M.; Slaughter, M. R.; Gao, B.; Kaludercic, N.; Angeline, A.; Bernardi, P.; Brain, P.; Hougham, C., High concordance of drug-induced human hepatotoxicity with in vitro cytotoxicity measured in a novel cell-based model using high content screening. *Archives of Toxicology* **2006,** *80* (9), 580-604.

40. Xu, J. J.; Diaz, D.; O'Brien, P. J., Applications of cytotoxicity assays and pre-lethal mechanistic assays for assessment of human hepatotoxicity potential. *Chemico-Biological Interactions* **2004,** *150* (1), 115-128.

41. Plymale, D. R.; Haskins, J. R.; Iglesia, F. A. d. l., Monitoring simultaneous subcellular events in vitro by means of coherent multiprobe fluorescence. *Nat Med* **1999,** *5* (3), 351-355.

42. Kann, O.; Kovacs, R., Mitochondria and neuronal activity. *Am J Physiol Cell Physiol* **2007,** *292* (2), C641-657.

43. Nicholls, D. G., Mitochondrial membrane potential and aging. *Aging Cell* **2004,** *3*, 35-40.

44. Orrenius, S.; Nicotera, P., The Calcium-Ion and Cell-Death. *Journal of Neural Transmission-Supplement* **1994,** (43), 1-11.

45. Monteith, G. R.; Bird, G. S. J., Techniques: High-throughput measurement of intracellular Ca2+ - back to basics. *Trends in Pharmacological Sciences* **2005,** *26* (4), 218-223.

46. Mattson, M. P., Calcium and neurodegeneration. *Aging Cell* **2007,** *6*, 337-350.

47. Chin, T.-Y.; Hwang, H.-M.; Chueh, S.-H., Distinct Effects of Different Calcium-Mobilizing Agents on Cell Death in NG108-15 Neuroblastoma X Glioma Cells. *Mol Pharmacol* **2002,** *61* (3), 486-494.

48. Orrenius, S.; McCabe, M. J.; Nicotera, P., Ca2+-dependent mechanisms of cytotoxicity and programmed cell death. *Toxicology Letters* **1992,** *64-65*, 357-364.

49. Zornetzer, M. S.; Stein, G. S., Gene Expression in Mouse Neuroblastoma Cells: Properties of the Genome. *PNAS* **1975,** *72* (8), 3119-3123.

50. Clarkson, E. D.; Edwards-Prasad, J.; Freed, C. R.; Prasad, K. N., Immortalized Dopamine Neurons: A Model to Study Neurotoxicity and Neuroprotection. *Proc Soc Exp Biol Med* **1999,** *222* (2), 157-163.

51. Kim, K.; Huang, S. W.; Ashkenazi, S.; O'Donnell, M.; Agarwal, A.; Kotov, N. A.; Denny, M. F.; Kaplan, M. J., Photoacoustic imaging of early inflammatory response using gold nanorods. *Applied Physics Letters* **2007,** *90* (22).

52. Bhattacharya, R.; Mukherjee, P.; Xiong, Z.; Atala, A.; Soker, S.; Mukhopadhyay, D., Gold nanoparticles inhibit VEGF165-induced proliferation of HUVEC cells. *Nano Letters* **2004,** *4* (12), 2479-2481.

53. Bhattacharya, R.; Patra, C. R.; Verma, R.; Kumar, S.; Greipp, P. R.; Mukherjee, P., Gold nanoparticles inhibit the proliferation of multiple myeloma cells. *Advanced Materials* **2007,** *19* (5), 711-716.

54. Mukherjee, P.; Bhattacharya, R.; Wang, P.; Wang, L.; Basu, S.; Nagy, J. A.; Atala, A.; Mukhopadhyay, D.; Soker, S., Antiangiogenic properties of gold nanoparticles. *Clinical Cancer Research* **2005,** *11* (9), 3530-3534.

55. Bianco, A.; Kostarelos, K.; Partidos, C. D.; Prato, M., Biomedical applications of functionalised carbon nanotubes. *Chemical Communications* **2005,** (5), 571-577.

56. Harrison, B. S.; Atala, A., Carbon nanotube applications for tissue engineering. *Biomaterials* **2007,** *28* (2), 344-353.

57. Tian, F. R.; Cui, D. X.; Schwarz, H.; Estrada, G. G.; Kobayashi, H., Cytotoxicity of single-wall carbon nanotubes on human fibroblasts. *Toxicology in Vitro* **2006,** *20* (7), 1202-1212.

58. Cui, D. X.; Tian, F. R.; Ozkan, C. S.; Wang, M.; Gao, H. J., Effect of single wall carbon nanotubes on human HEK293 cells. *Toxicology Letters* **2005,** *155* (1), 73-85.

59. Hu, H.; Ni, Y. C.; Montana, V.; Haddon, R. C.; Parpura, V., Chemically functionalized carbon nanotubes as substrates for neuronal growth. *Nano Letters* **2004,** *4* (3), 507-511.

60. Zanello, L. P.; Zhao, B.; Hu, H.; Haddon, R. C., Bone cell proliferation on carbon nanotubes. *Nano Letters* **2006,** *6* (3), 562-567.

61. Lifeng, D.; et al., Cytotoxicity of single-walled carbon nanotubes suspended in various surfactants *Nanotechnology* **2008,** *19* (25), 255702.

62. Haifei, X.; et al., Multi-walled carbon nanotubes suppress potassium channel activities in PC12 cells. *Nanotechnology* **2009,** *20* (28), 285102.

63. Kotov, N. A., Inverted colloidal crystals as three-dimensional cell scaffolds. *Langmuir* **2004,** *20* (19), 7887-7892.

64. Lee, J.; Lee, J., Inverted colloidal crystals as three-dimensional microenvironments for cellular co-cultures. *Journal of materials chemistry* **2006,** *16* (35), 3558-3564.

65. Yokoi, H.; Kinoshita, T.; Zhang, S., Dynamic reassembly of peptide RADA16 nanofiber scaffold. *Proceedings of the National Academy of Sciences* **2005,** *102* (24), 8414-8419.

66. Stachowiak, A. N.; Bershteyn, A.; Tzatzalos, E.; Irvine, D. J., Bioactive Hydrogels with an Ordered Cellular Structure Combine Interconnected Macroporosity and Robust Mechanical Properties. *Advanced Materials* **2005,** *17* (4), 399-403.

CHAPTER 3

Biocompatibility of Layer-by-Layer Assembled Single-Walled Carbon Nanotube Composites with Neural Stem Cells

3.1 Abstract

The same properties that made carbon nanotube (CNT) composites interesting for electronics, sensing and ultrastrong structural materials also make them an asset for biomedical engineering. The combination of electron conductivity, corrosion resistance and strength are essential for neuroprosthetic devices. All the studies in this area demonstrating cellular adhesion and signal transduction activity on CNT matrixes were conducted, so far, with terminally differentiated primary cells and cancerous cell lines. Neural stem cells are very plastic neural precursors capable of adapting to environmental conditions and recreating signal transduction pathways. Their intrinsic biological functionality not only makes the transition to stem cell cultures a difficult-to-avoid step but also implies several fundamentally important challenges. Here we demonstrate that mouse embryonic neural stem cells (NSCs) from the cortex can be successfully differentiated to neurons, astrocytes, and oligodendrocytes with clear formation of

neurites on layer-by-layer (LBL) assembled single-walled carbon nanotube (SWNT)-polyelectrolyte multilayer thin films. Biocompatibility, neurite outgrowth, and expression of neural markers were similar to those differentiated on poly-L-ornithine (PLO), one of the most widely used growth substratums for neural stem cells.

3.2 Introduction

The development of nanotechnology is penetrating biology and medicine at a remarkable speed.[1] Nanotechnology is poised to provide new tools to measure and understand biosystems,[2, 3] bring insights to challenges in biotechnology and biomedicine,[4, 5] and offer building components for advanced biomaterials.[6, 7] One area that will significantly benefit from the development of nanoscale engineering is the technology for neural medicine in its many manifestations.[8] The reasons are multifold:

(1) Nanomaterials were originally developed and still have the most widespread applicability for electronics and information processing which makes their functionalities quite similar to those of neural system.

(2) The neural tissue is highly complex in its anatomy, functional structuring, and information processing, which frustrates the applications of current technologies and requires the change of technological paradigm.

(3) The central nervous system is difficult to access and has a heterogeneous cellular and molecular environment, which, in turn, means that size reduction of any devices to interact with neurons is required to create the least possible interference with and disruption to the central nervous system's functionality.

Indeed, recently we are beginning to see emerging applications of nanotechnology in neuroscience using primarily organic and polymeric materials as scaffolds. In this study, we focus on the development of a new platform biomaterial based on single-walled carbon nanotubes (SWNTs) that can find applications in the treatment of neurological disorders and injuries. Why carbon nanotubes? The unique physical, chemical, mechanical, and electronic properties of carbon nanotubes[9-14] can be, in part, transferred into SWNT composites to combine high electrical conductivity, chemical stability, and physical strength with structural flexibility.[15-19] Such a unique combination of characteristics and the possibility for surface functionalization[20, 21] make these SWNT composites promising candidates for making neural prosthetic devices with capabilities for electrical field recording, sensing of neurotransmitters, and electrical stimulation. For example, several neurological disorders and injuries, such as Parkinson's disease, epilepsy, and stroke require an implantable device to generate electrical activity in the damaged or diseased tissue. One common problem of all chronically implanted electrodes lies in the tissue-electrode interface.[22] Tissue reactions typically lead to encapsulation around the electrode, reducing its performance and lifetime. Current neural prosthetic technology is in active search of a biocompatible material that allows chronic implantation of miniaturized electrodes.[23, 24] SWNT composites can exactly

satisfy these demands by providing a durable, electrically conductive, highly modifiable, and biocompatible interface for permanent long-term implantations. Various strategies can be similarly applied to SWNT composites to attract growing neurites[25, 26] and reduce inflammatory response.[27] The first results on neuronal excitation through SWNT films made by the layer-by-layer (LBL) assembly had already been demonstrated.[28]

All the latest studies of interactions of neural cells with carbon nanotubes were carried out with terminally differentiated primary cells or cell lines. The primary focus was on establishing biocompatibility of the proposed materials.[29, 30] In addition, carbon nanofiber reinforced composites were shown to increase neuronal cell functions while providing a mechanically strong and electrically conductive substrate.[31] Patterned carbon nanotubes were utilized to guide neural cell growth and demonstrate preferential cell attachment on carbon nanotubes.[32, 33] Neural signal transmission efficacy was also reported to increase on carbon nanotube-coated substrates.[34] We see strong possibilities, fundamental importance, and practical need to use neural stem cells (NSCs)[35] in the studies of SWNT materials for neural medicine. Terminally differentiated cells have limited capacities for extracellular matrix remodeling, axonal extension, and interfacing with implants.[36, 37] Successful implantation and long-term performance of a neural prosthetic device may and most likely will require an interface that can recruit NSCs. On the other hand, in many cases NSCs are necessary to regenerate the neural tissue,[38, 39] while the implantable device will be needed to establish and train a particular signal transmission path. Despite the obvious importance of NSCs, the overall body of knowledge of their behavior on engineered materials remains very limited. Young and

his colleagues have done work in this area with polymeric and biomimetic substrates.[40-42] Silva and Stupp have demonstrated the differentiation of NSCs in peptide fibrous matrices.[43] Interactions of quantum dots and nanoparticles have been investigated with neurons[44-46] and bone marrow stem cells[47, 48] but not with NSCs. Likewise, no information is available about the interaction of any possible carbon nanotube materials and NSCs. Considering the potential importance of these composites for neural medicine, one has to ask the two fundamental questions that are necessary for further development of the field and acquisition of knowledge regarding the interaction of nanoscale materials and transformable cells. First, are SWNT composites biocompatible enough to support the differentiation of stem cells, which are well known for their sensitivity to the environment? Second, if this is the case, do SWNT materials affect in any way the differentiation of NSCs? In this study, we demonstrate, for the first time, differentiation of mouse cortical NSCs on a SWNT-based composite. Our results provide us definite answers to the questions above regarding LBL assembled SWNT-polyelectrolyte composite films. The choice of the particular SWNT composite was made on the basis of previous success with culturing NG108-15 murine neuroblastoma × glioma hybrid cells on SWNT LBL films[49] and their neural excitation through the LBL films.[28]

3.3 Methods

3.3.1 Preparation of Substrates

Poly-L-ornithine (PLO, Sigma-Aldrich), a commonly used substratum for NSC studies, was used to produce a monolayer of PLO on 12mm #1 round German glass coverslips (Bellco Glass Inc.) as the control substrates. PLO coated coverslips were prepared 24 h before seeding by incubating the coverslips in 15 μg/ml PLO solution for 3 hours followed by 3 washes with PBS. Prior to coating, the glass coverslips were cleaned and sterilized by sonication in 70% ethanol and irradiation with UV light. The experimental substrates were fabricated by coating glass coverslips with layer-by-layer (LBL) assembled single-walled carbon nanotube (SWNT) composite multilayers. A stable dispersion of SWNTs was obtained by first dispersing purchased SWNTs (Carbon Nanotechnologies Inc.) in 1-wt% poly(sodium 4-styrene-sulfonate) (PSS, M_W 1,000,000, Sigma-Aldrich) solution[50] with 2 h of mild sonication in a ultrasonic cleaner followed by centrifuging the mixture at 5000 rpm and collecting the supernatant. To assemble multilayers of SWNTs, round glass coverslips cleaned by sonication in 70% ethanol were immersed in a 0.5 wt-% Poly(ethyleneimine) (PEI, M_W 750,000, Sigma-Aldrich) solution for 20 min followed by wash with high purity water and drying under a gentle air jet to form a stable monolayer of PEI molecules. Each subsequent layer was formed by immersing the coverslips in the dispersion of SWNTs or PEI for 20 min followed by the same washing and drying steps. The alternating layering process was repeated until 5 or 6 number of layers, designated as $(PEI/SWNT)_5$ or $(PEI/SWNT)_6$, were obtained. The

coated glass coverslips were sterilized with 70% ethanol and UV irradiation prior to cell seeding.

3.3.2 Culture of Mouse Cortex Embryonic 14-day Neurospheres

Mouse cortex embryonic 14-day neurospheres, basal medium, and all supplements for neural stem cell (NSC) culture were purchased from StemCell Technologies. Proliferation and differentiation media were prepared according to the manufacturer's technical manual. The proliferation medium contains 20 ng/ml of human epidermal growth factor (hEFG). Neurospheres were cultured in the proliferation medium for at least two passages (7 to 9 days each) before being used for differentiation experiments. Between passages, neurospheres at moderate densities were harvested, mechanically dissociated into single cells, and seeded at a density of 2×10^6 cells per 40 mL of medium. For the differentiation of neurospheres, neurospheres were harvested and seeded as whole spheres on coated glass coverslips in 24-well plates at a density of 200 neurospheres per well and cultured in differentiation medium. For the differentiation of single cells, neurospheres were dissociated into single cells using a chemical dissociation kit (StemCell Technologies) and seeded at a density of 2×10^5 cells per well. Cultures were observed for morphological changes at the indicated time point using a Nikon Eclipse TS100 inverted microscope equipped with a QImaging MicroPublisher 3.3 digital CCD color cameras. Images were captured using QImaging's QCapture software.

3.3.3 Quantification of Process Growth

The lengths of neural processes were determined from digital photomicrographs taken at the indicated experimental points. Quantification of process growth was evaluated from the end-to-end distances of neural processes in 10 independent fields. The lengths of 5 longest processes per field were measured from the edge of the neuropshere to the tip of the processes in a linear fashion using the NIH Image J software.

2.3.4 Assessment of Cell Viability

Viability of differentiated neurospheres was determined using the MTT assay. The MTT salt (3-(4,5-Dimethyl-2-thiazolyl)-2,5-diphenyl-2H-tetrazolium bromide, Sigma-Aldrich) is reduced to insoluble purple formazan by active mitochondrial reductase enzymes in the cell. At the indicated time points, 50 μL of MTT solution (5 mg MTT/ml PBS, sterile filtered) was added to each well and incubated for 4 h at 37°C. After incubation, the MTT formazan solution was collected, precipitated by centrifugation, and dissolved in 500 μL of DMSO. The optical density of the formazan solution was measured at 570 nm (reference at 650 nm) using a Maxline microplate reader (Molecular Devices). Viability of differentiated single cells was determined using the WST-8 assay. Unlike the MTT salt, the WST-8 salt (2-(2-methoxy-4-nitrophenyl)-3-(4-nitrophenyl)-5-(2,4-disulfophenyl)-2H-tetrazolium, monosodium) produces a water-soluble formazan dye upon reduction. At the indicated time point, 50 μL of WST-8 solution (Dojindo Molecular Technologies Inc.) was added to each well and incubated for

5 h at 37°C. The absorbance of the solution was measured at 450 nm (reference at 650 nm).

3.3.5 Scanning Electron Microscopy

For SEM analysis, samples were first washed briefly with PBS, fixed with 2.5% glutaraldehyde for 1 h, and then washed again with PBS three times for 5 min each. The samples were then dehydrated through a gradient series of ethanol (25%, 50%, 70%, 85%, 95%, and three times 100%) for 5 min each time and left overnight in the final 100% ethanol solution. Completely dried samples were mounted on aluminum stubs and coated sputter-coated with gold. Imaging was carried out using a Philips XL30FEG scanning electron microscope.

3.3.6 Immunocytochemistry

For immunocytochemical characterization, cultured cells were fixed in 4% paraformaldyde in PBS for 30 min and permeabilized in 0.3% Triton X-100 in PBS for 5 min. Cells were first incubated with primary antibody diluted in PBS containing 10% goat serum for 2 h at 37°C and then with secondary antibody diluted in PBS containing 2% goat serum for 30 min at 37°C. All primary and secondary antibodies were purchased from Chemicon. Primary antibodies and their dilutions are as follow: mouse anti-nestin (1:200), mouse anti-MAP2 (1:200), mouse anti-GFAP (1:200), chicken anti-GFAP (1:200), and mouse anti-O4 (1:200). Secondary antibodies and their dilutions are as follow: goat anti-mouse IgG-rhodamine conjugated (1:100), donkey anti-chicken Igy -

FITC conjugated (1:100). Samples were counter-stained for nuclei and mounted with Prolong Gold Anti-Fading Reagent with DAPI (Invitrogen). Immunostained samples were visualized using an Olympus FluoView FV500 confocal laser scanning microscope. The imaged were acquired using the Olympus Fluoview software version TIEMPO 4.3. Quantitative cell phenotype analysis was carried out using the NIH ImageJ software by counting immunopositive cells against DAPI-stained cells.

3.4 Results and Discussion

To investigate the behavior of NSCs on LBL assembled SWNT composite films, mouse embryonic 14-day neurospheres (ie. spherical clonal structures of NSCs) from the cortex were seeded and induced to differentiate on round glass coverslips (12 mm diameter) coated with 6 bilayers of SWNT-polyelectrolyte. SWNTs were dispersed in a 1-wt% poly(sodium 4-styrene-sulfonate) (PSS) solution and LBL assembled with the polyelectrolyte poly(ethyleneimine) (PEI). The resulted thin film of coating was designated as $(PEI/SWNT)_6$. As a control, neurospheres were also seeded and differentiated on coverslips coated with poly-L-ornithine (PLO), a standard substratum commonly used for NSC cultures and studies.

NSCs were first expanded in proliferation medium containing epidermal growth factor (EGF). To induce cell attachment and differentiation, they were seeded at a low density of 200 neurospheres per coated coverslip in 24-well plates and cultured with EGF

depleted differentiation medium. As suggested by Young et al.,[41] a high neurosphere seeding density encourages cell migration from neurospheres while a low seeding density does not support cell survival away from neurospheres and forces cells to extend long processes in search for other neurospheres. Therefore, a low neurospheres seeding density truly tests the interaction between cells and their substrate. In our study, neurospheres attached to both types of substrates and developed neural processes away from the edge of the neurospheres as early as 1 day in culture (Figure 3.1a). The lengths of processes from differentiated NSCs increased steadily over the 7-day culture period (Figure 3.1b). Throughout the culture period, neural processes developed on PLO coated substrates remained longer than those developed on $(PEI/SWNT)_6$ coated substrates; however, the differences were not very significant. By 5 days in culture, NSCs on both types of substrates had extended long and complex processes into the area surrounding the neurospheres. It is highly likely that, if the neurospheres were seeded at higher densities, the extending processes from individual neurospheres could reach and form networks with their neighboring neurospheres.

Viability of neurospheres was evaluated using the MTT assay (Figure 3.1c). There was no noticeable difference between the viability of neurospheres on $(PEI/SWNT)_6$ and PLO coated substrates. Cell viability was maintained at a steady level after day 3. The initial decline in cell activity between day 1 and day 3 is likely to be a consequence of cell damage during the EGF depletion process (repeated centrifugation and dispersion) and lost of weakly attached neurospheres during medium change. In any case, our viability assessment indicates that $(PEI/SWNT)_6$ coated substrates are as

biocompatible as PLO coated substrates in supporting neurosphere differentiation. The differentiated morphology of neurospheres was confirmed by scanning electron microscopy (SEM) (Figure 3.1d first row). Differentiated neurospheres developed abundant and highly branched neural processes on both types of substrates. SEM also revealed migration of individual cells away from the original neurospheres (Figure 3.1d second row). In addition, we observed more pronounced spreading of extracellular matrix (ECM) on PLO coated substrates which we believe is a consequence of PLO's adhesive nature. The SEM images are a straightforward indication, together with Figure 3.1a-b, that LBL assembled SWNT films can support the differentiation of neurospheres and their neurite outgrowth.

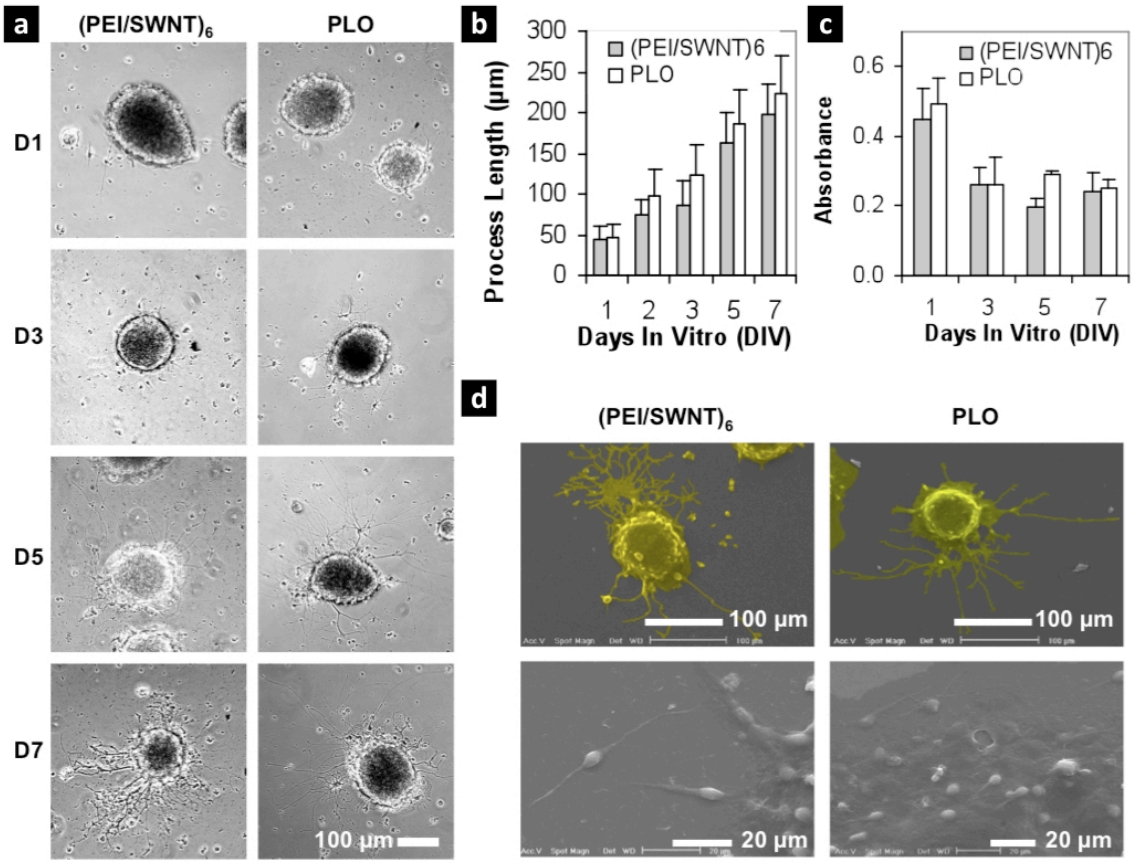

Figure 3.1 Mouse embryonic 14-day cortical neurospheres differentiated on and $(PEI/SWNT)_6$ and PLO coated coverslips in 24-well plate at a low seeding density of 200 neurospheres per well. (**a**) Light microscopy images of differentiated neurospheres. (**b**) Evaluation of the lengths of processes extending from the differentiated neurospheres for the 7-day culture period. (**c**) MTT reduction activity of differentiated neurospheres. (**d**) Color enhanced SEM images highlighting neurite outgrowth of differentiated neurospheres on day 7 (first row). SEM images at higher magnification showing migrating NSCs around neurospheres (second row).

It has been known since the discovery of NSCs that NSCs differentiate into a heterogeneous population of cells consisted primarily of neurons, astrocytes, and oligodendrocytes.[35] To analyze the differentiated phenotypes, neurospheres cultured for 7 days were immunostained with anti-nestin, anti-microtubule associated protein 2 (anti-MAP2), anti-glial fibrillary acidic protein (anti-GFAP), and anti-oligodendrocyte marker O4 (anti-O4) and countered stained with DAPI nuclei stain (Figure 3.2a). Nestin expression has been adopted as a marker for neural stem and precursor cells.[51] MAP2 is a cytoskeletal protein component in mature neurons and dendrites[52] while GFAP and O4 are established markers for intermediate filament proteins in astrocytes[53, 54] and surface antigens of developing oligodendrocytes[55, 56] respectively.

Immunostaining results on PLO and $(PEI/SWNT)_6$ coated substrates are qualitatively comparable (Figure 3.2a). Both types of substrates supported differentiation of neurospheres into the three primary neural cell types – neurons, astrocytes, and oligodendrocytes. In general, nestin expression is intense and abundant near the center of neurospheres. MAP2-positive cells are faintly stained and located near the center, while O4-positive cells are sparsely distributed throughout the neurospheres. GFAP is heavily expressed at the periphery of neurospheres, indicating that most migrating cells might be astrocytes. Quantitative assessment of cell phenotypes shows that there were slightly more neurons and oligodendrocytes on $(PEI/SWNT)_6$ coated substrates and more astrocytes on PLO coated substrates (Figure 3.2b). In general, the cell phenotype analysis is consistent with our observations from Figure 3.1 and 3.2a. Longer neural process formation (Figure 3.1a,b) and increased spreading of ECM (Figure 3.1d second

row) on PLO coated substrate seem to correlate with increased astrocyte population (Figure 3.2). Fibrous astrocyes are known to have long and slender processes, and ECM formation is characteristic for astrocytes. Similar results have also been obtained by Young and his colleagues[41] in which, under serum-free condition, a substrate that promotes longer processes generated primarily fibrous astrocytes and fewer neurons.

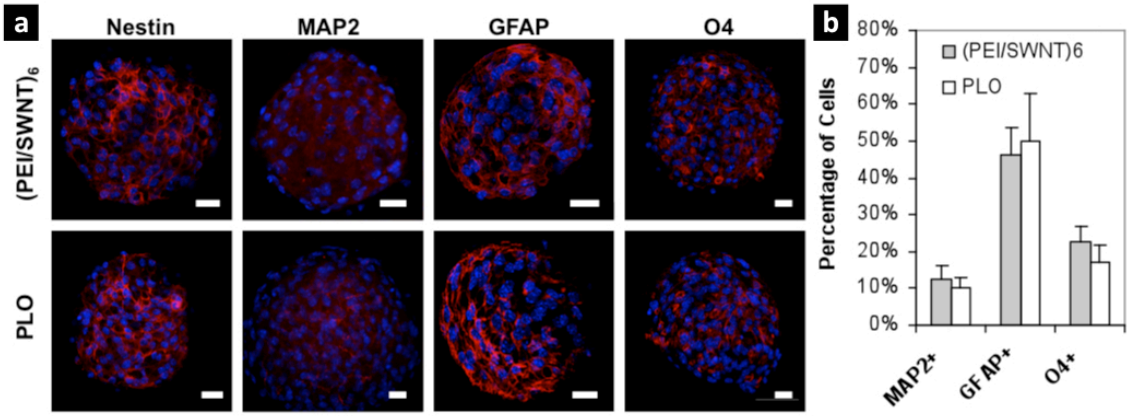

Figure 3.2 (**a**) Confocal microscopy images differentiated neurospheres on day 7. Neurospheres were stained for markers of NSCs (nestin), neurons (MAP2), astrocytes (GFAP), and oligodendrocytes (O4). Neural markers are shown in red, while the cell nuclei, counterstained with DAPI, are shown in blue. Images represent scans near the center of the neurospheres. Scale bars: 20 μm. (**b**) Average percentages of differentiated cell phenotypes after 7 days in culture.

Having successfully demonstrated the differentiation of mouse neurospheres on LBL assembled SWNT composite films, we sought to elucidate the differences between the different substrates by increasing cell-substrate contact. To accomplish this, we chemically dissociated neurospheres into single cells and differentiated them on

$(PEI/SWNT)_5$, PLO, and $(PEI/SWNT)_5$(PLO) coated glass coverslips. We added $(PEI/SWNT)_5$(PLO) coated substrates to help us determine whether the combination of PLO's adhesiveness and SWNT's nano-topology (Figure 3.3) would produce any additive cell behavior. However, we observed very little variations across NSCs cultured on the three different substrates (Figure 3.4a). As time progressed, NSCs transformed from a spherical morphology to a more elongated and spread-out morphology representative of differentiated neural cells. Differentiated NSCs also developed neural processes that intertwine with one another. The change in cell morphology was confirmed by scanning electron microscopy (SEM) images acquired on day 1 and day 5 after seeding (Figure 3.4b).

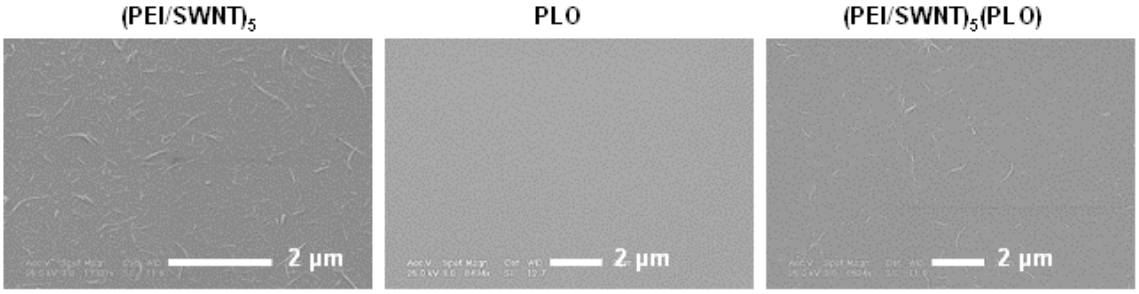

Figure 3.3 SEM images of $(PEI/SWNT)_5$, PLO, and $(PEI/SWNT)_5$(PLO) coated glass coverslips. Individual and bundles of carbon nanotubes are visible on $(PEI/SWNT)_5$ and $(PEI/SWNT)_5$(PLO) coated substrates, while PLO coated substrate is completely smooth under SEM.

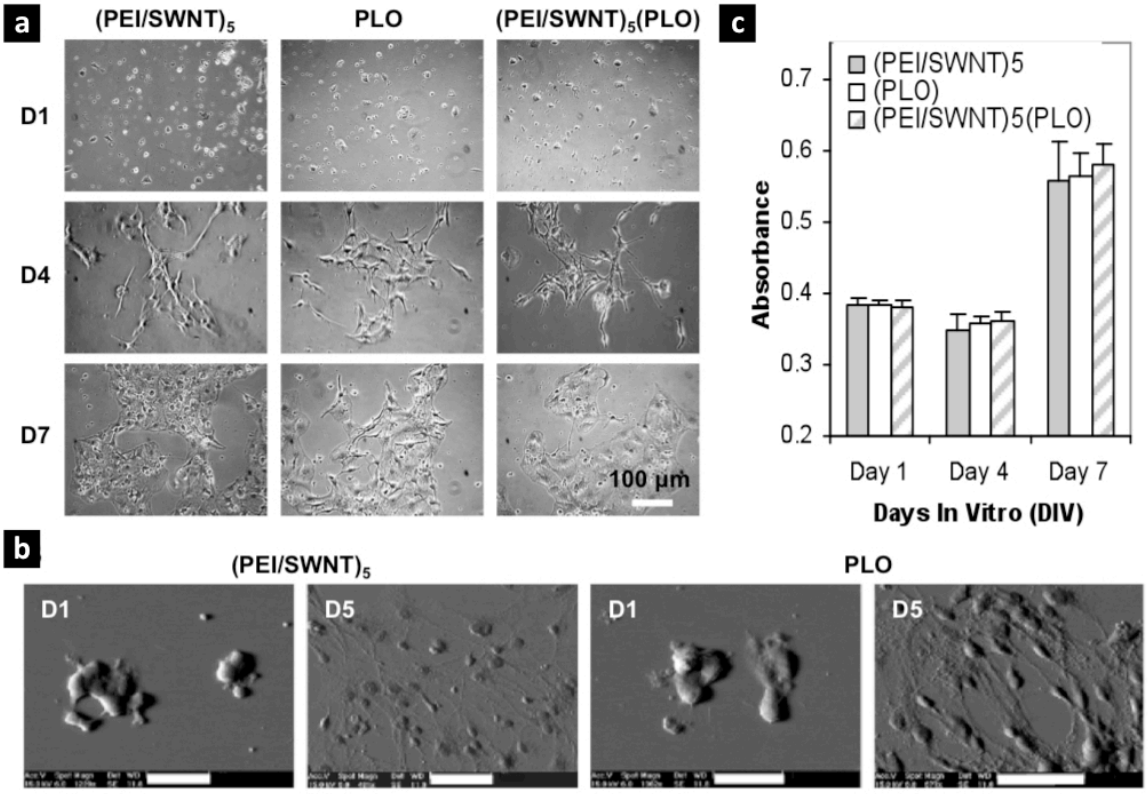

Figure 3.4 Mouse embryonic 14-day cortical neurospheres differentiated as dissociated single cells and small clusters on and $(PEI/SWNT)_6$, PLO, and $(PEI/SWNT)_6(PLO)$ coated coverslips in 24-well plate. (**a**) Light microscopy images of differentiated NSCs. (**b**) SEM images of differentiated NSCs. (**c**) WST-8 reduction activity of differentiated NSCs.

Viability of differentiated single cells was assessed using the WST-8 assay. We switched to using WST-8 because a previous study reported MTT's tendency to associate with carbon nanotubes to give false and cytotoxic results and recommended the use of water-soluble tetrazolium salts.[57] WST-8 is a tetrazolium salt that produces a highly

water soluble formazan upon cellular reduction and has been recently adopted as an indicator for use in viability assays.[58] Overall, NSCs on the three different substrates demonstrated similar viability throughout the 7-day culture period (Figure 3.4c). Cell activity appeared to be constant between day 1 and day 4 but increased significantly day 4 and day 7. We suspect this increase in cell activity to be the result of increased metabolic activity of the extensively differentiated cell populations.

The progression of NSC differentiation was monitored by immunostaining for nestin, MAP2, and GFAP expressions (Figure 3.5). Identical trends were observed on all three types of substrates, and differentiation was not affected by the SWNT-based substrates. While about 10% of differentiated neurospheres expressed MAP2, we observed insignificant amount of MAP2 expression in differentiated single cells throughout the culture period. This is not a surprising result considering no additional agent was added to the standard differentiation medium supplied by the manufacturer, which may be insufficient for inducing or maintaining neuronal differentiation. Our finding also indicates that the three dimensional structure of neurospheres and the junctions betweens individual cells in neurospheres may provide an environment similar to the neural stem cell niche, and therefore may be essential for neuronal differentiation. Despite the lack of MAP2 expression, NSC differentiation was nevertheless confirmed through changes in nestin and GFAP expressions. The entire cell population was nestin-positive and GFAP-negative on day 1, indicating an undifferentiated state. As time progressed, NSCs began to lose their nestin-expression and acquire GFAP-expression. By day 7, none of the cells stained positive for nestin and approximately 80 to 90% of all

cells were GFAP-positive. This transition is well documented.[59] As NSCs proliferate and differentiate into neurons and glia, nestin is down-regulated and distinct intermediate markers are expressed.

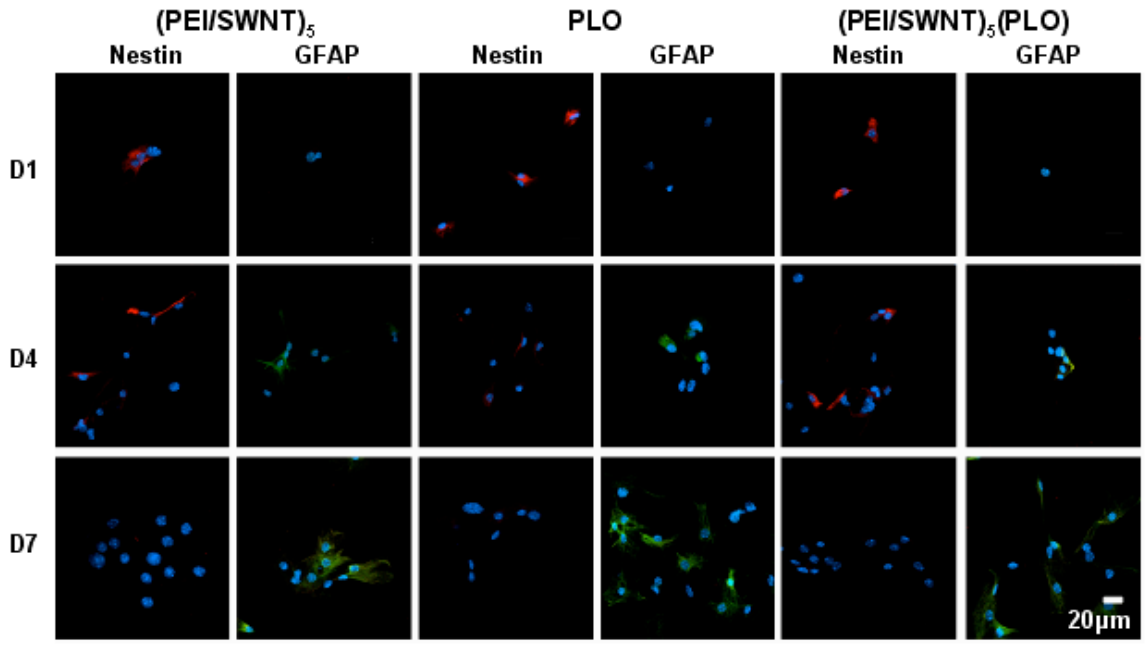

Figure 3.5 Confocal microscopy images of differentiated NSCs. Cells were stained for markers of NSCs (nestin, shown in red), astrocytes (GFAP, shown in green), and neurons (MAP2, not shown due to low level of expression). Cell nuclei were counterstained with DAPI and shown in blue.

3.5 Conclusions

We have demonstrated for the first time that the differentiation of environment-sensitive NSCs, both as neurospheres and single cells, on a CNT-based material. Our study has the critical importance for further development of nanomaterials for neural interfaces. The nanostructure of the LBL assembled SWNT-polyelectrolyte composite, which gives rise to the composite's structural flexibility, chemical stability, and physical properties, showed no adverse affect on the differentiation of NSCs. NSCs behaved similarly as those cultured on the standard and widely-used PLO substratum in terms of cell viability, the development of neural processes, and the appearance and progression of neural markers. We also see indications that SWNT substrates might induce preferential differentiation into the neuronal lineage; however, this aspect of the study as well as the potential mechanism(s) of the influence requires further investigation.

3.6 References

1. Roco, M. C., Nanotechnology: convergence with modern biology and medicine. *Current Opinion in Biotechnology* **2003,** *14* (3), 337-346.

2. Dubertret, B.; Skourides, P.; Norris, D. J.; Noireaux, V.; Brivanlou, A. H.; Libchaber, A., In Vivo Imaging of Quantum Dots Encapsulated in Phospholipid Micelles. *Science* **2002,** *298* (5599), 1759-1762.

3. Ishijima, A.; Yanagida, T., Single molecule nanobioscience. *Trends in Biochemical Sciences* **2001,** *26* (7), 438-444.

4. Curtis, A.; Wilkinson, C., Nantotechniques and approaches in biotechnology. *Trends in Biotechnology* **2001,** *19* (3), 97-101.

5. Bogunia-Kubik, K.; Sugisaka, M., From molecular biology to nanotechnology and nanomedicine. *Biosystems* **2002,** *65* (2-3), 123-138.

6. Seeman, N. C.; Belcher, A. M., Emulating biology: Building nanostructures from the bottom up. *PNAS* **2002,** *99* (90002), 6451-6455.

7. Whitesides, G. M.; Boncheva, M., Supramolecular Chemistry And Self-assembly Special Feature: Beyond molecules: Self-assembly of mesoscopic and macroscopic components. *PNAS* **2002,** *99* (8), 4769-4774.

8. Silva, G. A., Neuroscience nanotechnology: progress, opportunities and challenges. *Nat Rev Neurosci* **2006,** *7* (1), 65-74.

9. Dresselhaus, M. S.; Dresselhaus, G.; Jorio, A., Unsual Properties and Structure of Carbon Nanotubes. *Annual Review of Materials Research* **2004,** *34* (1), 247-278.

10. Niyogi, S.; Hamon, M. A.; Hu, H.; Zhao, B.; Bhowmik, P.; Sen, R.; Itkis, M. E.; Haddon, R. C., Chemistry of Single-Walled Carbon Nanotubes. *Acc. Chem. Res.* **2002,** *35* (12), 1105-1113.

11. Haddon, R. C., Carbon Nanotubes. *Acc. Chem. Res.* **2002,** *35* (12), 997-997.

12. Dai, H., Carbon Nanotubes: Synthesis, Integration, and Properties. *Acc. Chem. Res.* **2002,** *35* (12), 1035-1044.

13. Ouyang, M.; Huang, J. L.; Lieber, C. M., Fundamental Electronic Properties and Applications of Single-Walled Carbon Nanotubes. *Acc. Chem. Res.* **2002,** *35* (12), 1018-1025.

14. Zhou, O.; Shimoda, H.; Gao, B.; Oh, S.; Fleming, L.; Yue, G., Materials Science of Carbon Nanotubes: Fabrication, Integration, and Properties of Macroscopic Structures of Carbon Nanotubes. *Acc. Chem. Res.* **2002,** *35* (12), 1045-1053.

15. Mamedov, A. A.; Kotov, N. A.; Prato, M.; Guldi, D. M.; Wicksted, J. P.; Hirsch, A., Molecular design of strong single-wall carbon nanotube/polyelectrolyte multilayer composites. *Nature Materials* **2002,** *1* (3), 190-194.

16. O. Breuer, U. S., Big returns from small fibers: A review of polymer/carbon nanotube composites. *Polymer Composites* **2004,** *25* (6), 630-645.

17. Marquis, F. D. S., Fully integrated hybrid polymeric carbon nanotube composites. . *Materials Science Forum* **2003,** *437-438*, 85-88.

18. Thostenson, E. T.; Ren, Z.; Chou, T.-W., Advances in the science and technology of carbon nanotubes and their composites: a review. *Composites Science and Technology* **2001,** *61*, 1899-1912.

19. Blake, R.; Gun'ko, Y. K.; Coleman, J.; Cadek, M.; Fonseca, A.; Nagy, J. B.; Blau, W. J., A Generic Organometallic Approach toward Ultra-Strong Carbon Nanotube Polymer Composites. *J. Am. Chem. Soc.* **2004,** *126* (33), 10226-10227.

20. Fischer, J. E., Chemical Doping of Single-Wall Carbon Nanotubes. *Acc. Chem. Res.* **2002,** *35* (12), 1079-1086.

21. Bahr, J. L.; Tour, J. M., Covalent chemistry of single-wall carbon nanotubes. *Journal of Materials Chemistry* **2002,** *12*, 1952-1958.

22. Schwartz, A. B., Cortical Neural Prosthetics. *Annual Review of Neuroscience* **2004,** *27* (1), 487-507.

23. Patolsky, F.; Timko, B. P.; Yu, G.; Fang, Y.; Greytak, A. B.; Zheng, G.; Lieber, C. M., Detection, Stimulation, and Inhibition of Neuronal Signals with High-Density Nanowire Transistor Arrays. *Science* **2006,** *313* (5790), 1100-1104.

24. Chapin, J. K., Using multi-neuron population recordings for neural prosthetics. *Nat Neurosci* **2004,** *7* (5), 452-455.

25. Zhong, Y. H.; Yu, X. J.; Gilbert, R.; Bellamkonda, R. V., Stabilizing electrode-host interfaces: A tissue engineering approach. *Journal of Rehabilitation Research and Development* **2001,** *38* (6), 627-632.

26. Cui, X.; Lee, V. A.; Raphael, Y.; Wiler, J. A.; Hetke, J. F.; Anderson, D. J.; Martin, D. C., Surface modification of neural recording electrodes with conducting

polymer/biomolecule blends. *Journal of Biomedical Materials Research* **2001,** *56* (2), 261-272.

27. Shain, W.; Spataro, L.; Dilgen, J.; Haverstick, K.; Retterer, S.; Isaacson, M.; Saltzman, M.; Turner, J. N., Controlling cellular reactive responses around neural prosthetic devices using peripheral and local intervention strategies. *Neural Systems and Rehabilitation Engineering, IEEE Transactions on [see also IEEE Trans. on Rehabilitation Engineering]* **2003,** *11* (2), 186-188.

28. Gheith, M. K.; Pappas, T. C.; Liopo, A. V.; Sinani, V. A.; Shim, B. S.; Motamedi, M.; Wicksted, J. P.; Kotov, N. A., Stimulation of Neural Cells by Lateral Currents in Conductive Layer-by-Layer Films of Single-Walled Carbon Nanotubes. *Advanced Materials* **2006,** *18* (22), 2975-2979.

29. Mattson, M. P.; Haddon, R. C.; Rao, A. M., Molecular Functionalization of Carbon Nanotubes and Use as Substrates for Neuronal Growth. *Journal of Molecular Neuroscience* **2000,** *14*, 175.

30. Hu, H.; Ni, Y.; Montana, V.; Haddon, R. C.; Parpura, V., Chemically Functionalized Carbon Nanotubes as Substrates for Neuronal Growth. *Nano Lett.* **2004,** *4* (3), 507-511.

31. Waid, M. C.; McKenzie, J. L.; Price, R. L.; Ejiofor, J. U.; Webster, T. J., Nano-biotechnology: carbon nanofibres as improved neural and orthopaedic implants. *Nanotechnology* **2004,** *15*, 48-54.

32. Gabay, T.; Jakobs, E.; Ben-Jacob, E.; Hanein, Y., Engineered self-organization of neural networks using carbon nanotube clusters. *Physica A: Statistical and Theoretical Physics* **2005,** *350* (2-4), 611-621.

33. Zhang, X.; Prasad, S.; Niyogi, S.; Morgan, A.; Ozkan, M.; Ozkan, C. S., Guided neurite growth on patterned carbon nanotubes. *Sensors and Actuators B: Chemical* **2005,** *106* (2), 843-850.

34. Lovat, V.; Pantarotto, D.; Lagostena, L.; Cacciari, B.; Grandolfo, M.; Righi, M.; Spalluto, G.; Prato, M.; Ballerini, L., Carbon Nanotube Substrates Boost Neuronal Electrical Signaling. *Nano Lett.* **2005,** *5* (6), 1107-1110.

35. Reynolds, B. A.; Weiss, S., Generation of neurons and astrocytes from isolated cells of the adult mammalian central nervous system. *Science* **1992,** *255*, 1707-1710.

36. Ourednik, J.; Ourednik, W.; Mitchell, D. E., Remodeling of lesioned kitten visual cortex after xenotransplantation of fetal mouse neopallium. *The Journal of Comparative Neurology* **1998,** *395* (1), 91-111.

37. Grimaldi, P.; Carletti, B.; Rossi, F., Neuronal replacement and integration in the rewiring of cerebellar circuits. *Brain Research Reviews* **2005,** *49* (2), 330-342.

38. Martino, G.; Pluchino, S., The therapeutic potential of neural stem cells. *Nat Rev Neurosci* **2006,** *7* (5), 395-406.

39. Muller, F.-J.; Snyder, E. Y.; Loring, J. F., Gene therapy: can neural stem cells deliver? *Nat Rev Neurosci* **2006,** *7* (1), 75-84.

40. Young, T.-H.; Hung, C.-H., Behavior of embryonic rat cerebral cortical stem cells on the PVA and EVAL substrates. *Biomaterials* **2005,** *26* (20), 4291-4299.

41. Wang, J.-H.; Hung, C.-H.; Young, T.-H., Proliferation and differentiation of neural stem cells on lysine-alanine sequential polymer substrates. *Biomaterials* **2006,** *27* (18), 3441-3450.

42. Hung, C.-H.; Lin, Y.-L.; Young, T.-H., The effect of chitosan and PVDF substrates on the behavior of embryonic rat cerebral cortical stem cells. *Biomaterials* **2006,** *27* (25), 4461-4469.

43. Silva, G. A.; Czeisler, C.; Niece, K. L.; Beniash, E.; Harrington, D. A.; Kessler, J. A.; Stupp, S. I., Selective Differentiation of Neural Progenitor Cells by High-Epitope Density Nanofibers. *Science* **2004,** *303* (5662), 1352-1355.

44. Gomez, N.; Winter, J. O.; Shieh, F.; Saunders, A. E.; Korgel, B. A.; Schmidt, C. E., Challenges in quantum dot-neuron active interfacing. *Talanta* **2005,** *67* (3), 462-471.

45. Pappas, T. C.; Wickramanyake, W. M. S.; Jan, E.; Motamedi, M.; Brodwick, M.; Kotov, N. A., Nanoscale Engineering of a Cellular Interface with Semiconductor Nanoparticle Films for Photoelectric Stimulation of Neurons. *Nano Lett.* **2007,** *7* (2), 513-519.

46. Winter, J. O.; Liu, T. Y.; Korgel, B. A.; Schmidt, C. E., Recognition Molecule Directed Interfacing Between Semiconductor Quantum Dots and Nerve Cells. *Advanced Materials* **2001,** *13* (22), 1673-1677.

47. Chen, H. F.; Titushkin, I.; Stroscio, M.; Cho, M., Altered membrane dynamics of quantum dot-conjugated integrins during osteogenic differentiation of human bone marrow derived progenitor cells. *Biophysical Journal* **2007,** *92* (4), 1399-1408.

48. Hsieh, S.-C.; Wang, F.-F.; Lin, C.-S.; Chen, Y.-J.; Hung, S.-C.; Wang, Y.-J., The inhibition of osteogenesis with human bone marrow mesenchymal stem cells by CdSe/ZnS quantum dot labels. *Biomaterials* **2006,** *27* (8), 1656-1664.

49. Gheith, M. S., V.; Wicksted, J.; Matts, R.; Kotov, N., Single-Walled Carbon Nanotube Polyelectrolyte Multilayers and Freestanding Films as a Biocompatible Platform for Neuroprosthetic Implants. *Advanced Materials* **2005,** *17* (22), 2663-2670.

50. O'Connell, M. J.; Boul, P.; Ericson, L. M.; Huffman, C.; Wang, Y.; Haroz, E.; Kuper, C.; Tour, J.; Ausman, K. D.; Smalley, R. E., Reversible water-solubilization of single-walled carbon nanotubes by polymer wrapping. *Chemical Physics Letters* **2001,** *342* (3-4), 265-271.

51. Zimmerman L; Parr B; Lendahl U; Cunningham M; McKay R; Gavin B; Mann J; Vassileva G; A., M., Independent regulatory elements in the nestin gene direct transgene expression to neural stem cells or muscle precursors. *Neuron* **1994,** *12* (1), 11-24.

52. Johnson, G. V.; Jope, R. S., The role of microtubule-associated protein 2 (MAP-2) in neuronal growth, plasticity, and degeneration. *Journal of neuroscience research.* **1992,** *33* (4), 505-512.

53. Inagaki, M.; Nakamura, Y.; Takeda, M.; Nishimura, T.; Inagaki, N., Glial fibrillary acidic protein: dynamic property and regulation by phosphorylation. *Brain pathology* **1994,** *4* (3), 239-243.

54. McLendon, R. E.; Bigner, D. D., Immunohistochemistry of the glial fibrillary acidic protein: basic and applied considerations. *Brain pathology* **1994,** *4* (3), 221-228.

55. Sommer, I.; Schachner, M., Monoclonal antibodies (O1 to O4) to oligodendrocyte cell surfaces: an immunocytological study in the central nervous system. *Developmental biology.* **1981,** *83* (2), 311-327.

56. Bansal, R.; Warrington, A. E.; Gard, A. L.; Ranscht, B.; Pfeiffer, S. E., Multiple and novel specificities of monoclonal antibodies O1, O4, and R-mAb used in the analysis of oligodendrocyte development. *Journal of neuroscience research.* **1989,** *24* (4), 548-557.

57. Worle-Knirsch, J. M.; Pulskamp, K.; Krug, H. F., Oops They Did It Again! Carbon Nanotubes Hoax Scientists in Viability Assays. *Nano Lett.* **2006,** *6* (6), 1261-1268.

58. Tominaga, H.; Ishiyama, M.; Ohseto, F.; Sasamoto, K.; Hamamoto, T.; Suzuki, K.; Watanabe, M., A water-soluble tetrazolium salt useful for colorimetric cell viability study. *Analytical Communications* **1999,** *36* (2), 47-50.

59. McKay, R., Stem Cells in the Central Nervous System. *Science* **1997,** *276* (5309), 66-71.

CHAPTER 4

Electrochemical Properties of Layer-by-Layer Assembled Carbon Nanotube Composites

4.1 Abstract

The safety, function, and longevity of implantable neuroprosthetic and cardiostimulating electrodes depend heavily on the electrical properties of the electrode-tissue interface, which in many cases requires substantial improvement. While different variations of carbon nanotube materials have been shown to be suitable for neural excitation, it is critical to evaluate them vs. other materials used for bioelectrical interfacing. In this study, we found that composite multi-walled carbon nanotube-polyelectrolyte (MWNT-PE) multilayers electrodes substantially outperform state-of-the-art neural interface material available today, namely activated electrochemically deposited iridium oxide (IrOx). The MWNT-PE coated electrodes also share similar reductions in electrical impedance and augmentations in cathodic charge storage capacity (CSC) seen with promising conducting polymer coatings. Our findings suggest that MWNT-PE multilayers are excellent interfacing material for neural prosthetic

applications and can potentially be used to build a new generation of implantable electrodes.

4.2 Introduction

Neural and cardiac electrodes are currently utilized in an increasing number of diagnostic, therapeutic, and treatment strategies for various neurological, cardiac, sensory, and psychiatric conditions. Deep brain stimulators, artificial pacemakers, and cochlear implants are some of the most established and widely deployed electro-active prosthetic devices. They have been used to reduce symptoms of Parkinson's disease,[1] maintain regular heart rhythm,[2] and restore auditory function.[3, 4] Other neural prosthetic devices have been used to treat epilepsy,[5] depression[6] and chronic pain,[7] and to regulate breathing[8] and bladder and bowel control.[9] Regardless of their specific medical applications, all neural and cardiac electrodes operate by sensing or delivering electrical pulses to nearby tissues. Therefore, the safety, function, and longevity of these devices are ultimately dependent on the stability of the tissue-electrode interface, which dictates the electrode's sensitivity to small signals and the ability to transfer electro-ionic charges to the tissue. Currently used electrodes are made primarily from biocompatible noble metals, such as gold, platinum, and iridium, and other non-reactive materials, such as titanium, stainless steel, and silicon. These metallic electrodes often suffer from poor contact with tissue and suboptimal long-term stimulation and recording performance due in large part to scar formation.

To improve the performance of electrodes and to resolve these problems, researchers have turned to various surface modification strategies to render the electrodes more sensitive to electrical signals and more efficient in charge transfer. Most of these approaches focus on the reduction of electrical impedance (Z) and augmentation of charge storage capacity (CSC) by applying a thin layer of coating on the electrode to increase the effective surface area and improve charge transfer at the electrode-tissue interface. Further improvements in long-term device performance could be achieved with coatings that also provide enhanced biocompatibility and structural integrity. Iridium oxide (IrOx) has been extensively characterized as a coating material for electrodes[10-13] and is currently adopted for several commercially available medical devices. Compared to metal electrodes, IrOx permits significantly higher levels of charge injection without electrode dissolution or electrolysis of water[11] and has been used to coat a variety of electrodes including deep brain,[14, 15] nerve cuff,[16] pacing, and defibrillation electrodes.[17] Conducting polymers, including polyacetylene, polyaniline, polypyrrole, poly(3,4-ethylenedioxythiophene) (PEDOT), and their derivatives, are another class of material that has recently received significant attention as an interfacing material for implantable electrodes.[18, 19] PEDOT has been shown to be the most promising interfacing material among them since its ordered and well defined chemical structure gives rise to improved conductivity and thermal stability.[20] Recently, researchers have demonstrated the ability to dramatically improve the electrical properties of neural[21-23] and cochlear[24] electrodes by surface modification with PEDOT. In additions, various strategies have been explored

to improve biocompatibility of and incorporate drug release capabilities into the PEDOT coatings.[25-27]

Despite IrOx's initial success and PEDOT's promising outlook, there is still a strong demand for new interfacing materials with better combination of properties. IrOx is well known for its poor adhesion to underlying substrate, and low structural and chemical stability which worsens as increasingly thick oxide layers form during normal electrode activity.[28, 29] Unlike IrOx, PEDOT coatings do not grow thicker or degrade during normal device function. However, recent studies have revealed structural problems, such as cracking and delamination.[22]

Given that chemical and mechanical stability are fundamental to medical electrodes, a logical choice of material for interfacing electrodes with tissues is carbon nanotubes (CNTs), which are known for their extraordinary strength, toughness, chemical stability, electrical conductivity, high surface area[30] and supercapacitor properties[31, 32]. Indeed, many groups have investigated CNT materials and demonstrated promising results in biocompatibility with neuronal cells.[33-38] They have been shown to increase neuronal cell functions,[39] boost neural signal transmission efficacy,[40] stimulate and record brain circuit activity,[41, 42] and improve neural recordings.[43] Recently, successful growth and differentiation of neuroblastoma cells[44] and neural stem cells[45] on these films, as well as stimulation of cultured neurons were demonstrated.[46]

Thus far a substantial amount of data on CNTs interfaced with neural cells has been obtained. Yet, these data do not allow realistically compare CNTs with most

commonly used and probably the other state of the art materials used for similar purposes. To elucidate the potential of CNT-polyelectrolyte thin films for interfacing with electroactive cells, we investigated their ability to reduce interfacial impedance, increase charge storage capacity, deliver charge, and withstand continuous charge injection cycles by performing a multi-parameter side-by-side comparison with IrOx and PEDOT coatings. This knowledge is critical for the understanding of CNT's potential as an emerging technology. The obtained data also indicate that such comparison and materials evaluation is fundamental for future development of the technology of implantable electrodes.

4.3 Methods

4.3.1 Materials

CVD-produced multi-walled carbon nanotubes (MWNTs) were purchased from NanoLab, Inc. (Newton, MA), respectively. Poly(vinyl alcohol) (PVA; MW 70k) and poly(sodium 4-styrene-sulfonate) (PSS; MW 70k and MW 1000k) were obtained from Sigma-Aldrich. 3,4-Ethylenedioxythionphene (EDOT, BAYTRON® M; MW 142.17) was received from H.C. Stark Inc. (Newton, MA). Iridium tetrachloride was purchased from Alfa Aesar. All other chemicals were obtained from Sigma-Aldrich.

4.3.2 Electrodes

400 μm diameter ball electrodes were fabricated from 75 μm diameter Teflon® insulated platinum-iridium (90%-10%) wires obtained from A-M Systems, Inc. (Carlsborg, WA). The ball electrodes were made by melting the tip of the wire with a micro flame oxygen-methane torch. 6 mm diameter Au electrodes were fabricated in house by gold sputter coating a barbell-shaped pattern on polystyrene substrates using a mask.

4.3.3 Surface Modification of Electrodes

Surface modification of electrodes with MWNTs was carried out using the technique of layer-by-layer (LBL) assembly. MWNTs were dispersed at 0.5mg/ml in 0.1 wt% PSS (MW 1000k) solution by ultrasonication and alternately adsorbed with 1 wt% PVA solution. For each deposition, the electrode was immersed in the corresponding solution for 1 minute, following by rinsing with deionized water and drying with an air jet. The resulting thin film of coating was designated as (PVA/MWNT)n where n is the number of bilayers.

Surface modification with PEDOT was conducted by electrochemical deposition of the EDOT monomer. The monomer solution was prepared by dissolving EDOT in 0.2 wt% PSS (MW 70k). The electrochemical process was performed on each electrode by an Autolab PGSTAT 12 (EcoChemie, Utrecht, Netherlands) in glavanostatic mode with a conventional four-electrode configuration at room temperature. The reference and

counter electrodes were connected to a platinum wire within the monomer solution, and the working and sensing electrodes were connected to the electrode site. The thickness of the deposited material was controlled by the deposition time. For the ball electrodes, the deposition current was 1 μA, corresponding to a current density of 0.2 mA/cm2.

Surface modification with iridium oxide film was performed as described by Marzouk et al.[47] Briefly, the deposition solution was prepared by dissolving 75 mg iridium tetrachloride in 50 mL water, followed by addition of 0.5 mL aqueous 30% hydrogen peroxide and 250 mg oxalic acid dihydrate. The pH of the solution was adjusted to 10.5 by addition of anhydrous potassium carbonate, and the resulting solution was allowed to stabilize at room temperature for 2 days. Electrochemical deposition of iridium oxide was carried out using the same setup as EDOT but with a deposition current of 8 μA, corresponding to a current density of 1.6 mA/cm2.

For measurement of coating thicknesses, coatings were deposited on 6 mm diameter Au electrodes using the same LBL and electrochemical deposition processes described above above.

4.3.4 Electrochemical Impedance Spectroscopy (EIS)

An Autolab PGSTAT 12 and Frequency Response Analyzer software (EcoChemie, Utrecht, Netherlands) were used to record impedance spectra of the electrodes. A solution of 1 M phosphate buffered saline (PBS, pH = 7) was used as an electrolyte in a four-electrode configuration. The working and sensing electrodes were

connected to the electrode site. The counter electrode was connected to a platinum foil immersed in PBS, and an Ag/AgCl reference electrode was immersed in PBS. An AC sinusoidal signal of 5 mV in amplitude was used to record the impedance over a frequency range of 1-105 Hz.

4.3.5 Cyclic Voltammetry (CV) and Biphasic Stimulation

CV and biphasic stimulation were performed using an Autolab PGSTAT 12 instrument and General Purpose Electrochemical System software (EcoChemie, Utrecht, Netherlands) in a four-electrode configuration as described for EIS. For CV, a scan rate of 0.1 V/s was used and the potential on the working electrode was swept between -0.9 V and 0.5 V. Three cycles were swept to insure that the film had reached a stable state. For biphasic stimulation a 2 mC/cm2 (10 mA, 0.5 ms) biphasic, cathodic first current pulse was sourced.

4.3.6 Scanning Electron Microscopy (SEM)

SEM was conducted using a Philips XL30 FEG SEM and a FEI Nova Nanolab SEM. Samples were sputter coated with gold prior to imaging.

4.4 Results and Discussion

The functional properties of the neural interface depend not only on the properties of individual CNT but also on the technique of their deposition on the electrode surface. Typical CNT films are produced by solvent evaporation,[33, 34, 37, 40, 42] electrochemical deposition,[43] and chemical vapor deposition.[35, 36, 38, 41] While displaying excellent electrical properties, they are quite fragile. Implantable biomedical devices must withstand chronic low-level long-term stresses and harsh physical conditions and as such, require exceptional mechanical properties.[18] For this reason multilayered composites of CNTs with polyelectrolytes fabricated by the so called layer-by-layer (LBL) assembly capable of delivering such properties[48] appeared to us as an attractive technique for building a robust neural interface. Additionally, their ability to support both electronic and ionic current, store anti-inflammatory drugs,[49] and produce complex 3D surfaces also seem to be essential for a successful neuroprosthetic device.

The CNT LBL coated electrodes were prepared by assembling multi-walled carbon nanotubes (MWNTs) dispersed in a solution of poly(styrene sulfonate) (PSS)[50] with a solution of poly(vinyl alcohol) (PVA) on the ball-shaped tips of platinum-iridium (PtIr) model electrodes (Figure 4.1a). These model electrodes were made from commercially available Teflon-insulated 75 um diameter PtIr wires, which are widely used in the assembly of neural microelectrode arrays and have been adopted as model monopolar cochlear electrodes for *in vitro* and *in vivo* studies.[24] PEDOT and IrOx coatings were galvanostatically deposited on the model electrodes using methods that

have been described previously.[23, 47] For PEDOT deposition, PSS was also used as the dopant counter ion. The coating thickness of the MWNT coatings was controlled by the number of layers assembled on the surface. For PEDOT and IrOx deposition, thickness was varied by altering the deposition charge density. The presence of coatings can be easily recognized as the modified electrode changes color (Figure 4.1b-d). The surface morphology of the MWNT LBL coating (Figure 4.1e) consisted of intertwined MWNT bundles whose nanoscale, high aspect ratio features are essential to increasing surface area and improving charge transfer efficiency. Features of nanoscale roughness were also observed on the PEDOT coating (Figure 4.1f) while the IrOx coating (Figure 4.1g) appeared to have less visible surface roughness at the nanometer level.

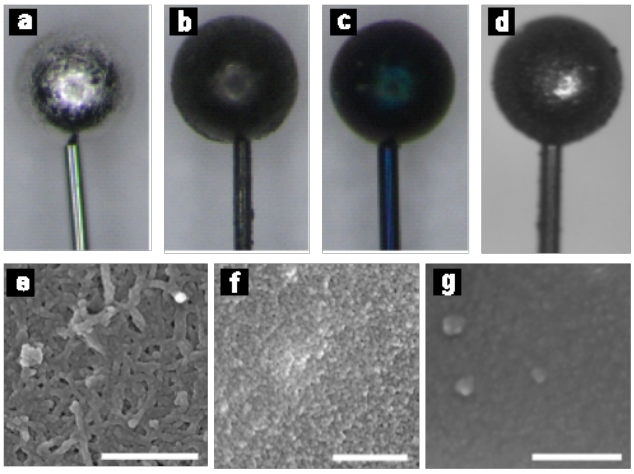

Figure 4.1 Surface modification of electrodes. Ball-tipped IrOx electrodes (**a**) made from Teflon® insulated 75 μm PtIr wires were surface modified with either LBL assembled MWNTs (**b**) or electrochemically deposited PEDOT (**c**) or IrOx (**d**). SEM images illustrate the differences in their surface morphology. The MWNT coating (**e**) consists of a nanofibrous network of MWNT bundles. The PEDOT coating (**f**) shows a moderate degree of roughness while the IrOx (**g**) coating is relatively featureless at the nanoscale level. Scale bars for the SEM images are 500 nm.

Electrochemical impedance spectroscopy (EIS) and cyclic voltammetry (CV) were used to characterize the electrochemical properties of the surface modified PtIr electrodes. All measurements were conducted in 1 M PBS. For EIS, an AC sinusoidal signal of 5 mV in amplitude was used to record the impedance over a frequency range of 1 to 10^5 Hz. For CV, a scan rate of 0.1 V/s was used and the potential on the working electrode was swept between -0.9 V and 0.5 V. The measurements showed that all three coatings progressively decreased the impedance (Figure 4.2a-c) and phase angle (Figure 4.2d-f) with increasing coating thickness, rendering the electrodes less capacitive at higher frequencies. Also as expected, the CV data (Figure 4.2g-i) indicated increasing charge storage capacity (CSC) with increasing coating thickness, which is proportional to the mass of material available for storing charges. As one may notice, the disparity in the magnitude of CSC across the three types of coatings is in fact due to differences in the coating thickness. To provide an accurate comparison on the electrochemical properties, we measured the thickness of the coatings (Figure 4.3) and translated our measurements to a per unit film thickness basis (Figure 4.4). The thickness of MWNT LBL film was found to depend linearly on the number of bilayers, averaging approximately 7 nm per bilayer. For PEDOT and IrOx, coatings thickness appeared to have a logarithmic-like dependence on the deposition charge density.

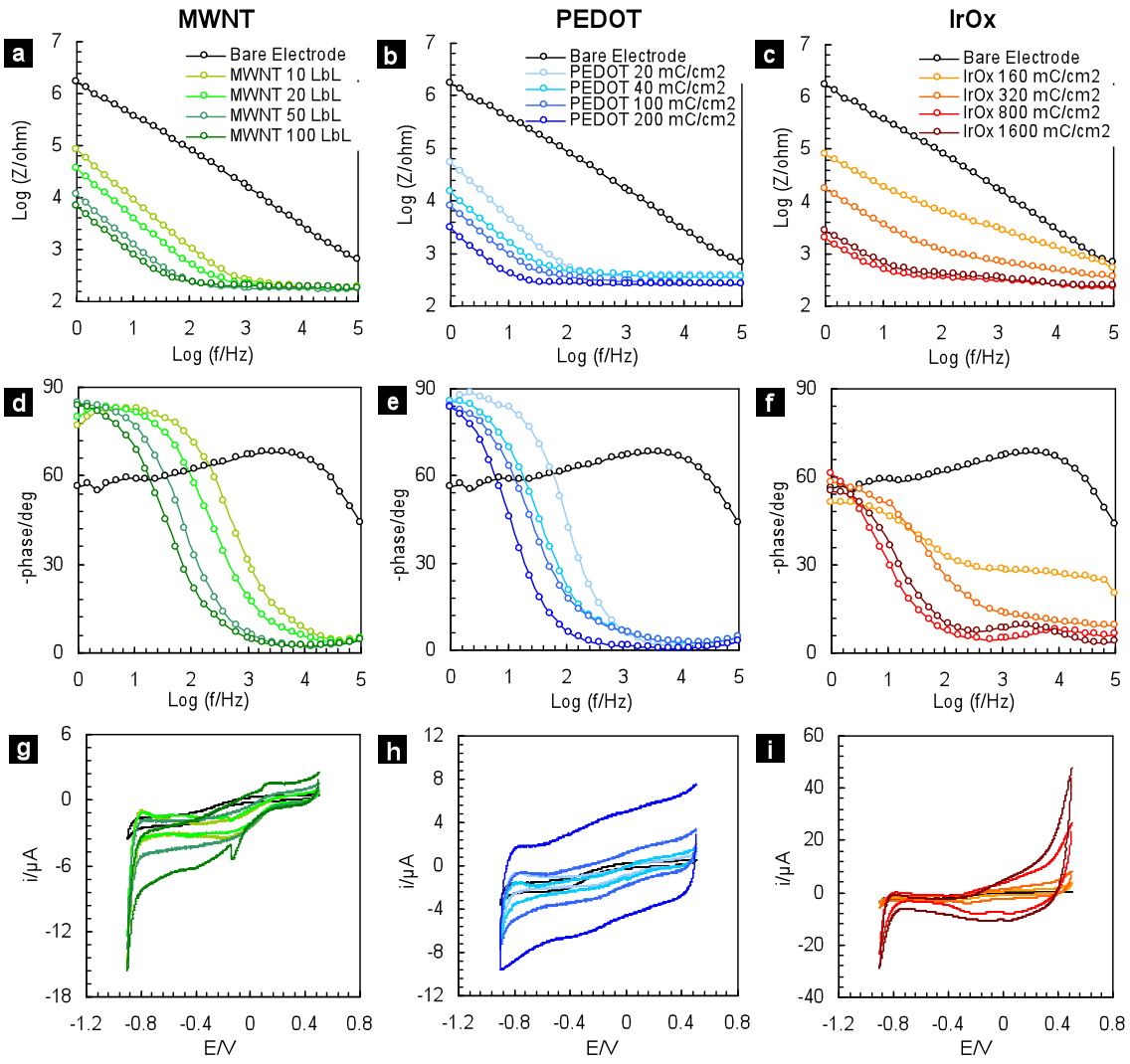

Figure 4.2 Characterization of MWNT, PEDOT, and IrOx coated electrodes. Electrochemical impedance spectroscopy revealed decreasing impedance (**a-c**) and phase angle (**d-f**) with increasing thickness of MWNT, PEDOT, and IrOx coatings on PtIr electrodes. The charge storage capacity of the surface modified electrodes also increased with increasing film thickness as illustrated by cyclic voltammetry (**g-i**).

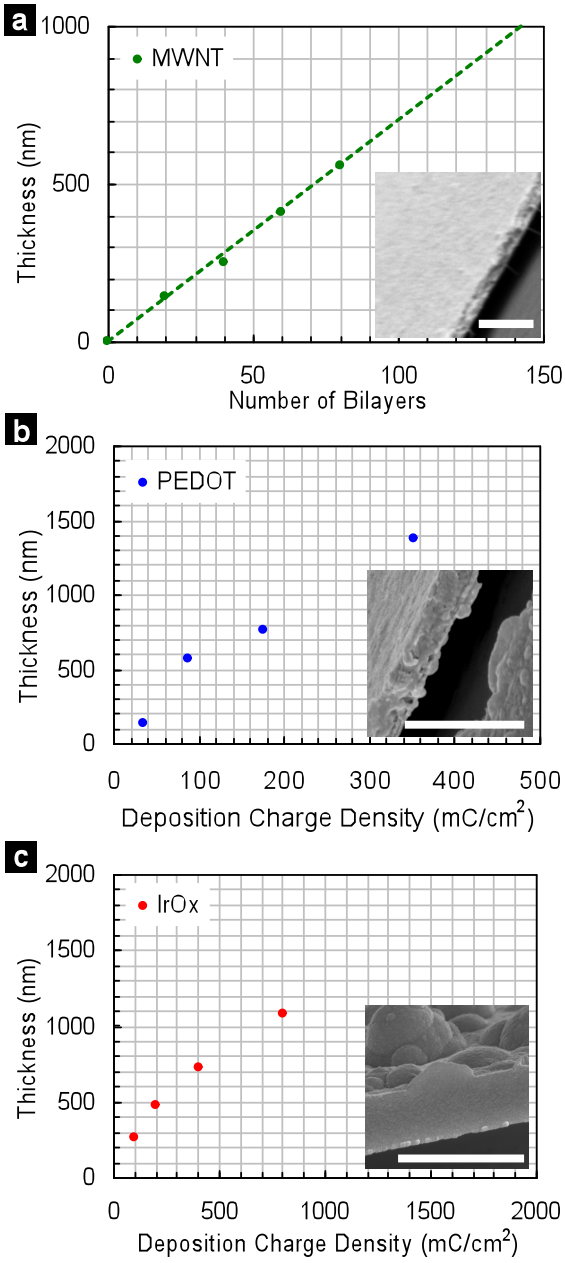

Figure 4.3 Coating thickness as a function of deposition parameters. MWNT (**a**), PEDOT (**b**), and IrOx (**c**) were coated with various numbers of bilayers or deposition charge densities on 6 mm diameter gold sputter coated electrodes, and the cross-sectional thickness of the coatings were measured under SEM. The insets illustrate the cross-sections of an 80-bilayer MWNT coating (**a**), and a PEDOT (**b**) and IrOx (**c**) coating deposited from a charge density of 90 mC/cm2 and 800 mC/cm2, respectively. Scale bars are 2 μm.

The thickness, deposition methods, and chemical composition of electrode coatings significantly affects the electrical and mechanical properties of the films. We chose to compare coatings at a given thickness that would be appropriate for use on clinical devices. By analyzing the measurements on a per unit film thickness basis, we find the MWNT LBL coating to be the most effective material for reducing the interfacial impedance value (Figure 4.4a). With only 10 bilayers of coating corresponding to a thickness of well below 100 nm, the MWNT LBL coating reduced the impedance of the PtIr electrode by two orders of magnitude, from over 17,400 Ω to 277 Ω at the physiologically relevant frequency of 1,000 Hz. At a thickness of 700 nm, the impedance of the MWNT coated electrodes at 1,000 Hz is approximately 30% and 60% lower those coated with PEDOT and IrOx, respectively. These findings suggest that MWNT LBL films can provide the greatest reduction in impedance with minimal impact on the electrode's physical profile, which has important consequence on the extent of tissue damage during the insertion of the electrode.[51]

Total CSC (Figure 4.4b) for the MWNT coated electrodes is higher than those coated with PEDOT and IrOx for the coatings of the same thickness. The total CSC of 11.4 mC/cm^2 reported here for a 600 nm thick PEDOT coating produced from a deposition charge density of 100 mC/cm^2 coincides well with previously published value of 11.3 mC/cm^2 obtained using the same dopant ion, deposition charge density, and CV scanning rate.[52] Note that coating thickness, method of measurements (CV sweep between -0.9 V and 0.5 V), and method of deposition (galvanostatic) were used as normalizing factors to make possible proper comparison of the three different materials.

The highest CSC for a sputtered IrOx film was reported to be 157 mC/cm^2.[53] These data were obtained for 3 µm thick films scanned under exclusively anodic bias and with a slow scanning rate of 0.05 V/s. All these factors obviously increase the apparent values of CSC of electrodes, while not necessarily being the working parameters of actual electrodes implanted in the tissue. The trend displayed in Figure 4.4b gives a systematic comparison of the three materials, which is the primary objective of this study.

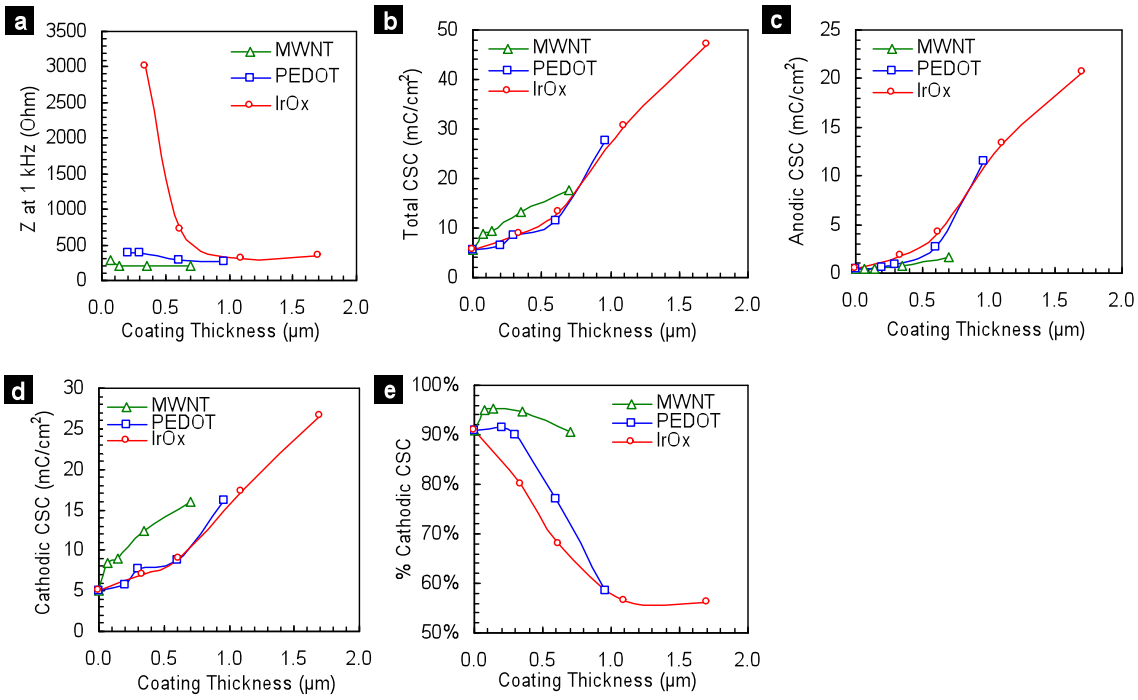

Figure 4.4 Comparison of electrochemical properties on a per unit film thickness basis. Measurements obtained from electrochemical impedance spectroscopy and cyclic voltammetry were normalized by the coating thickness. Impedance at 1 kHz (**a**), total CSC (**b**), anodic CSC (**c**), cathodic CSC (**d**), and % cathodic CSC (**e**) with increasing coating thickness are compared.

The distribution of anodic and cathodic CSCs for the MWNT coating is significantly different from the other two coatings for the potential range investigated. While the anodic CSCs (Figure 4.4c) of the MWNT coated electrodes are the lowest of all, their cathodic CSCs, i.e. the one determining the efficiency of implanted electrodes (Figure 4.4d), are nearly 70% higher than those of the PEDOT and IrOx coated electrodes at the same coating thicknesses. In addition, while the ratio of cathodic CSC to total CSC for the PEDOT and IrOx coatings dropped from 90% to less than 60% with increasing thickness, the MWNT coated electrodes appeared to maintain the ratio above 90% (Figure 4.4e). These are significant distinctions since cathodic stimuli, which initiate cellular action more efficiently, are typically used to stimulate neural tissues,[54] therefore making the cathodic CSC the physiologically relevant parameter in comparing interfacing materials.

To better understand the effect of surface modification, we examined the voltage response of coated electrodes to a 2 mC/cm^2 biphasic, cathodic-first current pulse (Figure 4.5). Such current pulses are commonly employed in the stimulation of nervous tissues.[55] The biphasic stimulation consisted of a 0.5 ms 10 mA cathodic current followed by an anodic current of the same length and magnitude after a 0.2 ms pause, corresponding to a frequency of approximately 1,000 Hz. For better comparison, the electrodes were coated to obtain a thickness of all the materials of ca. 700 nm. The total voltage excursions for the bare, MWNT, PEDOT, and IrOx coated PtIr electrodes were 5.8 V, 3.5 V, 3.8 V, and 4.1 V, respectively (Figure 4.5). As expected, this results correlates with the impedance values of the respective electrodes at 1,000 Hz, with lower impedance producing lower

voltage excursion. The MWNT coated electrodes produced the greatest reduction in voltage excursion, cutting the voltage differential by more than 40%, compared to 34% and 21% for the PEDOT and IrOx coated electrodes, respectively. The results indicate that the MWNT coated electrodes can deliver higher charge densities without producing the high voltages that are known to be extremely harmful to surrounding tissues.

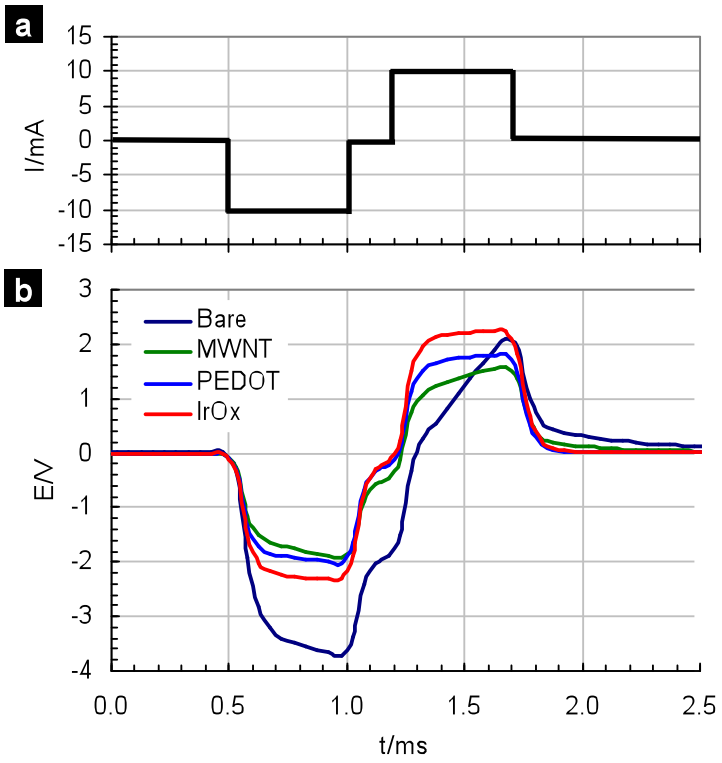

Figure 4.5 Biphasic charge injection. A 2 mC/cm^2 current waveform (**a**) was sourced through bare and coated electrodes and the resulting voltage responses were recorded (**b**). The bare, MWNT, PEDOT, and IrOx coated PtIr electrodes produced a total voltage excursion of 5.8 V, 3.5 V, 3.8 V, and 4.1 V, respectively. The MWNT coated electrode was most efficient in delivering charges, reducing the voltage differential by 40%.

The electrochemical stability of the MWNT LBL electrodes was also tested by subjecting the electrodes to 300 CV scanning cycles at a scan rate of 0.1 V/s. As Figure 4.6a illustrates, the total CSCs of MWNT and PEDOT coated electrodes decreased with increasing number of CV scanning cycles during the initial 100 cycles then gradually stabilized to relatively constant values. We found the MWNT electrode to be a stable interfacial material, losing just 5% of the original CSC, compared to 15% for the PEDOT electrodes. This level of decrease for the PEDOT coated electrodes is supported by previously published results for PSS-doped[52] and surfactant-templated[56] PEDOT coatings. The IrOx-coated electrode showed an initial decline of 8% but regained 3% before maintaining a stabilized percentage comparable to the MWNT coated electrode. Setting aside the possibility of artifacts generated from the sample preparation process, the SEM images suggest extensive cracking on the IrOx coated electrode (Figure 4.6d) that was not observed on the surface of MWNT- and PEDOT-coated electrodes (Figure 4.6b-c). This led to us to suspect that the increase in CSC was due to the formation of new IrOx surface as the layer cracked and exposed additional contact areas in the cracks. In an *in vivo* situation, the cracked brittle IrOx coating can probably easily delaminate, debilitating the electrode functionality and posing a threat to the surrounding tissues.

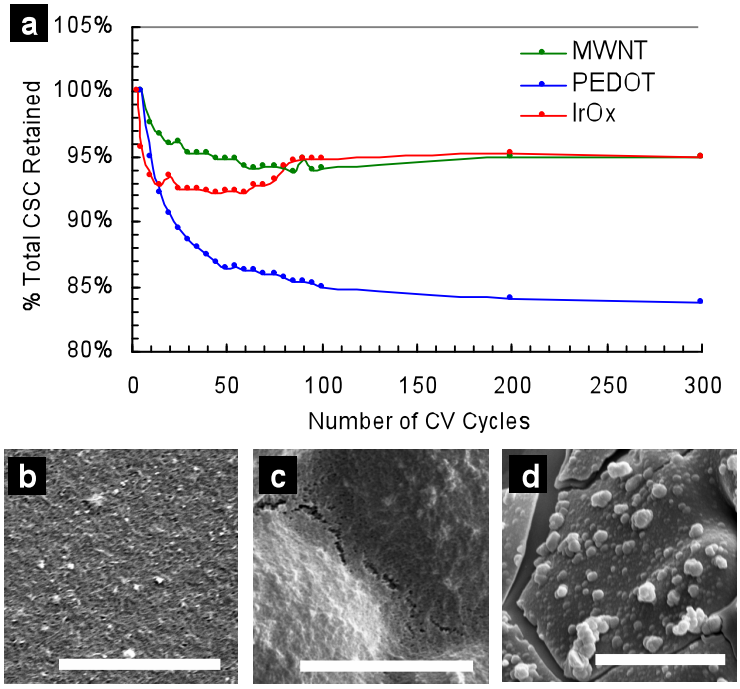

Figure 4.6 Electrochemical stability of MWNT, PEDOT, and IrOx coated PtIr electrodes under repeated cyclic voltammetry scanning cycles. The total charge storage capacities (CSC) of the coated electrodes were recorded while being subjected to 300 cyclic voltammetry scanning cycles (**a**). The data shows a 5% drop in total CSC for the MWNT and IrOx coated electrodes and a 15% decline for PEDOT. SEM images reveal a nearly intact surface on the MWNT coated electrode (**b**) and a slightly and extensively cracked surface for the PEDOT (**c**) and IrOx (**d**) coated electrodes, respectively. Scale bars are 5 μm.

The superior structural stability of LBL assembled CNT multilayer film can be related to its nanoscale morphology. Its stability in physiological conditions has been demonstrated in our previous cell culture studies.[44, 45] The multilayer design can be seen in many biomaterials evolved to exist at the interfaces of different tissues or tissue and environment. Some of the most intriguing biological systems found in nature, such as the sponge spicule[57] and nacre,[58, 59] have a layered architecture that gives rise to their

mechanical strength and unique material properties. Such design can help make use of CNT's electrical[60] and mechanical[48, 60] properties. The inter-digitated nanometer-thick multilayer structure yields flexible thin films[48] of remarkable stability and mechanical strength and creates intimate adhesion to the underlying substrate through molecular species acting at the nanometer length scale.

4.5 Conclusions

In summary, this study carried out a systematic multiparameter comparison of CNT LBL assembled composites in respect to PEDOT, and IrOx films as the most commonly used commercially available materials for biomedical electrodes. Unexpectedly, we found that CNT-PE electrodes substantially outperform most state-of-the art-electrodes in the ability to reduce impedance, increase cathodic charge capacity, and facilitate charge transfer. They successfully compete with promising conducting polymer coatings in respect to electrical impedance and cathodic CSC. The reasons for such performance of these materials are possibly related to CNT electrodes to function as supercapacitors[31, 32] as well as to structural characteristics of the prepared composites with dual electrical and ionic conductivities. The coatings made by LBL assembly are uniform and can carry both ionic and electronic currents and can be characterized as highly stable under electrochemical conditions retaining almost the entire CSC and showing no sign of failure after 300 CV scanning cycles. The morphology of CNT coatings with fibers oriented in parallel to the substrate closely mimics that of

extracellular matrix.[61] However it should be noted that for each of the three materials compared in this study, specifically CNT-PE, PEDOT, and IrOx thin film electrode coatings, the method of deposition, chemical composition, thickness, and micro/nanoscale morphology and topography has a significant effect on electrical, mechanical, and biological interfacing properties.

Despite these promising results, the MWNT-PE composites still have tremendous room for improvement in their electrochemical properties, durability, and biocompatibility. They have passed initial tests in biocompatiblity[44, 45] and the in-depth evaluation is expected to follow. The ultra-strong yet highly flexible characteristic of free-standing LBL films can be quite useful to minimizing mechanical stress exerted on surrounding tissues. Synergistic effects of combining CNT coatings with electrochemically deposited PEDOT and IrOx thin films, in which the functional properties of the resulting electrode surpass the sum of the individual coatings, should also be expected for the adhesion of the electrodeposited films as well as their mechanical and electrical properties.

4.6 References

1. Pena, C.; Bowsher, K.; Samuels-Reid, J., FDA-approved neurologic devices intended for use in infants, children, and adolescents. *Neurology* **2004,** *63* (7), 1163-1167.

2. Pollak, W. M.; Simmons, J. D.; Jr, A. I.; Castellanos, A.; Myerburg, R. J.; Mitrani, R. D., Pacemaker Diagnostics. *Pacing and Clinical Electrophysiology* **2003,** *26* (1p1), 76-98.

3. Middlebrooks, J. C.; Bierer, J. A.; Snyder, R. L., Cochlear implants: the view from the brain. *Current Opinion in Neurobiology* **2005,** *15* (4), 488-493.

4. Fallon, J. B.; Irvine, D. R. F.; Shepherd, R. K., Cochlear implants and brain plasticity. *Hearing Research* **2008,** *238* (1-2), 110-117.

5. Theodore, W. H.; Fisher, R. S., Brain stimulation for epilepsy. *The Lancet Neurology* **2004,** *3* (2), 111-118.

6. Mayberg, H. S.; Lozano, A. M.; Voon, V.; McNeely, H. E.; Seminowicz, D.; Hamani, C.; Schwalb, J. M.; Kennedy, S. H., Deep Brain Stimulation for Treatment-Resistant Depression. *Neuron* **2005,** *45* (5), 651-660.

7. Falowski, S.; Celii, A.; Sharan, A., Spinal Cord Stimulation: An Update. *Neurotherapeutics* **2008,** *5* (1), 86-99.

8. Exner, G.; Baer, G. A., Functional Electrical Stimulation in Paralyzed Respiratory Muscles: International Workshop in Hamburg, Germany. *Neuromodulation* **2000,** *3*, 211-217.

9. Peckham, P. H.; Knutson, J. S., Functional Electrical Stimulation for Neuromuscular Applications. *Annual Review of Biomedical Engineering* **2005,** *7* (1), 327-360.

10. Cogan, S. F.; Troyk, P. R.; Ehrlich, J.; Plante, T. D., In vitro comparison of the charge-injection limits of activated iridium oxide (AIROF) and platinum-iridium microelectrodes. *IEEE Trans. Biomed. Eng.* **2005,** *52* (9), 1612-1614.

11. Troyk, P. R.; Detlefsen, D. E.; Cogan, S. F.; Ehrlich, J.; Bak, M.; McCreery, D. B.; Bullara, L.; Schmidt, E. In *"Safe" charge-injection waveforms for iridium oxide (AIROF) microelectrodes*, Engineering in Medicine and Biology Society, 2004. IEMBS '04. 26th Annual International Conference of the IEEE, 2004; pp 4141-4144 Vol.6.

12. Stuart, F. C.; Philip, R. T.; Julia, E.; Christina, M. G.; Timothy, D. P., The influence of electrolyte composition on the in vitro charge-injection limits of activated

iridium oxide (AIROF) stimulation electrodes. *Journal of Neural Engineering* **2007,** (2), 79.

13. Weiland, J. D.; Anderson, D. J.; Humayun, M. S., In vitro electrical properties for iridium oxide versus titanium nitride stimulating electrodes. *IEEE Trans. Biomed. Eng.* **2002,** *49* (12), 1574-1579.

14. Meyer, R. D.; Cogan, S. E.; Nguyen, T. H.; Rauh, R. D., Electrodeposited iridium oxide for neural stimulation and recording electrodes. *Ieee Transactions on Neural Systems and Rehabilitation Engineering* **2001,** *9* (1), 2-11.

15. Weiland, J. D.; Anderson, D. J., Chronic neural stimulation with thin-film, iridium oxide electrodes. *Ieee Transactions on Biomedical Engineering* **2000,** *47* (7), 911-918.

16. Mailley, S.; Hyland, M.; Mailley, P.; McLaughlin, J. A.; McAdams, E. T., Thin film platinum cuff electrodes for neurostimulation: in vitro approach of safe neurostimulation parameters. *Bioelectrochemistry* **2004,** *63* (1-2), 359-364.

17. Niebauer, M. J.; Wilkoff, B.; Yamanouchi, Y.; Mazgalev, T.; Mowrey, K.; Tchou, P., Iridium Oxide–Coated Defibrillation Electrode : Reduced Shock Polarization and Improved Defibrillation Efficacy. *Circulation* **1997,** *96* (10), 3732-3736.

18. Green, R. A.; Lovell, N. H.; Wallace, G. G.; Poole-Warren, L. A., Conducting polymers for neural interfaces: Challenges in developing an effective long-term implant. *Biomaterials* **2008,** *29* (24-25), 3393-3399.

19. Guimard, N. K.; Gomez, N.; Schmidt, C. E., Conducting polymers in biomedical engineering. *Progress in Polymer Science* **2007,** *32* (8-9), 876-921.

20. Xiao, Y.; Cui, X.; Hancock, J. M.; Bouguettaya, M.; Reynolds, J. R.; Martin, D. C., Electrochemical polymerization of poly(hydroxymethylated-3,4-ethylenedioxythiophene) (PEDOT-MeOH) on multichannel neural probes. *Sensors and Actuators B: Chemical* **2004,** *99* (2-3), 437-443.

21. Yang, J. Y.; Lipkin, K.; Martin, D. C., Electrochemical fabrication of conducting polymer poly(3,4-ethylenedioxythiophene) (PEDOT) nanofibrils on microfabricated neural prosthetic devices. *Journal of Biomaterials Science-Polymer Edition* **2007,** *18* (8), 1075-1089.

22. Cui, X. T.; Zhou, D. D., Poly (3,4-Ethylenedioxythiophene) for Chronic Neural Stimulation. *Neural Systems and Rehabilitation Engineering, IEEE Transactions on* **2007,** *15* (4), 502-508.

23. Cui, X. Y.; Martin, D. C., Electrochemical deposition and characterization of poly(3,4-ethylenedioxythiophene) on neural microelectrode arrays. *Sensors and Actuators B-Chemical* **2003,** *89* (1-2), 92-102.

24. Hendricks, J. L.; Chikar, J. A.; Crumling, M. A.; Raphael, Y.; Martin, D. C., Localized cell and drug delivery for auditory prostheses. *Hearing Research* **2008,** *242* (1-2), 117-131.

25. Kim, D. H.; Richardson-Burns, S. M.; Hendricks, J. L.; Sequera, C.; Martin, D. C., Effect of immobilized nerve growth factor on conductive polymers: Electrical properties and cellular response. *Advanced Functional Materials* **2007,** *17* (1), 79-86.

26. Abidian, M. R.; Martin, D. C., Experimental and theoretical characterization of implantable neural microelectrodes modified with conducting polymer nanotubes. *Biomaterials* **2008,** *29* (9), 1273-1283.

27. Abidian, M. R.; Kim, D. H.; Martin, D. C., Conducting-polymer nanotubes for controlled drug release. *Advanced Materials* **2006,** *18* (4), 405-+.

28. Mailley, S. C.; Hyland, M.; Mailley, P.; McLaughlin, J. M.; McAdams, E. T., Electrochemical and structural characterizations of electrodeposited iridium oxide thin-film electrodes applied to neurostimulating electrical signal. *Materials Science and Engineering: C* **2002,** *21* (1-2), 167-175.

29. Cogan, S. F.; Guzelian, A. A.; Agnew, W. F.; Yuen, T. G. H.; McCreery, D. B., Over-pulsing degrades activated iridium oxide films used for intracortical neural stimulation. *Journal of Neuroscience Methods* **2004,** *137* (2), 141-150.

30. Chunsheng, D.; Ning, P., High power density supercapacitor electrodes of carbon nanotube films by electrophoretic deposition. *Nanotechnology* **2006,** (21), 5314.

31. An, K. H.; Kim, W. S.; Park, Y. S.; Choi, Y. C.; Lee, S. M.; Chung, D. C.; Bae, D. J.; Lim, S. C.; Lee, Y. H., Supercapacitors Using Single-Walled Carbon Nanotube Electrodes. *Advanced Materials* **2001,** *13* (7), 497-500.

32. Futaba, D. N.; Hata, K.; Yamada, T.; Hiraoka, T.; Hayamizu, Y.; Kakudate, Y.; Tanaike, O.; Hatori, H.; Yumura, M.; Iijima, S., Shape-engineerable and highly densely packed single-walled carbon nanotubes and their application as super-capacitor electrodes. *Nat Mater* **2006,** *5* (12), 987-994.

33. Hu, H.; Ni, Y.; Montana, V.; Haddon, R. C.; Parpura, V., Chemically Functionalized Carbon Nanotubes as Substrates for Neuronal Growth. *Nano Lett.* **2004,** *4* (3), 507-511.

34. Mattson, M. P.; Haddon, R. C.; Rao, A. M., Molecular functionalization of carbon nanotubes and use as substrates for neuronal growth. *J. Mol. Neurosci.* **2000,** *14* (3), 175-182.

35. Gabay, T.; Jakobs, E.; Ben-Jacob, E.; Hanein, Y., Engineered self-organization of neural networks using carbon nanotube clusters. *Physica A: Statistical Mechanics and its Applications* **2005,** *350* (2-4), 611-621.

36. Zhang, X.; Prasad, S.; Niyogi, S.; Morgan, A.; Ozkan, M.; Ozkan, C. S., Guided neurite growth on patterned carbon nanotubes. *Sensors and Actuators B: Chemical* **2005,** *106* (2), 843-850.

37. Hu, H.; Ni, Y.; Mandal, S. K.; Montana, V.; Zhao, B.; Haddon, R. C.; Parpura, V., Polyethyleneimine Functionalized Single-Walled Carbon Nanotubes as a Substrate for Neuronal Growth. *J. Phys. Chem. B* **2005,** *109* (10), 4285-4289.

38. Nguyen-Vu, T. D. B.; Hua, C.; Cassell, A. M.; Andrews, R. J.; Meyyappan, M.; Jun, L., Vertically Aligned Carbon Nanofiber Architecture as a Multifunctional 3-D Neural Electrical Interface. *Biomedical Engineering, IEEE Transactions on* **2007,** *54* (6), 1121-1128.

39. Thomas, J. W.; Michael, C. W.; Janice, L. M.; Rachel, L. P.; Jeremiah, U. E., Nano-biotechnology: carbon nanofibres as improved neural and orthopaedic implants. *Nanotechnology* **2004,** (1), 48.

40. Lovat, V.; Pantarotto, D.; Lagostena, L.; Cacciari, B.; Grandolfo, M.; Righi, M.; Spalluto, G.; Prato, M.; Ballerini, L., Carbon Nanotube Substrates Boost Neuronal Electrical Signaling. *Nano Lett.* **2005,** *5* (6), 1107-1110.

41. Yu, Z.; McKnight, T. E.; Ericson, M. N.; Melechko, A. V.; Simpson, M. L.; Morrison, B., Vertically Aligned Carbon Nanofiber Arrays Record Electrophysiological Signals from Hippocampal Slices. *Nano Lett.* **2007,** *7* (8), 2188-2195.

42. Mazzatenta, A.; Giugliano, M.; Campidelli, S.; Gambazzi, L.; Businaro, L.; Markram, H.; Prato, M.; Ballerini, L., Interfacing Neurons with Carbon Nanotubes: Electrical Signal Transfer and Synaptic Stimulation in Cultured Brain Circuits. *J. Neurosci.* **2007,** *27* (26), 6931-6936.

43. Keefer, E. W.; Botterman, B. R.; Romero, M. I.; Rossi, A. F.; Gross, G. W., Carbon nanotube coating improves neuronal recordings. *Nat Nano* **2008,** *3* (7), 434-439.

44. Gheith, M. K.; Sinani, V. A.; Wicksted, J. P.; Matts, R. L.; Kotov, N. A., Single-walled carbon nanotube polyelectrolyte multilayers and freestanding films as a biocompatible platformfor neuroprosthetic implants. *Advanced Materials* **2005,** *17* (22), 2663-+.

45. Jan, E.; Kotov, N. A., Successful differentiation of mouse neural stem cells on layer-by-layer assembled single-walled carbon nanotube composite. *Nano Letters* **2007,** *7* (5), 1123-1128.

46. Gheith, M. K.; Pappas, T. C.; Liopo, A. V.; Sinani, V. A.; Shim, B. S.; Motamedi, M.; Wicksted, J. R.; Kotov, N. A., Stimulation of neural cells by lateral layer-by-layer films of single-walled currents in conductive carbon nanotubes. *Advanced Materials* **2006,** *18* (22), 2975-+.

47. Marzouk, S. A. M.; Ufer, S.; Buck, R. P.; Johnson, T. A.; Dunlap, L. A.; Cascio, W. E., Electrodeposited Iridium Oxide pH Electrode for Measurement of Extracellular Myocardial Acidosis during Acute Ischemia. *Anal. Chem.* **1998,** *70* (23), 5054-5061.

48. Mamedov, A. A.; Kotov, N. A.; Prato, M.; Guldi, D. M.; Wicksted, J. P.; Hirsch, A., Molecular design of strong single-wall carbon nanotube/polyelectrolyte multilayer composites. *Nature Materials* **2002,** *1* (3), 190-194.

49. He, W.; Bellamkonda, R. V., Nanoscale neuro-integrative coatings for neural implants. *Biomaterials* **2005,** *26* (16), 2983-2990.

50. O'Connell, M. J.; Boul, P.; Ericson, L. M.; Huffman, C.; Wang, Y.; Haroz, E.; Kuper, C.; Tour, J.; Ausman, K. D.; Smalley, R. E., Reversible water-solubilization of single-walled carbon nanotubes by polymer wrapping. *Chemical Physics Letters* **2001,** *342*, 265-271.

51. Griffith, R. W.; Humphrey, D. R., Long-term gliosis around chronically implanted platinum electrodes in the Rhesus macaque motor cortex. *Neuroscience Letters* **2006,** *406* (1-2), 81-86.

52. Yamato, H.; Ohwa, M.; Wernet, W., Stability of polypyrrole and poly(3,4-ethylenedioxythiophene) for biosensor application. *Journal of Electroanalytical Chemistry* **1995,** *397* (1-2), 163-170.

53. Wessling, B.; Mokwa, W.; Schnakenberg, U., Sputtered Ir Films Evaluated for Electrochemical Performance I. Experimental Results. *Journal of The Electrochemical Society* **2008,** *155* (5), F61-F65.

54. Stieglitz, T.; Meyer, J.-U., Neural Implants in Clinical Practice. In *BioMEMS*, 2006; pp 41-70.

55. Merrill, D. R.; Bikson, M.; Jefferys, J. G. R., Electrical stimulation of excitable tissue: design of efficacious and safe protocols. *Journal of Neuroscience Methods* **2005,** *141* (2), 171-198.

56. Yang, J. Y.; Kim, D. H.; Hendricks, J. L.; Leach, M.; Northey, R.; Martin, D. C., Ordered surfactant-templated poly(3,4-ethylenedioxythiophene) (PEDOT) conducting polymer on microfabricated neural probes. *Acta Biomaterialia* **2005,** *1* (1), 125-136.

57. Aizenberg, J.; Sundar, V. C.; Yablon, A. D.; Weaver, J. C.; Chen, G., Biological glass fibers: Correlation between optical and structural properties. *Proceedings of the National Academy of Sciences of the United States of America* **2004,** *101* (10), 3358-3363.

58. Tang, Z.; Kotov, N. A.; Magonov, S.; Ozturk, B., Nanostructured artificial nacre. *Nat Mater* **2003,** *2* (6), 413-418.

59. Jackson, A. P.; Vincent, J. F. V.; Turner, R. M., The Mechanical Design of Nacre. *Proc. R. Soc. Lond. Ser. B-Biol. Sci.* **1988,** *234* (1277), 415-&.

60. Shim, B. S.; Tang, Z. Y.; Morabito, M. P.; Agarwal, A.; Hong, H. P.; Kotov, N. A., Integration of conductivity transparency, and mechanical strength into highly homogeneous layer-by-layer composites of single-walled carbon nanotubes for optoelectronics. *Chemistry of Materials* **2007,** *19* (23), 5467-5474.

61. Mwenifumbo, S.; Shaffer, M. S.; Stevens, M. M., Exploring cellular behaviour with multi-walled carbon nanotube constructs. *Journal of Materials Chemistry* **2007,** *17* (19), 1894-1902.

CHAPTER 5

Enhanced Differentiation and Electrical Stimulation of Neural Stem Cells Mediated by Carbon Nanotube Composites Containing Extracellular Matrix Protein

5.1 Abstract

One of the key challenges to engineering neural interfaces is to minimize their immune response toward foreign materials. One potential approach is to manufacture materials that bear greater structural resemblance to living tissues and by incorporating neural stem cells within the materials. The unique electrical and mechanical properties of carbon nanotubes make them an excellent candidate for neural interfaces, but their adoption hinges on finding approaches for "humanizing" nanotube-based materials. In this study, we demonstrated the fabrication of layer-by-layer assembled composites from single-walled carbon nanotubes (SWNTs) and laminin, which is an essential part of human extracellular matrix, and investigated the ability of the films to mediate the differentiation and electrical stimulation of neural stem cells (NSCs). Laminin-SWNT thin films were found to be conducive to NSC differentiation and suitable for their successful excitation. We observed extensive outgrowth from neurospheres and formation of functional neural network as indicated by the presence of synaptic

connections. Calcium imaging of the NSCs revealed generation of action potentials upon the application of a lateral current through the SWNT substrate, confirming the functionality of the differentiated NSCs and the utility of the conductive substrate. These results indicate that the protein-SWNT composite can serve as materials foundation of neural electrodes with chemical structure better adapted with long-term integration with the neural tissue.

5.2 Introduction

In recent years, carbon nanotubes have been widely explored for adoption in the biological realm in the form of biosensors and as agents of cellular transport and delivery.[1-4] Single-walled (SWNTs) and multi-walled carbon nanotubes (MWNTs) are also attractive candidates for developing interfaces with biological systems due to the promise of superior physical, electrical, mechanical and optical properties in comparison with traditional materials.[5] This research direction is of particular relevance to the field of neural prosthetics field as strategies for the diagnosis, therapy and treatment of neural disorders are increasingly relying on electrical stimulation techniques. However, these current techniques have several inherent problems that are associated with the traditional materials used for manufacturing of neural electrodes (NEs).[6, 7]

The interactions between various cell lines and carbon nanotubes[1, 3, 4, 8, 9] have been previously reported, including the adhesion, growth and differentiation of neuronal

cells on carbon nanotubes-based substrates. Most recently, the ability of such substrates to electrically stimulate neuronal cells was reported.[9-12] The strong interest in interfacing neuronal cells and carbon nanotubes is not accidental; the unique set of properties of carbon nanotubes make them an excellent candidate to address the acute need for better neural electrodes (NEs). The current problems facing neuroprosthetic devices include the following: (1) long-term inflammatory response of the neural tissues, which results in the neuron depletion around the electrodes and their replacement with reactive astrocytes preventing signal transduction, (2) delamination[6] and degradation[6, 7] of thin metal electrodes off the plastic substrates that drastically decrease the stimulation abilities, (3) the need for significant miniaturization of the electrodes which is currently limited not by manufacturing abilities but by electrical properties of the cell-electrode interface, and (4) the need to achieve mechanical compliance with the neural tissues to attain adequate long-term performance, which cannot be addressed by semiconductor devices that can partially resolve some of the above-mentioned issues.[13-15]

In this work we want to propose three current approaches to resolve these issues:

(1) Exploitation of on the mechanical and electrical properties of nanostructured materials to develop new electrodes. Such materials, including carbon nanotubes composites would be able to trigger a drastic decrease of delamination, while meeting the necessary mechanical and miniaturization requirements for NEs.

(2) Incorporation of neural stem cells (NSCs) with the NE due to their ability to differentiate into functional neurons, in damaged areas of the central nervous

system.[16, 17] This could result in significant reduction of inflammation of the neural tissue.

(3) Achieving better integration of tissues and NEs by "humanizing" the material, i.e. making it structurally and chemically more similar to tissues surrounding neurons.

Detailed evaluation of all of these approaches will probably require several years and, certainly, cannot be done in one paper. Nevertheless, what we intend to do here is to demonstrate the technical feasibility of manufacturing electrodes that satisfy the requirements of these hypotheses so that their evaluation can be carried out. In particular, the focus will be placed on feasibility of developing CNT-based electrodes that incorporate extracellular matrix proteins, one of the key components of tissues surrounding neurons and stem cell compatible materials.

5.3 Methods

5.3.1 Thin Film Fabrication

CNT thin films were fabricated by a layer-by-layer (LBL) method, with alternating layers of single-walled carbon nanotubes (SWNT) and the protein laminin. SWNT made by the Hipco process were obtained from Carbon Nanotechnologies Inc. and dispersed by bath sonication in a 1% aqueous solution of polystyrene-4-sulfonate

(PSS, MW 1,000, 000). The laminin was obtained from Sigma-Aldrich and used as a 100 μg/mL solution in PBS. Thin films were fabricated on a #1 glass coverslide by dipping the substrate in the SWNT suspension and protein solution alternatively, with thorough rinsing in DI water at each step. The dipping time for each step of laminin and SWNT adsorption was 30 min.

5.3.2 Cell Lines

Neural stem cells (NSC) were purchased from Stemcell Technologies and were grown and differentiated according to the company's protocols.

5.3.3 Cell Interfacing with Thin Films

To enable cell seeding onto the SWNT substrates, cloning rings are mounted on the substrate with high-vacuum grease serving as the adhesive. The attached cloning rings provide a chamber (with volume capacity of ~400 μL) for holding culture media required for cell growth. After the sterilization process, the SWNT samples are passivated with the appropriate cell media for at least 12 hr at 37ºC and in a humidified, 5% CO_2 environment. NSC cell suspensions are then seeded within the designed cell chambers in the appropriate differentiation medium. The cells are allowed to incubate for at least 12 hours prior to subsequent studies.

5.4 Results and Discussion

The development of these CNT-based electrodes for NEs hinges on the ability to process SWNTs or MWNTs in thin coatings or bulk composites. It is particularly important for the case of NSCs because some components of the composites and/or the nano-scale morphology of the interface can alter the differentiation pathway of the stem cells.[18, 19] While, there is a number of methods that can be used to yield carbon nanotubes film processing in substrates for neural growth, including simple solvent evaporation, chemical vapor deposition, and electrochemical deposition,[20-29] not all of them may be suitable for NE purposes. In particular, many of these methods do not yield coatings that possess the mechanical stability and actual conductivity that are key for NE as discussed above. On the other hand, the technique of layer-by-layer assembly (LBL) provides a high level of control and tailoring with respect to the film composition, including the polymeric components used.[30] It also makes the coating exceptionally mechanically robust.[31] The ability of carbon nanotubes thin films made by LBL to support growth, proliferation and differentiation and to electrically stimulate adult cancer cells of neuroblastoma NG108-15[9, 10] and their ability to support the growth of NSCs in culture[32] was reported recently. The LBL fabrication for the previous neuronal cell studies has however relied on the use of a synthetic non-biological polymer,[9, 10] which is one of the potential problems with this method. Along with other points addressing the hypotheses 1 and 2, we demonstrate in this study that LBL films consisting of SWNTs and natural polymers such as laminin, serve as a biocompatible substrate for promoting adhesion and differentiation as well as for mediating electrical stimulation of neuronal cell lines.

Overall, the interfacing of the biocompatible, electrically conductive and mechanically strong SWNT thin films with NSCs is likely to be of particular relevance for developing implantable prostheses.

The favorable biological properties of carbon nanotubesthat have been previously reported [12, 23, 24] provide an excellent foundation for exploitation of these properties in implantable medical devices. However, the critical issue of making tissue-friendly material still needs to be addressed for carbon nanotube-based NEs. One of the most logical ways to achieve this is to include molecules most familiar to the cells in the interfacial environment; such molecules are from extracellular matrix (ECM). While the incorporation of ECM proteins in carbon nanotubes composites made by many processing methods mentioned before, such as simple blending and solvent evaporation, might be faced with fast elution of the protein, the LBL technique can curtail this shortcoming. This technique, which is based on alternating the layers of nanotubes (or other nanoscale building blocks) and polymers, is versatile and can be easily adapted for the incorporation of biological components such as the ECM proteins. In this study, we explore and evaluate the performance of CNT-based NEs made by LBL method and that incorporate ECM proteins. The LBL films consisted from SWNTs (HIPCO, Tubes@Rice.com) wrapped with poly(styrene-4-sulfonate) (PSS, MW = 1,000,000, 1% in water, Sigma-Aldrich) and the glycoprotein laminin (MW ~ 900 kD, 100 μg/mL in PBS at pH 7.4). The latter is an important protein in the basement membrane that is widely used for coating substrate to promote cell adhesion and neurite outgrowth.[33]

Dipping time of 30 min per single step of laminin and SWNT adsorption was used throughout the project.

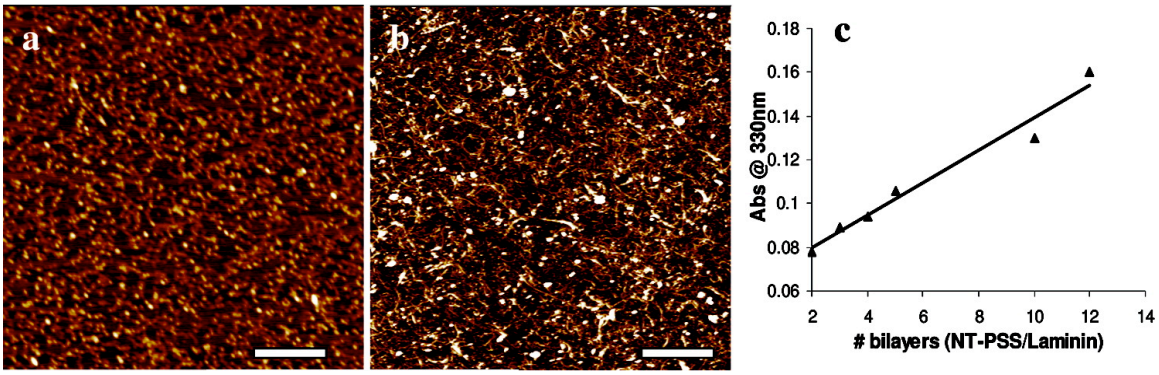

Figure 5.1 Fabrication of LBL films of SWNTs and laminin. Atomic force microscopy image of (**a**) one monolayer of laminin on piranha-treated SiO_2 substrate and (**b**) 6 bilayers of SWNT/laminin on the same substrate. (**c**) Successful accumulation of laminin-SWNT layers on glass substrate monitored by UV-vis absorption.

Despite its large size, laminin (isoelectric point is pH 7) appeared to interact strongly with the negatively charged, piranha-treated substrate upon deposition of the first layer. Atomic force microscopy (AFM) image of a single layer of laminin on a silicon oxide substrate indicated a uniform coating of the protein (Figure 5.1a). AFM was also utilized to assess the subsequent interactions between the deposited laminin and the SWNT dispersions and confirmed deposition of SWNT onto the laminin layer (Figure 5.1b). This observation is consistent with reports of strong electrostatic and nonspecific adsorption of proteins to carbon nanotubes.[34, 35] The film progress of multilayer depositions was monitored by UV-VIS absorption, which indicated linear increase in

SWNT concentration on the thin films with increasing number of bilayers (Figure 5.1c) as expected for the traditional mode of LBL growth observed before.

As the first step in examination of suitability of SWNT-laminin composites suitability for the use as NEs, LBL films of up to 30 bilayers were made and the ability of cells to adhere on the SWNT/laminin substrate was assessed (Table 4.1). The architectures of the LBL films tested, that is number of deposition cycles, their sequence and the composition of the final layer, were chosen based on several factors: the fact that cells typically adhere better to positively charged surfaces and that heat treatment enhances cross-linking among the layers within SWNT LBL films and causes an increase in electrical conductivity.[36, 37] In particular the influence of the structure of the polymeric component(s) of the LBL film and the annealing step were investigated. We found that cell adhesion markedly depended on the composition of the final layer. The initial ability of cells to adhere to the substrate was assessed 24 h following seeding and at various time points leading to 7 days post-seeding (Table 4.1). The substrate that was most conducive to cell adhesion and attachment was the LBL film that contained SWNT as the topmost layer and that was heat treated. Control experiments with laminin coated slides (no SWNT) that were either used as made or following heat treatment were also carried out in parallel. Interestingly enough, not all "humanized" protein composites revealed sufficient adhesion of the cells. As-made films did not reveal any cell adhesion after 7 days (Table 4.1). This is likely to be related with gel-like behavior of laminin. Swelling of its composites in water apparently reduced stiffness of the substrates and prevented cell adhesion. On the contrary, SWNT-laminin films obtained after annealing,

i.e. after cross-linking, exhibited sufficient stiffness[38] and served as excellent adhesion support for cells (Table 4.1). Note that SWNTs and other inorganic materials substantially increase thermal stability of proteins and other macromolecules and drastically reduce the decomposition of these materials at high temperature.[39, 40] So, while altering the structure of the proteins, thermal annealing for a fairly short time used here does not certainly destroy laminin structure completely as one might expect from pure laminin coatings.

LBL film configuration (15 bilayers)	**Cell adhesion (day 1)**	**Cell adhesion (day 7)**
Laminin as final layer	Yes	No
PSS-wrapped SWNT as final layer	Yes	No
Laminin as final layer, annealed at 300 °C (10 min)	No	No
PSS-wrapped SWNT as final layer, annealed at 300 °C (10 min)	Yes	Yes

Table 5.1 Summary of various LBL configurations investigated in cell seeding and cell adhesion experiments.

The interfacing between neuronal cells and the heat-treated SWNT/laminin LBL film was monitored more closely by measuring neuronal outgrowth from the cells. When compared to neuronal behavior on laminin-coated glass slides, longer outgrowths were noted at every time point (24 h -120 h) on the heat treated SWNT/laminin substrate. The

biocompatibility of the annealed SWNT/laminin substrate was also verified via a commercial cell viability assay that confirmed previous reports on the biocompatibility of SWNT substrates (Figure 5.2e). They indicated that 98% of cells on the surface of SWNT-laminin composite were viable.

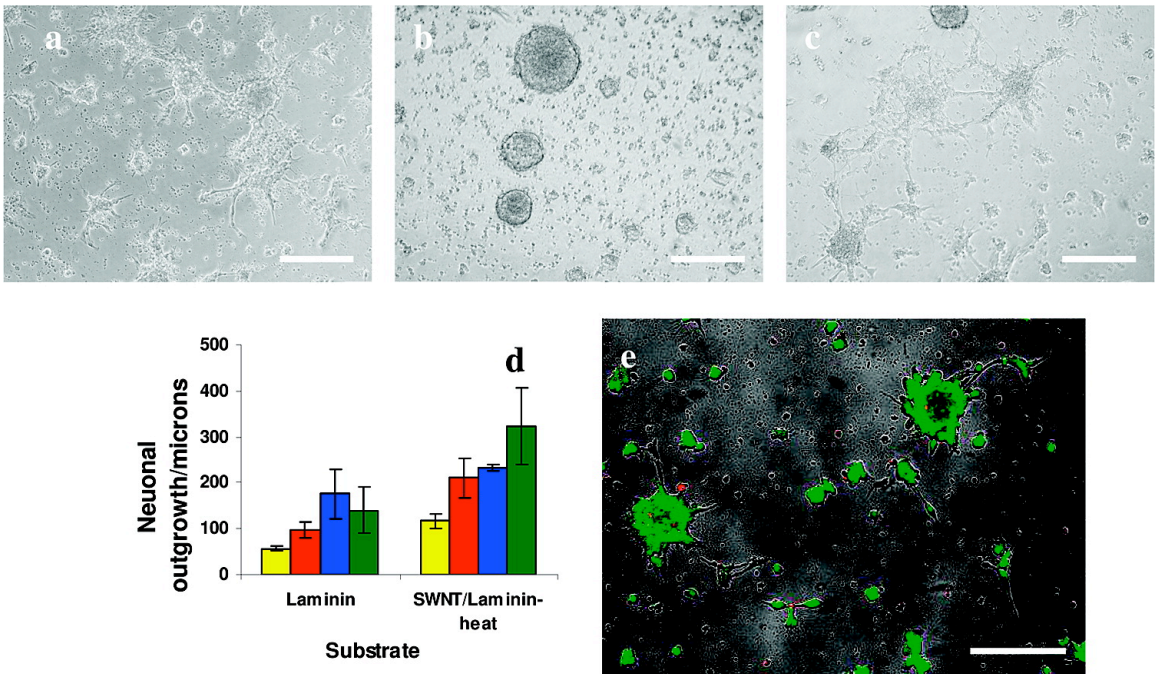

Figure 5.2 Micrograph assessing NSC cell adhesion and differentiation 72 h after initial seeding on (**a**) laminin-coated glass slides and on 10 bilayers SWNT/laminin thin films that were (**b**) used as is or (**c**) heated at 300 °C for 10 min. (**d**) Distance of outgrowth from neurospheres after 24h (yellow), 48h (red), 72h (blue) and 120h (green) on laminin-coated slides and heat-treated SWNT/laminin film on slide. (**e**) Live-dead viability assay on seeded cells where live cells are stained green and dead cells are red. (scale bar = 200 μm)

The observation of neuronal outgrowths from the adhered cells is a promising indication of successful cell differentiation. However, in the context of this study more concrete evidence is required to indicate that neural stem cells are capable of transforming into neuronal cells following adhesion to the SWNT substrate. Neural stem cells have been shown to transform into functioning neurons as well as glial cells such as astrocytes and oligodendrocytes.[17, 41] Following cell seeding on the SWNT substrates, the NSCs were immunostained with neuronal markers and observed by confocal fluorescence microscopy. The protein markers studied included MAP-2 (for neurons), glial fibrillary acidic protein, GFAP (for astrocytes), and nestin (for NSCs). The results indicate that even though neural stem cells precursors still exist 7 days post-seeding on the heat-treated SWNT/laminin substrate, differentiated neurons and glial cells are also present in large amounts due to spontaneous differentiation caused probably by the physical properties of the SWNT-laminin composites. Interestingly, most of the adhered cells showed some signs of differentiation, which can be advantageous from NE perspective. The strong presence of neurons (MAP-2, Figure 5.3a, green staining) provides indication that successful neuronal communication could possibly be established between cells grown on the CNT substrate and the surrounding tissue.

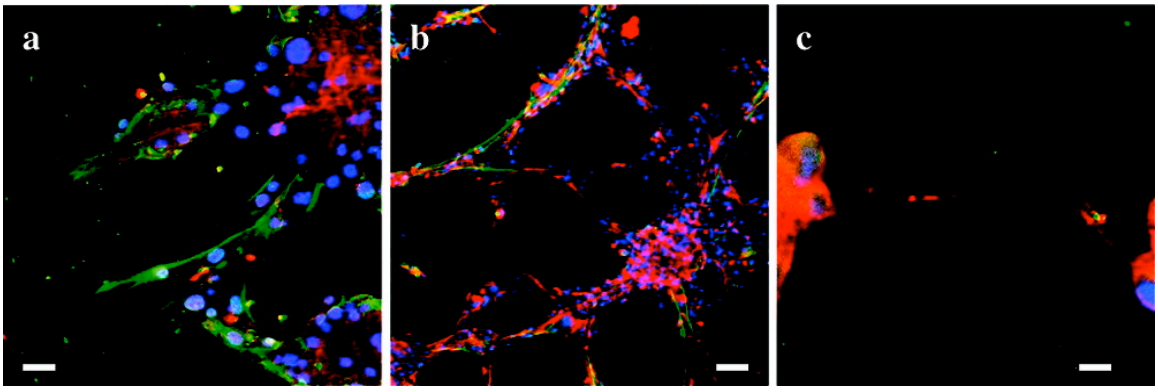

Figure 5.3 Immunostaining of spontaneously differentiated NSCs on heat-treated SWNT/laminin thin films. The blue color in all images indicates DAPI staining of cell nuclei. In (**a**) GFAP staining is red and MAP-2 staining is green. In (**b**) GFAP staining is red and nestin staining is green. In (**c**) cell were stained red for the presence of synapsin.

It is interesting to verify the presence of synaptic connection between differentiated cells, which would also show the possibility of connectivity between the cells grown on the SWNT-composite and fairly efficient signal transmission. Synapses or synaptic nodes are crucial elements in the propagation of electrochemical signals from cells to cells that ensure communication within a neuronal population.[42] The cells seeded on the CNT surface were thus immunostained for the presence of synapsin protein with the appropriate markers. Synapsin is present between the differentiated cells, thus further confirming that neuronal cell growth and differentiation on the SWNT/laminin thin films result in functional neuronal networks (Figure 5.3c).

Once the biocompatibility and cellular composition on the laminin-SWNT substrates is established, it is necessary to demonstrate the possibility to excite the neuronal cells residing on the nanotubes-protein films. The conductivity of a 10-bilayer

SWNT/laminin thin film was estimated to be 430 and 2,140 S/m before and after heat treatment, respectively. Drastic increase of conductivity after heat treatment is not surprising, and is also related to reduced swelling behavior. It is certainly beneficial for the design of NEs based on these composites. An electrical signal was applied to the cells via application of a lateral current through the nanotube substrate. The electrical stimulus was applied in a similar fashion as in the previous study,[10] via electrical leads that induce a lateral electric field within the entire SWNT/laminin substrate. The device set up used is shown in Figure 5.4a: two cloning rings were mounted on the LBL film to serve as chambers for the cell and aqueous media. The electrical leads were attached directly the dry area of the SWNT film by using silver paste and copper tape. The input stimulation was applied with the aid of a function generator (Instek Instruments) that gave flexibility in the stimulus signal to be applied. Constant DC signals as well as pulsed signals were utilized in this study and were typically verified by the use of an oscilloscope prior to cell stimulation/recording.

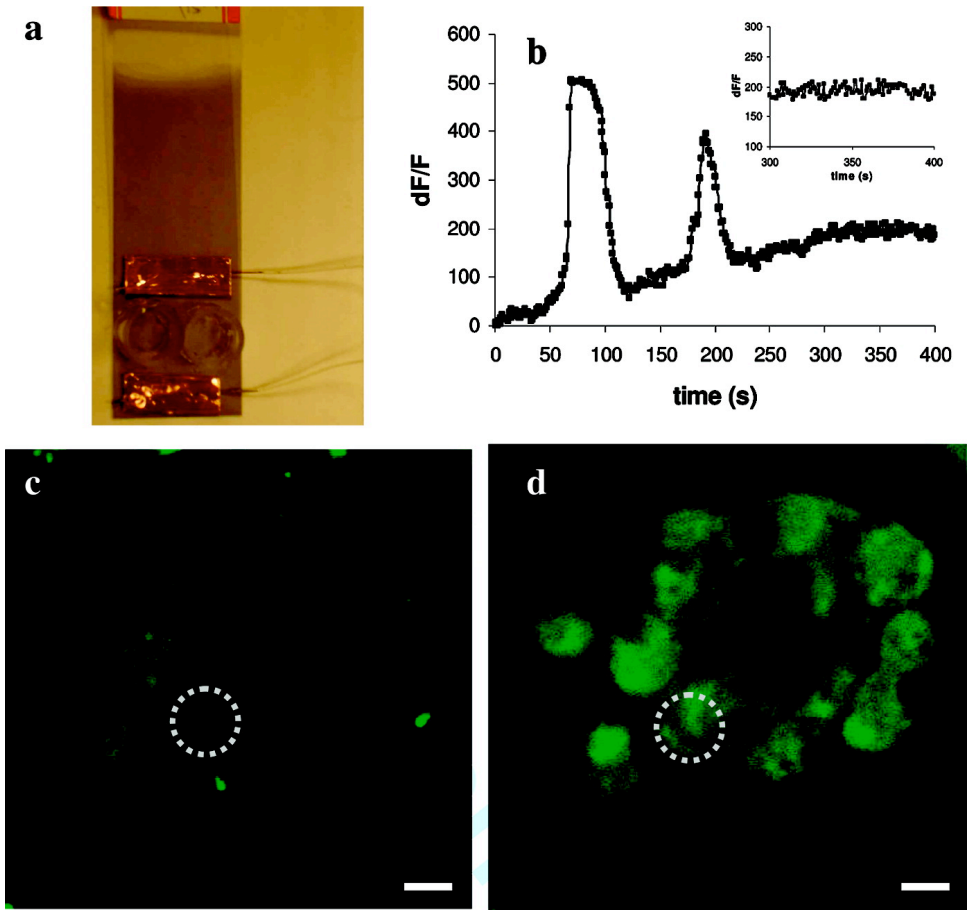

Figure 5.4 (**a**) Experimental set-up for electrical stimulation studies indicating the cell chambers and electrical leads. (**b**) Change in fluorescence intensity of Fluo-4-AM dye (ΔF/F) in one cell during electrical stimulation by CNT substrate. Change in fluorescence once stimulation is turned off at time t = 300s is shown in inset. (**c**) Confocal image of a cell cluster before start of stimulation and (**d**) confocal image of same cluster during stimulation. Data shown in (**b**) is from the circled cell in (**c**) and (**d**).

Cell response to chemical and electrical stimuli typically results in a change in the membrane voltage of the cells, commonly referred to as an action potential. Detection of action potentials can be achieved via the invasive patch clamp method[43] used before or via non-invasive optical detection techniques. Transparency of SWNT LBL films

previously reported by our group[44] affords the utilization of optical methods for monitoring that can be a great advantage for fundamental studies. The fluorescence detection method was chosen for our studies due to its convenience, clarity, and high information content. Ion-sensitive dyes undergo a change in fluorescence intensity as a result of change in ion concentrations upon application of an action potential. A Ca^{2+} dependent dye (Fluo-4-AM, Molecular Probes) was used for our study that is membrane-permeable, thus allowing facile imaging of a large population of live cells.[45] The versatile nature of the LBL fabrication allowed for simultaneous detection of fluorescence changes in cells pre-incubated with Fluo-4-AM during electrical stimulation. The experimental setup for the cells thus underwent minor adjustments to ensure that (1) the cells were kept in their physiological media during experiment, (2) electrical leads were kept isolated from any aqueous media and (3) that a #1 cover-glass slide was used as the substrate for the LBL film to allow cell recording with an inverted confocal fluorescence microscope.

The cell response appeared to be independent of the type of stimulus applied. The results reported here were obtained from cells that were excited with a pulsed signal. The latter was generally the preferred stimulus in order to minimize any heating effect in the SWNT thin films and to ensure that SWNT electrodes as well as cells are not constantly under stress during stimulation. The typical stimulation signal employed consisted of a series (~10-15) of 1 ms pulses spaced in 1-10 s intervals. The pulses were applied at these intervals rather than continuously in order to allow both the electrodes and the cells

to discharge. Cellular stimulations were carried out over areas of the films of about 4 cm^2, and output currents from the film range from the order of 1-10 $\mu A/cm^2$.

The cells were seeded on the pre-heated SWNT/laminin substrate for at least 72 h, incubated with Fluo-4-AM dye and washed prior to electrical stimulation studies. The cells were observed by confocal microscopy during the application of the stimulus. A representative confocal microscope image of a cell cluster is shown after Fluo-4-AM incubation/washing step but prior to stimulation is given in Figure 5.4c. The fluorescence level was adjusted such that minimal background fluorescence from the cells was present. A clear increase in fluorescence was observed in the cell cluster following electrical stimulation (Figure 5.4d). In order to obtain a quantitative measurement of the fluorescence fluctuation in the cells, the image processing software ImageJ was used to measure the fluorescence intensity in the cells during stimulation. The change in fluorescence over stimulation time is plotted as $\Delta F/F$ (Figure 5.4b) and is shown for one cell from the cluster (circled in Figure 5.4c, d). In addition to the increase in fluorescence observed, the presence of two peaks on the fluorescence curve suggests that an individual cell can be stimulated more than once upon application of the pulsed stimulus in the form of the sequence of two pulses, which what expected from NEs. The fluorescence level is also monitored after the electrical stimulation is stopped at time ~ 300s. Upon turning off of the electrical pulses, a leveling off is noticed in the cell fluorescence (Figure 5.4b). This indicates that the observed cell signal is indeed due to the stimulation through the electrode and not due to spontaneous firing. Recording of the cell excitation after the excitation process also indicated that generation of action

potential in individual cell is dependent on the status of the surrounding cells. Once one cell is excited, the train of the excitation is spreading from one cell to another in a nearly sequential manner, which can be identified by video recording of excitation. Although the main source of stimulation comes from the electrode underneath the cells, excited state of the neighboring cells causes the next cell to fire with lower threshold. This is another fact that confirms communication between the differentiated NSCs probably as early neurons.

5.5 Conclusions

In conclusion, this study establishes the ability of composite SWNT/laminin thin films to mediate the differentiation and electrical stimulation of NSCs. The protein-SWNT composite can serve as a foundation of a new type of NEs which (1) incorporate SWNTs as superior conductor and strengthening agent; (2) are conducive to NSCs growth and proliferation; (3) and are suitable for excitation of NSCs and the products of their differentiation. Additional studies to further understand the effect of electrical stimulus on NSC during the differentiation cycle and in a longer time frame are still needed.

5.6 References

1. Kam, N. W. S., Liu, Z. and Dai H., Functionalization of Carbon Nanotubes via Cleavable Disulfide Bonds for Efficient Intracellular Delivery of siRNA and Potent Gene Silencing. *J. Am. Chem. Soc.* **2005,** *127*, 12492-12493.

2. Kam, N. W. S., Liu, Z. and Dai H., Carbon Nanotubes Intracellular Transporters for Proteins and DNA: An Investigation of the Uptake Mechanism and Pathway. *Angew. Chem. Int. Ed.* **2006,** *45*, 577-581.

3. Kam, N. W. S.; Dai, H., Carbon Nanotubes as Intracellular Protein Transporters: Generality and Biological Functionality. *J. Am. Chem. Soc.* **2005,** *127*, 6021-6026.

4. Bianco, A.; Kostarelos, K.; Partidos, C. D.; Prato, M., Biomedical applications of functionalised carbon nanotubes. *Chem. Comm.* **2005,** *5*, 571-577.

5. Dai, H., Carbon nanotubes: synthesis, integration, and properties. *Acc. Chem. Res.* **2002,** *35*, 1035-1044.

6. Cogan, S. F.; Guzelian, A. A.; Agnew, W. F.; Yuen, T. G. H.; McCreery, D. B., Over-pulsing degrades activated iridium oxide films used for intracortical neural stimulation. *Journal of Neuroscience Methods* **2004,** *137* (2), 141-150.

7. Harnack, D.; Winter, C.; Meissner, W.; Reum, T.; Kupsch, A.; Morgenstern, R., The effects of electrode material, charge density and stimulation duration on the safety of high-frequency stimulation of the subthalamic nucleus in rats. *Journal of Neuroscience Methods* **2004,** *138* (1-2), 207-216.

8. Chen, R. J.; Bangsaruntip, S.; Drouvalakis, K. A.; Kam, N. W. S.; Shim, M.; Li, Y. M.; Kim, W.; Utz, P. J.; Dai, H. J., Noncovalent functionalization of carbon nanotubes for highly specific electronic biosensors. *Proc. Nat. Acad. Sci. USA.* **2003,** *100*, 4984-4989.

9. Gheith, M. K.; Sinani, V. A.; Wicksted, J. P.; Matts, R. L.; Kotov, N. A., Single-walled carbon nanotube polyelectrolyte multilayers and freestanding films as a biocompatible platform for neuroprosthetic implants. *Adv. Mat.* **2005,** *17*, 2663-2670.

10. Gheith, M. K.; Pappas, T. C.; Liopo, A. V.; Sinani, V. A.; Shim, B. S.; Motamedi, M.; Wicksted, J. P.; Kotov, N. A., Stimulation of Neural Cells by Lateral Currents in Conductive LBL Films of Single-Walled Carbon Nanotubes. *Adv. Mat.* **2006,** *18*, 2975.

11. Mattson, M. P.; Haddon, R. C.; Rao, A. M., Molecular functionalization of carbon nanotubes and use as substrates for neuronal growth. *J. Molecular Neurosci.* **2000,** *14*, 175-182.

12. Liopo, A. V.; Stewart, M. P.; Hudson, J.; Tour, J. M.; Pappas, T. C., Biocompatibility of native and functionalized single-walled carbon nanotubes for neuronal interface. . *J Nanosci Nanotechnol.* **2006,** *6*, 1365-74.

13. Patolsky, F.; Timko, B. P.; Yu, G.; Fang, Y.; Greytak, A. B.; Zheng, G.; Lieber, C. M., Detection, Stimulation, and Inhibition of Neuronal Signals with High-Density Nanowire Transistor Arrays. *Science* **2006,** *313* (5790), 1100-1104.

14. Zeck, G.; Fromherz, P., Noninvasive neuroelectronic interfacing with synaptically connected snail neurons immobilized on a semiconductor chip. *Proc. Natl. Acad. Sci. U. S. A.* **2001,** *98* (18), 10457-10462.

15. Fromherz, P.; Offenhausser, A.; Vetter, T.; Weis, J., A neuron-silicon junction: a Retzius cell of the leech on an insulated-gate field-effect transistor. *Science* **1991,** *252* (5010), 1290-1293.

16. Martino, G.; Pluchino, S., The therapeutic potential of neural stem cells. *Nat Rev Neurosci* **2006,** *7* (5), 395.

17. Okano, H., Stem cell biology of the central nervous system. *J. Neurosci. Res.* **2002,** *69* (6), 698-707.

18. Webster, T. J.; Waid, M. C.; McKenzie, J. L.; Price, R. L.; Ejiofor, J. U., Nano-biotechnology: carbon nanofibres as improved neural and orthopaedic implants. *Nanotechnology* **2004,** *15* (1), 48-54.

19. McKenzie, J. L.; Waid, M. C.; Shi, R. Y.; Webster, T. J., Decreased functions of astrocytes on carbon nanofiber materials. *Biomaterials* **2004,** *25* (7-8), 1309-1317.

20. Hu, H.; Ni, Y.; Mandal, S. K.; Montana, V.; Zhao, B.; Haddon, R. C.; Parpura, V., Polyethyleneimine Functionalized Single-Walled Carbon Nanotubes as a Substrate for Neuronal Growth. *J. Phys. Chem. B* **2005,** *109* (10), 4285-4289.

21. Mattson, M. P.; Haddon, R. C.; Rao, A. M., Molecular functionalization of carbon nanotubes and use as substrates for neuronal growth. *J. Mol. Neurosci.* **2000,** *14* (3), 175-182.

22. Mazzatenta, A.; Giugliano, M.; Campidelli, S.; Gambazzi, L.; Businaro, L.; Markram, H.; Prato, M.; Ballerini, L., Interfacing Neurons with Carbon Nanotubes: Electrical Signal Transfer and Synaptic Stimulation in Cultured Brain Circuits. *J. Neurosci.* **2007,** *27* (26), 6931-6936.

23. Lovat, V.; Pantarotto, D.; Lagostena, L.; Cacciari, B.; Grandolfo, M.; Righi, M.; Spalluto, G.; Prato, M.; Ballerini, L., Carbon Nanotube Substrates Boost Neuronal Electrical Signaling. *Nano Lett.* **2005,** *5* (6), 1107-1110.

24. Hu, H.; Ni, Y.; Montana, V.; Haddon, R. C.; Parpura, V., Chemically Functionalized Carbon Nanotubes as Substrates for Neuronal Growth. *Nano Lett.* **2004,** *4* (3), 507-511.

25. Zhang, X.; Prasad, S.; Niyogi, S.; Morgan, A.; Ozkan, M.; Ozkan, C. S., Guided neurite growth on patterned carbon nanotubes. *Sensors and Actuators B: Chemical* **2005,** *106* (2), 843-850.

26. Gabay, T.; Jakobs, E.; Ben-Jacob, E.; Hanein, Y., Engineered self-organization of neural networks using carbon nanotube clusters. *Physica A: Statistical Mechanics and its Applications* **2005,** *350* (2-4), 611-621.

27. Yu, Z.; McKnight, T. E.; Ericson, M. N.; Melechko, A. V.; Simpson, M. L.; Morrison, B., Vertically Aligned Carbon Nanofiber Arrays Record Electrophysiological Signals from Hippocampal Slices. *Nano Lett.* **2007,** *7* (8), 2188-2195.

28. Nguyen-Vu, T. D. B.; Hua, C.; Cassell, A. M.; Andrews, R. J.; Meyyappan, M.; Jun, L., Vertically Aligned Carbon Nanofiber Architecture as a Multifunctional 3-D Neural Electrical Interface. *Biomedical Engineering, IEEE Transactions on* **2007,** *54* (6), 1121-1128.

29. Keefer, E. W.; Botterman, B. R.; Romero, M. I.; Rossi, A. F.; Gross, G. W., Carbon nanotube coating improves neuronal recordings. *Nat Nano* **2008,** *3* (7), 434-439.

30. Tang, Z.; Wang, Y.; Podsiadlo, P.; Kotov, N. A., Biomedical Applications of Layer-by-Layer Assembly: From Biomimetics to Tissue Engineering *Advanced materials* **2006,** *18*, 3203-3224.

31. Mamedov, A. A.; Kotov, N. A.; Prato, M.; Guldi, D. M.; Wicksted, J. P.; Hirsch, A., Molecular design of strong single-wall carbon nanotube/polyelectrolyte multilayer composites. *Nat Mater* **2002,** *1* (3), 190-194.

32. Jan, E.; Kotov, N. A., Successful Differentiation of Mouse Neural Stem Cells on Layer-by-Layer Assembled Single-Walled Carbon Nanotube Composite. *Nano Lett.* **2007,** *7* (5), 1123-1128.

33. Freire, E.; Gomes, F. C. A.; Linden, R.; Neto, V. M.; Coelho-Sampaio, T., Structure of laminin substrate modulates cellular signaling for neuritogenesis. *J Cell Sci* **2002,** *115* (24), 4867-4876.

34. Shim, M.; Shi Kam, N. W.; Chen, R. J.; Li, Y.; Dai, H., Functionalization of Carbon Nanotubes for Biocompatibility and Biomolecular Recognition. *Nano Lett.* **2002,** *2* (4), 285-288.

35. Lin, Y.; Taylor, S.; Li, H.; Fernando, K. A. S.; Qu, L.; Wang, W.; Gu, L.; Zhou, B.; Sun, Y.-P., Advances toward bioapplications of carbon nanotubes. *Journal of Materials Chemistry* **2004,** *14* (4), 527-541.

36. Shim, B.; Kotov, N. A., Single-Walled Carbon Nanotube Combing during Layer-by-Layer Assembly: From Random Adsorption to Aligned Composites. *Langmuir* **2005,** *21* (21), 9381-9385.

37. Wang, J.-H.; Hung, C.-H.; Young, T.-H., Proliferation and differentiation of neural stem cells on lysine-alanine sequential polymer substrates. *Biomaterials* **2006,** *27* (18), 3441.

38. Thompson, M. T.; Berg, M. C.; Tobias, I. S.; Rubner, M. F.; Van Vliet, K. J., Tuning compliance of nanoscale polyelectrolyte multilayers to modulate cell adhesion. *Biomaterials* **2005,** *26* (34), 6836-6845.

39. Asuri, P.; Karajanagi, S. S.; Yang, H.; Yim, T. J.; Kane, R. S.; Dordick, J. S., Increasing Protein Stability through Control of the Nanoscale Environment. *Langmuir* **2006,** *22* (13), 5833-5836.

40. Eggers, D. K.; Valentine, J. S., Molecular confinement influences protein structure and enhances thermal protein stability. *Protein Sci* **2001,** *10* (2), 250-261.

41. Mehler, M. F.; Kessler, J. A., Progenitor Cell Biology: Implications for Neural Regeneration. *Arch Neurol* **1999,** *56* (7), 780-784.

42. Hopf, F. W.; Waters, J.; Mehta, S.; Smith, S. J., Stability and Plasticity of Developing Synapses in Hippocampal Neuronal Cultures. *J. Neurosci.* **2002,** *22* (3), 775-781.

43. Stuart, G. J.; Sakmann, B., Active propagation of somatic action potentials into neocortical pyramidal cell dendrites. *Nature* **1994,** *367* (6458), 69-72.

44. Shim, B. S.; Tang, Z.; Morabito, M. P.; Agarwal, A.; Hong, H.; Kotov, N. A., Integration of Conductivity, Transparency, and Mechanical Strength into Highly Homogeneous Layer-by-Layer Composites of Single-Walled Carbon Nanotubes for Optoelectronics. *Chem. Mater.* **2007,** *19* (23), 5467-5474.

45. Smetters, D.; Majewska, A.; Yuste, R., Detecting Action Potentials in Neuronal Populations with Calcium Imaging. *Methods* **1999,** *18* (2), 215-221.

CHAPTER 6

Neuronal Programming of Multipotent Cells via Gene Delivery on Functionalized Carbon Nanotube Nanocomposites

6.1 Abstract

Inflammatory reactions, encapsulation of implanted electrodes with scar tissues and gradual withdrawal of neurons from them are the key problems for the neural tissue interfacing. These issues must be resolved for treatments of several well-known debilitating conditions to be effective. If an implanted electrode acquires ability to control cell response via in-situ gene transfection, all these problems can be successfully mitigated. Taking advantage of layer-by-layer assembled carbon nanotubes composites, purposeful engineering of the electrostimulating implants with these functionalities becomes realistic. They are conductive and can incorporate plasmid DNA capable of altering the response/functionality of surrounding cells. Successful expression of Lyn-citrine plasmid DNA was achieved in attached neurons. The transfection efficiency was found to be remarkably higher than conventional solution-mediated techniques. Most importantly, by using plasmid expression vectors for neural basic helix-loop-helix proteins, neurons were generated from multipotent P19 embryonal carcinoma cells

adhering to SWNT multilayers. This illustrates the possibility of recruiting resident stem cells in brain by the electrostimulating implant, programming of surrounding cells, and substantially improved level of tissue-device integration.

6.2 Introduction

The acute and long-term inflammatory tissue responses around implanted electrodes represent the long-standing problems for neural stimulation necessary for the treatment of many diseases. Scarring of the tissue around implants is difficult to avoid due to the fundamental limitations on electrical properties of the materials used, discrepancy in mechanical properties of hard implants and soft tissues, and physical dimensions of the electrodes.[1] However, encapsulation with resident immune cells and related loss of electrostimulation performance can potentially be avoided by *in-situ* gene therapy. It can be particularly suitable for the activation of resident neural stem cells or genetic re-programming of scar-forming astroglial cells into neurons.[2] Enhanced neural population in the vicinity of electrode will improve signal transduction, decrease pathological symptoms, and reduce inflammatory reactions at the implantation site.[3, 4]

The same approach can be applied to correction of defective genes at the implantation site responsible for various neurological and cardiac diseases. For example, gene delivery was demonstrated in animal models to prevent the development of neuritic plaques in Alzheimer's disease,[5] reverse motor dysfunction in Parkinson's disease,[6] and

decrease seizure activity[7] in epilepsy. By delivering appropriate genes, researchers were also able to prevent degeneration[8] and induce generation[9] of cochlear hair cells. For cardiac conditions such as a heart block, gene delivery effectively generated ventricular biological pacemakers.[10] Furthermore, by exploiting the highly migratory stem cells as delivery vehicles, gene therapy can be combined with stem cell therapy as a new treatment strategy for neurodegenerative diseases.[11]

Unfortunately, traditional and state-of-the-art inorganic electrode materials, such as gold, iridium oxide, doped silicon, and *etc.,* do not have mechanical compliance with soft tissues, which results in the activation of astroglial cells. Also, they present multiple problems for realization of gene delivery.[12] Although conducting polymers have received tremendous attention as a promising class of materials for producing functional neural interfaces, most developments have so far focused on biocompatibility and incorporation of small-molecule drugs.[13, 14]

Conductive organic-inorganic composites fabricated from carbon nanotubes (CNTs) represent a promising class of materials for neuroprosthetic electrodes. According to the data from many groups, these CNT-based materials are not only biocompatible[15, 16] but can also boost the efficacy of neural signal transmission,[17] stimulate and record neural circuit activities,[18, 19] and improve neural recordings.[20] As electrical/mechanical properties and accessibility of genes are highly dependent on nano- and micro-scale morphology of the electrode material, the choice of processing technique for preparing CNT composites is extremely essential. Layer-by-layer (LBL) assembly has

several advantages significant in this respect. (1) It allows for simple integration of biological species into the resulting material.[21] The incorporation of deliverable genes in the matrix of implants avoids many tough problems of more traditional methods of gene therapy, such as systemic administration and solution-based gene delivery.[22, 23] (2) The composites made by LBL display remarkable mechanical properties,[24, 25] which come into play during implantation and long-term performance of the implants. (3) High loading of CNTs and control over nanotube-nanotube contacts produce high electrical conductivity.[25] (4) LBL composites can be used as coatings and free-standing materials for electrode manufacturing, providing necessary flexibility for device engineering.[26-28] (5) Importantly, they do not interfere with the differentiation pattern of stem cells.[29, 30]

Such a complementary set of properties motivated us to test whether single-walled carbon nanotube (SWNT) LBL composites can be used for *in-situ* gene delivery. As background for this idea, electroporation has been used in conjunction with conductive materials to deliver genes,[31, 32] but such methods require a counter electrode to initiate the delivery which is unlikely to be implemented with implantable electrodes and can cause additional damage to the neural tissue. Electrical potential was demonstrated to successfully release genetic material from LBL films built on conductive surfaces, but unassisted genetic expression in cells was not demonstrated because manual incorporation of a transfection agent was subsequently required to enable delivery into cells.[33, 34] Functionalized individual SWNTs have been shown to condense and deliver DNA into cells in solution similar to little spears.[35, 36] However, it is unclear how this

function may be utilized in conjunction with conductive materials for neuroprosthetic applications.

6.3 Methods

6.3.1 SWNT Multilayer Composite Preparation

Purified single-walled carbon nanotubes (SWNTs) were purchased from Carbon Solutions, Inc. (Riverside, CA). Poly(vinyl alcohol) (PVA; MW 70k), poly(sodium 4-styrene-sulfonate) (PSS; MW 1000k) were obtained from Sigma-Aldrich (St. Louis, MO). SWNT-PVA multilayers were prepared on round glass coverslips (Bellco Glass, Vineland, NJ) using the technique of layer-by-layer (LBL) assembly. SWNTs were dispersed at 0.5 mg/ml in 0.1 wt% PSS solution by sonication, and the SWNT-PSS dispersion was alternately adsorbed onto glass coverslips with 0.2 wt% PVA solution. For each deposition, the coverslips were immersed in the corresponding solution for 5 minutes, followed by rinsing with deionized water and drying with an air jet. The process was repeated to obtain 3 bilayers of PVA/SWNT-PSS on the surface which we designated as $(PVA/SWNT\text{-}PSS)_3$.

6.3.2 PEI-pDNA Complex Preparation

Plasmid DNA (pDNA), pLyn-citrine, was provided by Professor Ronald W. Holz (Department of Pharmacology, University of Michigan, Ann Arbor, MI). This plasmid

vector encodes a citrine fluorescent protein, a YFP variant, fused to a sequence from Lyn, a member of the Src-family kinases, for plasma membrane localization. The pUS2MT-MASH1, pUS2MT-ngn2, and pUS2MT plasmids were provided by Professor David L. Turner (Neuroscience Program, University of Michigan, Ann Arbor, MI). The pUS2MT-MASH1 and pUS2MT-ngn2 plasmids are vectors for the neural bHLH proteins MASH1 and ngn2, respectively.[37] The plasmids were amplified in *Escherichia coli* DH5-alpha strain, which was provided to us by Professor Xiaoxia Lin (Department of Chemical Engineering, University of Michigan, Ann Arbor, MI), and purified using Promega's PureYield Plasmid Midiprep System (San Luis Obispo, CA) according to the manufacturer's instructions. The concentration of pDNA was estimated spectrophotometrically using a quartz cuvette. To prepare PEI-pDNA complexes for transfection studies, linear polyethylenimine (PEI; MW 25k; Polysciences, Inc., Warrington, PA) and pDNA were diluted separately in 150 mM NaCl. Appropriate amount and concentration of PEI solutions were added to pDNA solutions to create mixtures of desired nitrogen-to-phosphorous (N/P) ratios. For cotransfection of P19 cells, the ratio of neural bHLH vector to pLyn-citrine in the mixture was 3 to 1. The mixtures were vortexed, incubated at room temperature for 15 min, and used immediately following preparation.

6.3.3 Cell Cultures

NG108-15 (murine neuroblastoma/glioma) cells, P19 cells, and hypoxanthine, aminopterin, and thymidine (H.A.T.) were obtained from American Type Culture

Collection (ATCC, Manassas, VA). NG108-15 cells were maintained in Dulbecco's Modified Eagle's Medium (DMEM) without sodium pyruvate (Invitrogen, Carlsbad, CA) supplemented with 0.1 mM hypoxanthine, 400 nM aminopterin, 0.016 mM thymidine, 100 IU penicillin and 100 μg/ml streptomycin, and 10% fetal bovine serum (FBS). NG108-15 neural cells were seeded and cultured in serum-depleted culture media to induce neuronal differentiation. P19 cells were cultured in MEMα medium (Invitrogen, Carlsbad, CA) supplemented with 10% FBS. All cells were maintained at 37 °C in a humidified 5% CO_2 atmosphere.

6.3.4 Cell Transfection

NG108-15 transfection studies were performed by two different methods in triplets – multilayer mediated delivery and solution mediated delivery. For multilayer mediated delivery, an additional layer of PEI-pDNA was deposited on top of the PVA/SWNT-PSS multilayers. The $(PVA/SWNT)_3$ coated glass coverslips were immersed in PEI-pDNA solutions to produce a film structure of $(PVA/SWNT)_3$(PEI-pDNA). Prior to cell seeding, the glass substrates were washed with cell culture medium twice to remove weakly attached PEI-pDNA complexes. Cells were seeded on the substrates in 24-well plates at a concentration of 20,000 cells per well in DMEM with 1% FBS to induce neuronal differentiation. For solution mediated delivery,[38, 39] cells were seeded similarly on $(PVA/SWNT\text{-}PSS)_3$ coated coverslips. In 2 h, following cell seeding and cell attachment, 30 μl of PEI-pDNA solution containing 1 μg of pDNA was added to each well. As an additional control to the untreated group, cells were also seeded on

$(PVA/SWNT\text{-}PSS)_3(PEI)$ multilayers or treated with just PEI alone. Cells were cultured for 2 days before being assayed for transfection efficiency and metabolic activity.

P19 cotransfection was performed using the multilayer mediated delivery method. P19 cells were seeded and cultured on top of $(PVA/SWNT\text{-}PSS)_3(PEI\text{-}pDNA)$ multilayers, where the PEI-pDNA complexes were prepared from a mixture of linear PEI, Lyn-citrine plasmid, and a neural bHLH vector (MASH1 or ngn2) at an N/P ratio of 20. This N/P ratio was selected to achieve high transfection efficiency while avoiding the cytotoxic effects, as the P19 cells may be more vulnerable than the NG108-15 cells. As a control, cells were also co-transfected such that the bHLH vector was replaced with an empty vector. Cells were seeded in MEMα with 10% FBS. After 2 days in culture, the serum content was lowered to 1% and the media was replaced every 2 days.

6.3.5 Gene Expression

Gene expression was examined using confocal microscopy. In brief, at indicated time points following cell seeding and treatment, NG108-15 cells were fixed with 4% paraformaldehyde, stained with DAPI, mounted on coverslides, and observed using an Olympus FluoView 500 laser scanning confocal microscope. For each sample, random fields were selected under 20X magnification. For each field, total number of all cells (DAPI stained nuclei) and transfected cells (YFP expressed cells) were counted. The transfection efficiency for each treatment was calculated as the number of transfected cells divided by the number of total cells. For P19 cotransfection, the cells were also stained with primary antibodies for β-tubulin III (anti-TuJ1, 1:500 diluation, Sigma-

Aldrich, St. Louis, MO) and visualized with Alexa Fluor-conjugated secondary antibodies (Invitrogen, Calrsbad, CA).

6.3.6 Cell Metabolic Activity Assay

Cell metabolic activity was determined by MTT assay (thiazolyl blue tetrazolium bromide, Sigma-Aldrich, St. Louis, MO). In brief, 2 days after cell seeding and treatment, cells were added with 1.2 mM of MTT solution. After incubation at 37 °C for 2 h, isopropanol containing 10% Triton X-100 and 0.1 N HCl was added to dissolve the purple formazan crystals formed by dehydrogenase reduction of MTT. The absorbance of the resulting solution was measure at a test wavelength of 570 nm and a reference wavelength of 690 nm. Absorbance readings were converted to percentage cell viability by referencing the untreated cells as 100%.

6.4 Results and Discussion

SWNT multilayers were fabricated from poly(vinyl alcohol) (PVA) and poly(sodium 4-styrene-sulfonate) (PSS) dispersed SWNTs (SWNT-PSS). The conductivity of such composites was as high as 4.15×10^4 S/m determined as described in [27, 30]. It is sufficient or exceeds the requirements for different modes of neuronal excitation. As the first step, the delivery of the Lyn-citrine plasmid DNA (pDNA) to NG108-15 neuroblastoma cells was attempted. The NG108-15 cell line was chosen because these neural cells can be easily differentiated into neurons with distinctive

neuronal morphology, and they are routinely used as a model system for studying neuronal tissue. Lyn-citrine encodes a protein with strong luminescence similar to that of yellow fluorescent protein and gives strong membrane labeling that makes possible easy detection of successful transfection. To impart the SWNT films with gene delivery functionality, the pDNA was complexed with polyethylenimine (PEI) and deposited on the SWNT films in LBL fashion. The PEI protects pDNA against degradation, prolonging pDNA retention in the cell and the nucleus. Because the SWNT-PSS layer has a negative charge, the positively charged PEI-pDNA complexes were able to form a stable nanoscale layer with the LBL multilayers of SWNTs after thorough rinsing.[21] To optimize the transfection efficiency, PEI-pDNA complexes of various nitrogen-to-phosphorous (N/P) ratios were tested. To evaluate the comparative efficiency of gene transfer in the SWNT-pDNA multilayer composites, we also conducted in parallel PEI-mediated gene delivery using the conventional solution method.

In general, the transfection efficiency was higher in multilayer-mediated gene transfer across all N/P ratios tested (Figure 1a, d, e). The maximum transfection efficiency achieved in this study was *ca.* 50% and 30% for the multilayer and solution mediated delivery modes, respectively. The data for solution mediated delivery correlates very well with previous studies, which have demonstrated efficiencies ranging from less than 10% to 50% with increasing N/P ratio, as well as being highly variable depending on the cell line used.[40, 41] While both transfected and untransfected NG108-15 cells differentiated into mature neurons with long neural processes, many which extended over 100 μm in length, only those transfected with the Lyn-citrine pDNA developed

elaborated neural networks that were fluorescently labeled (Figure 1f). This is a clear indication that the delivery of functional genes through LBL films does not interfere with cellular developments, such as differentiation and neurite outgrowth unless such action is purposefully designed in the transferred gene.

There are several factors contributing to the higher transfection efficiency observed in multilayer mediated gene delivery. LBL deposition distributed the PEI-pDNA complexes evenly across the coated surface and elevated the concentration of the complexes on the surface of cells, increasing the number of cells exposed to the vectors and the likelihood of the vectors being transported across the cell membrane. Furthermore, immobilization of the PEI-pDNA complexes provided additional stabilization to the vectors, preventing unwanted degradation and prolonging their bioactivity.

The efficiency monotonously increased with increasing N/P ratio for the multilayer composites, while it dropped solution mediated delivery after N/P = 40 and was significantly diminished at an N/P = 80 (Figure 1a) because for these ratios PEI-plasmid complexes become less stable without immobilization onto a solid substrate. For both delivery modes, the increase in N/P ratio also adversely effects cell viability (Figure 1b) and cell metabolic activity (Figure 1c) due to the cytotoxicity of PEI. Importantly, in all cases the cytotoxicity was more severe in solution mediated delivery.

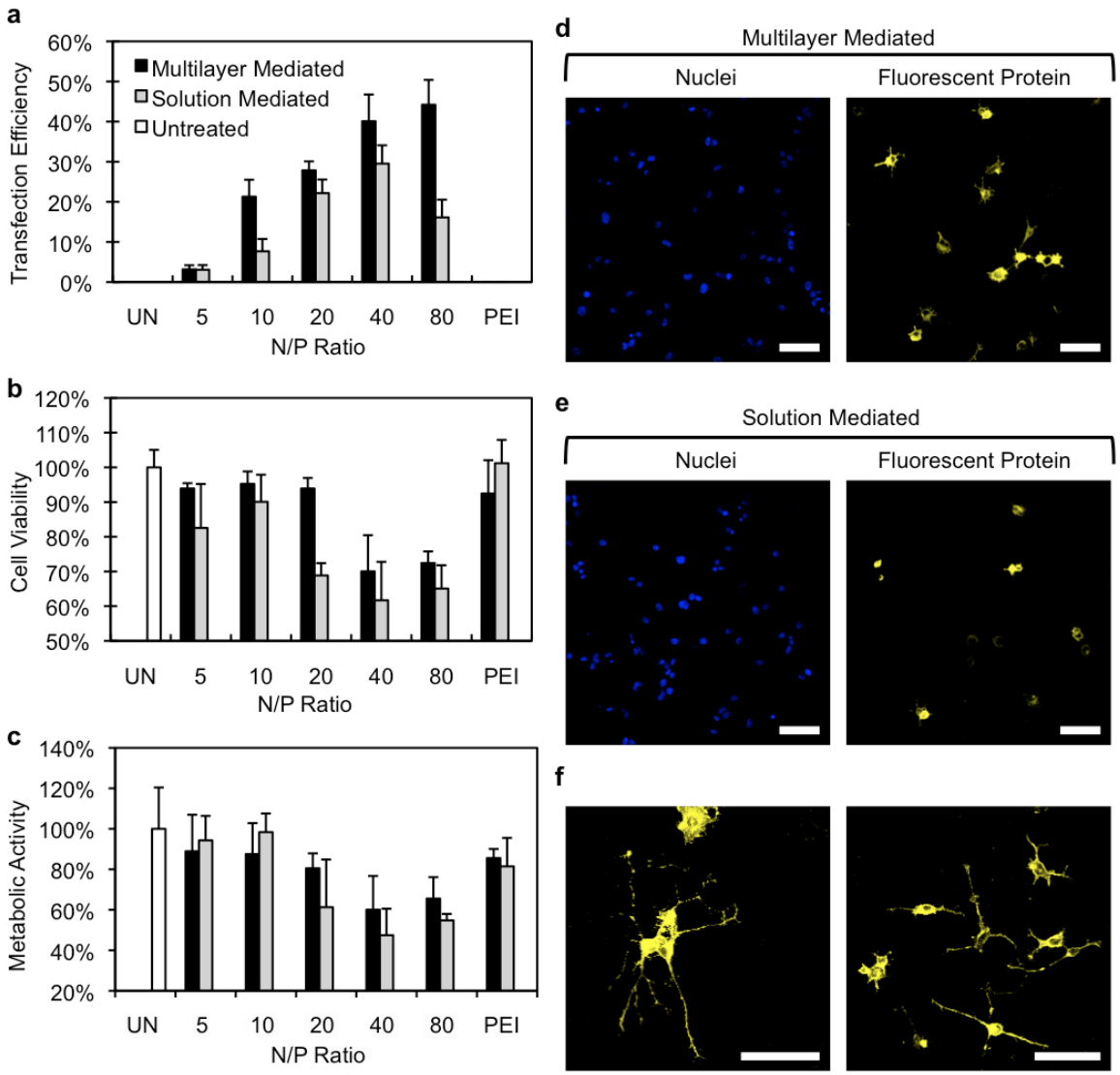

Figure 6.1 Transfection of NG108-15 neural cells. Comparison of transfection efficiency (**a**), cell viability (**b**), and metabolic activity (**c**) in NG108-15 neural cells transfected with pLyn-citrine by multilayer mediated (black bars) and solution mediated (grey bars) gene delivery. Untreated cells (white bars) were cultured on SWNT multilayers without any additional coating or treatments. Comparison of citrine fluorescent protein expression using multilayer mediated (**d**) and solution mediated (**e**) gene delivery. Expression of the plasmid gave a very strong plasma membrane labeling. Expression of the plasmid not only had no noticeable adverse effect on neuronal differentiation, but also improved the definition of the neural processes (**f**). Scale bars are 100 μm.

The possibility to generate neurons from resident stem and astroglial cells by delivering appropriate genes from the SWNT films would lead to the opportunity to control cellular processes around the neuroprosthetic implants. To demonstrate this, we decided to deliver both genes encoding a fluorescent protein and the neural basic helix-loop-helix (bHLH) proteins to the multipotent P19 embryonal carcinoma cells. The P19 cells are derived from mouse embryo and have been used extensively as a model system for studying *in vitro* differentiation of neural cells, and skeletal and cardiac muscle cells.[42, 43] Studies have shown that they appear to differentiate by the same mechanisms as normal embryonic stem cells.[44-46] Forced expression of bHLH proteins, such as NeuroD2, MASH1, and neurogenins (ngn1, ngn2, ngn3), which are essential during mammalian neuronal determination and differentiation,[47] have led to formation of neurons.[48, 49] Note the exactly the same set of genes is necessary to re-program astroglial cells into neurons.[2] Genetic control of neural population never been carried out using a surface mediated delivery system, which is the most logical approach for electroactive implantable devices.

Indeed, P19 cells cultured on multilayer composites functionalized with fluorescent protein and neural bHLH expression vectors gradually adopted a neuronal morphology (Figure 2) while reducing proliferation rate. By 4 days in culture, these cells expressed both the fluorescent protein and the neuronal specific β-tubulin III protein stained with the antibody TuJ1 (Figure 3). The staining of β-tubulin III protein outlines the formation of neural processes, which became much more elaborated and intricate by day 6 in culture. In general, the outcomes of either MASH1 or ngn2 expression were very

similar. In contrast, P19 cells co-transfected with pLyn-citrine and the empty vector remained in their undifferentiated morphology and continued to proliferate, generating large islands of cells (Figure 2). As expected, some of these cells expressed the fluorescent protein but none of them showed expression for β-tubulin III (Figure 3).

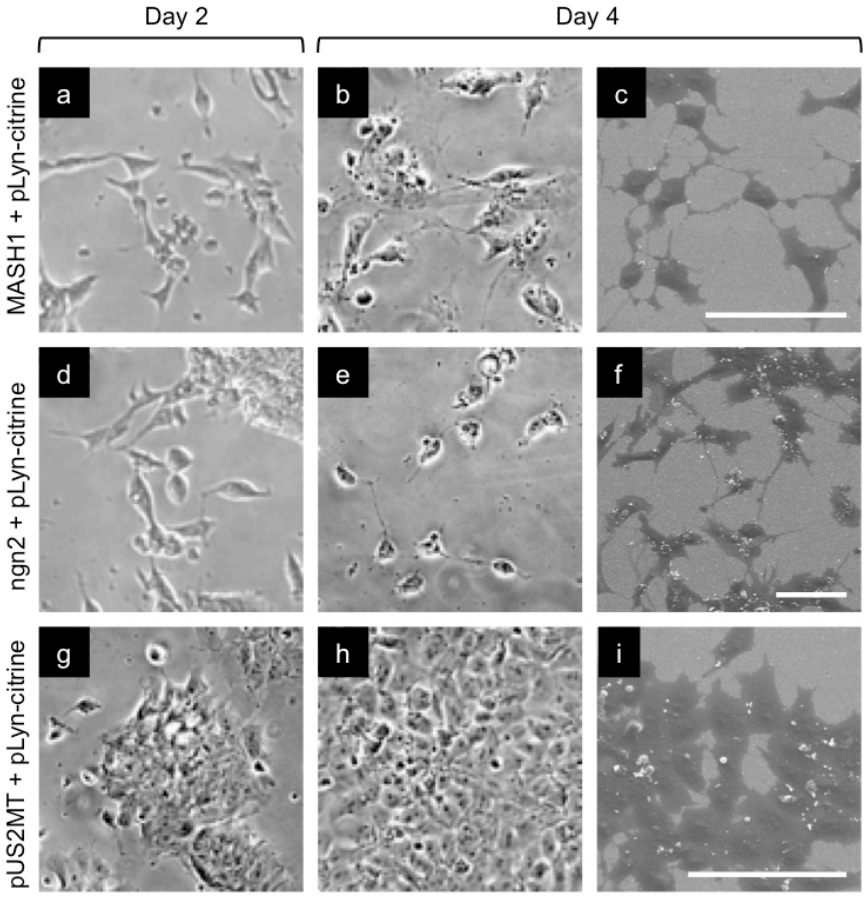

Figure 6.2 Morphology of transfected P19 embryonal carcinoma cells. Light microscope (**a, b, d, e, g, h**) and scanning electron microscope (**c, f, i**) images of P19 embryonal carcinoma cells cultured on functionalized SWNT multilayers on day 2 (**a, d, g**) and day 4 (**b, c, e, f, h, i**) after seeding. The SWNT multilayers were functionalized with PEI-pDNA complexes containing pLyn-citrine and either a neural bHLH protein expression vector (**a-f**) or an empty vector (**g-i**). Cells transfected with the MASH1 (**a-c**) and ngn2 (**d-f**) vectors adopted a neuronal morphology while those transfected with the empty vector continued to proliferated and remained in their undifferentiated morphology (**g-i**). Scale bars are 100 μm.

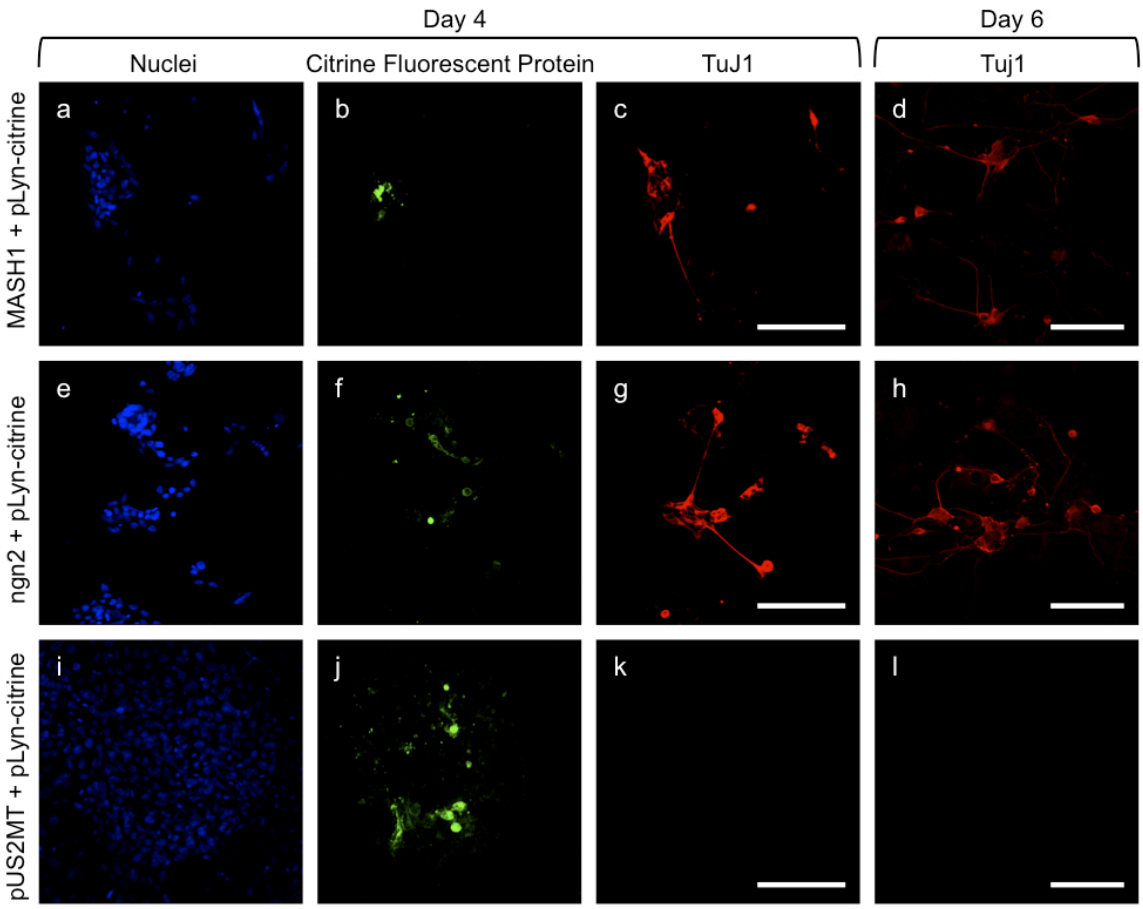

Figure 6.3 Neuronal differentiation of transfected P19 embryonal carcinoma cells. Confocal microscope images of P19 embryonal carcinoma cells cultured on functionalized SWNT multilayers on day 4 (**a-c, e-g, i-k**) and day 6 (**d, h, l**) after seeding. Cells were transfected with PEI-pDNA complexes containing pLyn-citrine, in addition to a vector for either MASH1 (**a-d**), ngn2 (**e-h**), or an empty vector (**i-l**). The cells were labeled for their nuclei with DAPI and expression for the neuronal specific β-tubulin III protein with the antibody TuJ1. While all cells showed citrine fluorescence (**b, f, j**), only those transfected with the neural bHLH protein expression vectors stained positive for β-tubulin III (**c, d, g, h**), which indicates successful neuronal differentiation.

6.5 Conclusions

In conclusion, it is clear that successful delivery of bHLH vectors was sufficient to program into the material the generation of neuron from the surrounding cells. Also essential, the direct delivery of genes using SWNT LBL multilayers incorporating pDNA was demonstrated to be more efficient and safer than the conventional solution mediated delivery. The use of SWNT composites makes possible integration of essential biological properties and signaling functions into the conductive materials, for which the reliable delivery of the genes on the implant during the surgical procedure was either difficult or impossible. This ability is critical to the development of new generation of neuroprosthetic devices potentially eliminating inflammatory reactions[50] that often lead to the demise of implanted electrodes. It can also be used for stimulation of cell regeneration[51] promoting much better integration of the electrode in the tissue.

6.6 References

1. Kotov, N. A.; Winter, J. O.; Clements, I. P.; Jan, E.; Timko, B. P.; Campidelli, S.; Pathak, S.; Mazzatenta, A.; Lieber, C. M.; Prato, M.; Bellamkonda, R. V.; Silva, G. A.; Kam, N. W. S.; Patolsky, F.; Ballerini, L., Nanomaterials for Neural Interfaces. *Advanced Materials* **2009,** *21* (40), 3970-4004.

2. Berninger, B.; Costa, M. R.; Koch, U.; Schroeder, T.; Sutor, B.; Grothe, B.; Gotz, M., Functional Properties of Neurons Derived from In Vitro Reprogrammed Postnatal Astroglia. *J. Neurosci.* **2007,** *27* (32), 8654-8664.

3. Ben-Hur, T., Immunomodulation by neural stem cells. *Journal of the Neurological Sciences* **2008,** *265* (1-2), 102-104.

4. Schwarting, S.; Litwak, S.; Hao, W.; Bahr, M.; Weise, J.; Neumann, H., Hematopoietic Stem Cells Reduce Postischemic Inflammation and Ameliorate Ischemic Brain Injury. *Stroke* **2008,** *39* (10), 2867-2875.

5. Dodart, J.-C.; Marr, R. A.; Koistinaho, M.; Gregersen, B. M.; Malkani, S.; Verma, I. M.; Paul, S. M., Gene delivery of human apolipoprotein E alters brain Abeta burden in a mouse model of Alzheimer's disease. *Proceedings of the National Academy of Sciences of the United States of America* **2005,** *102* (4), 1211-1216.

6. Isacson, O.; Kordower, J. H., Future of cell and gene therapies for Parkinson's disease. *Annals of Neurology* **2008,** *64* (S2), S122-S138.

7. Riban, V.; Fitzsimons, H. L.; During, M. J., Gene therapy in epilepsy. *Epilepsia* **2009,** *50* (1), 24-32.

8. Staecker, H.; Gabaizadeh, R.; Federoff, H.; Van De Water, T. R., Brain-derived neurotrophic factor gene therapy prevents spiral ganglion degeneration after hair cell loss, , , : Second Place--Resident Clinical Science Award 1997. *Otolaryngology - Head and Neck Surgery* **1998,** *119* (1), 7-13.

9. Kawamoto, K.; Ishimoto, S.-I.; Minoda, R.; Brough, D. E.; Raphael, Y., Math1 Gene Transfer Generates New Cochlear Hair Cells in Mature Guinea Pigs In Vivo. *J. Neurosci.* **2003,** *23* (11), 4395-4400.

10. Piron, J.; Quang, K. L.; Briec, F.; Amirault, J.-C.; Leoni, A.-L.; Desigaux, L.; Escande, D.; Pitard, B.; Charpentier, F., Biological Pacemaker Engineered by Nonviral Gene Transfer in a Mouse Model of Complete Atrioventricular Block. *Mol Ther* **2008,** *16* (12), 1937-1943.

11. Muller, F.-J.; Snyder, E. Y.; Loring, J. F., Gene therapy: can neural stem cells deliver? *Nat Rev Neurosci* **2006,** *7* (1), 75-84.

12. Grill, W. M.; Norman, S. E.; Bellamkonda, R. V., Implanted Neural Interfaces: Biochallenges and Engineered Solutions. *Annual Review of Biomedical Engineering* **2009,** *11* (1), 1-24.

13. Richardson, R. T.; Wise, A. K.; Thompson, B. C.; Flynn, B. O.; Atkinson, P. J.; Fretwell, N. J.; Fallon, J. B.; Wallace, G. G.; Shepherd, R. K.; Clark, G. M.; O'Leary, S. J., Polypyrrole-coated electrodes for the delivery of charge and neurotrophins to cochlear neurons. *Biomaterials* **2009,** *30* (13), 2614-2624.

14. Abidian, M. R.; Martin, D. C., Multifunctional Nanobiomaterials for Neural Interfaces. *Advanced Functional Materials* **2009,** *19* (4), 573-585.

15. Mattson, M.; Haddon, R.; Rao, A., Molecular functionalization of carbon nanotubes and use as substrates for neuronal growth. *Journal of Molecular Neuroscience* **2000,** *14* (3), 175-182.

16. Hu, H.; Ni, Y.; Montana, V.; Haddon, R. C.; Parpura, V., Chemically Functionalized Carbon Nanotubes as Substrates for Neuronal Growth. *Nano Letters* **2004,** *4* (3), 507-511.

17. Lovat, V.; Pantarotto, D.; Lagostena, L.; Cacciari, B.; Grandolfo, M.; Righi, M.; Spalluto, G.; Prato, M.; Ballerini, L., Carbon Nanotube Substrates Boost Neuronal Electrical Signaling. *Nano Letters* **2005,** *5* (6), 1107-1110.

18. Wang, K.; Fishman, H. A.; Dai, H.; Harris, J. S., Neural Stimulation with a Carbon Nanotube Microelectrode Array. *Nano Letters* **2006,** *6* (9), 2043-2048.

19. Yu, Z.; McKnight, T. E.; Ericson, M. N.; Melechko, A. V.; Simpson, M. L.; Morrison, B., Vertically Aligned Carbon Nanofiber Arrays Record Electrophysiological Signals from Hippocampal Slices. *Nano Letters* **2007,** *7* (8), 2188-2195.

20. Keefer, E. W.; Botterman, B. R.; Romero, M. I.; Rossi, A. F.; Gross, G. W., Carbon nanotube coating improves neuronal recordings. *Nat Nano* **2008,** *3* (7), 434-439.

21. Tang, Z.; Wang, Y.; Podsiadlo, P.; Kotov, N. A., Biomedical Applications of Layer-by-Layer Assembly: From Biomimetics to Tissue Engineering. *Advanced Materials* **2006,** *18* (24), 3203-3224.

22. Bengali, Z.; Shea, L. D., Gene delivery by immobilization to cell-adhesive substrates. *Mrs Bulletin* **2005,** *30* (9), 659-662.

23. Wong, S. Y.; Pelet, J. M.; Putnam, D., Polymer systems for gene delivery--Past, present, and future. *Progress in Polymer Science* **2007,** *32* (8-9), 799-837.

24. Mamedov, A. A.; Kotov, N. A.; Prato, M.; Guldi, D. M.; Wicksted, J. P.; Hirsch, A., Molecular design of strong single-wall carbon nanotube/polyelectrolyte multilayer composites. *Nat Mater* **2002,** *1* (3), 190-194.

25. Shim, B. S.; Tang, Z.; Morabito, M. P.; Agarwal, A.; Hong, H.; Kotov, N. A., Integration of Conductivity, Transparency, and Mechanical Strength into Highly Homogeneous Layer-by-Layer Composites of Single-Walled Carbon Nanotubes for Optoelectronics. *Chemistry of Materials* **2007,** *19* (23), 5467-5474.

26. Gheith, M. K.; Sinani, V. A.; Wicksted, J. P.; Matts, R. L.; Kotov, N. A., Single-walled carbon nanotube polyelectrolyte multilayers and freestanding films as a biocompatible platformfor neuroprosthetic implants. *Advanced Materials* **2005,** *17* (22), 2663-+.

27. Gheith, M. K.; Pappas, T. C.; Liopo, A. V.; Sinani, V. A.; Shim, B. S.; Motamedi, M.; Wicksted, J. R.; Kotov, N. A., Stimulation of neural cells by lateral layer-by-layer films of single-walled currents in conductive carbon nanotubes. *Advanced Materials* **2006,** *18* (22), 2975-+.

28. Jan, E.; Hendricks, J. L.; Husaini, V.; Richardson-Burns, S. M.; Sereno, A.; Martin, D. C.; Kotov, N. A., Layered Carbon Nanotube-Polyelectrolyte Electrodes Outperform Traditional Neural Interface Materials. *Nano Letters* **2009,** *9* (12), 4012-4018.

29. Jan, E.; Kotov, N. A., Successful differentiation of mouse neural stem cells on layer-by-layer assembled single-walled carbon nanotube composite. *Nano Letters* **2007,** *7* (5), 1123-1128.

30. Kam, N. W. S.; Jan, E.; Kotov, N. A., Electrical Stimulation of Neural Stem Cells Mediated by Humanized Carbon Nanotube Composite Made with Extracellular Matrix Protein. *Nano Letters* **2009,** *9* (1), 273-278.

31. Koda, S.; Inoue, Y.; Iwata, H., Gene Transfection into Adherent Cells Using Electroporation on a Dendrimer-Modified Gold Electrode. *Langmuir* **2008,** *24* (23), 13525-13531.

32. Jen, C.-P.; Chen, Y.-H.; Fan, C.-S.; Yeh, C.-S.; Lin, Y.-C.; Shieh, D.-B.; Wu, C.-L.; Chen, D.-H.; Chou, C.-H., A Nonviral Transfection Approach in Vitro: The Design of a Gold Nanoparticle Vector Joint with Microelectromechanical Systems. *Langmuir* **2004,** *20* (4), 1369-1374.

33. Recksiedler, C. L.; Deore, B. A.; Freund, M. S., A Novel Layer-by-Layer Approach for the Fabrication of Conducting Polymer/RNA Multilayer Films for Controlled Release. *Langmuir* **2006,** *22* (6), 2811-2815.

34. Wang, F.; Li, D.; Li, G.; Liu, X.; Dong, S., Electrodissolution of Inorganic Ions/DNA Multilayer Film for Tunable DNA Release. *Biomacromolecules* **2008,** *9* (10), 2645-2652.

35. Pantarotto, D.; Singh, R.; McCarthy, D.; Erhardt, M.; Briand, J.-P.; Prato, M.; Kostarelos, K.; Bianco, A., Functionalized Carbon Nanotubes for Plasmid DNA Gene Delivery. *Angewandte Chemie International Edition* **2004,** *43* (39), 5242-5246.

36. Singh, R.; Pantarotto, D.; McCarthy, D.; Chaloin, O.; Hoebeke, J.; Partidos, C. D.; Briand, J.-P.; Prato, M.; Bianco, A.; Kostarelos, K., Binding and Condensation of Plasmid DNA onto Functionalized Carbon Nanotubes: Toward the Construction of Nanotube-Based Gene Delivery Vectors. *Journal of the American Chemical Society* **2005,** *127* (12), 4388-4396.

37. Yu, J. Y.; Chung, K. H.; Deo, M.; Thompson, R. C.; Turner, D. L., MicroRNA miR-124 regulates neurite outgrowth during neuronal differentiation. *Experimental Cell Research* **2008,** *314* (14), 2618-2633.

38. Lungwitz, U.; Breunig, M.; Blunk, T.; Gˆpferich, A., Polyethylenimine-based non-viral gene delivery systems. *European Journal of Pharmaceutics and Biopharmaceutics* **2005,** *60* (2), 247-266.

39. Boussif, O.; Lezoualch, F.; Zanta, M. A.; Mergny, M. D.; Scherman, D.; Demeneix, B.; Behr, J. P., A versatile vector for gene and oligonucleotide transfer into cells in culture and in vivo: polyethylenimine. *Proceedings of the National Academy of Sciences of the United States of America* **1995,** *92* (16), 7297-7301.

40. Huh, S.-H.; Do, H.-J.; Lim, H.-Y.; Kim, D.-K.; Choi, S.-J.; Song, H.; Kim, N.-H.; Park, J.-K.; Chang, W.-K.; Chung, H.-M.; Kim, J.-H., Optimization of 25 kDa linear polyethylenimine for efficient gene delivery. *Biologicals* **2007,** *35* (3), 165-171.

41. Godbey, W. T.; Ku, K. K.; Hirasaki, G. J.; Mikos, A. G., Improved packing of poly(ethylenimine)/DNA complexes increases transfection efficiency. *Gene Therapy* **1999,** *6* (8), 1380-1388.

42. McBurney, M.; Reuhl, K.; Ally, A.; Nasipuri, S.; Bell, J.; Craig, J., Differentiation and maturation of embryonal carcinoma-derived neurons in cell culture. *J. Neurosci.* **1988,** *8* (3), 1063-1073.

43. Bain, G.; Kitchens, D.; Yao, M.; Huettner, J. E.; Gottlieb, D. I., Embryonic Stem Cells Express Neuronal Properties in Vitro. *Developmental Biology* **1995,** *168* (2), 342-357.

44. Laplante, I.; Paquin, J.; BÈliveau, R., RhoB expression is induced after the transient upregulation of RhoA and Cdc42 during neuronal differentiation and influenced by culture substratum and microtubule integrity. *Developmental Brain Research* **2001,** *129* (2), 157-168.

45. McBurney, M. W., P19 Embryonal Carcinoma Cells. *International Journal of Developmental Biology* **1993,** *37* (1), 135-140.

46. Paquin, J.; Danalache, B. A.; Jankowski, M.; McCann, S. M.; Gutkowska, J., Oxytocin induces differentiation of P19 embryonic stem cells to cardiomyocytes. *Proceedings of the National Academy of Sciences of the United States of America* **2002,** *99* (14), 9550-9555.

47. Reynolds, B. A.; Weiss, S., Generation of neurons and astrocytes from isolated cells of the adult mammalian central nervous system. *Science* **1992,** *255* (5052), 1707-1710.

48. Farah, M. H.; Olson, J. M.; Sucic, H. B.; Hume, R. I.; Tapscott, S. J.; Turner, D. L., Generation of neurons by transient expression of neural bHLH proteins in mammalian cells. *Development* **2000,** *127* (4), 693-702.

49. McCormick, M.; Tamimi, R.; Snider, L.; Asakura, A.; Bergstrom, D.; Tapscott, S., NeuroD2 and neuroD3: distinct expression patterns and transcriptional activation potentials within the neuroD gene family. *Mol. Cell. Biol.* **1996,** *16* (10), 5792-5800.

50. Ghisletti, S.; Meda, C.; Maggi, A.; Vegeto, E., 17{beta}-Estradiol Inhibits Inflammatory Gene Expression by Controlling NF-{kappa}B Intracellular Localization. *Mol. Cell. Biol.* **2005,** *25* (8), 2957-2968.

51. Bonadio, J., Review: Local Gene Delivery for Tissue Regeneration. *e-biomed: The Journal of Regenerative Medicine* **2000,** *1* (2), 25-29.

CHAPTER 7

Development of an In Vitro 3D Neural Tissue Model for Testing of Electrode-Induced Cellular Reactions

7.1 Abstract

The emergence of new neural interfacing materials, such as layer-by-layer assembled composites of carbon nanotubes, offer novel opportunities for addressing the problem of inflammatory reactions that current neural electrode designs suffer from. While a wide variation of features can be designed into these new neural interfacing materials, validation of their efficacy will require a new biological testing platform that is accurate, affordable, and high-throughput. In this study, we report the development of an in vitro 3D neural tissue model based on high-density culture of cell lines in hydrogel scaffolds with inverted colloidal crystal structure. We showed that P19 embryonal carcinoma multipotent cells have the potential to differentiate into a mixture of neural cell types that are essential for modeling the neural inflammatory process. We also demonstrated that co-culture of Neuro-2A neuronal cells, C8-D1A astrocytic cells, and HAPI microglial cells represents a promising neural tissue model as the cells were dynamic and responsive to their environment.

7.2 Introduction

Implantable neural electrodes are important and valuable tools in both research and clinical medicine. Neuromotor prosthetic devices have allowed researchers to investigate the biological basis of planning and control of movement by recording brain activity from animals.[1, 2] New knowledge and technological advances acquired from these studies are now being translated into clinical settings. For example, it was recently demonstrated that neuronal activity recorded through a microelectrode array enabled a tetraplegic human to control a prosthetic hand, opening up the possibilities for such patients to communicate and interact with the outside world.[3]

Despite the promise offered by advances in neurotechnologies, implantable neural electrodes often fail to function reliably in chronic settings, suffering from inflammatory tissue responses that prevent a stable, long-term interface to be maintained for acquisition of neural signals.[4] The inflammatory tissue responses occur in acute and chronic stages. The acute responses consist of activated microglia and astrocytes that are recruited to the implant site due to mechanical injuries inflicted by the implantation process.[5, 6] The persistent presence of the electrode induces chronic responses characterized by the formation of a dense, encapsulating tissue sheath consisted of microglia and astorcytes.[5, 7] This process, also known as glial scarring, displaces neuronal bodies at the implant site, and ultimately leads to loss of electrode connections.

The need for better neural interfaces has called for the development of new materials that are not only biocompatible but possess properties that can mitigate

inflammatory responses. Conducting polymers[8, 9] and carbon nanotubes (CNTs)[10, 11] are emerging neural interfacing materials with potentials unmatched by conventional metallic electrodes. For example, layer-by-layer (LBL) assembled CNT composites have demonstrated excellent biocompatibility[12, 13] and electrochemical properties,[14, 15] as well as endless possibilities for biofunctionalization afforded by LBL assembly.[16, 17]

The realization of new neural interfacing materials, especially those made from nanomaterials,[18] will necessitate extensive biological testing, which has always involved in vivo animal models that are time-consuming and labor-intensive.[19-21] In order to test the wide range of functionalities promised by new neural interfacing materials in an affordable, high-throughput, and accurate fashion, in vitro models that can closely mimic the neural tissue must be developed.

The goal of this study is to develop an in vitro 3D neural tissue model that can be used to investigate cellular responses inflicted by neural electrodes. While several 2D[22-25] and 3D[26-28] in vitro models have been reported in the literature, they all employ primary cells, which require animals to be sacrificed. In this study, we report on the progress we have made in the development of an in vitro 3D neural tissue model based on culturing of cell lines in hydrogel scaffolds with inverted colloidal crystal (ICC) geometry.[29-31] The ICC hydrogel scaffold design is characterized by its highly porous and uniform architecture consisted of interconnecting spherical cavities. This highly controlled and regular structure is the key to reproducible experimental results. Successful development

of such an in vitro 3D neural tissue model will enable faster screening of neural electrode designs and will make the study of glial scarring easier to advance.

7.3 Methods

7.3.1 Fabrication of Inverted Colloidal Crystal (ICC) Hydrogel Scaffolds

Colloidal crystals were first constructed from glass beads with diameters between 212 and 230 μm. The glass beads were dispersed in ethylene glycol (EG) and slowly added to glass vials through long glass Pasteur pipets. The vials were gently shaken using an ultrasonic cleaner to allow self-assembly of the glass mircospheres into a colloidal crystal with a hexagonally packed geometry. After evaporation of excess EG at 160°C, the colloidal crystal arrays were heated at 700°C for 3 h to anneal the glass particles. To obtain hydrogel scaffolds with ICC geometry, the glass colloidal crystal arrays were first infiltrated with a monomer solution containing 30 wt.-% acrylamide (AAm), a crosslinking agent, and an accelerating agent. The solution was then initiated to polymerize with a 1 wt.-% potassium peroxide solution. Following removal of excess polyacrylamide (PAAm) hydrogel from the exterior of the colloidal crystal arrays, the hydrogel infiltrated crystals were immersed in 5% HF solution to remove the glass colloids. The resulting 3D hydrogel scaffolds were washed extensively with deionized water and phosphate buffered saline (PBS) and then sterilized with 70% ethanol and UV irradiation.

7.3.2 Cell Culture

P19 embryonal carcinoma multipotent cells, Neuro-2a neuroblastoma cell, and C8-D1A type I astrocytic cells were purchased from American Type Culture Collection. HAPI microglia cells were a generous gift from Professor Marina Mata of the Department of Neurology at the University of Michigan. Neuro-2a, C8-D1A, and HAPI cells were cultured in Dulbecco's Modified Eagle's Medium (DMEM) supplemented with 10% fetal bovine serum (FBS). The serum concentration was lowered as needed to reduce proliferation and induce differentiation of the cells. P19 cells were cultured in alpha Minimum Essential Medium (αMEM) supplemented with 10% FBS. To induce differentiation into neural lineages, P19 cells were cultured in αMEM containing 5% FBS and 2.5 μM retinoic acid for 4 days, during which cells formed aggregates. Subsequently, the aggregates were dissociated into single cells and cultured in a differentiation medium consisted of neural basal medium supplemented with B27 and L-glutamine.

For culture in 3D ICC hydrogel scaffolds, sterilized scaffolds were immersed in 100% ethanol and allowed to completely dehydrate with evaporation of the ethanol. Cells were then seeded into scaffolds by carefully dispensing 20 μl of concentrated cell solution containing 50% Matrigel into each scaffold. A cell seeding density of 2×10^6 cells per scaffold was used. The addition of cell solution caused the scaffolds to gradually expand, rehydrate and uptake the dispersed cells. Once in the scaffolds, the cell solution was allowed to gel for 30 min before the scaffolds were transferred into 6-well culture

plates containing culture medium. For regular 2D culture, cells were seeded in 24-well culture plates.

To inflict damage on the 3D cell culture model, a piece of copper wire (254 μm in diamater) was inserted into each scaffold. Alternatively, two to three holes were punched in each cell seeded scaffold, resulting in three-dimensional wounds. For 2D culture, cells were inflicted with mechanical injury or foreign body response by creating scrape wounds on the cell layer or placing 50 μm diamater stainless steel wires on the cutlure.

7.3.3 Characterization

At the end of each time point, the 3D scaffolds were fixed with 4% paraformaldehyde, dehydrated, paraffinized, and sectioned into circular slices at the Histology Core at the University of Michigan. To prepare samples for immunocytochemical characterization, the scaffold sections mounted on glass slides were deparaffinized and rehydrated. Fixed samples from 2D and 3D cultures were permeabilized and blocked in PBS containing 0.3% Triton X-100 and 10% goat serum. The samples were first incubated with primary antibody diluted in PBS containing 10% goat serum for 24h at 4°C and then with secondary antibody diluted in PBS containing 2% goat serum for 3h at room temperature. Primary antibodies were purchased from Chemicon, Millipore, and Sigma. Primary antibodies and their dilutions are as follow: mouse anti-NeuN (1:100), mouse anti-MAP2 (1:200), mouse anti-GFAP (1:200), mouse anti-OX-42. rabbit anti-GFAP (1:200), and rabbit anti-MAP2 (1:100), rabbit anti-β-tubulin III (anti-Tuj1) (1:100), and rat anti-MAC-1 (1:100). Secondary Alexa Fluor

antibodies were purchased from Invitrogen and a 1:100 dilution was used. Samples were counter-stained for nuclei and mounted with Prolong Gold Anti-Fading Reagent with DAPI (Invitrogen). Immunostained samples were visualized using an Olympus FluoView FV500 confocal laser scanning microscope. The imaged were acquired using the Olympus Fluoview software version TIEMPO 4.3.

Histological characterization consisted of H&E staining. Samples were visualized using a Nikon Eclipse TS100 inverted microscope equipped with a QImaging MicroPublisher 3.3 digital CCD color cameras. Images were captured using QImaging's QCapture software. For SEM analysis, fixed samples were dehydrated through a gradient series of ethanol (25%, 50%, 70%, 85%, 95%, and three times 100%) for 5 min each time and left overnight in the final 100% ethanol solution. Completely dried samples were mounted on aluminum stubs and sputter-coated with gold. Imaging was carried out using a Philips XL30FEG scanning electron microscope.

7.4 Results and Discussion

7.4.1 3D Culture of P19 Embryonal Carcinoma Multipotent Cells

In order to mimick the cellular reactions inflicted by electrode materials in neural tissues, the in vitro model must contain the three major cell types that are involved in the inflammatory process - neurons, astrocytes, and microglia. Therefore, our approach was to generate a dense 3D structure of cells consisted of these three cell types. The P19

embryonal carcinoma multipotent cells appeared to be a logical choice of cell line for obtaining a mixed population of neural cells as they have been known to differentiate into various neural cell types when treated with retinoic acid.[32, 33]

In this study, P19 cells were treated with retinoic acid for 4 days before the cell aggregates were dissociated into single cells and seeded into polyacrylamide hydrogel ICC scaffolds at a cell density of 2×10^6 cells per scaffold. The cells were allowed to differentiate and adjust to the scaffold environment for 5 days, after which a piece of copper wire with a diameter of 254 μm was inserted into each scaffold to inflict mechanical injury and present a foreign material to the cells in the scaffold. The treatment day was denoted as Day 0, and the 3D culture was harvested, sectioned, and examined 1, 5, and 10 days after the treatment.

Hematoxylin and eosin (H&E) staining of the sectioned 3D scaffolds was used to examine the overall health and distribution of cells within the scaffolds following the insertion of testing electrodes. Figure 7.1 shows H&E staining of sectioned scaffolds at the different time points. The images indicate that the overall health of cells declined in the scaffolds as time progressed. The number of cell nuclei, which are darkly stained in H&E staining, dropped significantly between the time points. By Day 10, there were very cells remaining in the scaffolds as illustrated by the few dark spots present in the H&E stained section. The loss in cell population is mostly likely the result of a combination of factors, including a highly dense and crowded population of cells, insufficient diffusion

of nutrients through the scaffolds, and inability of the culture medium in keeping the differentiated P19 culture healthy for extended period of time.

The distribution of cells appeared to be even throughout the scaffolds. The locations of the inserted testing electrodes can be easily identified by the circular void space in the scaffold sections. The testing electrodes did not seem to impact the surrounding cells as cell nuclei were present around the electrode site on Day 1 and Day 5 (Figure 7.1). We also did not observe clustering of cells around the electrode site that would indicate possible migration of glial cells and formation of glial scars. It must be pointed out that the distribution and motility of the cells are highly dependent on the density and health of the cell population, both of which were observed to deteriorate with time in this study.

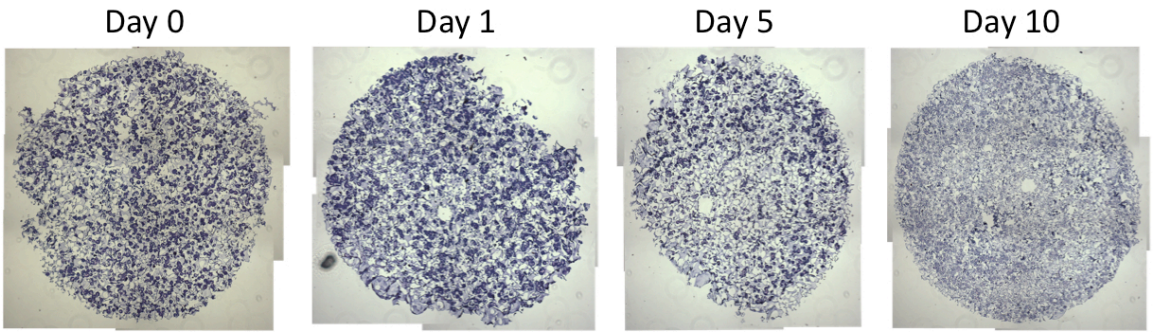

Figure 7.1 H&E staining of sectioned 3D scaffolds on Day 0, Day 1, Day 5, and Day 10 after insertion of copper wire electrodes. Retinoic acid treated P19 cells were cultured in the ICC hydrogel scaffolds for 5 days prior to the placement of the testing electrodes. Void space created by the inserted electrodes can be easily identified in the images.

To identify the phenotypes of differentiated P19 cells cultured in the scaffolds, the scaffold sections were stained and observed under a confocal microscope for various neural markers, including NeuN for mature neuronal nuclei, β-tubulin III for neuronal microtubule, GFAP for astrocytes, and MAC-1 for microglia. Figure 7.2 shows that the retinoic acid treated P19 cells were capable of differentiating into mature neurons and astrocytes when cultured in the 3D hydrogel scaffolds. However, no presence of microglial cells was observed. The morphology of differentiated neuronal cells are easily distinguished under scanning electron microcopy (SEM) as the cells developed elongated cell bodies with extensive network of neurites (Figure 7.3). The retinoic acid treated P19 cells formed cell aggregates that occupied the interconnected spherical cavities of the scaffolds. As cell differentiation progressed, cellular contacts were formed between adjacent cavities and many cells developed neurites with long extensions that passed through multiple cavities.

The two biggest drawbacks of this experiment are the decline in the health of the 3D culture and the absence of microglial cells. These two factors could limit the 3D model's ability in producing a noticeable cellular response to mechanical injuries and foreign materials. The ability to generate and maintain a mixed population of neurons, astrocytes, and microglia would be a challenging task for the adoption of the P19 multipotent cell line. Although many studies have reported the generation of neurons, astrocytes, oligodendrocytes from P19 cells,[33-35] very few studies have demonstrated the differentiation of P19 cells into microglial cells. Researchers were able to generate microglia-like cells from P19 cells only at late stages of neural differentiation, requiring a

culture period of 18 or more days.[36] According to the same study, the initial appearance of microglia coincided with the disappearance of neurons.[36] Therefore, the ability to maintain differentiated P19 cells in culture using 3D scaffolds for extended period of time will be essential. This is also important as it takes time for cells to migrate and reorganize after the culture is challenged with a testing electrode. Optimization of the culture condition and media formulation will be required to keep mature neurons alive in the culture. Alternatively, neurons from a second delayed culture could be introduced into the first culture once microglial cells have emerged.

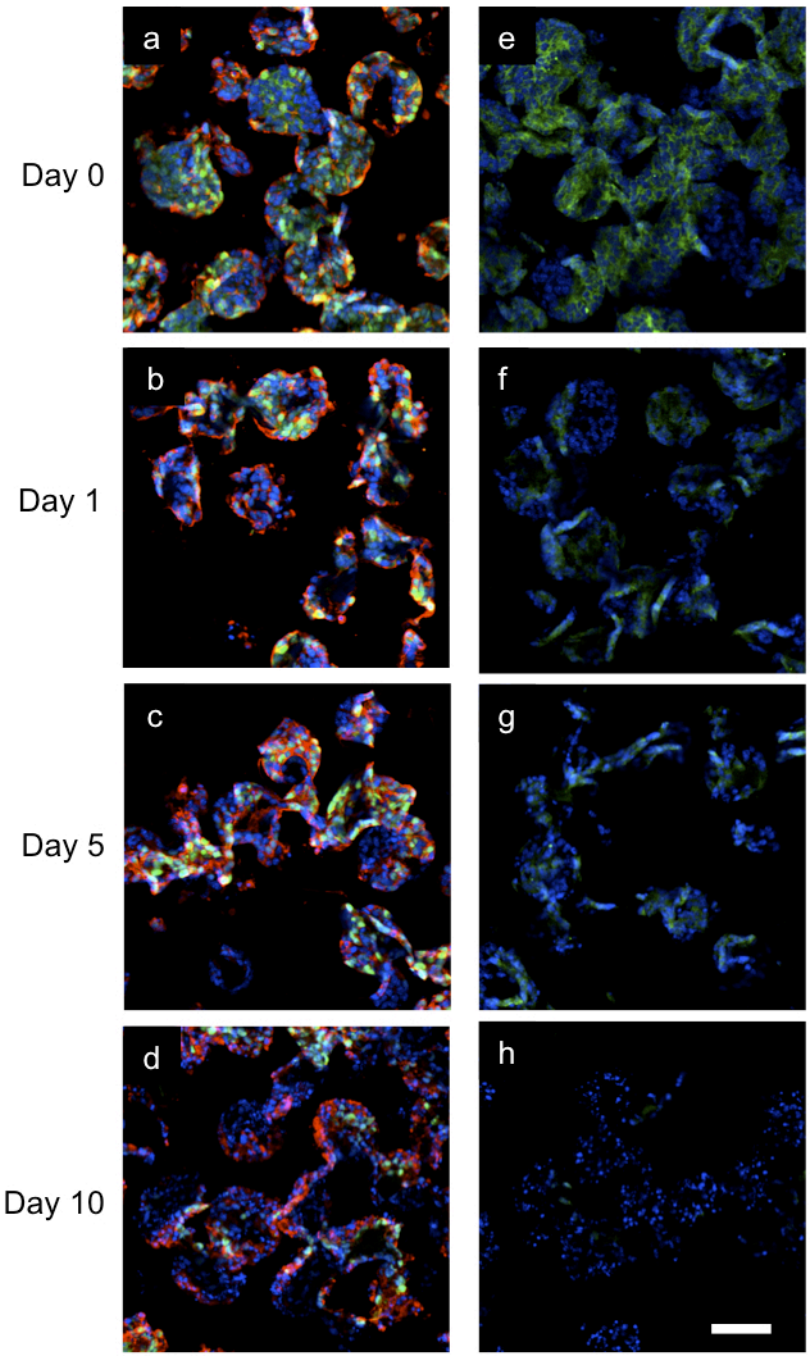

Figure 7.2 Confocal microscopy images of sectioned scaffolds on Day 0, Day 1, Day 5, and Day 10 after insertion of copper wire electrodes. Differentiated P19 cells were stained for markers of matured neuronal neuclei (NeuN, shown in green) and neuronal microtubule (β-tubulin III, shown in red) (**a-d**). Cells were also stained for markers of astrocytes (GFAP, shown in green) and microglia (MAC-1, shown in red) (**e-h**). Cell nuclei were counterstained with DAPI and are shown in blue. Scale: 100 μm.

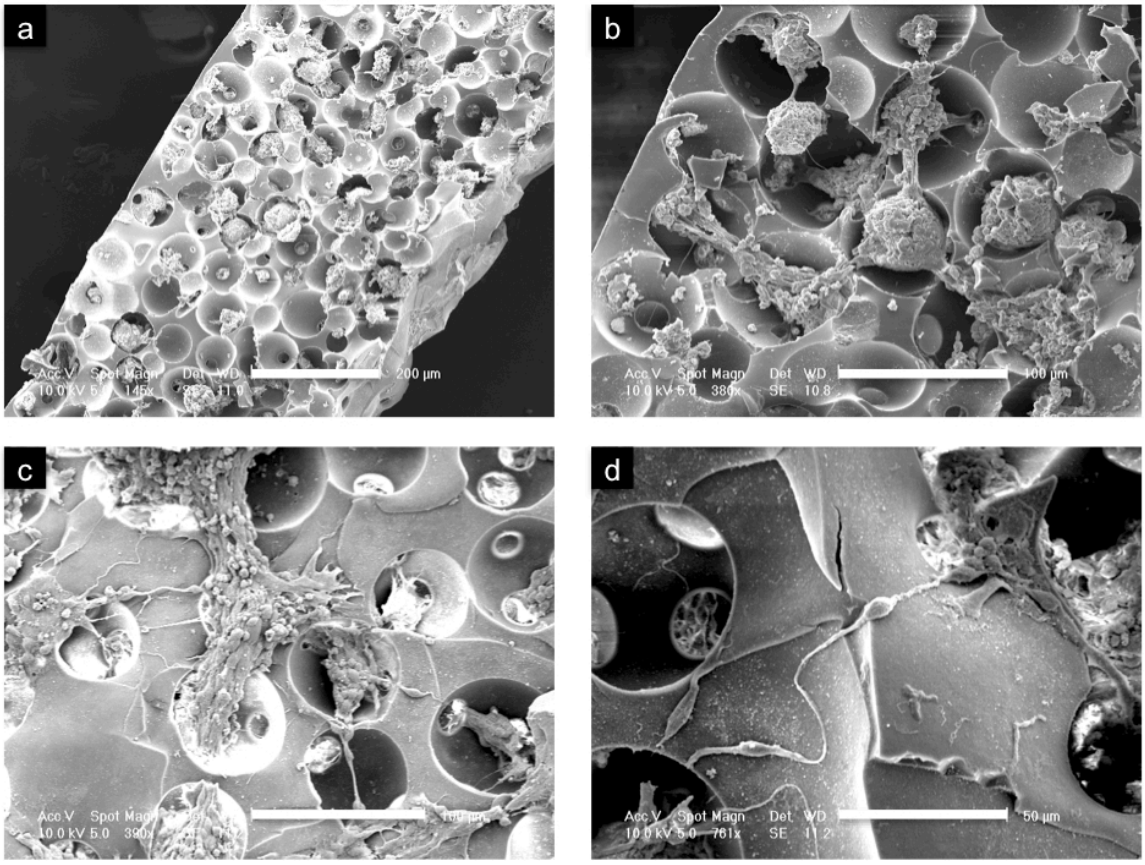

Figure 7.3 SEM images of vertical cross-section (**a, b**) and outer surface (**c, d**) of a scaffold 5 days after cell seeding (**a, b**). Cells aggregates formed by the seeded P19 cells not only occupied the spherical pores, but were also interconnected with those in adjacent pores (**b**). Highly differentiated neurons formed neurites with long extensions that passed through multiple pores and interfaced with multiple cells (**c, d**). Scale bars: 200 µm (**a**), 100 µm (**b, c**), 50 µm (**d**).

7.4.2 3D Co-culture of Neuronal, Astrocytic, and Microglial Cell Lines

Another approach to obtain neurons, astrocytes, and microglia in the same culture is through co-culture of three cell lines, each representing a different neural cell type. To achieve this, we decided to culture Neuro-2A neuronal cells, C8-D1A astrocytic cells, and HAPI microglial cells together. These three cell lines were selected because they can be conveniently cultured together using the same culture medium.

One convenient feature of using a co-culture approach is that the percentage of each cell type can be easily controlled during cell seeding. However, the growth rates of the cell lines must be taken into consideration as they are different across different cell lines, and therefore the distribution of cell population can change substantially after seeding. The distribution of neural cell types can be varied accordingly to model different regions of the brain. For example, the ratio of neuronal to non-neuronal cells is approximately 1 for the whole brain, 4 for the cerebral cortex, 0.2 for the cerebellum, and 11.4 for the rest of the brain.[37] In mice, the proportion of microglia ranges from 5% in the cortex to 12% in the substantia nigra,[38] and microglia can comprise up to 20% of the total non-neuronal population.[39] In general, the ratio of all non-neuronal cell to neurons across different primate species is roughly constant and not much larger than 1.[40] With these numbers in mind, we decided to use a ratio of 50% neurons, 30% astrocytes, and 20% microglia for our culture system.

We began this study by looking at the cellular behavior of the co-culture system of Neuro-2A, C8-D1A, and HAPI cells in regular 2D culture, as such a combination of

cells has never been reported in the literature. The cells were seeded and allowed to stabilize for three days under reduced serum condition to limit the extent of cell proliferation, after which the culture was challenged two treatments. In one scenario, stainless steel wires with a diameter of 50 μm were place on top of the cells, whereas in another case, scrapes were made to the cell layer.

Figure 7.4 illustrates the response of the co-culture system during the 6 days following the two treatments. For the wire placement scenario, we observed a very slight compacting and clustering of cells around the wire. However, the effect was not very significant, and we did not observe considerable attachment of cells to the wires as occurred in experiments using primary cells.[23] In the scrape test, we found that the co-culture to be highly migratory. By day 3 after treatment, many cells had already migrated into the area once cleared of cells on the treatment day. Overall, we demonstrated a co-culture system where three different cell lines were able to co-exist with each other at high density. Although we did not observe an overwhelming cellular response, perhaps due to the lack of effecting inducing conditions, the culture seemed to be dynamic as cell were able to migrate and rearrange around foreign objects.

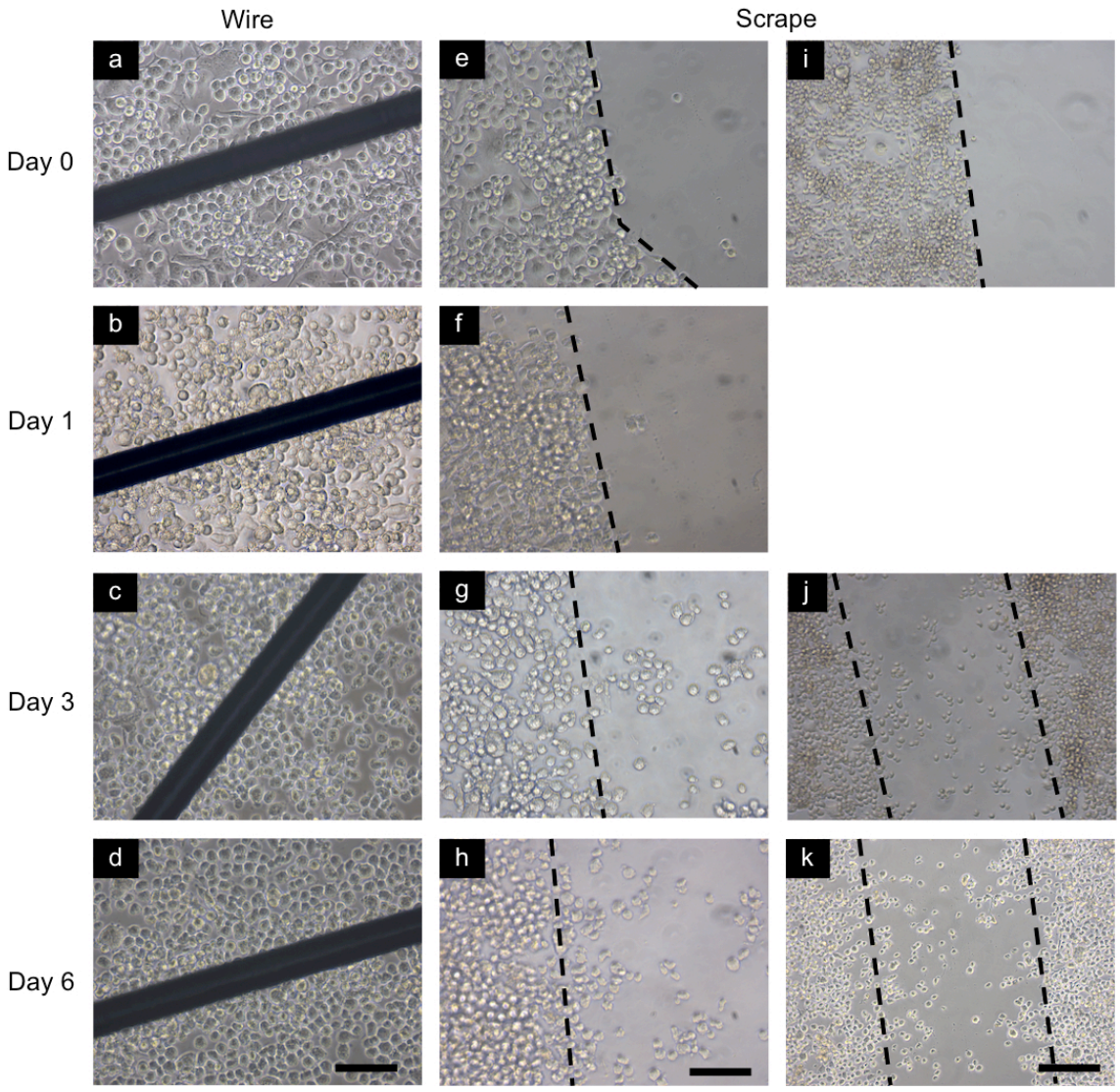

Figure 7.4 Time course of cellular events in response to the wire placement (**a-d**) or the scrape wound (**e-k**) in 2D co-culture of Neuro-2A neuronal cells, C8-D1A astrocytic cells, and HAPI microglial cells. The area scraped free of cells is on the right of the dotted line (**e-h**) or between the dotted lines (**i-k**). Scale bars: 100 µm (**a-h**), 200 µm (**i-l**).

The co-culture of Neuro-2A, C8-D1A, and HAPI cell lines was also demonstrated in 3D culture with ICC hydrogel scaffolds. Cells were seeded at a concentration of 2×10^6 cells per scaffold and allowed to stabilize for 3 days under low serum condition. On the day of treatment, two to three holes (Figure 7.5) were punched in the scaffolds to inflict injury on the cell culture. On day 0, 1, 3, and 5 following treatment, the scaffolds were harvested, sectioned, and analyzed. Figure 7.5 shows the H&E staining of sections collected from the various time points. Overall, we did not observe reorganization of the cells around the punched holes at any of the time points. Although the number of cell nuclei within the scaffolds declined as time progressed, interestingly cell population actually increased around the periphery of the scaffolds. The layer of cells on the periphery had small cell nuclei that are characterisc of microglial cells. In addition, this cell layer appeared to thicken with time, resembling that of a glial scarring and encapsulation reaction. A couple of factors could have contributed to this reorganization of cells. The poor transport of nutrients near the center of the scaffolds might have caused cells to migrate toward the edges for more nutrients. Also the exterior of the scaffolds consist of open spherical pore structure that are rough in texture. This microscale roughness could have attracted microglia and astrocytes to encasuplate the structure.

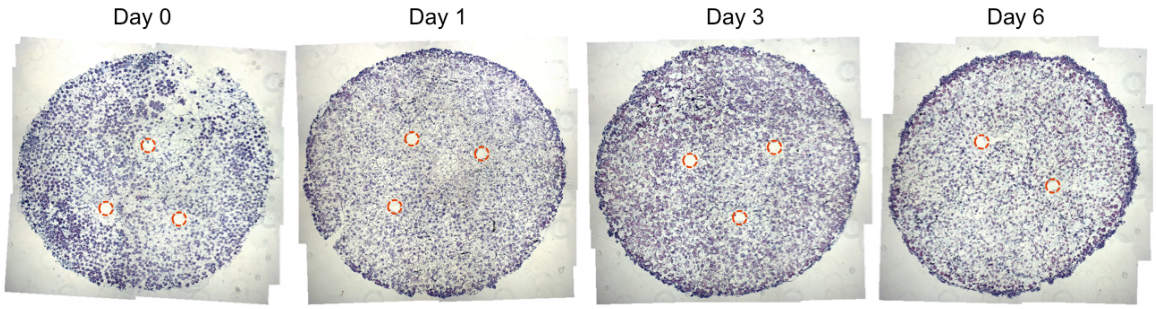

Figure 7.5 H&E staining of sectioned scaffolds on Day 0, Day 1, Day 5, and Day 10 after insertion of copper wire electrodes. Neuro-2A neuronal cells, C8-D1A astrocytic cells, and HAPI microglial cells were seeded at a ratio of 5:3:2, respectively, and cultured in the ICC hydrogel scaffolds for 3 days prior to infliction of wound on the 3D culture. On the day of treatment, two to three holes were punched in each scaffold, creating void spaces that can be easily identified in the stained sections (outlined with red circles).

There are a few adjustments that could improve the performance of the 3D culture system. First, coating of the culture plates and 3D scaffolds with biomolecules such as polylysine might be necessary to improve cell adhesion as detachment of small patches of cells were observed toward the end of the experiment. Secondly, the transport of nutrients in the scaffolds must be improved. A healthy culture is critical to inducing a significant cellular response. Vibration could be introduced using a shaker to facilitate the exchange of medium around the scaffolds. Alternatively, a rotary vessel could be used for the 3D culture. Lastly, the cells should be allowed to differentiate and mature for a longer period of time under low serum or no serum condition prior to treatment. However, serum should be introduced into the culture system with the treatment as serum has been found to be an effective stimulant for more pronounced level of scarring.[22]

7.5 Conclusions

In this study we made very important progress toward the development of an in vitro 3D neural tissue model that is free of primary cells. Our overall approach was to obtain a 3D cell structure consisted of neurons, astrocytes, and microglia, the three essential cell types in neural inflammatory process, by culturing cell lines in 3D hydrogel scaffolds. Through this study, we obtained valuable knowledge and established important protocols for 3D co-culture of neural cells. Our study shows that generation of the three target cell types from P19 multipotent cells would be possible if the right culture conditions could be provided. However, control over the proportion of the differentiated cell types would be difficult. To resolve this, we developed a co-culture system consisted of three different cell lines, each representing a different cell type (Neuro-2A neurons, C8-D1A astrocytes, HAPI microglia). We demonstrated that this combination of cell lines is promising and concluded that the culture conditions should be further optimized to achieve a more robust and responsive neural tissue model.

7.6 References

1. Wessberg, J.; Stambaugh, C. R.; Kralik, J. D.; Beck, P. D.; Laubach, M.; Chapin, J. K.; Kim, J.; Biggs, J.; Srinivasan, M. A.; Nicolelis, M. A. L., Real-time prediction of hand trajectory by ensembles of cortical neurons in primates. *Nature* **2000,** *408* (6810), 361-365.

2. Musallam, S.; Corneil, B. D.; Greger, B.; Scherberger, H.; Andersen, R. A., Cognitive Control Signals for Neural Prosthetics. *Science* **2004,** *305* (5681), 258-262.

3. Hochberg, L. R.; Serruya, M. D.; Friehs, G. M.; Mukand, J. A.; Saleh, M.; Caplan, A. H.; Branner, A.; Chen, D.; Penn, R. D.; Donoghue, J. P., Neuronal ensemble control of prosthetic devices by a human with tetraplegia. *Nature* **2006,** *442* (7099), 164-171.

4. Polikov, V. S.; Tresco, P. A.; Reichert, W. M., Response of brain tissue to chronically implanted neural electrodes. *Journal of Neuroscience Methods* **2005,** *148* (1), 1-18.

5. Szarowski, D. H.; Andersen, M. D.; Retterer, S.; Spence, A. J.; Isaacson, M.; Craighead, H. G.; Turner, J. N.; Shain, W., Brain responses to micro-machined silicon devices. *Brain Research* **2003,** *983* (1-2), 23-35.

6. Fujita, T.; Yoshimine, T.; Maruno, M.; Hayakawa, T., Cellular Dynamics of Macrophages and Microglial Cells in Reaction to Stab Wounds in Rat Cerebral Cortex. *Acta Neurochirurgica* **1998,** *140* (3), 275-279.

7. Schultz, R. L.; Willey, T. J., ULTRASTRUCTURE OF SHEATH AROUND CHRONICALLY IMPLANTED ELECTRODES IN BRAIN. *J. Neurocytol.* **1976,** *5* (6), 621-642.

8. Green, R. A.; Lovell, N. H.; Wallace, G. G.; Poole-Warren, L. A., Conducting polymers for neural interfaces: Challenges in developing an effective long-term implant. *Biomaterials* **2008,** *29* (24-25), 3393-3399.

9. Abidian, M. R.; Ludwig, K. A.; Marzullo, T. C.; Martin, D. C.; Kipke, D. R., Interfacing Conducting Polymer Nanotubes with the Central Nervous System: Chronic Neural Recording using Poly (3,4-ethylenedioxythiophene) Nanotubes. *Advanced Materials* **2009,** *21* (37), 3764-3770.

10. Keefer, E. W.; Botterman, B. R.; Romero, M. I.; Rossi, A. F.; Gross, G. W., Carbon nanotube coating improves neuronal recordings. *Nat. Nanotechnol.* **2008,** *3* (7), 434-439.

11. Wang, K.; Fishman, H. A.; Dai, H. J.; Harris, J. S., Neural stimulation with a carbon nanotube microelectrode array. *Nano Lett.* **2006,** *6* (9), 2043-2048.

12. Gheith, M. K.; Sinani, V. A.; Wicksted, J. P.; Matts, R. L.; Kotov, N. A., Single-walled carbon nanotube polyelectrolyte multilayers and freestanding films as a biocompatible platformfor neuroprosthetic implants. *Advanced Materials* **2005,** *17* (22), 2663-+.

13. Jan, E.; Kotov, N. A., Successful differentiation of mouse neural stem cells on layer-by-layer assembled single-walled carbon nanotube composite. *Nano Lett.* **2007,** *7* (5), 1123-1128.

14. Gheith, M. K.; Pappas, T. C.; Liopo, A. V.; Sinani, V. A.; Shim, B. S.; Motamedi, M.; Wicksted, J. R.; Kotov, N. A., Stimulation of neural cells by lateral layer-by-layer films of single-walled currents in conductive carbon nanotubes. *Advanced Materials* **2006,** *18* (22), 2975-+.

15. Jan, E.; Hendricks, J. L.; Husaini, V.; Richardson-Burns, S. M.; Sereno, A.; Martin, D. C.; Kotov, N. A., Layered Carbon Nanotube-Polyelectrolyte Electrodes Outperform Traditional Neural Interface Materials. *Nano Lett.* **2009,** *9* (12), 4012-4018.

16. Tang, Z. Y.; Wang, Y.; Podsiadlo, P.; Kotov, N. A., Biomedical applications of layer-by-layer assembly: From biomimetics to tissue engineering. *Advanced Materials* **2006,** *18* (24), 3203-3224.

17. Kam, N. W. S.; Jan, E.; Kotov, N. A., Electrical Stimulation of Neural Stem Cells Mediated by Humanized Carbon Nanotube Composite Made with Extracellular Matrix Protein. *Nano Lett.* **2009,** *9* (1), 273-278.

18. Kotov, N. A.; Winter, J. O.; Clements, I. P.; Jan, E.; Timko, B. P.; Campidelli, S.; Pathak, S.; Mazzatenta, A.; Lieber, C. M.; Prato, M.; Bellamkonda, R. V.; Silva, G. A.; Kam, N. W. S.; Patolsky, F.; Ballerini, L., Nanomaterials for Neural Interfaces. *Advanced Materials* **2009,** *21* (40), 3970-4004.

19. Purcell, E. K.; Seymour, J. P.; Yandamuri, S.; Kipke, D. R., In vivo evaluation of a neural stem cell-seeded prosthesis. *Journal of Neural Engineering* **2009,** *6* (2).

20. Rohatgi, P.; Langhals, N. B.; Kipke, D. R.; Patil, P. G., In vivo performance of a microelectrode neural probe with integrated drug delivery. *Neurosurgical Focus* **2009,** *27* (1).

21. Purcell, E. K.; Thompson, D. E.; Ludwig, K. A.; Kipke, D. R., Flavopiridol reduces the impedance of neural prostheses in vivo without affecting recording quality. *Journal of Neuroscience Methods* **2009,** *183* (2), 149-157.

22. Polikov, V. S.; Su, E. C.; Ball, M. A.; Hong, J. S.; Reichert, W. M., Control protocol for robust in vitro glial scar formation around microwires: Essential roles of bFGF and serum in gliosis. *Journal of Neuroscience Methods* **2009,** *181* (2), 170-177.

23. Polikov, V. S.; Block, M. L.; Fellous, J. M.; Hong, J. S.; Reichert, W. M., In vitro model of glial scarring around neuroelectrodes chronically implanted in the CNS. *Biomaterials* **2006,** *27* (31), 5368-5376.

24. Kimura-Kuroda, J.; Teng, X.; Komuta, Y.; Yoshioka, N.; Sango, K.; Kawamura, K.; Raisman, G.; Kawano, H., An in vitro model of the inhibition of axon growth in the lesion scar formed after central nervous system injury. *Molecular and Cellular Neuroscience 43* (2), 177-187.

25. Wanner, I. B.; Deik, A.; Torres, M.; Rosendahl, A.; Neary, J. T.; Lemmon, V. P.; Bixby, J. L., A New In Vitro Model of the Glial Scar Inhibits Axon Growth. *Glia* **2008,** *56* (15), 1691-1709.

26. Cullen, D. K.; Stabenfeldt, S. E.; Simon, C. M.; Tate, C. C.; LaPlaca, M. C., In vitro neural injury model for optimization of tissue-engineered constructs. *Journal of Neuroscience Research* **2007,** *85* (16), 3642-3651.

27. Irons, H. R.; Cullen, D. K.; Shapiro, N. P.; Lambert, N. A.; Lee, R. H.; LaPlaca, M. C., Three-dimensional neural constructs: a novel platform for neurophysiological investigation. *Journal of Neural Engineering* **2008,** *5* (3), 333-341.

28. LaPlaca, M. C.; Cullen, D. K.; McLoughlin, J. J.; Cargill, R. S., High rate shear strain of three-dimensional neural cell cultures: a new in vitro traumatic brain injury model. *Journal of Biomechanics* **2005,** *38* (5), 1093-1105.

29. Lee, J.; Shanbhag, S.; Kotov, N. A., Inverted colloidal crystals as three-dimensional microenvironments for cellular co-cultures. *Journal of Materials Chemistry* **2006,** *16* (35), 3558-3564.

30. Nichols, J. E.; Cortiella, J. Q.; Lee, J.; Niles, J. A.; Cuddihy, M.; Wang, S. P.; Bielitzki, J.; Cantu, A.; Mlcak, R.; Valdivia, E.; Yancy, R.; McClure, M. L.; Kotov, N. A., In vitro analog of human bone marrow from 3D scaffolds with biomimetic inverted colloidal crystal geometry. *Biomaterials* **2009,** *30* (6), 1071-1079.

31. Zhang, Y. J.; Wang, S. P.; Eghtedari, M.; Motamedi, M.; Kotov, N. A., Inverted-colloidal-crystal hydrogel matrices as three-dimensional cell scaffolds. *Advanced Functional Materials* **2005,** *15* (5), 725-731.

32. Berg, R. W.; McBurney, M. W., Cell density and cell cycle effects on retinoic acid-induced embryonal carcinoma cell differentiation. *Developmental Biology* **1990,** *138* (1), 123-135.

33. McBurney, M.; Reuhl, K.; Ally, A.; Nasipuri, S.; Bell, J.; Craig, J., Differentiation and maturation of embryonal carcinoma-derived neurons in cell culture. *J. Neurosci.* **1988,** *8* (3), 1063-1073.

34. Staines, W. A.; Craig, J.; Reuhl, K.; McBurney, M. W., Retinoic acid treated P19 embryonal carcinoma cells differentiate into oligodendrocytes capable of myelination. *Neuroscience* **1996,** *71* (3), 845-853.

35. Matsuda, Y.; Koito, H.; Yamamoto, H., Induction of myelin-associated glycoprotein expression through neuron-oligodendrocyte contact. *Developmental Brain Research* **1997,** *100* (1), 110-116.

36. Aizawa, T.; Haga, S.; Yoshikawa, K., Neural differentiation-associated generation of microglia-like phagocytes in murine embryonal carcinoma cell line. *Developmental Brain Research* **1991,** *59* (1), 89-97.

37. Azevedo, F. A. C.; Carvalho, L. R. B.; Grinberg, L. T.; Farfel, J. M.; Ferretti, R. E. L.; Leite, R. E. P.; Filho, W. J.; Lent, R.; Herculano-Houzel, S., Equal numbers of neuronal and nonneuronal cells make the human brain an isometrically scaled-up primate brain. *The Journal of Comparative Neurology* **2009,** *513* (5), 532-541.

38. Lawson, L. J.; Perry, V. H.; Dri, P.; Gordon, S., Heterogeneity in the distribution and morphology of microglia in the normal adult mouse brain. *Neuroscience* **1990,** *39* (1), 151-170.

39. Santambrogio, L.; Belyanskaya, S. L.; Fischer, F. R.; Cipriani, B.; Brosnan, C. F.; Ricciardi-Castagnoli, P.; Stern, L. J.; Strominger, J. L.; Riese, R., Developmental plasticity of CNS microglia. *Proceedings of the National Academy of Sciences of the United States of America* **2001,** *98* (11), 6295-6300.

40. Hilgetag, C.; Barbas, H., Are there ten times more glia than neurons in the brain? *Brain Structure and Function* **2009,** *213* (4), 365-366.

CHAPTER 8

Conclusions and Future Directions

8.1 Conclusions

In this dissertation, we demonstrated key properties of layer-by-layer (LBL) assembled carbon nanotube (CNT) composites that are essential for neural interfacing. Specifically, we showed that these nanostructured materials are biocompatible and possess excellent electrochemical properties for neural prosthetic applications. Most importantly, we were able to design biofunctional interfaces that can modulate cellular behaviors by integrating biological molecules into LBL assembled CNT composites. The combination of LBL assembly with CNTs is the enabling ingredient of this platform technology, allowing the unique properties of CNTs to be exploited and additional functionalities to be incorporated with high level of control over the material structure and composition.

In **Chapter 2**, we demonstrated the novel usage of high content screening assays as a convenient and universal tool for investigating the cytotoxicity of nanomaterials. We found that unlike CdTe quantum dots, gold nanoparticles, and freely dispersed CNTs,

which produced various cytotoxic effects on cells, LBL assembled CNT composite thin films were found to be nearly inert. Specifically, we observed little to no change in the cell number, nuclear area, mitochondrial membrane potential, and intracellular free calcium concentration of neural cells cultured on the CNT composite films, indicating their inertness and biocompatibility as a cellular interfacing material.

In **Chapter 3**, we investigated the potential of interfacing LBL assembled CNT composites with neural stem cells (NSCs) because their plasticity and ability to reestablish neuronal circuits may be an important component in the engineering of an stable, biocompatible, and effective neural interface. In this chapter, we demonstrated that mouse embryonic NSCs from the cortex can be successfully differentiated to neurons, astrocytes, and oligodendrocytes with clear formation of neurites on LBL CNT thin films. The results suggest that LBL CNT films are a suitable substrate for NSCs as cell viability, metabolic activity, neurite outgrowth, and expression of neural markers were found to be similar to those obtained from NSCs differentiated on poly-L-ornithine coated surface, a commonly employed growth substratum for NSCs.

In **Chapter 4**, the electrochemical properties of electrodes made from LBL assembled CNT composites were established and compared with electrodes made from iridium oxide and poly(3,4-ethylenedioxythiophene) (PEDOT). A thorough investigation was carried out to study properties such as electrochemical impedance, charge storage capacity, voltage excursion, and electrochemical stability, showing that the CNT electrodes outperformed the other electrodes. The LBL assembled CNT composites were

not only more stable electrochemically but also demonstrated more pronounced reductions in electrical impedance and augmentations in cathodic charge storage capacity. This clearly indicates that they are an excellent electrode material for neural prosthetic applications.

In **Chapter 5**, LBL composites were prepared from CNTs and laminin to create an interface that can mediate the differentiation and electrical stimulation of neural stem cells. The laminin-CNT composite films were found to enhance the differentiation of NSCs. Cells exhibited extensive neurite outgrowth and formed functional neural network. In addition, excitation of cells was demonstrated by applying a lateral current through the CNT film, confirming the functionality of the differentiated NSCs, as well as the utility of the conductive CNT substrate.

In **Chapter 6**, LBL assembled CNT composite films were engineered to incorporate plasmid DNAs, allowing that composites to deliver genetic materials to surrounding cells and thus altering their biological properties. The transfection efficiency of these functionalized CNT composites was found to be remarkably higher than the conventional solution-mediated technique. By using plasmid expression vectors for neural basic helix-loop-helix proteins, neurons were generated from multipotent cells adhering to the CNT multilayers. This chapter illustrates the possibility of a substantially improved level of tissue-device integration through recruiting and programming of resident stem cells in the nervous system.

In **Chapter 7**, we described our approach in developing an in vitro three-dimensional neural tissue model for testing electrode coatings designed to mitigate electrode-induced gliosis. Our goal is to build a model system solely based on cell lines, which will negate the use of primary cells and the sacrifice of animals, making the testing of electrode materials much cheaper, faster, and easier.

In summary, the studies presented in this dissertation provide a detailed characterization of the biocompatibility and electrochemical properties of LBL assembled CNTs composites. In addition, these studies also serve as valuable examples regarding the design and implementation of biofunctionalities in the CNT composites and provide important insights into the interaction between nanomaterials and cellular behaviors. All of the work presented in this dissertation clearly and strongly supports our hypothesis that LBL assembly of CNT composites is a powerful and versatile platform for creating a multifunctional neural interface that cannot be achieved using traditional electrode materials.

8.2 Future Directions

Despite the many exciting results generated from this dissertation, there is still much to be explored in realizing the full potential of a neural interface platform based on LBL assembled CNT composites. One property that remains to be characterized and optimized is the long-term stability of CNT composites in biologically relevant conditions. Since neural prosthetic devices need to stay inside the body for many years, accelerated stability testing of CNT composites would be necessary and could yield valuable information. Such testing may involve incubating the nanostructured CNT material in a simulated body fluid at body temperature with stirring of the fluid.[1, 2] The physical structure, surface morphology, and electrochemical properties of the CNT LBL composites should be monitored as material degradation can significantly impact the biocompatibility and functionality of an implanted neural interface. Post processing of LBL assembled CNT composites, such as chemical crosslinking or heat treatment, may be required to achieve optimal stability since the high concentration of ions in simulated body fluid could destabilize the native composite films, which are held together by a combination of electrostatic and weak forces. Post processing strategies are promising as they have been shown to be effective in optimizing the mechanical strength and stiffness of CNT LBL composites.[3]

Another direction of research that deserves attention is the fabrication of conductive CNT LBL films with neural tissue-like stiffness. While LBL assembled CNT films with high tensile strength and stiffness have been produced in the development of

ultra-strong materials,[3, 4] very little work has been devoted to the engineering of soft multilayer materials.[5] Several studies have demonstrated that matrix stiffness not only affects the adhesion of cells, but also controls the differentiation of stem cells.[6-9] For example, mesenchymal stem cells were shown to commit to the lineage specified by matrix elasticity. Specifically, soft matrices that mimicked brain elasticity induced differentiation toward neurons while stiffer matrices that mimicked muscles were favorable for differentiation into myoblasts.[8, 9] Both neurons and myoblasts are electroactive cells that can be electrically stimulated using conductive substrates like CNT LBL films.[10] By engineering CNT LBL films with elasticity resembling that of the neural tissue (E~0.1-1 kPa),[9] it may be possible to reduce acute inflammatory responses caused by mismatch in mechanical properties and increase neuronal differentiation of resident stem/progenitor cells. The level of control afforded by LBL assembly, as well as the wide selection of molecular species available to this nanostructuring technique, will be essential for this task. Since the desired material is most likely going to be a hydrogel film, the key challenge will be the ability to achieve sufficient electrical conductivity in this hydrated multilayer structure.

The last direction of research to be discussed here is the fabrication of a thin film electrode array based on LBL assembled CNT composites. This challenge could generate the most impact and encompasses several aspects that go hand in hand with each other, including miniaturization, patterning, and packaging of the conductive CNT LBL films. One important function highly desired by neural prosthetic devices is the ability to acquire high temporal and spatial frequency signals. This function requires the

deployment of multiple number of recording electrodes that are not only small (< 0.5 mm^2) but also positioned close to each other.[11] The ability to precisely fabricate such an array of electrode pads will require a patterning technology that is compatible with LBL assembled composite films. Conventional lithography techniques have been successfully utilized to create fine patterns on thin films fabricated from LBL assembly.[12-14] This interesting combination of top-down and bottom-up techniques can be similarly applied to CNT LBL films. Although patterning of LBL films using soft-lithography has been demonstrated, the fine balance of forces required at the interface may be a limiting factor for certain combinations of materials.[15] Another interesting strategy for generating patterns on LBL films is the use of laser ablation techniques. Femtosecond laser patterning of conducting polymer thin films[16] has already been demonstrated and should be equally applicable to CNT LBL films. The ability to precisely pattern CNT LBL films would allow both a dense array of electrodes and their interconnection wires to be constructed solely from LBL assembled CNT composites. However, the interconnection wires must be packaged and protected with an insulating material to prevent contact with the surrounding tissue and fluids. The insulating layer or packaging material can also be fabricated from LBL films, and the electrodes can be selectively exposed using lithographic techniques. The large surface area covered by this outer insulating layer requires it to be biocompatible but also offers opportunities for additional functions to be incorporated, such as selective adhesion, anti-inflammatory, and drug delivery.[17] With careful engineering and selection of materials, it would be possible to fabricate a thin film electrode array built entirely from LBL composite films. With a thickness of only a few

micrometers, this thin film electrode array would provide highly conformal coverage over the convoluted brain surface, which is critical to the establishment of a stable neural interface and the acquisition of quality signals. We envision that such a device would be most suitable and successful as a new generation of subdural, non-penetrating surface electrode system.[18, 19]

8.3 References

1. Fekry, A. M.; El-Sherif, R. M., Electrochemical corrosion behavior of magnesium and titanium alloys in simulated body fluid. *Electrochimica Acta* **2009,** *54* (28), 7280-7285.

2. Kaufmann, C. R.; et al., Long-term stability of self-assembled monolayers on 316L stainless steel. *Biomedical Materials 5* (2), 025008.

3. Shim, B. S.; Zhu, J.; Jan, E.; Critchley, K.; Ho, S.; Podsiadlo, P.; Sun, K.; Kotov, N. A., Multiparameter Structural Optimization of Single-Walled Carbon Nanotube Composites: Toward Record Strength, Stiffness, and Toughness. *ACS Nano* **2009,** *3* (7), 1711-1722.

4. Mamedov, A. A.; Kotov, N. A.; Prato, M.; Guldi, D. M.; Wicksted, J. P.; Hirsch, A., Molecular design of strong single-wall carbon nanotube/polyelectrolyte multilayer composites. *Nat Mater* **2002,** *1* (3), 190-194.

5. Francius, G. g.; Hemmerl√©, J.; Ball, V.; Lavalle, P.; Picart, C.; Voegel, J.-C.; Schaaf, P.; Senger, B., Stiffening of Soft Polyelectrolyte Architectures by Multilayer Capping Evidenced by Viscoelastic Analysis of AFM Indentation Measurements. *The Journal of Physical Chemistry C* **2007,** *111* (23), 8299-8306.

6. Engler, A. J.; Richert, L.; Wong, J. Y.; Picart, C.; Discher, D. E., Surface probe measurements of the elasticity of sectioned tissue, thin gels and polyelectrolyte multilayer films: Correlations between substrate stiffness and cell adhesion. *Surface Science* **2004,** *570* (1-2), 142-154.

7. Discher, D. E.; Janmey, P.; Wang, Y.-l., Tissue Cells Feel and Respond to the Stiffness of Their Substrate. *Science* **2005,** *310* (5751), 1139-1143.

8. Engler, A. J.; Griffin, M. A.; Sen, S.; B√∂nnemann, C. G.; Sweeney, H. L.; Discher, D. E., Myotubes differentiate optimally on substrates with tissue-like stiffness. *The Journal of Cell Biology* **2004,** *166* (6), 877-887.

9. Engler, A. J.; Sen, S.; Sweeney, H. L.; Discher, D. E., Matrix Elasticity Directs Stem Cell Lineage Specification. **2006,** *126* (4), 677-689.

10. Gheith, M. K.; Pappas, T. C.; Liopo, A. V.; Sinani, V. A.; Shim, B. S.; Motamedi, M.; Wicksted, J. R.; Kotov, N. A., Stimulation of neural cells by lateral layer-by-layer films of single-walled currents in conductive carbon nanotubes. *Advanced Materials* **2006,** *18* (22), 2975-+.

11. Kim, D.-H.; Viventi, J.; Amsden, J. J.; Xiao, J.; Vigeland, L.; Kim, Y.-S.; Blanco, J. A.; Panilaitis, B.; Frechette, E. S.; Contreras, D.; Kaplan, D. L.; Omenetto, F. G.; Huang, Y.; Hwang, K.-C.; Zakin, M. R.; Litt, B.; Rogers, J. A., Dissolvable films of silk fibroin for ultrathin conformal bio-integrated electronics. *Nat Mater 9* (6), 511-517.

12. Hua, F.; Shi, J.; Lvov, Y.; Cui, T., Patterning of Layer-by-Layer Self-Assembled Multiple Types of Nanoparticle Thin Films by Lithographic Technique. *Nano Letters* **2002,** *2* (11), 1219-1222.

13. Mohammed, J. S.; McShane, M., Polymer/Colloid Surface Micromachining: Micropatterning of Hybrid Multilayers. *Langmuir* **2008,** *24* (23), 13796-13803.

14. Hua, F.; Lvov, Y.; Cui, T., A lithographic approach of spatial separation for multiple types of layer-by-layer self-assembled nanoparticles. *Thin Solid Films* **2004,** *449* (1-2), 222-225.

15. Park, J.; FouchÈ, L. D.; Hammond, P. T., Multicomponent Patterning of Layer-by-Layer Assembled Polyelectrolyte/Nanoparticle Composite Thin Films with Controlled Alignment. *Advanced Materials* **2005,** *17* (21), 2575-2579.

16. McDonald, J. P.; Hendricks, J. L.; Mistry, V. R.; Martin, D. C.; Yalisove, S. M., Femtosecond pulsed laser patterning of poly(3,4-ethylene dioxythiophene)-poly(styrenesulfonate) thin films on gold/palladium substrates. *J. Appl. Phys.* **2007,** *102* (1), 5.

17. Tang, Z. Y.; Wang, Y.; Podsiadlo, P.; Kotov, N. A., Biomedical applications of layer-by-layer assembly: From biomimetics to tissue engineering. *Advanced Materials* **2006,** *18* (24), 3203-3224.

18. Freeman, W. J.; Rogers, L. J.; Holmes, M. D.; Silbergeld, D. L., Spatial spectral analysis of human electrocorticograms including the alpha and gamma bands. *Journal of Neuroscience Methods* **2000,** *95* (2), 111-121.

19. Wilson, J. A.; Felton, E. A.; Garell, P. C.; Schalk, G.; Williams, J. C., ECoG factors underlying multimodal control of a brain-computer interface. *IEEE Trans. Neural Syst. Rehabil. Eng.* **2006,** *14* (2), 246-250.